

http://researchcommons.waikato.ac.nz/

Research Commons at the University of Waikato

Copyright Statement:

The digital copy of this thesis is protected by the Copyright Act 1994 (New Zealand).

The thesis may be consulted by you, provided you comply with the provisions of the Act and the following conditions of use:

- Any use you make of these documents or images must be for research or private study purposes only, and you may not make them available to any other person.
- Authors control the copyright of their thesis. You will recognise the author's right to be identified as the author of the thesis, and due acknowledgement will be made to the author where appropriate.
- You will obtain the author's permission before publishing any material from the thesis.

MODELLING VOLCANIC TSUNAMIS

A thesis submitted in partial fulfilment of the requirements

for the Degree of

Master of Science

in Earth Sciences

at the University of Waikato

by

Gegar Sapta Prasetya

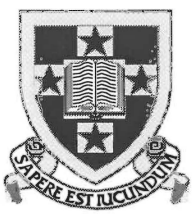

1998
Hamilton, New Zealand

ABSTRACT

Tsunamis generated by volcanic eruptions have caused about 25% of all deaths associated with volcano activity. The 1883 Krakatau eruption is one example of a fairly recent eruption that produced large tsunamis (~35 m) which caused a high death toll. Concern has also been raised by the potential tsunami generation of the Auckland Volcanic Field, and the impact of such events on the Auckland Region.

Although the generation of tsunamis by volcanic eruptions is a major hazard, the processes of tsunami generation are poorly understood. A review of volcanic tsunamis identified 10 main mechanisms. Four of these - caldera collapse, debris avalanches, submarine explosions, and pyroclastic flows - have been suggested as the mechanisms producing the largest tsunamis. All four mechanisms have also been suggested as being responsible for the tsunamis produced by the Krakatau eruption.

A combination of physical and numerical modelling was used to develop predictive tools to be applied to volcanoes in Indonesia and New Zealand. The physical modelling involved two main investigations:

- A 3 dimensional scale model of the Straits of Sunda and Krakatau. This examined the nature of tsunamis produced by caldera collapse, submarine explosions, and water displacement by debris avalanches and pyroclastic flows.
- A series of 2 dimensional simulations of the entrance of pyroclastic flows into the sea.

A finite element numerical model was applied to the simulation of pyroclastic flow, maar formation and submarine explosion generation of tsunamis within the Auckland Volcanic Field.

The physical and numerical model results indicate that large scale pyroclastic flows are probably the cause of the main 1883 Krakatau tsunamis. A tsunami wave can easily be generated by gravity flows entering the water, regardless of the slope. The wave properties depend on the relative densities of the flow and the receiving body, and the

velocity of the flow. The angle of entry of the flow into the water determines the deposition pattern of sediment. The formation of the Calmeyers and Steers shallow area on Krakatau event 1883 was reproduced by the pyroclastic experiments using coarse sand and mud with steep entry angle ($\geq 60^{o}$). The more dilute upper component of the pyroclastic flow that traveled along the sea surface for up to 45 km and killed more than 1000 people at Katimbang, Sumatera Island can also be explained. The experiments showed that less dense material from the pyroclastic flow propagates near the water surface. This is even more likely if the material is hot and gas-rich.

Physical and numerical model results showed that a single explosion cannot produce a high wave . If a super violent explosion did occur during the Krakatau event, then the water waves (tsunamis) that caused the devastating effect on the surrounding island coastal land were not caused by the direct transfer of explosive forces. Instead a sequence of one or more pyroclastic flows, or collapsing column in and around the Krakatau complex are the most likely mechanism causing the largest tsunami.

Numerical modelling of the Auckland Volcanic Field examined 4 scenarios:

- A series of submarine explosion;
- Pyroclastic flows from Rangitoto Island;
- Pyroclastic flows from Browns (Motukorea) Island;
- Submarine explosion within the Tamaki Estuary.

The first 3 scenarios produced regional effects, while the last was purely local event.

It was also found that the efficiency of the submarine explosion mechanism was increased by using a sequence of smaller explosions, instead of one large explosion. However the timing between explosions was found to be critical; if the explosions are too close together or too far apart, the efficiency decreases. It is considered that the optimal timing will vary with water depth and explosive yield.

The numerical modelling showed that volcanic tsunamis are not a major threat to Auckland. However under suitable conditions a volcanic eruption could produce moderately large tsunamis that generate strong currents.

ACKNOWLEDGEMENTS

I wish to take the opportunity to thank people who have aided me to complete this thesis.

My most sincere thanks go to my chief supervisor Professor Terry Healy for initiating the thesis topic, organizing the scholarship to undertake this study, and for his continued support and editing.

I would like to thank Dr. Willem de Lange for his endless patient and time; his support has been a key feature to the completion of this thesis.

Many thanks go to Rossane Bjerring for her support since I came to Hamilton and Ministry of Foreign and Trade for the Scholarships, International Student Office Staff for their general assistance.

All engineers, scientists and technicians of Tsunami Research Center, Coastal Engineering Laboratory LPTP BPP Teknologi, Indonesia, are thanked for their support during the physical modelling experiments.

I am indebted to Prof. Efim Pelinovsky, Institute of Applied Physic, Russian Academy of Sciences for the latest literature on pyroclastic flow modelling.

I would also like to thank Dr. Richard Smith and Assoc.Prof. Roger Briggs for their valuable discussions on pyroclastic flow and submarine explosion mechanisms, and volcanic activities in the Auckland region.

Many thanks to Michele Daly, Auckland Regional Council for providing valuable information on the volcanology of the Auckland region.

The Earth Sciences secretaries, Sydney Wright and Elaine Norton, are thanked for their valuable general assistance over the past 2 years. Thanks Sydney for your care and attention to my family.

Special thanks to Dr. Yacov Nier and Dr. Klaus Michels for all discussions in 'rainy days'.

To Sohail, Joseph, Tian, Nick Brown, Mike, Ed Brown, Rick, Cam, Louise, Vermoon, Nenad, Hamish, Ross, Paul, Jens, Joan, Glenn, Dion, Julie, Flint, Bruce, Grant, John and John Meneer, many thanks for the help and jokes.

My friends Irvan, Azul & Nia, Vano, Sarah, Rani and Ran-ran, thanks for everything.

Finally, I would like to thank my wife, Bekti Poedjihastoeti and my family for all their love and support.

CONTENTS

Abstract ii
Acknowledgements iv
Contents v
List of Figures viii
List of Tables xvii

Chapter 1 Introduction 1
1.1. Aims and Objectives 2
1.2. Study Area 2
1.3. Summary of Thesis 3
1.4. References 6

Chapter 2 Fundamental Tsunami Processes 7
2.1. Introduction 7
2.2. Tsunami Generation 7
2.2.1. Submarine Faulting 8
2.2.2. Landslides and Submarine Slumps 10
2.2.3. Volcanic Activity 12
2.3. Tsunami Propagation 17
2.3.1. Refraction 18
2.3.2. Difraction 19
2.3.3. Reflection 20
2.4. Tsunami Runup and Inundation 21
2.5. References 22

Chapter 3 Mathematical Model 26
3.1. Introduction 26
3.2. Derivation of Governing Equation 26
3.3. Model for Deep Sea Propagation 31
3.4. Model for Propagation in Shallow Water 32
3.5. Runup Model 35
3.6. References 36

Chapter 4 The Finite Element Method 37
4.1. Introduction 37
4.2. The Method 37
4.3. Tsunami Model Approach 40
4.4. Tsunami Finite Element Model 41
4.4.1. Deep Water Generation and Propagation 41

4.4.2. Near Land Propagation Model 42
4.4.3. Time Stepping Method 43
4.4.4. Limitations and Sources of Error 45
4.5. The Tsunami Finite Element Computer Program 47
4.6. References 50

Chapter 5 Physical Modelling 51
5.1. Introduction 51
5.2. Overview of Krakatau Event 51
5.3. Overview of The Physical Model (Overview of The Scale Model) 53
5.4. Test Facility 54
5.5. Background of Events Simulated 57
5.6. Model Test 60
5.6.1. Two Dimensional (2D) Model Test 60
5.6.2. Three Dimensional (3D) Model Test 61
5.7. Results and Discussions 65
5.7.1. Two Dimensional (2D) Pyroclastic Flow Experiments 65
5.7.2. Three Dimensional (3D) Model Test 71
5.8. References 78

Chapter 6 Mathematical Modelling of Volcanogenic Tsunamis 79
6.1. Introduction 79
6.2. Overview of Auckland Volcanic Field 79
6.3. Events Simulated 82
6.4. Numerical Simulation 85
6.4.1. Construction of the Finite Element Grid 85
6.4.2. Boundary and Initial Conditions 93
6.5. Results 95
6.5.1. The Initial Test 95
6.5.2. Events Simulated Results 97
6.6. References 102

Chapter 7 Conclusions 103
7.1. Introduction 103
7.2. Major Findings 103
7.3. Implications for Civil Defence 106
7.4. Further Research 106
7.5 Reference 108

Appendix.1. File Description and Simulation Results

Trigrid File Description 2
Digit(.dig) 2
Node(.nod) 4
Neighbour (neigh)(.ngh) 5
Triangle(.tri) 5
Tsunami Files 6

Command File 6
Boundary Condition File 6
Time History File 8
Simulation Results 28

Appendix.2. Photographic Sequence of The Experiments

Preparation 2
Submarine Explosion 5
Free Fall Circular Plate 16
Caldera Formation Test 23
The Typical Wave Dynamic in the Coast 26
Two Dimensional Experiments 30

Appendix.3. Result of Wave and Current Measurements

Flume Test 2
Three Dimensional Test 10

LIST OF FIGURES

FIGURE CHAPTER :

1.1. The Hauraki Gulf 4
1.2. The Auckland Volcanic Field 5
2.1. Fault geometry and parameters in 2D and 3D 9
2.2. Geometry of landslide 11
2.3. Sequence of an ultraplniean volcanic eruption leading to up a pyroclastic flow 13
2.4. Schematic of pyroclastic flow mechanism 14
2.5. Sequence of shallow water explosion generated wave 16
2.6. Schematic diagram of refraction process 18
2.7. Schematic diagram of diffraction process 19
2.8. Schematic diagram of reflection process 20
3.1. Cartesian coordinate system 28
3.2. Cartesian coordinate of sea floor displacement and initial wave, following the method of Manshina and Smylie(1971) 31
3.3. Modified coordinate system (de Lange, 1997) 34
4.1. The simplest type of 2-dimensional (2D) finite element with triangular mesh generated by automatic grid generation software package TRIGRID 38
5.1. The Krakatau volcanic comples lay between the Indonesian island of Java and Sumatera in Sunda Straits(modified from Mathew, 1988) 52
5.2. The lay out of laboratory facilities at the Tsunami Research Center 58
5.3. The bathymetry changed surrounding the Krakatau before and after 1883 event (source: Sigurdsson et al.1991) 59
5.4. Lay out of 2-dimensional (2D) test facility 60
5.5. The photograph of 3-dimensional model in wave basin 63
5.6. The sequences dynamic of pyroclastic flow shows the turbulent and well mixed flow and the first stage of wave initiations and its propagation 67
5.7. The changes of wave height with slope angle shows the tendency of decreasing of the wave height from 20° - 60° and increased after 60°. It also shows that the denser material of flow generated higher wave. 68
5.8. The sediments were deposited further from the base of ramp for angle > 30° 69
5.9. The typical wave formation produced by a point source mechanism is consistent with the aerial photograp of Eruption 1929 of Anak Krakatau. There are clear concentric eruption-waves emanating from the eruption point (Simkin and Fiske, 1983) 73
6.1. The Auckland Volcanic Field has been active for over

140,000 years and has formed 49 small basaltic volcanoes within an area of about 360 km^2 centre on Auckland (source: Nairn et al.,1996) 80
6.2. The trend towards an increase in the size of the average eruption at Auckland Volcanic Field (source: Smith and Allen, 1993) 81
6.3. The 4 locations (A, B, C, D) considered as having the potential to generate the tsunamis and affect the auckland region (modified from Nairn et al, 1996) 83
6.4. The finite element grid mesh produced by TRIGRID for the Auckland region consists of 6383 nodes, with maximum of 11 neighbours 86
6.5. The flowchart of depth grid preparation 90
6.6. The flowchart of model grid preparation 91
6.7. The finite element grid for the Hauraki Gulf showing that for the area with rapid change of contour bathymetry are represented by fine elements 92
6.8. The schematic diagram of dynamic initial condition of the pyroclastic flow 94
6.9. The time history of the submarine explosion with multiple explosion and collapsing of caldera 98

FIGURE APPENDIX:

APPENDIX.1.

1. Dome shape at the sea surface one second after explosion completed 28
2. The dome one second after the last explosion. Time gap between explosion is 30 s 28
3. The dome one second after the last explosion. Time gap between explosion is 60 s 29
4. The dome one second after the last explosion. Time gap between explosion is 120 s 29
5. The dome one second after the last explosion. Time gap between explosion is 5 minutes 30
6. The dome one second after the last explosion. Time gap between explosion is 10 minutes 30
7. The patterns of wave propagation after 1 minute from explosion 31
8. The patterns of wave propagation after 5 minutes from explosion 31
9. The patterns of wave propagation after 1 minute from the last explosion 32
10. The patterns of wave propagation after 5 minutes from the last explosion 32
11. The patterns of wave propagation after 1 minute from the last explosion 33
12. The patterns of wave propagation after 5 minutes from the last explosion 33
13. The patterns of wave propagation after 1 minute from the last explosion 34
14. The patterns of wave propagation after 5 minutes from the last explosion 34
15. The patterns of wave propagation after 1 minute from the last explosion 35
16. The patterns of wave propagation after 5 minutes from the last explosion 35
17. The patterns of wave propagation after 1 minute from the last explosion 36
18. The patterns of wave propagation after 5 minutes from the last explosion 36
19. The variation of dome height produce by multiple explosion

with variable time gaps at one second after the last explosion.
Time gap 0 means a single explosion 37
20. The variation of dome height produce by multiple explosion
with variable time gaps at one minute after the last explosion.
Time gap 0 means a single explosion 37
21. The initial condition of maar formation with negative displacement - 6 m 38
22. The pattern of sea disturbances one minute after the initial condition 38
23. The sea elevations after 3 minutes from initial condition
showing that the sea recession took place around the Rangitoto Channel 39
24. The pattern after 5 minutes showing that the center of disturbance
has almost disapeared 39
25. The current pattern for initial negative displacements for maar
formation immediately after collapse 40
26. The current pattern for negative displacements
after one minute from the initial condition 40
27. The current pattern for negative displacements
after two minutes from the initial condition 41
28. The current pattern for negative displacements
after 5 minutes from the initial condition 41
29. The result of static initial condition for pyroclastic flow test
after 10 seconds from the initial condition where with maximum
displacement is 7 m 42
30. The results of dynamic initial condtion after 10 seconds
from the initial condition with maximum displacement 7 m 42
31. Initial condition overlapping explosions at Rangitoto Channel 43
32. The patterns of waves one minute after 1st explosion 43
33. Three minutes after 1st explosion 44
34. Five minutes from 1st explosion, collapsing of sea bottom
is started 30 seconds before second explosion 44
35. Second explosion is started with dome reaching 21.0 m height 45
36. The waves pattern one minute after thelast explosion 45
37. Five minutes after the last explosion 46
38. Ten minutes after the last explosion 46
39. Twenty minutes after the last explosion 47
40. Thirty minutes after the last explosion 47
41. Forty minutes after the last explosion 48
42. Fifty minutes after the last explosion 48
43. The water levels condition in Waitemata Harbour and
its vicinity 50 minutes after the last explosion 49
44. Sixty minutes after the last explosion 49
45. Current pattern one minute after 1st explosion 50
46. Three minutes after 1st explosion 50
47. Current pattern at final stage of second explosion
(five minutes after 1st explosion) 51
48. Five minutes after the last explosion strong currents
enter the Tamaki Estuary 51
49. General view of current pattern 5 minutes after the last explosion.
Strong current flows along the coastline to the north, around

the Rangitoto Volcano and down to St. Heliers Bay and
entrance of Waitemata Harbour. To the southeast the flow
enter Tamaki Estuary 52
50. Current pattern 10 minutes after the last explosion.
Strong current occured along the coastline move up to
the north, along the northern and southern part of
Rangitoto Volcano, and at the mouth of Tamaki Estuary. 53
51. General view of current pattern after 10 minutes from the last explosion 53
52. Curent pattern after 40 minutes from the last explosion.
The intensity of the flows are decreasing. 54
53. General view of current pattern 40 minutes from the last explosion 54
54. The initial condition of the submarine explosion for Tamaki Estuary 55
55. Wave and current pattern 1 minute after the explosion 55
56. The condition of the estuary 5 minutes after explosion 56
57. Ten minutes after explosion, at the end of estuary thewave height is 0.2 m 56
58. At 15 minutes after explosion the water level at
the end of estuary (upstream) reaches 0.32 m and
the current flow start to change direction to downstream. 57
59. Initial condition of a pyroclastic flow enetering the sea at
Brown Island using dynamic initial condition 58
60. The pattern of waves and currents one minute after initial condition.
Curents are rapidly flowing towards the mouth of Tamaki Estuary 58
61. The pattern of waves and currents 5 minutes after the initial condition 59
62. After 30 minutes from the initial condition,
current flows into Tamaki Estuary are reduced
and stronger current flows occur in Rangitoto Channel 59
63. Sixty minutes from the initial condition, strong current still flows
along the coastline from eastern beach of Musick Point down
to Motukaraka Island and around the Rangitoto Island.
The waves propagate up to the north with 0.02 m height.
In Waitemata Harbour the wave varies from 0.02 m to 0.25 m 60
64. Initial condition of pyroclastic flow entering the sea at
Rangitoto Island using dynamic initial condition 61
65. The pattern of curents and waves 5 minutes after initial condition 61
66. The waves and currents pattern after 10 minutes from initial condition 62
67. The waves and currents pattern 20 minutes from initial condition. 62

APPENDIX.2.

Ap2.1. Overall view of wave basin and the three dimensional model. Sixteen wave sensors (blue tripods) and five current meters were installed and connected with HP data logger and computer for further processesing
2

Ap.2.2. The capacitance wave sensor (white colour) and tripod (blue colour) used to measure the tsunami waves in the model 2

Ap.2.3. Water from the reservoir starting to fill the wave basin 3

Ap.2.4. The water level at the shoreline could be adjusted by controlling the outlet and intake pumps 3

Ap.2.5. The water surface in the wave basin before instrument calibration. It is necessary to keep the water surface calm to set the zero levels for measurement of wave height and current velocities 4

Ap.2.6. The computer and HP data logger before start the experiments 4

Ap.2.7. The initial stage of submarine explosion test. The typical disruption of the water surface resulting from a point source mechanism can be seen at the source of explosion with the small quantity of explosive used, a dome formed in the water surface. This dome had just begin to break up when the photo was taken 5

Ap.2.8. Concentric eruption-waves emanating from the explosion point have propagated outside the Krakatau complex. The first three waves are evident 5

Ap.2.9. The initial waves reaching the main shores of the wave basin. The concentric pattern is still clearly evident 6

Ap.2.10. The first wave reaches the west coast of Java causing inundation of low lying areas 6

Ap.2.11. With increasing the intensity of explosion, the water surface at the source of explosion no longer formed a dome shape, but developed a crater instead. The initial crater is showing in this photo 7

Ap.2.12. Shortly after the explosion, the water surrounding the crater rush inwards and collide to form the jet shown in the centre of the crater. Waves then start to propagate outwards from the centre as the jet collapses 7

Ap.2.13. A few seconds after explosion, the bore and accompanying waves leave the vicinity of the crater at Krakatau 8

Ap.2.14. The waves start approaching the west coast of Java 8

Ap.2.15. The preparation of explosion test with a confining chamber. The area around the chamber were infilled with sand to represent the Krakatau Island before it exploded 9

Ap.2.16. The initial stages of the explosion with a confining chamber. The white in the centre of the Krakatau complex was smoke from the explosion. The initial waves formed by the explosion were obscured 9

Ap.2.17. A second after explosion, no waves have formed outside the Krakatau Island complex 10

Ap. 2.18. A few seconds after Ap.2.17, the first wave starts to move towards the East, approaching the west coast of Java. The smoke still remains around the Krakatau complex 10

Ap.2.19. Shortly afterwards three to five leading waves are evident approaching the Sumatera coast and west coast of Java 11

Ap.2.20. The waves inundating the west coast of Java 11

Ap.2.21. The medium intensity explosion test severely disrupted the water and formed a crater instead of forming a dome 12

Ap.2.22. A second after the explosion, the disrupted water dropped back into the crater. The white colour is the smoke from the explosion 12

Ap.2.23. Three seconds after explosion the initial wave has formed due to the expansion of the crater 13

Ap.2.24. The pattern of the waves approaching the west coast of Java and the Sumatera coast 13

Ap.2.25. The high intensity explosion with a confining chamber showing the initial stage of the explosion (above) and the initial wave formation (below). The leading waves were generated mainly by the expansion of the crater 14

Ap.2.26. The first wave reaches the west coast of Java and the Sumatera coast. There are obviously three 'large' waves generated by this mechanism 15

Ap.2.27. The inundation of the shoreline after the arrival of the first wave 15

Ap.2.28. The initial condition for the free-fall circular plate experiments. The suspended plate was dropped into the water to simulate an explosion 16

Ap.2.29. Calibration of all instruments before dropping the circular plate 16

Ap.2.30. Immediately after the plate impacted the water surface. The crater and the first wave have formed 17

Ap.2.31. Shorthly after the water surged back into the crater to form a jet before collapsing to generate waves. Clearly,a single leading wave was formed 17

Ap.2.32. The waves have propagated outside the generation area 18

Ap.2.33. There are clearly three main waves approaching the coast 18

Ap.2.34. The waves interacting with the Sumatera coast 19

Ap.2.35. Close-up of the first wave arriving at the Sumatera coast 19

Ap.2.36. Different view of the free-fall circular plate experiment at the initial stage when the circular plate has just dropped into the water 20

Ap.2.37. The height of the jet of water formed the water surged back into the crater is clearly seen in this picture 20

Ap.2.38. The propagation of the leading solitary waves outside the generation area 21

Ap.2.39. The propagating waves approaching the coastline 21

Ap.2.40. The first wave hits the west coast of Java 22

Ap.2.41. The interaction of the first and second waves after they hit the tip of the west coast of Java 22

Ap.2.42. The preparation for the caldera formation test showing the final caldera configuration 23

Ap.2.43. Filling of the wave basin with water and adjustment to the mean water level used for the tests 23

Ap.2.44. Calibration of instruments prior to caldera formation tests 24

Ap.2.45. The caldera plug has been uplifted and the first wave is starting to form 24

Ap.2.46. The withdrawal of water along the west coast of Java before the first crest arrives 25

Ap.2.47. Inundation of the coast after the arrival of the first wave crest 25

Ap.2.48. A maximum of five waves were observed during the experiments as seen in this photograph 26

Ap.2.49. Half of the first wave has inundated the northern part of the west coast of Java.
27

Ap.2.50. The wave interaction at the coastline one second after .Ap.2.49 27

Ap.2.51. The wave interaction at the coastline one second after .Ap.2.50 28

Ap.2.52. The wave interaction at the coastline one second after .Ap.2.51 28

Ap.2.53. Different view of waves approaching the west coast of Java. The first wave is clearly shown in the photograph 29

Ap.2.54. The first wave breaks and rushes up the coastline 29

Ap.2.55. This photographic sequence shows the main stages of the dyed freshwater water experiments in Flume. The initial condition (above) shows the calibration of the water level. Next is the initiation of the first wave (middle) when the pyroclastic flow hits the water surface in flume causing high turbulent and flow mixing. The waves propagate leaving the generation area. The dark red colour beneath the waves (photo in the middle) and behind the waves (below) in the water column shows the continuation of the pyroclastic flow
30

Ap.2.56. The wave still maintains its shape and propagates at a speed of 1.85 m/sec. The lighter material of the pyroclastic flow propagates at the upper surface of the water column 31

Ap.2.57. Behind the first wave, there is a second low angle wave. This wave was generated due to the turbulence and the force of buoyant fluid which pushed the water up behind the flow 32

Ap.2.58. A trace of light material remained on the glass-walls of the flume. A thick layer occured close to the source and it thinned along the flume indicating increased mixing and dispersion
33

Ap.2.59. The cross-sectional view of the dyed freshwater within the water column showing that close to the generation area the dyed freshwater was well mixed with the water in flume 34

Ap.2.60. Overhead photograph showing the trace of dyed freshwater which remained on the bottom of the glass-walled flume close to generation area. It shows the area where the flow material hit the bottom of the flume.
34

Ap.2.61. The interaction of the mass flow and the water in flume is still in progress; the first wave has left the generation area. The water level behind the first wave remains calm and level.

35

Ap.2.62. The denser mass flow material flowing along the bottom of the flume without affecting the water surface.

35

Ap.2.63. The propagation of the first wave with a small surface roller formation. 35

Ap.2.64. The condition of the water in flume close to generation area after the test. The sediment in the flow was deposited at the base of the ramp.

36

Ap.2.65. The head of the flow is still flowing at the bottom of the flume, and some heavier sediment has deposited in the base of the ramp. 36

Ap.2.66. The initial wave starts to change its shape; the roller in the wave crest becomes larger.

36

Ap.2.67. A cross section of the flume showing the same characteristic distribution of material within the water column, with lighter material flowing at the top of water surface. 37

Ap.2.68. The flow sediment material was deposited further away from the base of the ramp for the experiment with angle of ramp $\alpha = 60\ ^{o}$. This behaviour was evident during the 1883 eruption.

37

LIST OF TABLES

Table 5.1. A combination of experiments 61
Table 5.2. A number of experiments 65
Table 5.3. The form of initial disturbances with analytical solution 75

Chapter One

INTRODUCTION

A tsunami is a progressive wave with a long wavelength and period, generated by a disturbance of seafloor associated with various geologic processes such as: submarine fault movements accompanying earthquakes; submarine volcanism; landslides; or a combination of these sources. The tsunami's size and effect on the shoreline are often decomposed into several factors: the amplitude of the wave at the source, which is primarily controlled by the size and geometry of the source; the response of the coastal features, such as bays and harbours (which are capable of resonance, thereby amplifying selected wave frequencies), to the wave; and the nonlinear hydrodynamics of the breaking wave as it climbs up the shore. In order to predict detailed and quantitative information, the modelling of tsunami behaviour is essentially required.

Coastal areas in the Pacific Ocean have suffered damage by tsunamis for a long time: more than 3000 lives were lost to disastrous tsunamis since 1992 in Indonesia, Nicaragua, Japan and Philippines. However, their effects are often underestimated as an earthquake hazard, possibly because of their infrequent occurrence. Based on historical data of tsunami events in the Pacific Ocean, tsunami affecting New Zealand Coast have been generated by a variety of different mechanism. Some sources can be categorised into far field tsunami, which are generated at some distance from New Zealand and propagate through the deep water of Pacific Ocean before reaching the coast, while some are near field tsunami generated close to New Zealand's coastline and propagate through relatively shallow water.

1.1. Aims and Objectives

The major aim of this study is to examine the behaviour of tsunamis within the Hauraki Gulf, generated from the possible volcanogenic tsunami sources within the Auckland Volcanic Field. This will be achieved by

i) undertaking physical modelling studies of the Krakatau 1883 event in order to understand the physical behaviour of volcanogenic tsunamis and associated generation processes;

ii) applying the tsunami finite element model to volcanogenic tsunamis within the Hauraki Gulf. Particular attention is given to the generation processes and coastal response of tsunami such as: harbour resonance, wave focusing, current patterns, trapping and edge wave phenomena, and maximum wave heights.

The results of this study will be used to assess the Volcanic Tsunami Hazard within the Auckland Region.

1.2. Study Area

The Hauraki Gulf is a semi enclosed sea with many small islands scattered within its' coastal area (Figure 1.1). Two relatively large islands are located within the Gulf, Rangitoto island (volcanic) and Waiheke Island. Further offshore, in the mouth of the Gulf are Great Barrier Island and Little Barrier Island. The Hauraki Gulf is extensively used for recreation and has a significant amount of infrastructure located around its' shores. The Auckland metropolitan region, the largest population centre in New Zealand, is located within this area. Since the last significant tsunami event in 1964, there has been considerable investment in coastal infrastructure including new marinas and upgraded port facilities.

From the historical record, since 1840, the Hauraki Gulf has recorded 11 tsunamis and one meteorological tsunami (rissaga) caused by Krakatau 1883 event (de Lange, 1983). Most of these were small events, except 3 tsunamis (Chile 1868, Chile 1960, and Alaska 1964) and the rissaga (Krakatau event 1883). These damaging tsunamis were tele-tsunami (far field tsunami). However, it is considered possible that a local source may also produce damaging tsunamis, and hence the potential of tsunami hazard is of concern to regional and local planners around the Hauraki Gulf.

A volcanic eruption within the Auckland Volcanic Field is considered as the main source of volcanogenic tsunamis during this study. This field has involved a series of mainly monogenetic basaltic eruptions over the last 140,000 years (Figure 1.2). Phreatomagmatic eruptions around the coastal margins, or within the shallow waters close to Auckland are considered to be a likely future event given the history of the field.

1.3. Summary of the Thesis

This research study consist of eight chapters which is structured to achieve the major objectives of the research as follows:

Chapter 1 : Explain the background, objectives and aim, and region of interest for this research study.

Chapter 2 : Elaborate the fundamental processes of tsunami generation, propagation, runup and inundation of coastal areas.

Chapter 3 : Discuss mathematical models of tsunami generation, propagation, runup and inundation. Resulting equations can be solved numerically to simulate tsunami behaviour.

Chapter 4 : Presents the finite element method which is used to simulate the behaviour of tsunami.

Chapter 5 : Elaborate the physical, or scale, modelling studies of volcanogenic tsunamis with special emphasis on submarine explosion, caldera formation and pyroclastic flow based on Krakatau event 1883.

Chapter 6 : Presents the results and discussion of numerical simulations based on ARC scenarios.

Chapter 7 : Conclusion of this study and the possible further research.

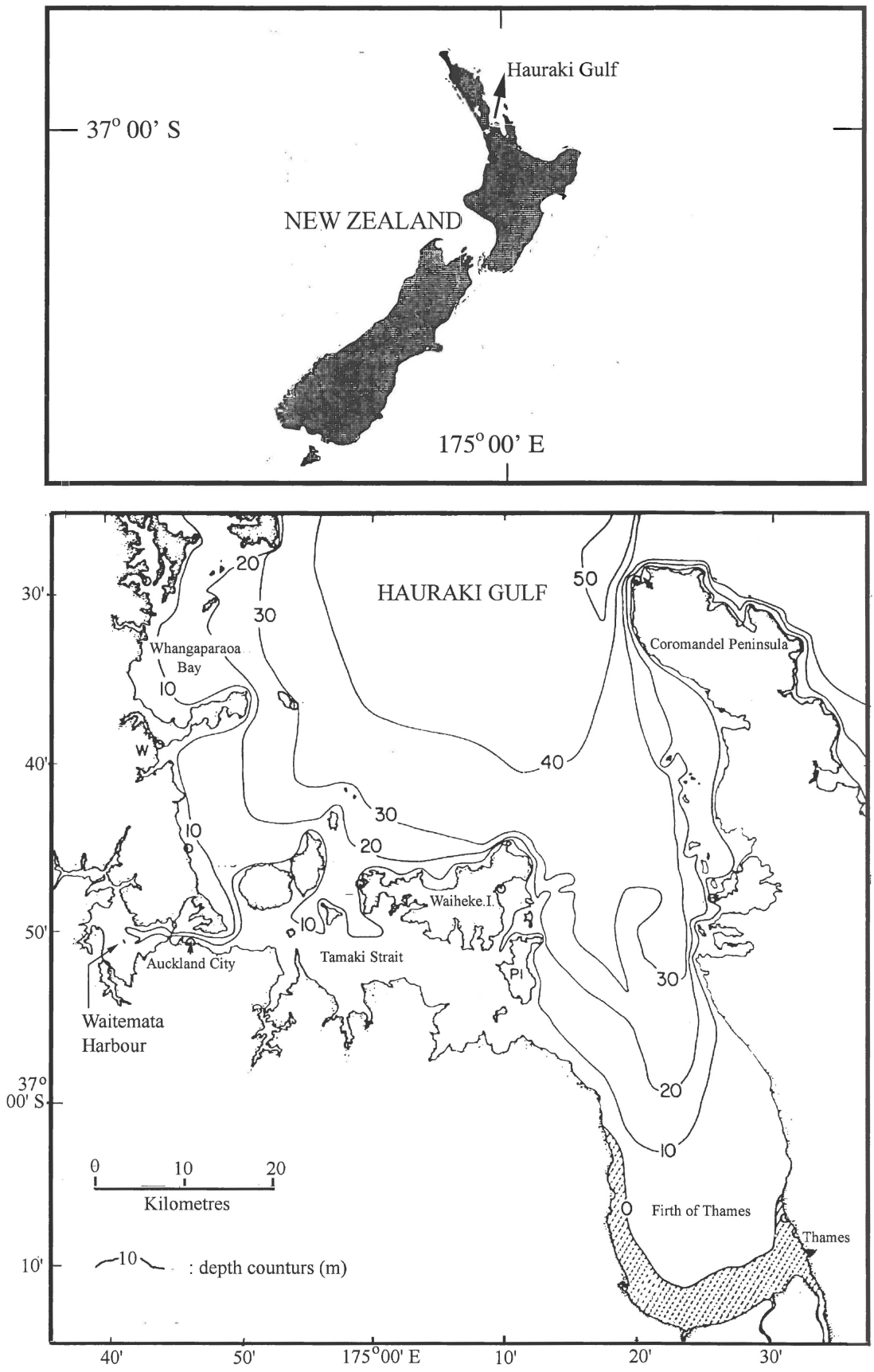

Figure 1.1. The Hauraki Gulf (modified from Bowman and Chiswell, 1982).

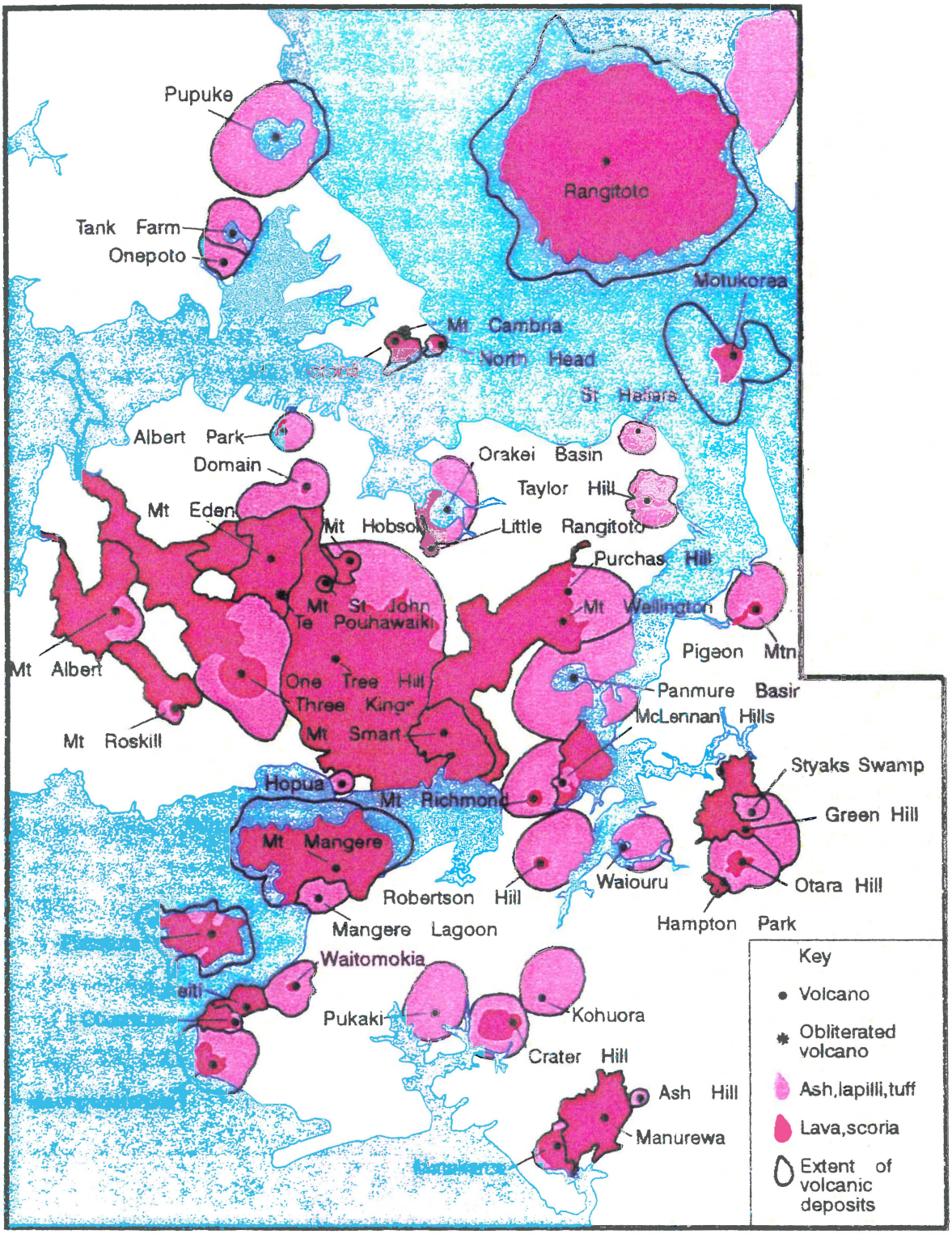

Figure 1.2. The Auckland Volcanic Field (source: Nairn et al. 1996).

1.4. References

Bowman, M.J., and Chiswell, S.M.,(1982), Numerical tidal Simulations within the Hauraki Gulf, New Zealand., in : Hydrodynamics od semi-enclosed seas., J.C.J. Nihoul (ed)., Elsevier Oceanography series., Elsevier scientific Pub. Netherland. p. 349-385.

De Lange, W.P., (1983), Tsunami Hazard: an investigation into the potential tsunami hazards of the Bay of Plenty Region using numerical models. M.Sc. Thesis., University of Waikato, Hamilton, New Zealand., 275 p.

Nairn, I.A., Johnston, D.M.,and Thordarson, T.,(1996), Eruption scenarios for Auckland Volcanic Field, Institute of Geological and Nuclear Sciences.

Chapter Two

FUNDAMENTAL TSUNAMI PROCESSES

2.1. Introduction

The fundamental processes that must be well understood in studying tsunamis are their generation, propagation and runup on land. The mechanics of tsunami generation involves the source mechanism and its' interaction with the body of water, which gives the initial profile at the sea surface. Once the initial profile is generated, it will travel outward from the source and its' characteristics will change as it moves into shallower water and begins to approach the shore. The main feature of the near-shore dynamics and runup of tsunami is non-linearity.

This chapter presents a general overview of the fundamental processes of tsunami generation, propagation and runup on land. The main forces which dominate each process are identified and limitations of existing methods are considered.

2.2. Tsunami Generation

The movement of the seafloor that causes tsunami can be produced by various geological processes. At least three different types of geologic activities can produce tsunami: submarine faulting associated with an earthquake; submarine volcanic eruption or explosion; and landslides or submarine slumps. Each of these sources involves a different generating mechanism. The characteristics of the generated waves are dependent on the generating mechanism involved.

Theoretical, numerical and physical modelling studies are used as tools to study the initial wave form of tsunami during their generation phase. In reality, the initial wave form is difficult to observe due to the very small amplitude compared to

the length and width of generating area. A discussion of the generating mechanism of tsunami by major geologic processes is given in the following section.

2.2.1. Submarine Faulting

The generation of tsunamis by earthquakes has been studied extensively (viz., Ward, 1980 and Okal, 1988, 1994). There is a little doubt that earthquake mechanism, along with other factors such as earthquake moment and focal depth, plays a critical part in tsunami generation. Empirical formulae that relate the earthquake moment magnitude and focal depth can be used to determined the tsunamigenic earthquake. As an example: mostly, earthquakes and moment magnitudes more than 5.6 with focal depths less than 70 km are needed to generate tsunami.

The most frequent and important mechanism of the earthquake for tsunami generation is submarine faulting, when a block of the ocean floor is thrust upward or suddenly drops accompanied by earthquakes. This kind of fault is known as dip-slip (thrust and normal) faulting. Another fault mechanism, strike-slip faults, are infrequent in generating tsunamis and when tsunamis have formed, they have been of a local nature and did not propagate long distances (Murty, 1979).

Fault mechanism and fault parameters for tsunamis are determined from seismic data collected locally and world-wide by United State Geological Survey (USGS) and Harvard University. The vertical displacement of the sea bottom can be calculated using the Manshina and Smyle (1971) methods. The fault parameters used in the calculation of bottom deformation are divided into two: static parameters (length, width, dislocation, strike, slip, and dip angle); and dynamic parameters (rupture velocity and rising time of dislocation). Usually rapid deformation of seafloor over an extensive area produces a disastrous tsunami.

A tsunami generated from a dip-slip fault source will have the characteristics of being generated from a line source; i.e., the length of the generating area is much greater than width. When displacement occurs along a substantial length of fault line, the divergence of the wave rays of the generated wave (i.e. the spreading of wave energy along the wave crest) will be much less than for a wave generated from a small source (Camfield, 1980). In the case of a wave generated near to the coastline, the main component of the wave energy will travel perpendicular to the faultline and propagates seaward. However, some of it is manifested in the run-up on the coastal

segment alongside the source region and then reflected seaward and some, in the form of trapped edge waves, propagates along the shelf with dispersive attenuation (Carrier 1995; Gonzalez et al., 1995).

The direction of the initial sea surface deformation determined the wave form to a significant degree. A rise or fall of the sea surface results in a wave form with a leading positive or negative (or trough) displacement. The first case will result in bore formation and an increasing water level as the wave approaches the coast, and the second case will give drawdown effects or recession of sea surface as the wave approach the coast. These effects have been demonstrated by physical and numerical modelling investigation, and also by an eye-witness accounts (de Lange, 1983; Synolakys, 1991; de Lange and Hull, 1994 ; Yeh, 1995).

Reconstruction of the initial wave form at the source can be done by using anti-refraction diagrams based on field measurements immediately after the event. The accuracy of this method is depend on the quality of field data measurements.

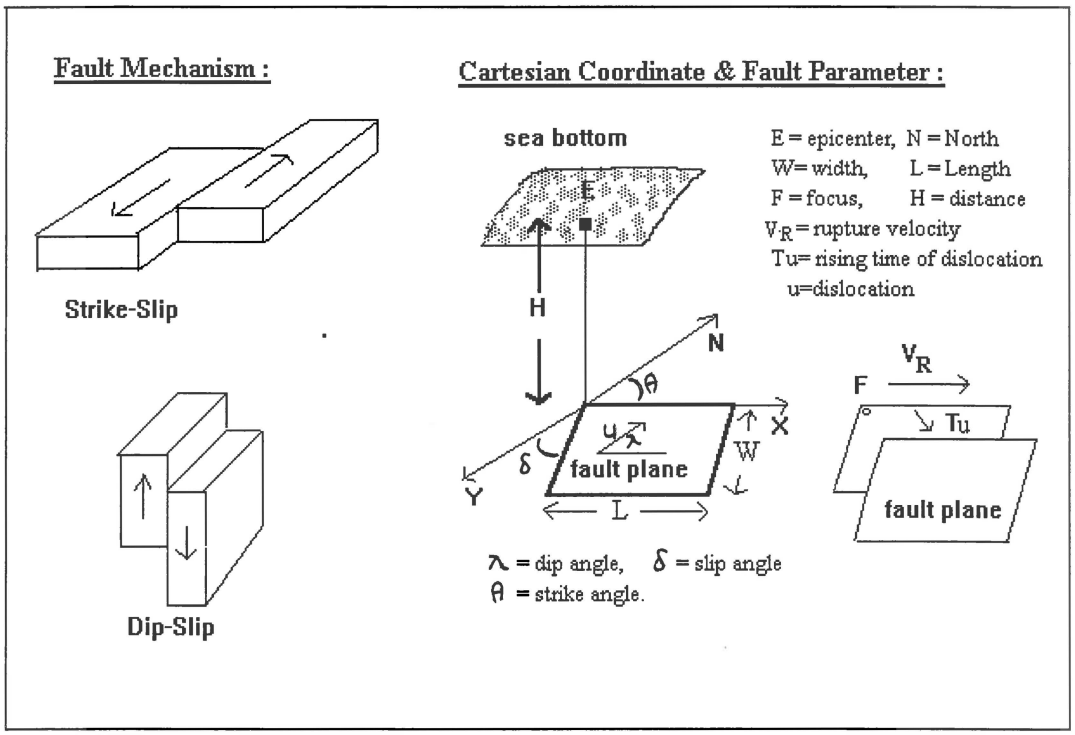

Figure 2.1. Fault geometry and parameters in 2 D and 3D

2.2.2 Landslides and Submarine Slumps

Landslides and submarine slumps can occur from various causes, and may take place in the open ocean, bays or inlets where they can generate tsunamis. Generally, landslide tsunamis have a much smaller horizontal scale than tsunamis generated by an earthquake and have been considered as point sources with local characteristics (Kulikov et al., 1996). Most documented tsunamis associated with known slumping have involved large masses of sediment moving down relatively steep slopes, usually the continental slope (de Lange, 1983; de Lange and Hull, 1994). The waves generated by such events will spread geometrically as they propagate from their source in an open ocean. This directly reduces the wave height, but they can be very high near their origin. This type of tsunami is characterised by short wave lengths and high amplitude waves in the generation area (Rzadkiewicz et al., 1997). Waves can be particularly high if they occur in confined inlet or harbour, or if resonance or refraction effects exist such as at Lituya Bay, Alaska 1958 (Camfield, 1980), Kitimat Inlet - British Columbia 1974 (Murty, 1979) and Skagway- Alaska 1994. This last event was due to a local abrupt failure of the sediment material in the region of wharf construction (Kulikov et al., 1996).

Following Murty (1979) and Kulikov et al. (1996), the wave generated is assumed to have the characteristics of a Solitary wave. Further, it is assumed that the fraction of potential energy in the slide that is converted into wave energy is small (< 0.01). Van Dorn (1965), indicate that under ideal conditions only about 2% of the potential energy of the sliding mass is converted into tsunami. In confined waters it would seem that more energy is transferred to the tsunami, since documented tsunamis which have occurred in confined water bodies have been very large (de Lange, 1983).

Analytical theory to estimate tsunami height from landslides was developed by Striem and Miloh (1976), Murty (1979) and Kulikov et al. (1996). The following method is based on a somewhat simplified analytical theory for solitary waves. The required landslide parameters are defined schematically in Figure 2.2. The wave height H may be estimated as :

$$H = \frac{1}{D_0}\left[8(3)^{0.5}\mu l w(\delta - 1)(D_0 - D_s)\right]^{2/3} \qquad (2.1)$$

where w is the average thickness of the slide material, l is the length of the slide, D_s and D_o are the water depths at ends of the slide and slope, respectively, δ is the relative sediment bulk density, and μ is the fraction of potential energy transformed into wave energy. Clearly the most difficult parameter to define is μ.

To attempt to develop a classify of submarine landslides based on feature geometry and the nature of the solid material (chemical composition, grain size, solid concentration, etc), Rzadkiewicz et al., (1997) studied submarine flow slides (viz., mass flows resulting from initial slide) and their hydraulic effects by numerical means using a two-dimensional fluid mechanics mixture model based on the Navier-Stokes' equation. This initial approach was improved by using the NASA-Vof3D model which is a three dimensional model. Their study is based on submarine flow slides generating tsunamis at Nice, France 1979, when part of the building site of a new port slumped into the Mediterranean Sea, and at Skagway Harbour, Alaska 1994, where the waves were estimated by eyewitness as to be 5-6 m in the inlet and 9 - 11 m at the shoreline. Dawson et al. (1993) and Harbitz (1992) discuss a tsunami in the Norwegian Sea and North Sea caused by the Storegga Submarine Landslide that produced waves up to 20 m. This event was caused by continental slope failure.

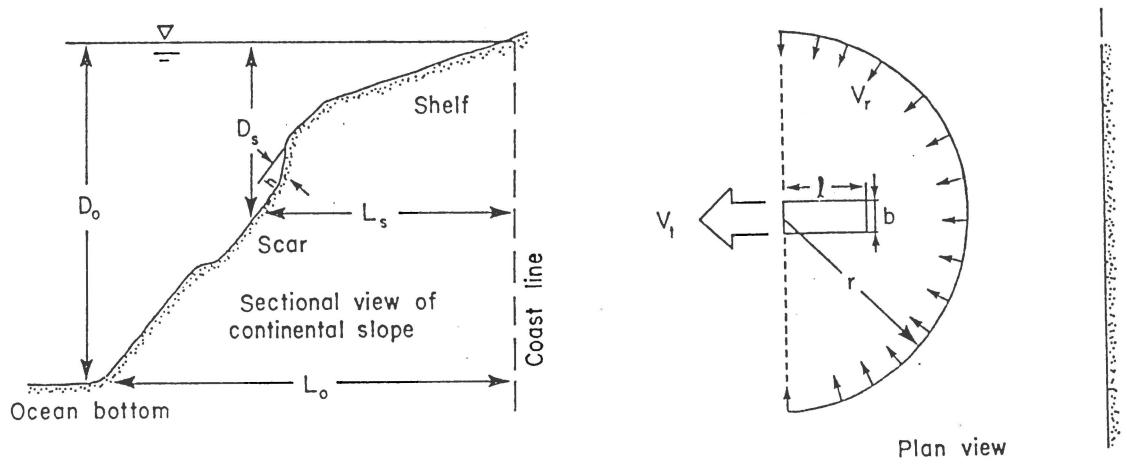

Figure 2.2. Geometry of landslide (source: Murty, 1979).

2.2.3. Volcanic Activity

Tsunamis generated by volcanic eruptions are much less frequent than tsunamis produced by submarine earthquakes. The assessment of tsunami potential must be performed in a substantially different way to that used in analysing earthquakes by taking into account all the known active volcanoes and volcanic areas individually. For each volcano we could inquire for example whether geographical position and eruption mechanism are compatible with tsunami generation (Tinti and Saraceno, 1991). Recently, some studies have been done in this field by de Lange et al. (in press) and Monaghan et al. (1997) by using physical and numerical modelling approaches focused on pyroclastic flow generated tsunamis, submarine (underwater) explosion and caldera formation.

Latter (1981), with particular reference to Krakatau event in 1883 recognised 10 distinct processes whereby volcanic activity may generate tsunamis as follows :

- pyroclastic flows or nuees ardantes (impacting on water): 20 %
- earthquake accompanying eruptions: 22%
- landslides and avalanches of cold rock: 7%
- submarine explosions: 19 %
- caldera collapse or subsidence: 9 %
- basal surges and accompanying shock waves: 7%
- avalanches of hot rock: 6%
- lahars: 4.5 %
- air waves associated with large explosion: 4.5%
- lava flows: 1%

It was noted that the efficiency of these processes varies, depending primarily on the amount of seawater displaced, the direction of displacement and the duration of the disturbance (Latter, 1981; Sigurdsson and Carey,1991; de Lange and Hull, 1994; de Lange et al., in press). In the following section I will summarise the generation mechanisms, focusing on atmospheric coupling, pyroclastic flow and underwater explosion involving crater formation.

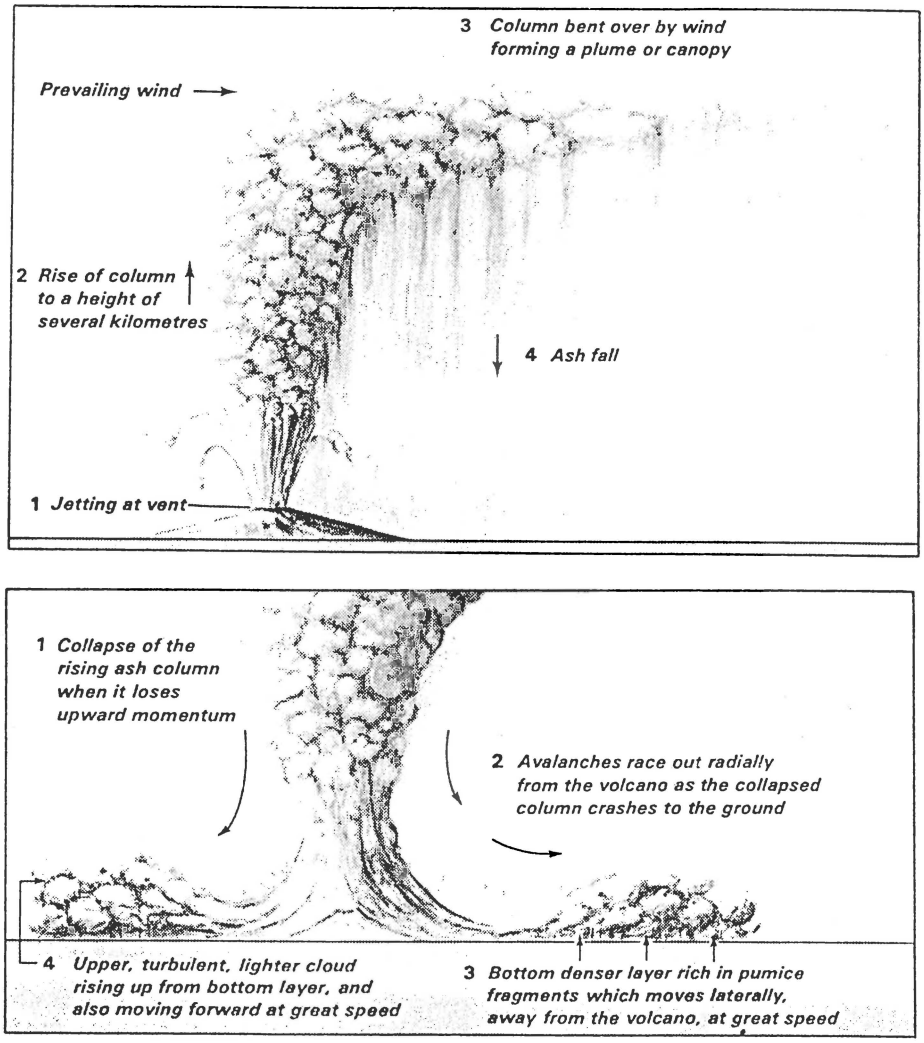

Figure 2.3. Sequence of an ultraplinean volcanic eruption leading to a pyroclastic flow (source: Johnson & Threlfall, 1985)

2.2.3.1. Atmospheric Coupling

The theory of an interaction between the atmosphere and the ocean, namely the coupled system, generating a tsunami was proposed by Press and Harkrider (1966) based on the 1883 Krakatau event. Coupling occurs at the atmosphere-ocean interface when gravity waves with velocities of about 220 ms^{-1} are generated in the atmosphere. Such waves were detected at the time of the Krakatau eruption at a number of location and this mechanism has been accepted as the probable cause of the distantly detected tsunamis. The tsunami observed at Auckland, where 2 m wave height was recorded, was probably produced in this way (de Lange, 1983).

2.2.3.2. Pyroclastic Flow

Pyroclastic flows have important features that derive from their high temperature and the turbulent mixing of volcanic gases, air, pumice, lithic fragments, ash and dust. The basic flow involved is a gravity current driven by density differences between the pyroclastic flow, the atmosphere and the sea (Battaglia, 1993; Monaghan et al., 1997). Eventhough the exact nature of the interaction between a hot pyroclastic flow and seawater is poorly understood (Figure 2.4), factors that would favour the smooth transition of pyroclastic flow are known to be a steep slope, large flow rates and great thickness (de Lange, 1983; Sigurdsson et al., 1991; de Lange et al., in press). Sigurdsson et al. (1997) stated that tsunamis were generated by pyroclastic flows during the Krakatau event 1883 that had flow velocities excess of 100 miles per hour and involved an enormous volume of debris ~10 - 11 km^3.

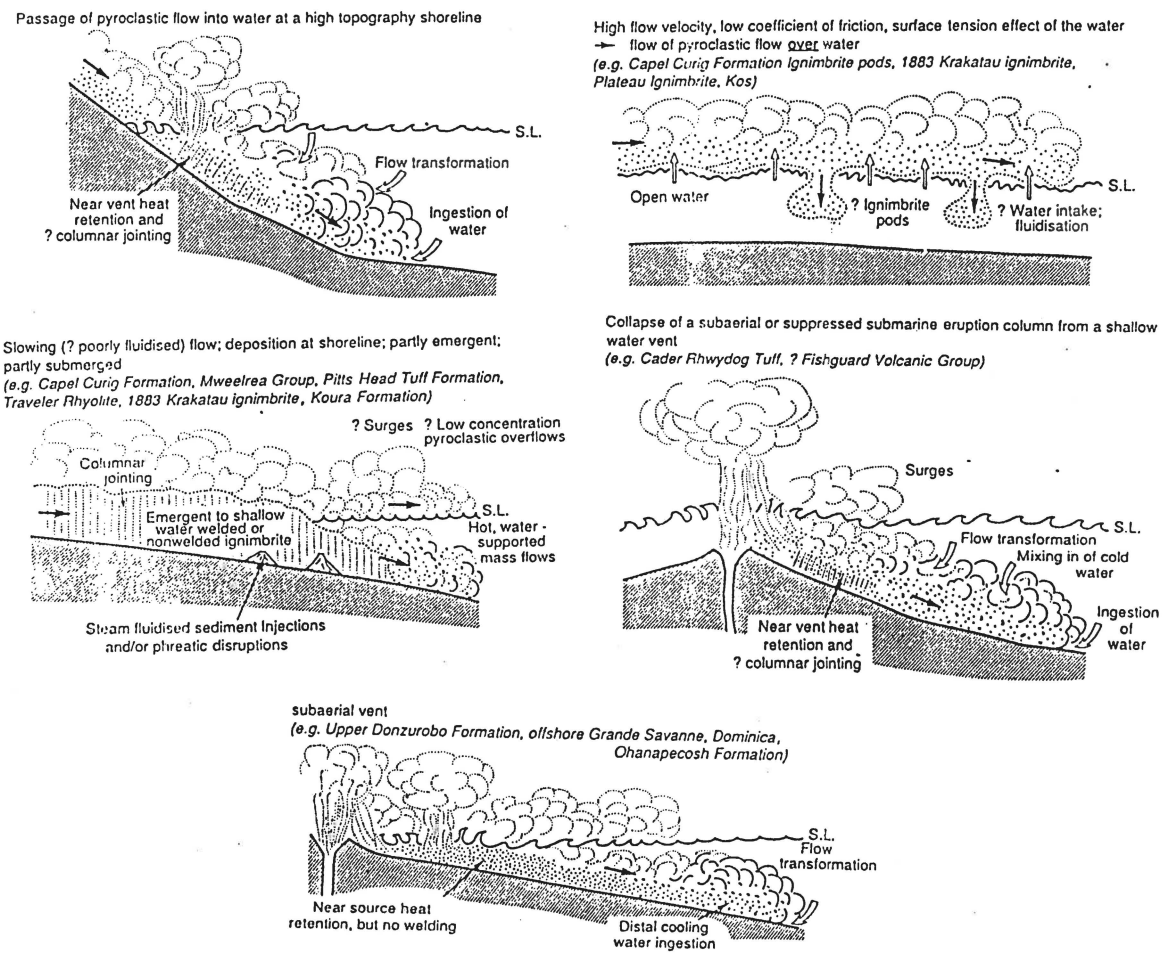

Figure 2.4. Schematic of pyroclastic flow mechanism (modified from Cas and Wright, 1991).

2.2.3.3. Underwater Explosion

For tsunami generation submarine volcanism is assumed to behave like a large scale underwater explosion. Like any other physical event, this explosion produces a localised disturbance of the water surface, that generates a group of surface gravity waves that expand radially and disperse. Based on underwater explosion research (Le Mehaute and Wang, 1996), the wave characteristics are determined by a number of parameters characterising the explosion and the medium. Three main parameters are recognised : the yield W the weight coefficient of high explosive; the depth of burst, z, defined by the distance from the center of mass of the explosive to the free surface; and the water depth (d). If the water depth is sufficiently shallow that the expanding gas bubble generated by the explosion interacts with the bottom , the wave field generation will be affected.

Underwater explosions may be categorised into three types (Le Mehaute and Wang, 1996). Deepwater explosions are those where the explosion crater on the water surface is small compared to the water depth. The waves created are analogous to those created by throwing a pebble in a pond, and linear theory can be applied for this phenomena. Shallow water explosions are those where the water depth is small compared to the explosion crater size. The ground is exposed and the wave generation mechanism is nonlinear, highly dissipative, and significantly different from deep water explosions. In very shallow water explosions, the wave generation process is affected by ground cratering. The soil is left with a significant crater surrounded by a lip. The debris from the water is projected into the atmosphere and falls randomly adding considerable noise to the main wave field. On this case, the wave generation process is also a function of the soil characteristics.

The explosion from a submarine volcano can be treated as a shallow water explosion phenomena. Le Mehaute and Wang (1996) described the complex free surface disturbance for the wave generation processes in shallow water as follows:

"Initially, the water is expelled upwards and radially, forming a plume and a water crater with a watery rim or lip. The lip evolves into small cylindrical bore which expands radially and decays rapidly to form a leading wave. The water crater exposes the soil to the atmosphere. After reaching its maximum size, the water crater collapses and the water rushes inwardly under the influence of gravity onto soil crater,

analogous to the dam break problem. The local reduction in sea level following the first wave crest caused by the inrush of water is transmitted outwards as a long shallow wave trough. When the water edge of the inward motion reaches the center, a very high peak of water is thrown up in the center and a surge is formed which also expands radially on the top of the inward flow. This surge is analogous to a cylindrical bore, and dissipates a large amount (near 40%) of the potential and kinetic energy initially imparted by the explosion to the water. As the bore expands radially and decays, it is transformed into a nonbreaking (nondissipative) undulated cylindrical bore, with a number of smaller undulations. The number of undulations increases with time and distance. The time interval between the leading wave generated by the initial lip and the following wave is directly related to the size of the limited crater and the initial water depth ".

The sequences of wave generation process can be seen in Figure 2.5. below :

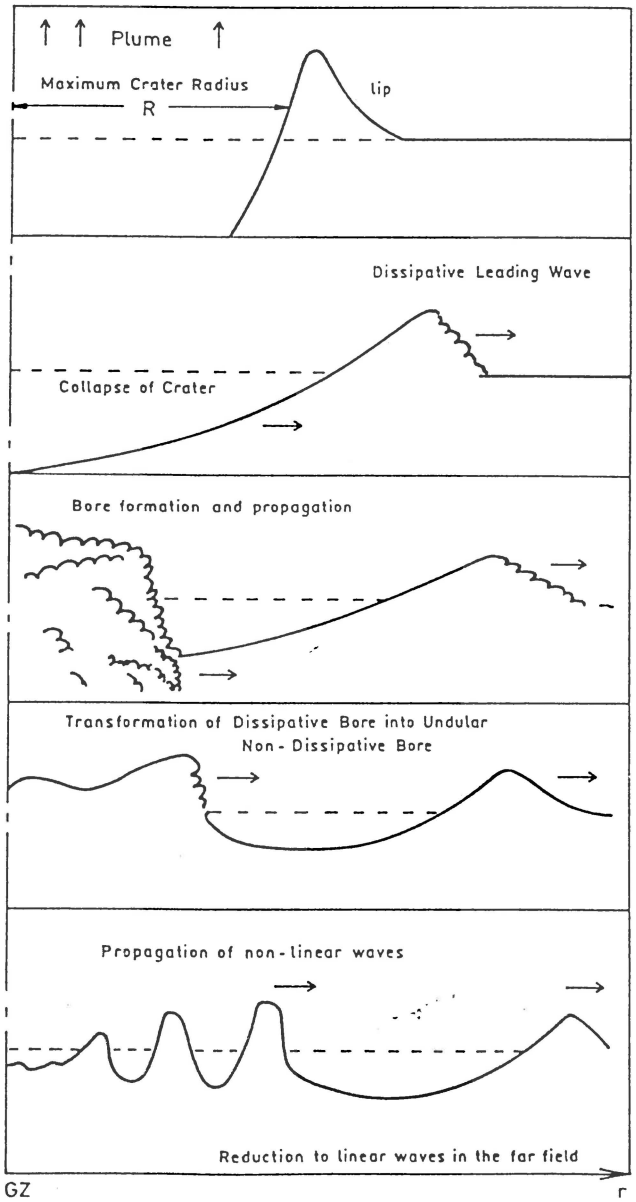

Figure 2.5. Sequence of shallow water explosion generated wave (source: Le Mehaute and Wang 1996)

2.3. Tsunami Propagation

Once tsunami waves have been generated, regardless of their generating mechanism, they begin to propagate away from their source region in all directions. Tsunami travels as a shallow long wave, and can travel for longer distances without loosing their energy. They consist of 5 or more main waves, forming a tsunami wave train. The individual waves follow one behind the other, between 5 and 60 minutes apart. Because tsunamis are long-period waves with a long wavelength in relation to both the water depth and the wave height, shallow water theory can be used to examine the behaviour of tsunamis during propagation. The velocity of the tsunami waveform and the associated energy is given by :

$$C = \sqrt{g.h} \tag{2.2}$$

The travel time T of a tsunami wave from its source point to a point of interest can be predicted by summing the travel times along successive increments of the wave orthogonal connecting the two points by the equation (Sorensen, 1978) :

$$T = \sum \frac{\Delta S}{\sqrt{g.ds}} \tag{2.3}$$

where ds is the average water depth over the increment of length Δ S.

The main processes affecting tsunami propagation are shoaling, refraction, diffraction and reflection, both for far-field tsunamis - generated beyond the continental margins and cross the continental margin before reaching the coast and near-field tsunamis- generated within the continental margins (de Lange and Hull, 1994; Carrier, 1995; Liu et al., 1995). In reality, all these processes frequently occur simultaneously and are interdependent because of the complex bathymetry of the continental margins.

Tsunami may interact with a shoreline in number of different ways, including: standing wave resonance at the shoreline; generation of edge waves by the impulse of the incident waves; trapping of reflected incident waves by refraction and reflection of wave energy from an abrupt change in water depth at the seaward edge of a shelf. Also a Macht-stem phenomena may occur along the shoreline when the wave arrives at an oblique angle to the shoreline (Camfield, 1980).

For long distance propagation, the Coriolis Effect has a great influence on tsunami propagation. The Coriolis Effect leads to a concentration of the tsunami

2.3.1. Refraction

The refraction process for tsunami waves is the same as other water waves in the ocean (i.e. wind waves) where the direction of wave propagation is influenced by changes in water depth. Therefore, a simple evaluation of refraction can be done by using Snells Law. Clearly wave refraction involves the bending waves towards regions of lower wave phase velocity and Equation 2.2 indicates that tsunami waves will bend towards shallow water (Figure 2.6). As a result, the wave crest approaches the orientation of the bottom contours (Sorensen, 1972; de Lange and Hull, 1994). The refraction process indirectly affects the wave energy concentration. In deep water propagation, shallow water areas act as a lens to concentrate tsunami energy (such as sea mounts and guyots). Trenches and ocean deeps will disperse tsunami energy along a coast. Ridges may steer the tsunami wave energy along their crest.

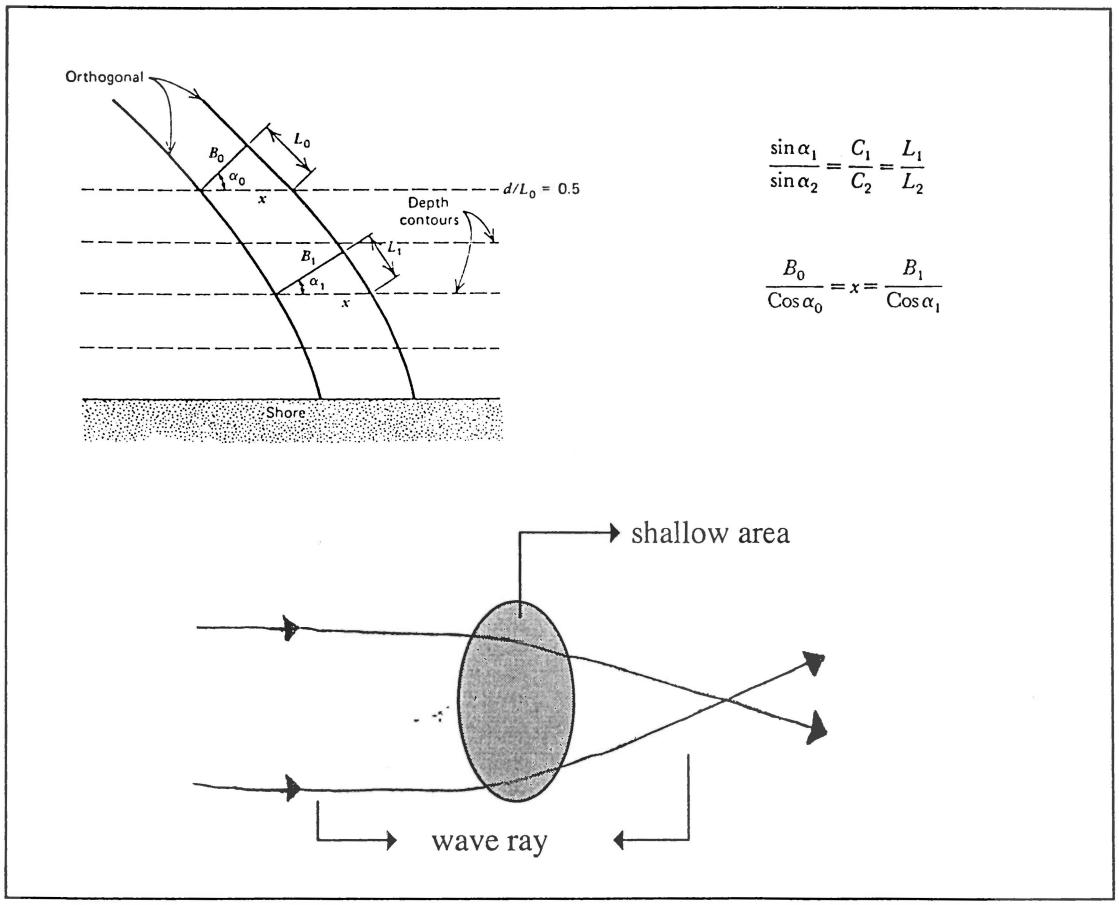

Figure 2.6. Schematic diagram of refraction process

2.3.2. Diffraction

Wave diffraction occurs when a train of waves passes an obstruction during their propagation and the wave energy is transferred laterally along a wave crest behind the obstruction (Sorensen, 1972; Mei, 1989). The presence of an obstruction sets up radiating disturbances and these combine to give rise to wave trains in the lee or shadow of the obstruction (Figure 2.7). Simple analysis of diffraction of water waves can be done by using the mathematical solution for the diffraction of light to predict the wave crest pattern and height variation of water wave. Following Huygens' principles, each point along a wave crest becomes a point source for the propagation of further wave forms. These waves propagate in all directions and their interaction causes the reduction or amplification of wave energy in the direction of wave energy propagation.

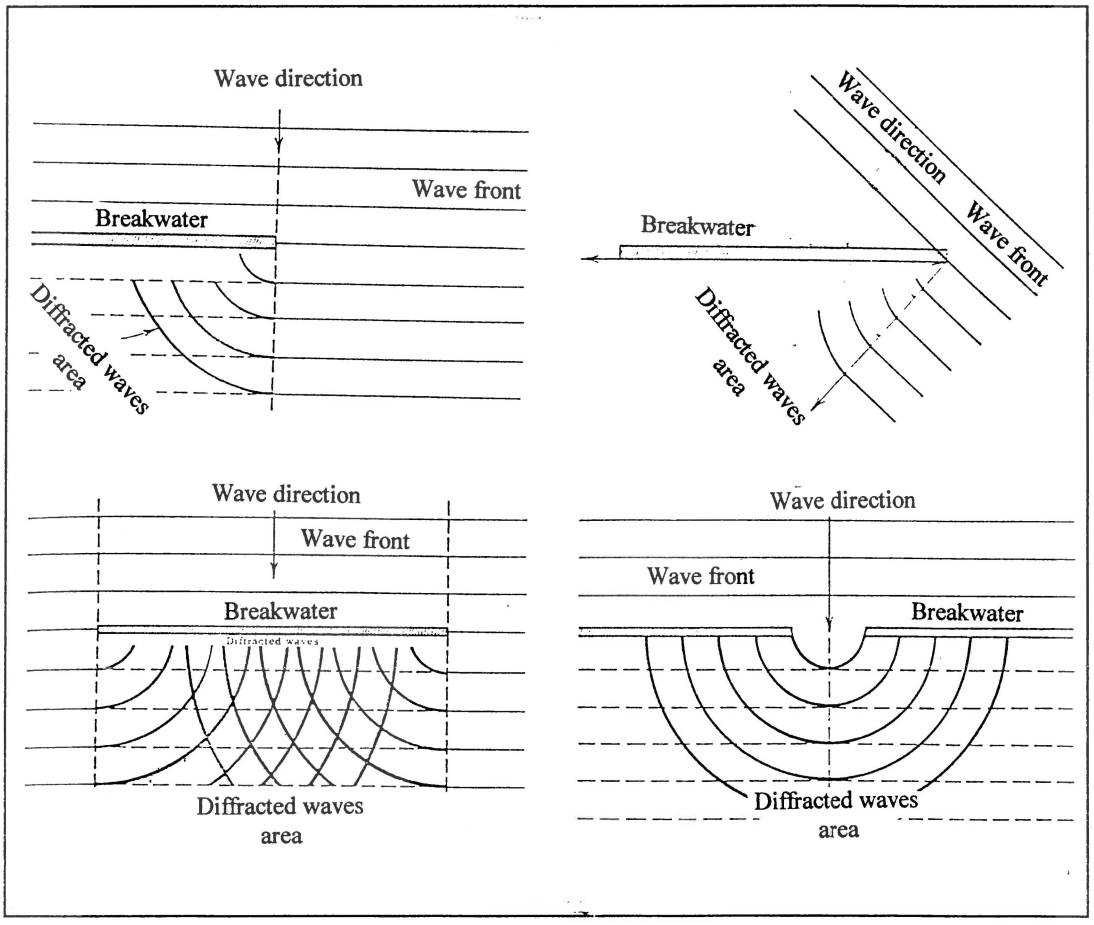

Figure 2.7. Schematic diagram of diffraction process

2.3.3. Reflection

The process of water wave reflection is analogous to the reflection of light and acoustic waves. There are two main types of reflection for water waves (Figure 2.8): full reflection where the energy of the wave is fully reflected back; and partial reflection, which allows the wave energy to be transmitted or absorbed by the reflecting boundary. A reflecting boundary can be considered as the source of a secondary wave train, by assuming an appropriate phase relation between the incident and reflected wave trains and by imposing the boundary condition of no flow through the boundaries (Bretschneider, 1966; Mei, 1989). The superposition of two such wave trains traveling in opposite directions leads to the formation of standing wave, where there is no progressive horizontal motion, but the water surface oscillates vertically with well developed of nodes and antinodes. Partial reflection is caused by a sudden change of water depth met by wave trains, some of the wave energy is absorbed (i.e. by continental slopes, offshore bars and beach) or transmitted through the reflecting boundaries (such as reefs and submerged or permeable coastal structures).

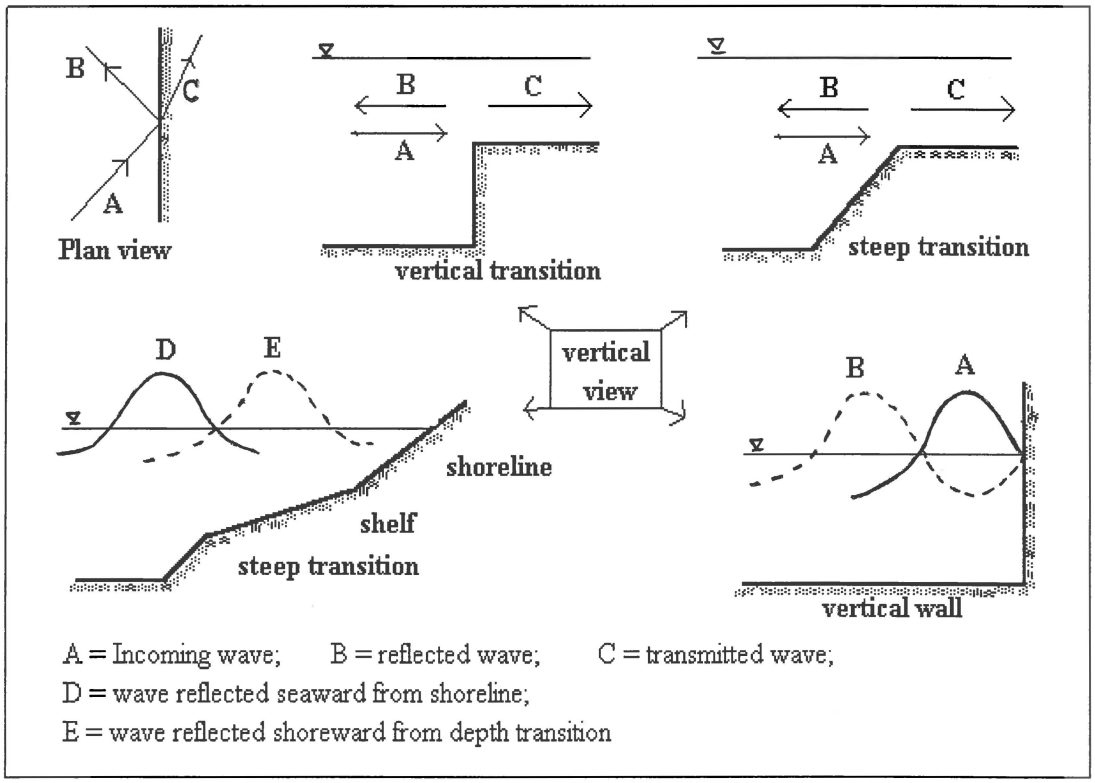

Figure 2.8. Schematic diagram of reflection process

As the leading wave of a tsunami propagates into shallower water in the coastal zone, the wavelength of the incident tsunami becomes shorter and the amplitude becomes larger. The shape of harbour, bay and local nearshore bathymetry has an important influence on how the tsunami wave behaves. Water level records for different tsunamis at the same coastal location show greater similarity than records for the same tsunami at different locations. This indicates the importance of local effects on tsunami characteristics (Sorensen, 1978; Dudley & Lee, 1988; Liu et al., 1995; Henry and Murty, 1995).

2.4. Tsunami Runup and Inundation

When the tsunami wave reaches the shoreline, it may climb up and flood the coastal land areas. The tsunami runup level depends on the nature of the tsunami wave form when it reaches the shore. The wave runup can reach 30 m in height or greater, and inundate the low lying area up to 650 m inland (depending on the topography of the coastal area). Even though the process is poorly understood, a manifestation of the difficulty of the underlying basic hydrodynamic problem, two main types of wave form are recognised before they reach the shoreline (Synolakis, 1991; Yeh, 1991; Pelinovsky and Mazova, 1992; Titov and Synolakis, 1995):

1. Non-breaking waves , where theory can predict, not only the maximum runup height, but also the runup process itself on plane beach. In this case the tsunami wave is considered as either a Solitary or a Cnoidal waves.
2. Breaking waves, where the incoming tsunami breaks offshore and creates a tsunami bore runup. In this case, some of the wave energy must be dissipated offshore via turbulence during the propagation. The maximum runup height of the tsunami bore is lower than the equivalent non-breaking tsunami runup.

There is much evidence that the tsunami bore can cause significant structural damage and casualties. This is because of violent flow actions (viz., strong turbulence) as a result of momentum exchange at the transition of tsunami bore to the runup, together with the rapidly-accelerated mean flow motion which is released onto dry bed (Yeh, 1991). Tsunami runup is the most devastating hazard associated with tsunami waves.

2.5. References

Battaglia, M. (1993), On pyroclastic flow emplacement, Journal of Geophysical Research, 98(B12): p.22.269-22.272

Bretschneider, C.L. (1966), Wave Refraction, Diffraction and Reflection, in Ippen, A.T (eds) : Estuarine and Coastline Hydrodynamic, p.257-280, McGraw-Hill Book Comp.

Camfield, F.E.(1980), Tsunami Engineering. US Army Coastal Engineering Research Center, Special Report 6, 222 p.

Carrier, G.F.(1995), On-shelf Tsunami Generation and Coastal Propagation, in : Tsuchiya.Y and Shuto.N, (eds), Tsunami: Progress in Prediction, Disaster Prevention and Warning, p. 1-20, Kluwer Academic Publ. Netherland.

Dawson, A.G., Long, D., Smith, D.E., Shi, S., and Foster, I.D.L.(1993), Tsunamis in the Norwegian Sea and North Sea caused by The Storegga submarine landslides., in Tinti.S, (eds) : Tsunamis in the world, Kluwer Academic Publ. p.31-42.

de Lange, W.P.(1983), Tsunami Hazard: an investigation into the potential tsunami hazards of the Bay of Plenty Region using numerical models. M.Sc.Thesis, University of Waikato, Hamilton., New Zealand. 275 p.

de Lange, W.P., and Hull, A.G.(1994), Tsunami Hazard for the Auckland region, Institute of Geologicaland Nuclear Sciences. 37 p.

de Lange, W.P., Prasetya, G.S. and Healy, T.R.(in press), Modelling of Tsunamis generated by pyroclastic flows (Ignimbrites).

Dudley, W.C. and Lee, M.(1988), Tsunami , University of Hawaii Press, 132 p.

Gonzalez, F.I., Satake, K., Boss, E.F., and Mofjeld, H.O.(1995), Edge wave and non-trapped modes of the 25 April 1992 Cape Mendocino Tsunami., Tsunami Project - Cape Mendocino, 19 p.

Hammack, J.L. and Segur, H.(1978), Modelling Criteria for Long Water Waves, Journal of Fluid Mechanics.Vol.84.part2.p.359-373., Cambridge University Press, England.

Harbitz, C.B. (1992), Model Simulation of Tsunamis Generated By The Storegga Slides, Marine Geology, 105, p.1-21.

Henry, R.F and Murty, T.S. (1995), Tsunami Amplification Due to Resonance in Alberni Inlet: Normal Modes, in : Tsuchiya.Y and Shuto.N, (eds), Tsunami: Progress in Prediction, Disaster Prevention and Warning, p.117 - 128, Kluwer Academic Publ. Netherland.

Jiang , L and LeBlond P.L. (1994), Three-Dimensional Modeling of Tsunami Generation Due to a Submarine Mudslide, Journal of Physical Oceanography, Vol.24., p.559-572.

Johnson, R.W., and Threlfall, N.A. (1985), Volcano Town : The 1937-43 Rabaul Eruptions., Robert Brown & Asc. Australia, 151 p.

Kulikov, E.A, Rabinovich, A.B, Thomson, R.E, Bornhold, B.D. (1996), The Landslide Tsunami of November 3, 1994, Skagway Harbor, Alaska, Journal of Geophysical Research, Vol.101.No.C3. p.6609-6615. American Geophysical Union, Washington DC.

Latter, J.H.(1981), Tsunamis of volcanic origin: summary of causes, with particular reference to Krakatoa, 1883.Bulletin Volcanologique.Vol.44. p.467-490.

Le Mehaute, B., and Wang, S.(1996), Water waves generated by underwater explosion. Advanced series in Ocean Engineering. Vol. 10. 367 p.

Liu, P.L.F, Synolakis, C.E. and Yeh, H.H (1991), Report on The International Workshop on Long-Wave Runup, Journal Fluid Mechanics, Vol.229. p.675-688, Cambridge University Press, England.

Liu, P.L.F , Cho, Y.S, Yoon.S.B and Seo, S.N. (1995), Numerical Simulations of the 1960 Chilean Tsunami Propagation and Inundation at Hilo, Hawaii, in : Tsuchiya.Y and Shuto.N, (eds), Tsunami: Progress in Prediction, Disaster Prevention and Warning, p.99 - 116, Kluwer Academic Publ. Netherland.

Manshina, L., and Smylie, D.E.(1971), The displacement fields of inclined faults, Bulletin of the Seismological Society of America. Vol.61.No.5.p. 1433-1440.

Mei, C.C.(1989), The Applied Dynamics of Ocean Surface Waves, World Scientific, 740 p. Singapore.

Monaghan, J.D., Cas, R.A.F., Kos, A.M., and Hallworth, M.,(1997), Tsunami generation by pyroclastic flows, Applied Mathematics Report and Preprints, Department of Mathematics, Monash University, Australia, 47 p.

Murty, T.S.(1979), Submarine Slide-Generated Water Waves in Kitimat Inlet, British Columbia, Journal OF Geophysical Research, 84(C12).p.7777-7779. American Geophysical Union, Washington DC.

Okal, E.A.(1988), Natural Hazards. Vol.1. p.67-96

Okal, E.A. (1994), Tsunami warning: beating the waves to death and destruction., Endeavour, New Series.Vol.18.No.1.p.38-434.

Pelinovsky, E. N., and Mazova, R.K.(1992) , Exact Analytical Solutions of Nonlinear Problems of Tsunami Wave Runup on slopes with different profiles, Journal of Natural Hazards, Vol.6.No.3.p.227-250.,Kluwer Academic Publ., The Netherland.

Press, F., and Harkrider, D.(1966), Air-sea waves from the explosion of Krakatoa. Science.Vol.154. p.1325-1327.

Rzadkiewicz, S.A., Mariotti, C., and Heinrich, P.(1997), Numerical Simulation of submarine landslides and their hydraulic effects, Journal of Waterway, Port, Coastal, and Ocean Engineering. Vol.123.No.4.p. 149-157.

Sigurdsson, H., Carey, S., Mandeville, C., and Bronto, S.,(1991), Pyroclastic flows of the 1883 Krakatau eruption., EOS, Transaction, American Geophysical Union, Vol.72.No.3., p.377-392.

Sigurdsson, H., and Carey, S.,(1997), comments in article : Wave of destruction., Earth Magazine. p.28-29.

Sorensen, R.M.(1978), Basic Coastal Engineering, John Willey & Sons, 227 p. New York.

Striem, H.L., and Miloh, T.(1976), Tsunamis induced by submarine slumping off the coast of Israel. International Hydrographic Review. Vol.53. p.41-55

Synolakis, C.E. (1991), Tsunami Runup on Steep Slopes: How Good Linear Theory Really Is, in : Bernard, E.N.(eds) : Tsunami Hazard, A practical Guide for Tsunami Hazard Reduction, p.221-234, Kluwer Academic Publ., The Netherland.

Tinti, S.(1991), Assessment of Tsunami Hazard in the Italian Seas, in : Bernard, E.N.(eds) : Tsunami Hazard, A practical Guide fro Tsunami Hazard Reduction, p.267-284, Kluwer Academic Publ., The Netherland.

Tinti, S., and Saraceno, A.(1993), Tsunamis related to volcanic activity in Italy, in : Tinti.S, (eds) : Tsunamis in the world, Kluwer Academic Publ.p.43-63.

Titov, V.V. and Synolakis C.E. (1995), Numerical Modeling of 2D and 3D Long Wave Runup using VTCS-2 and VTCS-3, in International Long wave Runup Workshop, Part Discussion, Friday Harbour - Seattle, Washington USA.

Van Dorn, W.G.(1964), Tsunamis, Advances in Hydroscience, Vol.2. New York: Academic Press. p.1-48.

Verriere, M and Lenoir, M. (1992), Computation of Waves Generated By Submarine Landslides, International Journal for Numerical Methods in Fluids, Vol.14.p.403-421. John Willey & Sons.

Ward, S.N.(1980), Journal of Physic of the Earth. Vo.28.p. 441-474.

Yeh, H.H.(1991), Tsunamis Bore Runup, in : Bernard, E.N.(eds) : Tsunami Hazard, A practical Guide fro Tsunami Hazard Reduction, p.209-220, Kluwer Academic Publ., The Netherland.

Chapter Three

MATHEMATICAL MODEL

3.1. Introduction

In order to predict detailed and quantitative information about tsunami behaviour, the modelling is essentially required. The modelling can be done using a physical (scale) model or a mathematical model which solves the complex phenomena of tsunamis; their generating mechanism, propagation and runup on land. Mathematical modelling requires developing, constructing, verifying, and testing a set of mathematical or logical expressions for a solution (usually on a high-speed digital computer) to yield the desired parameters.

This chapter presents the wave theory which can be used to develop a mathematical model of tsunami, which represents the dynamic behaviour of tsunami in deep sea, nearshore dynamics and runup on land.

3.2. Derivation of Governing Equation

Tsunami are categorised as long waves due to the wavelength and the ratio to water depth. Their propagation can be adequately described by a set of shallow water equations. Shallow water wave theory is based on the depth-averaged equations of mass and momentum conservation. General assumptions for the derivations of these equation are that the fluid is incompressible and inviscid with no tension, the water depth is small in comparison with the characteristic horizontal lengthscale of the motion. The consequences of these assumptions are that the pressure field is hydrostatic everywhere, and that the velocity is uniform throughout the depth.

Equation of Motion

An Eularian form of general equation of motion in three-dimensional cartesian coordinate system can be written as follows :

$$\begin{aligned}
&\frac{\partial u}{\partial t}+u\frac{\partial u}{\partial x}+v\frac{\partial u}{\partial y}+w\frac{\partial u}{\partial z}-fv=-\frac{1}{\rho}\frac{\partial p}{\partial x}-\frac{1}{\rho}\left(\frac{\partial \tau_{xx}}{\partial x}+\frac{\partial \tau_{xy}}{\partial y}+\frac{\partial \tau_{xz}}{\partial z}\right)+\mathrm{A}\,\Delta u\\
&\frac{\partial v}{\partial t}+u\frac{\partial v}{\partial x}+v\frac{\partial v}{\partial y}+w\frac{\partial v}{\partial z}-fu=-\frac{1}{\rho}\frac{\partial p}{\partial y}-\frac{1}{\rho}\left(\frac{\partial \tau_{xy}}{\partial x}+\frac{\partial \tau_{yy}}{\partial y}+\frac{\partial \tau_{yz}}{\partial z}\right)+A\,\Delta \mathrm{v}\\
&\frac{\partial w}{\partial t}+u\frac{\partial w}{\partial x}+v\frac{\partial w}{\partial y}+w\frac{\partial w}{\partial z}=-\frac{1}{\rho}\frac{\partial p}{\partial z}-\frac{1}{\rho}\left(\frac{\partial \tau_{xz}}{\partial x}+\frac{\partial \tau_{yz}}{\partial y}+\frac{\partial \tau_{zz}}{\partial z}\right)-g+\mathrm{A}\,\Delta \mathrm{w}
\end{aligned} \tag{3.1}$$

The origin and the (x,y) plane lie on the undisturbed water surface (Figure 3.1). The x and y-axes are directed to east and north respectively (horizontal coordinate) with the z axis directed vertically upwards. The velocity components in the directions of x, y, and z are denoted by u, v and w respectively. The other quantities appearing in the equation of motion are :

p = pressure;

ρ = sea water density;

g = gravitational acceleration;

t = time;

f = Coriolis parameter = 2 ω sin ϕ;

ω = Earth's angular velocity = 7.29 x 10^{-3} rad.s^{-1};

ϕ = latitude;

$\tau_{i,j}$ = normal and tangential shear stress in direction of i on normal plane j;

A = Lateral eddy viscosity coefficient or coefficient of exchange of momentum in horizontal direction; and

$\Delta = \frac{\partial^2}{\partial x^2}+\frac{\partial^2}{\partial y^2}$, two dimensional Laplace operator.

Using the same cartesian coordinates, the equation of continuity, with sea water considered as an incompressible fluid can be written as follows :

$$\frac{\partial u}{\partial x}+\frac{\partial v}{\partial y}+\frac{\partial w}{\partial z}=0 \tag{3.2}$$

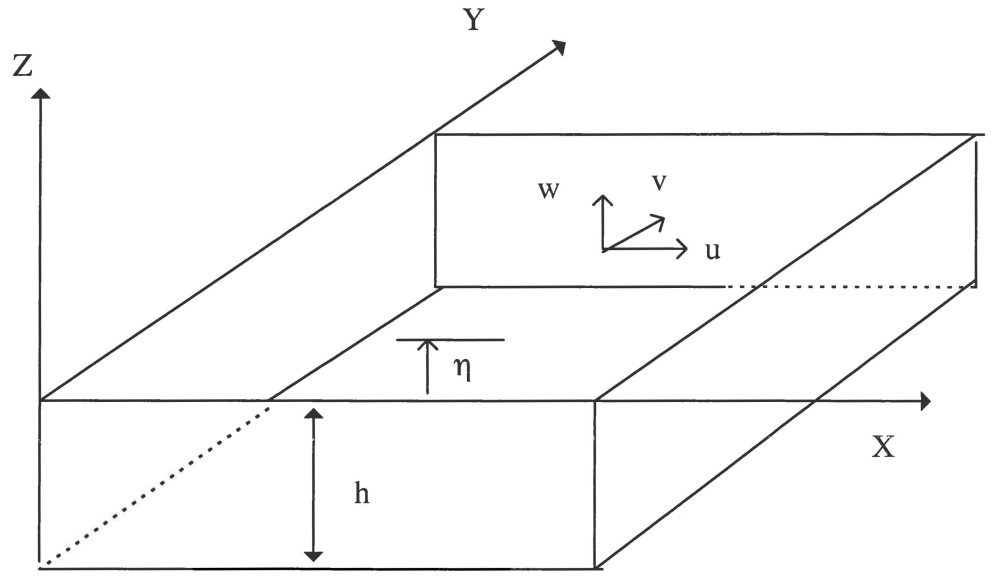

Figure 3.1. Cartesian coordinates system

Assumptions and Simplifications

Considering the long wave condition, the vertical velocity is small compared to the horizontal velocity, therefore the vertical velocity (w) may be ignored. Consequently the vertical movement water particles does not influence the pressure distribution through the water column, meaning the pressure field is hydrostatic everywhere. Also the vertical acceleration term $(\frac{\partial w}{\partial t})$ becomes smaller than gravitational acceleration and may be ignored. This conclusion is wrong when the dimensions of horizontal and vertical motion are the same order (Ramming and Kowalik, 1980). Through these assumptions and simplifications, equation 3.1 becomes :

$$\frac{\partial u}{\partial t}+u\frac{\partial u}{\partial x}+v\frac{\partial u}{\partial y}-fv=-\frac{1}{\rho}\frac{\partial p}{\partial x}-\frac{1}{\rho}\left(\frac{\partial \tau_{xx}}{\partial x}+\frac{\partial \tau_{xy}}{\partial y}\right)+A\Delta u$$

$$\frac{\partial v}{\partial t}+u\frac{\partial v}{\partial x}+v\frac{\partial v}{\partial y}+fu=-\frac{1}{\rho}\frac{\partial p}{\partial y}-\frac{1}{\rho}\left(\frac{\partial \tau_{xy}}{\partial x}+\frac{\partial \tau_{yy}}{\partial y}\right)+A\Delta v \qquad (3.3)$$

$$0=-\frac{1}{\rho}\frac{\partial p}{\partial z}-g$$

The momentum equation in the z direction (equation 3.3) gives a simple hydrostatic balance combined with a dynamic condition at the surface where $p_a = 0$, giving hydrostatic pressure :

$$p = - \rho \, .g \, . \, (z - \eta) \tag{3.4}$$

Taking the spatial derivatives of the hydrostatic balance in equation 3.3 in three dimensions gives :

$$\begin{aligned} \frac{\partial p}{\partial x} &= \rho g \frac{\partial \eta}{\partial x} \\ \frac{\partial p}{\partial y} &= \rho g \frac{\partial \eta}{\partial y} \\ \frac{\partial p}{\partial z} &= \rho g \frac{\partial \eta}{\partial z} \end{aligned} \tag{3.5}$$

and substitution into the equation of motion yields :

$$\begin{aligned} \frac{\partial u}{\partial t} + u\frac{\partial u}{\partial x} + v\frac{\partial u}{\partial y} - fv &= -g\frac{\partial \eta}{\partial x} - \frac{1}{\rho}\left(\frac{\partial \tau_{xx}}{\partial x} + \frac{\partial \tau_{xy}}{\partial y}\right) + A\Delta u \\ \frac{\partial v}{\partial t} + u\frac{\partial v}{\partial x} + v\frac{\partial v}{\partial y} + fu &= -g\frac{\partial \eta}{\partial y} - \frac{1}{\rho}\left(\frac{\partial \tau_{xy}}{\partial x} + \frac{\partial \tau_{yy}}{\partial y}\right) + A\Delta v \end{aligned} \tag{3.6}$$

Integrating equation (3.6) from the bottom z = -h to $z = \eta$ using the Leibtnitz rule, as an example, the first term of momentum equation in x direction can be written as:

$$\int_{-h}^{h} \frac{\partial u}{\partial t} dz = \frac{\partial}{\partial t}\int_{-h}^{h} u dz - u\frac{\partial h}{\partial t}\Big|_{z=h} + u\frac{\partial(-h)}{\partial t}\Big|_{z=-h} \tag{3.7}$$

Using a dynamic and kinematic boundary for shallow water condition and defining the flux discharge as:

$$\begin{aligned} P &= \int_{-h}^{\eta} u dz = \bar{u}(h + \eta) \\ Q &= \int_{-h}^{\eta} v dz = \bar{v}(h + \eta) \end{aligned} \tag{3.8}$$

yields :

$$\frac{\partial P}{\partial t}+\frac{\partial}{\partial x}\left(\frac{P^2}{D}\right)+\frac{\partial}{\partial y}\left(\frac{PQ}{D}\right)+gD\frac{\partial \eta}{\partial x}+\frac{\tau_x}{\rho}D=A\left(\frac{\partial^2 P}{\partial x^2}+\frac{\partial^2 P}{\partial y^2}\right)$$
$$\frac{\partial Q}{\partial t}+\frac{\partial}{\partial x}\left(\frac{PQ}{D}\right)+\frac{\partial}{\partial y}\left(\frac{Q^2}{D}\right)+gD\frac{\partial \eta}{\partial y}+\frac{\tau_y}{\rho}D=A\left(\frac{\partial^2 Q}{\partial x^2}+\frac{\partial^2 Q}{\partial y^2}\right) \quad (3.9)$$

as a shallow water wave equation, in which P and Q are the volume flux components per unit width in the x- and y- direction, respectively, $D = h + \eta$ is the total depth and τ_x and τ_y denote the x and y components of bottom frictional force per unit mass, respectively. The frictional model can be written by using either the Chezy's formula or the Manning's formula.

The bottom friction force for x- and y- direction by using Chezy's formula can be written as:

$$\frac{\tau_x}{\rho}=\frac{g}{C_f^2 D^3}P\sqrt{(P^2+Q^2)}$$
$$\frac{\tau_y}{\rho}=\frac{g}{C_f^2 D^3}Q\sqrt{(P^2+Q^2)} \quad (3.10)$$

where C_f is the Chezy's frictional coefficient. This coefficient is dependent on the flow condition ,i.e. the Reynolds number, and the surface roughness of the beach. Similarly the equation of continuity becomes:

$$\frac{\partial \eta}{\partial t}+\frac{\partial M}{\partial x}+\frac{\partial N}{\partial y}=0 \quad (3.11)$$

The equation of motion (3.9) or conservation of momentum equation and equation of continuity (3.11) or conservation of mass provides a set of shallow water equations which can be used to model a tsunami.

When modelling tsunami, some terms have to be reevaluated according to the boundary and initial conditions. Further simplification of equations may be possible to allow numerical solution to simulate the ' real ' condition of tsunami behaviour in deep sea, nearshore and runup on land.

3.3. Model for deep sea propagation

To simulate deep sea tsunami including tsunami generation, there are two initial conditions. First condition involves the dynamic movement of fault (ground velocity and increasing time), and second condition is without dynamic fault movement. If the dynamic condition can be neglected for the initial propagation of tsunami, the final sea bottom deformation caused by the fault is given as the initial condition of sea surface. The modified cartesian coordinate system to permit the inclusion of the initial tsunami wave and a generating sea floor displacement using the Manshina and Smylie Method (1971) can be seen in Figure 3.2

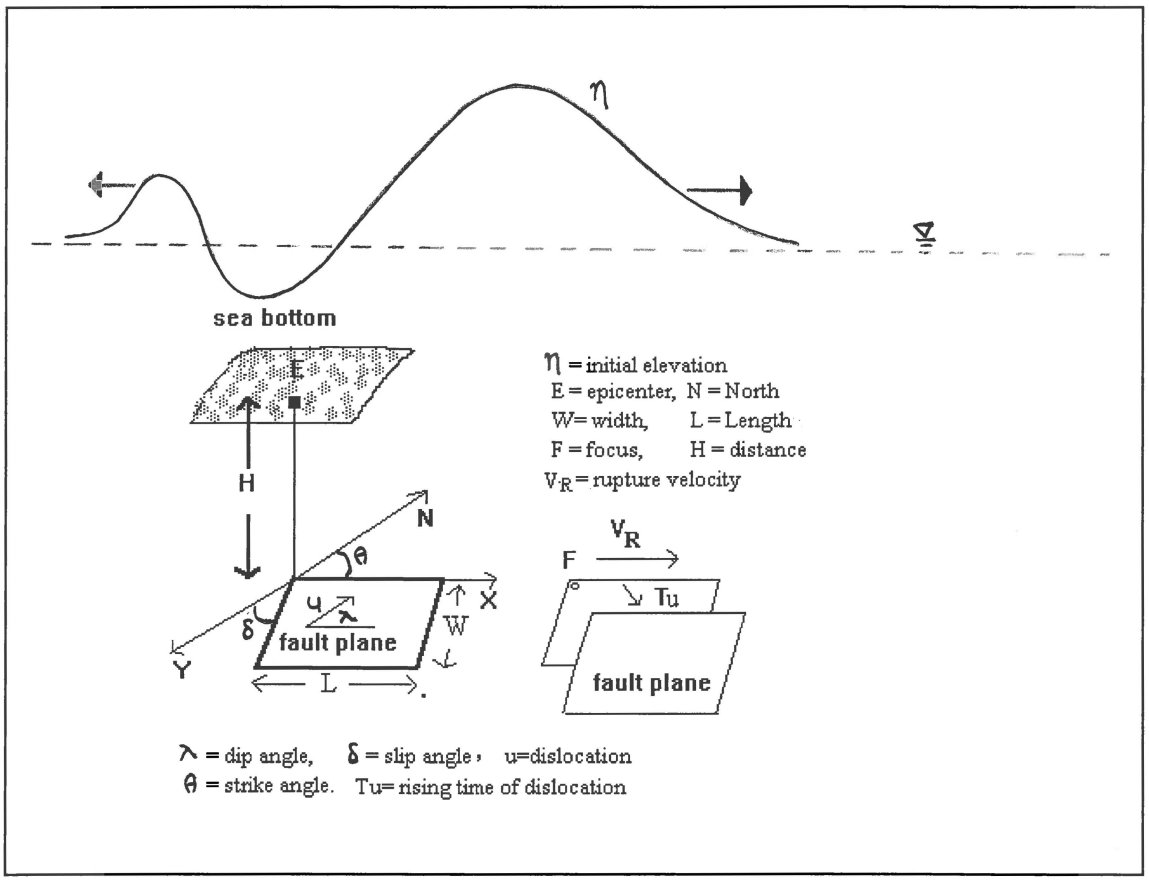

Figure 3.2. Cartesian coordinate of sea floor displacement and initial wave, following the method of Manshina and Smylie (1971)

If the dynamic condition is considered, the equation of continuity or conservation of mass (equation 3.11) becomes:

$$\frac{\partial \eta}{\partial t} + \frac{\partial M}{\partial x} + \frac{\partial N}{\partial y} = \frac{\partial \zeta}{\partial t} \tag{3.12}$$

where ζ is the deformation of the sea bottom. This deformation is based on the shear stress theory of an elastic body (Manshina and Smylie, 1971) and can be estimated through fault parameter as mentioned in chapter 2.

For the equation of motion, during propagation of tsunami in deep sea, Liu et al., (1995) estimated the relative importance of nonlinear inertia force, pressure force, Coriolis force, bottom friction and frequency dispersion with respect to the local inertia force, and concluded that nonlinear inertia force and bottom friction are relatively insignificant and may be neglected. The horizontal friction forces are important in the narrow nearshore zone. The Coriolis force becomes important if tsunami travel over a long distance from the source region. The frequency dispersion effects are dependent on the wavelength of the tsunami generated. Taking these factors into consideration, the equation of motion can be expressed as :

$$\frac{\partial P}{\partial t} + \frac{\partial}{\partial x}\left(\frac{P^2}{D}\right) + \frac{\partial}{\partial y}\left(\frac{PQ}{D}\right) + gD\frac{\partial \eta}{\partial x} = 0 \tag{3.13}$$

$$\frac{\partial Q}{\partial t} + \frac{\partial}{\partial x}\left(\frac{PQ}{D}\right) + \frac{\partial}{\partial y}\left(\frac{Q^2}{D}\right) + gD\frac{\partial \eta}{\partial y} = 0$$

This provides a mathematical model for tsunami propagation in deep sea with initial generation by using the equation 3.12

3.4. Model for propagation in shallow water

When a tsunami propagate into shallower water (i.e., in the coastal zone), the wavelength of the incident tsunami become shorter, increase their amplitude, steepness and curvature of water level. All of forces acting on a water column must be considered to represent this phenomena. Convective inertia force and bottom friction become increasingly important. The Coriolis force and the inertia force caused by the vertical acceleration (i.e., frequency dispersion) diminishes. Therefore, a set equation

of shallow water wave theory for tsunami propagation as governing equations for mathematical model in shallower region (i.e., coastal zone) can be written as :

$$\frac{\partial \eta}{\partial t} + \frac{\partial M}{\partial x} + \frac{\partial N}{\partial y} = 0 \tag{3.14}$$

The equation of continuity and equation of motion as :

$$\begin{aligned} &\frac{\partial P}{\partial t} + \frac{\partial}{\partial x}\left(\frac{P^2}{D}\right) + \frac{\partial}{\partial y}\left(\frac{PQ}{D}\right) + gD\frac{\partial \eta}{\partial x} + \frac{\tau_x}{\rho}D = 0 \\ &\frac{\partial Q}{\partial t} + \frac{\partial}{\partial x}\left(\frac{PQ}{D}\right) + \frac{\partial}{\partial y}\left(\frac{Q^2}{D}\right) + gD\frac{\partial \eta}{\partial y} + \frac{\tau_y}{\rho}D = 0 \end{aligned} \tag{3.15}$$

with bed or bottom friction as :

$$\begin{aligned} \frac{\tau_x}{\rho} &= \frac{g}{C_f^2 D^3} P\sqrt{(P^2 + Q^2)} \\ \frac{\tau_y}{\rho} &= \frac{g}{C_f^2 D^3} Q\sqrt{(P^2 + Q^2)} \end{aligned} \tag{3.16}$$

The bed friction for tsunami propagation in very shallow water area and runup on dry land can also use the Manning roughness coefficient.

A different approach of derivation of tsunami model is given following McKenzie (1993) and de Lange (1997). Using the modified coordinate system, the total water depth is defined by :

$$d = \eta + h - b \tag{3.17}$$

and equation of motion for deep sea propagation (equation 3.13) using standard matrix notation can be written as :

$$\frac{\partial M_i}{\partial t} + g(\eta + h - b)\eta_{,i} = 0 \tag{3.18}$$

The equation of continuity with inclusion of the generating zone becomes :

$$\frac{\partial(\eta - b)}{\partial t} + M_{i,i} = 0 \tag{3.19}$$

where $M_i = dU_i$, with i indicates cartesian coordinate for velocity in x, y, z as u, v, w respectively and $_{,i}$ is conventional notation for partial derivative in x, y and z direction as : $\frac{\partial}{\partial x}, \frac{\partial}{\partial y}, \frac{\partial}{\partial z}$. The coordinate system is illustrated on Figure 3.3.

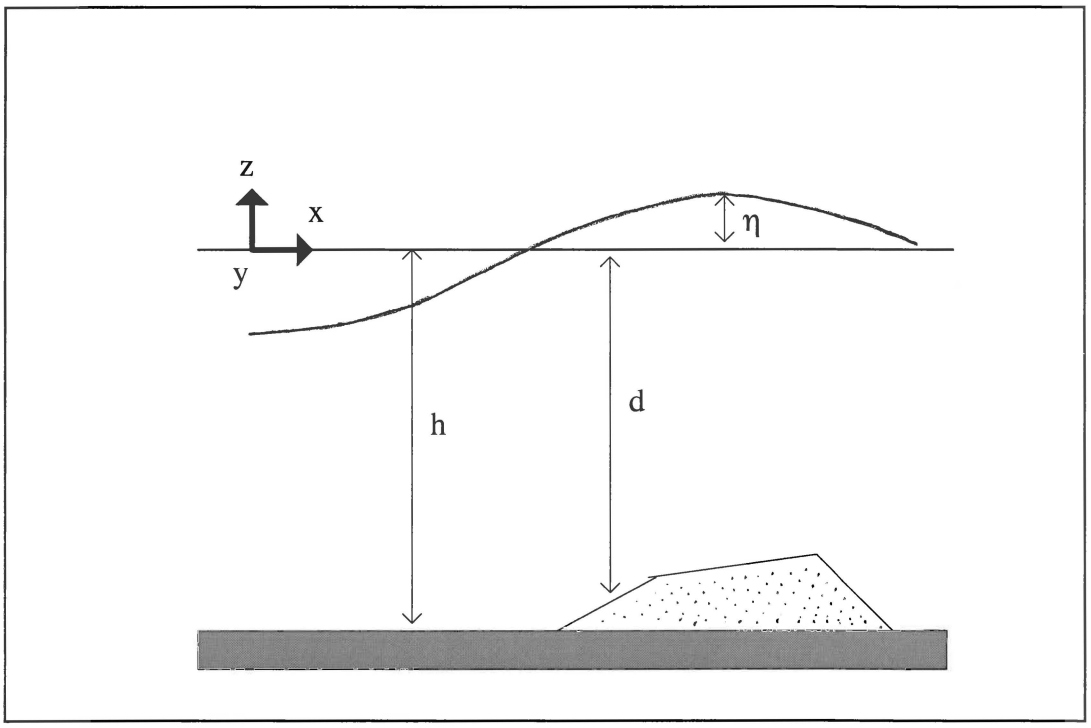

Figure.3.3. Modified coordinate system (de Lange, 1997)

For shallow water propagation close to the coastal land, the convection term cannot be neglected and the displacement of sea bottom become zero, hence, the equations of continuity and motion become :

$$\frac{\partial \eta}{\partial t} + M_{i,i} = 0 \tag{3.20}$$

$$\frac{\partial U_i}{\partial t} + U_j U_{i,j} + g(\eta + h - b)\eta_{,i} = 0 \qquad (3.21)$$

These equations can be solved numerically either by using Finite Difference or Finite Element methods.

3.5. Runup Model

When tsunami reach the shoreline, they start to propagate onto dry land, as they flood the area. Incorporating of this phenomena into a mathematical model is really difficult due to the basic hydrodynamic problem of high turbulence flow on a dry bed. Dam- break flow is one solution used to represent tsunami runup onto a dry bed. Several models have been developed for the one dimensional (1D) problem (Synolakis, 1991; Pelinovsky and Mazova, 1992; Carrier, 1995). In a two dimensional (2D) model, the runup computation depend on the numerical solution and grid arrangement of flooding and drying areas of the equation of continuity and motion above. The numerical solution and grid arrangement will be discussed in Chapter 4.

3.6. References

Carrier, G.F.(1995), On-shelf Tsunami Generation and Coastal Propagation, in : Tsuchiya.Y and Shuto.N, (eds), Tsunami: Progress in Prediction, Disaster Prevention and Warning, p. 1-20, Kluwer Academic Publ. Netherland.

de Lange, W.P.(1997), Tsunami Manual., Dept.of Earth Sciences., University of Waikato. New Zealand.

de Lange, W.P., Prasetya, G.S. and Healy, T.R.(in press), Modelling of Tsunamis generated by pyroclastic flows (Ignimbrites).

Hammack, J.L. and Segur, H.(1978), Modelling Criteria for Long Water Waves, Journal of Fluid Mechanics.Vol.84.part2.p.359-373.,Cambridge University Press, England.

Liu, P.L.F , Cho, Y.S, Yoon.S.B and Seo, S.N. (1995), Numerical Simulations of the 1960 Chilean Tsunami Propagation and Inundation at Hilo, Hawaii, in : Tsuchiya.Y and Shuto.N, (eds), Tsunami: Progress in Prediction, Disaster Prevention and Warning, p.99 - 116, Kluwer Academic Publ. Netherland.

Manshina, L., and Smylie, D.E.(1971), The displacement fields of inclined faults, Bulletin of the Seismological Society of America. Vol.61.No.5.p. 1433-1440.

McKenzie, D.D.J.,(1993), Numerical modelling of Tsunamis in the Bay of Plenty. M.Sc. Theses. Department of Earth Science. University of Waikato., New Zealand.

Pelinovsky, E. N., and Mazova, R.K.(1992) , Exact Analytical Solutions of Nonlinear Problems of Tsunami Wave Runup on slopes with different profiles, Journal of Natural Hazards, Vol.6.No.3.p.227-250.,Kluwer Academic Publ., The Netherland.

Ramming, R.H., and Kowalik, Z.(1980), Numerical modelling of marine hydrodynamics, Elsevier, New York. 368 p.

Synolakis, C.E. (1991), Tsunami Runup on Steep Slopes: How Good Linear Theory Really Is, in : Bernard, E.N.(eds) : Tsunami Hazard, A practical Guide for Tsunami Hazard Reduction, p.221-234, Kluwer Academic Publ., The Netherland.

Weir, G.J., and White, S.P.,(1982), Mathematical modelling of volcanic tsunamis. New Zealand Journal of Marine and Freshwater. Vol.16. p. 373-382.

Chapter Four

THE FINITE ELEMENT METHOD

4.1. Introduction

The finite element method is a useful numerical analysis technique. Its ability to incorporate boundaries with complicated features and without requiring a uniform spatial grid has made this method popular in the field of environmental computational fluid dynamics. The method uses a model domain that is subdivided into a number of smaller regions or elements. The elements can be any regular polygon of variable, provided that the whole domain is covered by elements with no gaps or overlaps (McKenzie, 1993; Tinti and Gavagni, 1995; de Lange, 1997).

This chapter introduces the finite element's method and its application for tsunami modelling. It will also investigate its ability to reproduce the tsunami generation, propagation and run up on land.

4.2. The Method

A cursory analysis of finite element method reveals that there are two principles that appear to be essential from a mathematical point of view. The choice of local parameters of the solution and the use of various types of variational principles for transforming the given equations to relations among the parameters of the solution (Babuska and Aziz, 1972). To simulate the real world systems, a series of approximating functions is used.

The first step of the method is discretization of the problem by the selection of elements interconnected at the nodal points. The real world system that is simplified and represented by model domain is divided into a number of smaller regions or elements. The unknowns are given at certain points of these elements, called nodal

points or nodes. Each element is analyzed separately and its properties are generally derived from the minimization of a functional or Galerkin type expression governing the problem, after choosing some approximate functions for the element variables. The approximate functions have to satisfy the admissibility and completeness condition for the problem (Connor and Brebbia, 1976).

The simplest type of 2-dimensional (2D) finite element is the triangle (Figure 4.1). The model domain is discretized into a finite number of triangular elements. The generation of this triangular mesh should be done automatically by a computer program that includes the numbering of the elements (triangles) and the nodes (vertices of the triangles). The numbering scheme of the nodes will affect the computational time and accuracy of the solution.

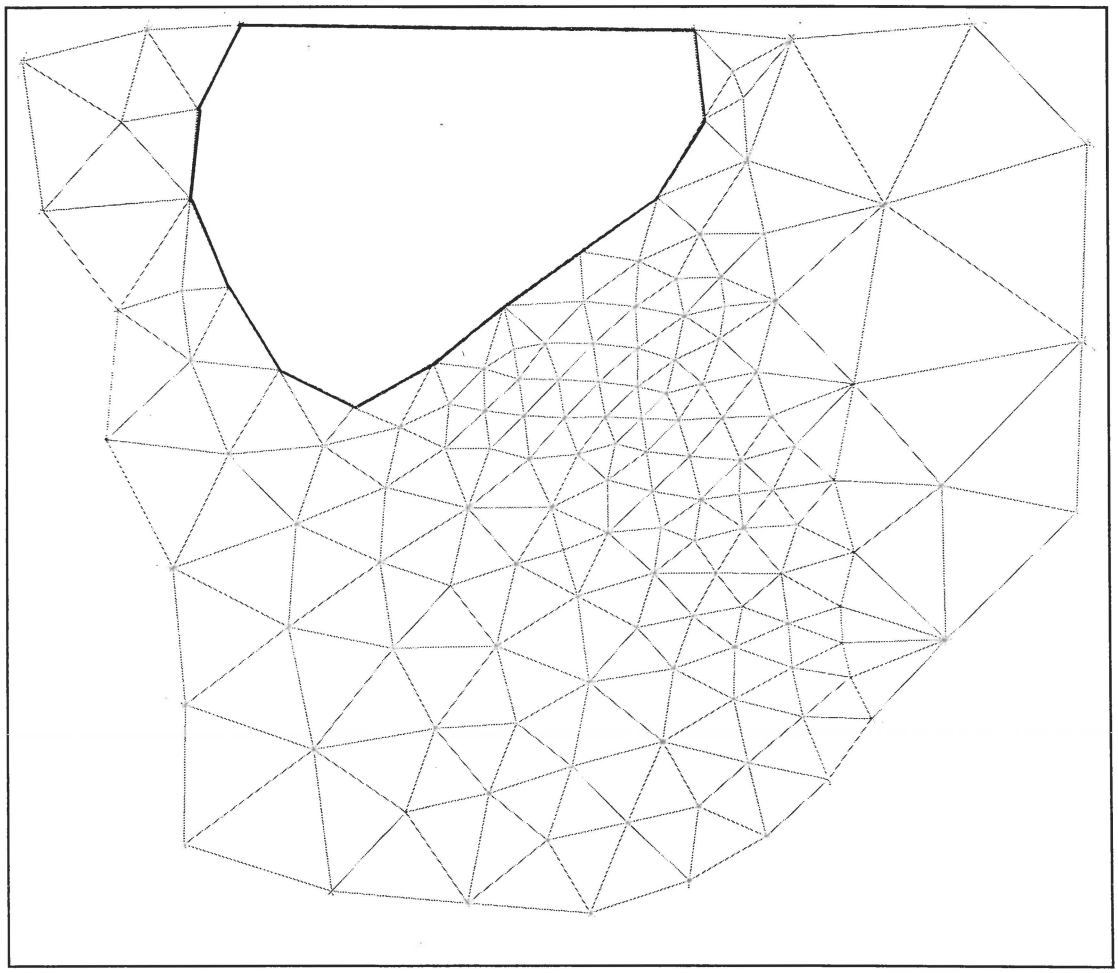

Figure 4.1. The simplest type of 2-dimensional (2D) finite element with triangular mesh generated by automatic grid generation software package TRIGRID.

After the finite element grid is developed, the behavior of the real system is considered to be explained by some unknown continuous function (F). The function is characterized by a finite number or discrete set of *n* nodal values, f_α that is connected by interpolating function (ϕ_α). The function can be formulated as follows:

$$F = \sum_{\alpha=1}^{n} f_\alpha \phi_\alpha \tag{4.1}$$

where F : unknown continuous function;

f_α : value at the α_{th} nodal point;

ϕ_α : interpolating function.

The interpolating function is a piece-wise linear function (McKenzie, 1993; de Lange, 1997) with :

$\phi_\alpha = 1$ at vertex a;

$\phi_\alpha = 0$ at all other vertices;

ϕ_α varies linearly over each element.

The nodal values must satisfy the governing differential equations, and fit all existing boundary conditions. Errors can arise due to the discretisation and the finite element method attempts to minimize the discretisation errors.

Discretisation Errors

If a differential operator is applied to equation 4.1, the residual error due to the discrete representation of a continuous function is defined (de Lange, 1997) by :

$$r(x,y) = D.\ f_\alpha.\ \phi_\alpha. \tag{4.2}$$

where r(x,y) : residual due to discretion.

D : differential operator.

To minimize the residuals, the Galerkin Method multiplies equation 4.2 by *n* weighting functions. The resulting matrix is then integrated over the whole domain,

while requiring that each resulting weighted residual be zero (McKenzie, 1993; de Lange , 1997). This approach may be expressed as

$$\int_R W \hat{D} f_\alpha \phi_\alpha dR = 0 \tag{4.3}$$

where W is the weighting function and R is domain or region of interest.

Applying the interpolation function (ϕ_k) as the weight function (W), equation 4.3 may be expressed as :

$$\int_R \phi_k \hat{D} f_\alpha \phi_\alpha dR = 0 \tag{4.4}$$

Equation 4.4 cannot be applied if the differential operator is second order, or higher, because the interpolating functions are piece-wise linear that can only be differentiated once. This problem is avoided by integrating in parts, using Gauss's or Green's Theorem (Connor and Brebbia, 1976; McKenzie, 1993; de Lange, 1997).

4.3. Tsunami Model Approach

For the tsunami model, the nodal values depend only on time. Equation 4.4 can be simplified (de Lange, 1997) as follows :

$$A_{k\alpha} f_\alpha = 0 \tag{4.5}$$

where

$$A_{k\alpha} = \int_R \phi_k \hat{D} \phi_\alpha dR = 0$$

Equation 4.5 with an appropriate boundary condition produces a system of linear equations that can be used to determine the nodal values. These can be expressed as

$$\sum_{\alpha=1}^{n} a_{\alpha k} f_\alpha = b_k \tag{4.6}$$

Here the values of $a_{\alpha k}$ and b_k depend on the interpolating function f_α and the boundary conditions (de Lange, 1997).

In summary the basic steps of the method (Connor and Brebbia, 1976; McKenzie, 1993; de Lange, 1997)are :

- discretisation of the problem by selection of elements interconnected at the nodal points
- evaluation of the matrices of the elements
- formulation of the complex matrix of the continuum and the input vector
- application of the boundary conditions
- solution of the resulting system of equations
- calculation of any other functions based on the nodal unknowns.

4.4. Tsunami Finite Element Model

The finite element model for tsunami is derived from the mathematical model in Chapter 3. It covers deep water generation and propagation; and near land propagation. Different governing equations can be applied to these condition with results a sets of linear equations. The derivations of the finite element model for tsunami are given in the work of McKenzie (1993) and de Lange (1997).

4.4.1. Deep Water Generation and Propagation Model

The governing equations of tsunami generation and propagation in deep water are given in chapter 3, equations 3.18 and 3.19 as follow:

$$\frac{\partial M_i}{\partial t} + g(\eta + h - b)\eta_{,i} = 0 \tag{4.7}$$

$$\frac{\partial(\eta - b)}{\partial t} + M_{i,i} = 0 \tag{4.8}$$

The variables (M, η, b, d) in governing equations can be expressed by the following interpolating functions

$$\begin{aligned} M_i &= \phi_\alpha M_{\alpha i} \\ \eta &= \phi_\alpha \eta_\alpha \\ h &= \phi_\alpha h_\alpha \\ b &= \phi_\alpha b_\alpha \\ d &= \phi_\alpha d_\alpha \end{aligned} \tag{4.9}$$

Applying the Galerkin Method, the governing equations become (de Lange, 1997)

$$\begin{aligned} &\dot{M}_{\alpha i} A_{k\alpha} + \eta_\beta d_\alpha B_{k\alpha\beta i} = 0 \\ &\text{where :} \\ &A_{k\alpha} \equiv \int_R \phi_k \phi_\alpha dR \\ &B_{k\alpha\beta i} \equiv \int_R g\phi_k \phi_\alpha \phi_{\beta,i} dR \end{aligned} \tag{4.10}$$

for the equation of motion, $\dot{M}_{\alpha i}$ is the time derivative of M, and

$$\begin{aligned} &(\dot{\eta}_\beta - \dot{b}_\beta) A_{k\beta} + M_{\alpha i} C_{k\alpha i} = 0 \\ &\text{where :} \\ &C_{k\alpha i} \equiv \int_R \phi_k \phi_{\alpha,i} dR \end{aligned} \tag{4.11}$$

for the equation of continuity.

4.4.2. Near Land Propagation Model

Near land propagation model of tsunami are derived from the governing equations in chapter 3 as follow:

$$\frac{\partial U_i}{\partial t} + U_j U_{i,j} + g\eta_{,i} = 0 \tag{4.12}$$

$$\frac{\partial \eta}{\partial t} + ((\eta + h)U_j)_{,j} = 0 \tag{4.13}$$

The discrete variables and interpolating equations approximation for the variables (U, η, h) in the governing equations are as follow :

$$\begin{aligned} U_i &= \phi_\alpha U_{\alpha i} \\ \eta &= \phi_\alpha \eta_\alpha \\ h &= \phi_\alpha \eta_\alpha \end{aligned} \tag{4.14}$$

Applying the Galerkin Method, the governing equations become (de Lange, 1997)

$$U_{\alpha i} A_{k\alpha} + U_{\alpha j} U_{\beta i} \frac{1}{B} B_{k\alpha\beta j} + \eta_\alpha g C_{k\alpha i} = 0 \tag{4.15}$$

for the equation of motion, and

$$\dot{\eta} A_{k\alpha} + U_{\alpha j} (h_\alpha + \eta_\alpha) \frac{1}{g} (B_{k\alpha i\beta} + B_{k\alpha\beta i}) = 0 \tag{4.16}$$

for the equation of continuity.

The equations 4.10 and 4.11 are the finite element equations for tsunami generation and propagation in deep water. The quations 4.15 and 4.16 are the finite element equations for near land tsunami propagation..

4.4.3. Time Stepping Method

Applying a numerical time stepping technique to the finite element equations for tsunami is necessary in order to predict the evolution of the system with time. The tsunami model uses the Lax-Wendroff numerical time stepping method for this purpose (de Lange, 1997).

The method

The Taylor expansion of an arbitrary function of time *f(t)* may be expressed as

$$f(t+\Delta t) = f(t) + \Delta t\, \dot{f}(t) + \frac{(\Delta t)^2\, \ddot{f}(t)}{2} + \ldots\ldots \tag{4.17}$$

The first order coupled system can be derived by retaining the first three terms as

$$f(t+\frac{\Delta t}{2}) = f(t) + \frac{\Delta t}{2} \dot{f}(t) \tag{4.18}$$

$$f(t) = f(t) + \Delta t\, \dot{f}(t + \frac{\Delta t}{2}) \tag{4.19}$$

which eliminates the second order derivative $\ddot{f}(t)$, and constitutes the two step Lax-Wendroff Method.

Deep water propagation and generation

The time function for the finite element equations of tsunami generation and propagation in deep water (equation 4.10 and 4.11) for the nth time step

$$f(t) = A_{k\alpha} M_{\alpha}^{n}\ , \tag{4.20}$$

for the equation of motion, and

$$f(t) = A_{k\alpha} \eta_{\alpha}^{n}\ , \tag{4.21}$$

for the equation of continuity.

Applying the Lax-Wendroff Method produces the following equations

$$\begin{aligned} f(t + \frac{\Delta t}{2}) &= \bar{A}_{k\alpha}\, M_{\alpha}^{n+1/2} = A_{k\alpha}\, M_{\alpha}^{n} - \frac{\Delta t}{2} B_{k\alpha\beta} d_{\alpha}^{n} \eta_{\beta}^{n} \\ f(t + \Delta t) &= \bar{A}_{k\alpha}\, M_{\alpha}^{n+1} = A_{k\alpha}\, M_{\alpha}^{n} - \Delta t B_{k\alpha\beta} d_{\alpha}^{n+1/2} \eta_{\beta}^{n+1/2} \end{aligned} \tag{4.22}$$

for the equation of motion, and

$$\begin{aligned} f(t + \frac{\Delta t}{2}) &= \bar{A}_{k\alpha}\, \eta_{\alpha}^{n+1/2} = A_{k\alpha}\, \eta_{\alpha}^{n} - \frac{\Delta t}{2} C_{k\alpha} M_{\alpha}^{n} + A_{k\alpha} (b_{\alpha}^{n+1/2} - b_{\alpha}^{n}) \\ f(t + \Delta t) &= \bar{A}_{k\alpha}\, \eta_{\alpha}^{n+1} = A_{k\alpha}\, \eta_{\alpha}^{n} - \Delta t C_{k\alpha} M_{\alpha}^{n+1/2} + A_{k\alpha} (b_{\alpha}^{n+1} - b_{\alpha}^{n}) \end{aligned} \tag{4.23}$$

for the equation of continuity.

Given the initial and boundary conditions on these equations, the variables M_{α} and η_{α} can be evaluated for all subsequent time steps.

Near Land Propagation

The time function for the finite element equations of tsunami propagation near land (equation 4.15 and 4.16) for the nth time step

$$f(t) = A_{k\partial} U_{\alpha}^{n} \tag{4.24}$$

and applying the Lax-Wendroff Method produces the following equations

$$f\left(t + \frac{\Delta t}{2}\right) = \bar{A}_{k\alpha}\, U_{\alpha}^{n+1/2} = A_{k\alpha} U_{\alpha}^{n} - \frac{\Delta t}{2}\left(\frac{1}{g} B_{k\alpha\beta} U_{\alpha}^{n} U_{\alpha}^{n} + g C_{k\alpha} \eta_{\alpha}^{n}\right)$$

(4.25)

$$f(t+\Delta t) = \bar{A}_{k\alpha}\, U_{\alpha}^{n+1} = A_{k\alpha} U_{\alpha}^{n} - \Delta t\left(\frac{1}{g} B_{k\alpha\beta} U_{\alpha}^{n+1/2} U_{\alpha}^{n+1/2} + gC_{k\alpha}\eta_{\alpha}^{n+1/2}\right)$$

for the equation of motion, and

$$f\left(t+\frac{\Delta t}{2}\right) = \bar{A}_{k\alpha}\, \eta_{\alpha}^{n+1/2} = A_{k\alpha}\eta_{\alpha}^{n} - \frac{\Delta t}{2}\left(h_{\alpha}+\eta_{\alpha}^{n}\right)U_{\beta}^{n}\frac{1}{g}\left(B_{k\alpha\beta}+B_{k\beta\alpha}\right)$$

(4.26)

$$f\left(t+\frac{\Delta t}{2}\right) = \bar{A}_{k\alpha}\, \eta_{\alpha}^{n+1} = A_{k\alpha}\eta_{\alpha}^{n} - \Delta t\left(h_{\alpha}+\eta_{\alpha}^{n+1/2}\right)U_{\beta}^{n+1/2}\frac{1}{g}\left(B_{k\alpha\beta}-B_{k\beta\alpha}\right)$$

for the equation of continuity. The variables U_{α} and η_{α} can be evaluated for all subsequent time steps by giving the initial and boundary conditions into these equations.

The term $\bar{A}$ in the above equations denotes a lumped matrix. It's defined as a matrix where all of the off-diagonal elements are 'lumped' or combine onto diagonal elements. These allows the matrix to be inverted relatively easily. The errors introduced on simplification of matrix inversion are small if the elements on the leading diagonal of the original matrix are dominant terms in the matrix (McKenzie, 1993; de Lange, 1997).

The application of Lax-Wendroff method to the governing finite element equations results in a non-linear equation of motion. This is because the total water depth *d* in the equation of motion is a function of the wave elevation η (McKenzie, 1993; de Lange, 1997).

4.4.4. Limitations and Sources of Error

Generally, two main sources of error are identified in the numerical model before it is converted to computer code (de Lange, 1997). The first source of error is come from assumptions made relate to the controlling of physical processes; and second is due to the limitations of the mathematical techniques used to generate the numerical model (McKenzie, 1993; de Lange, 1997).

Basic assumptions

The basic assumptions for tsunami model have been discussed in chapter 3, and in summary :

- Shallow water theory is used as governing equations
- Frictional forces due to sea floor, and the Coriolis force have been neglected
- In deep water, the convection terms and high order term have been omitted.

All of the assumptions are reasonable. However, the assumptions relating to frictional forces and Corioli force have to be considered carefully. It might be source of error and invalidate the computational results.

Numerical technique

There are at least five potential sources of error arising from the numerical technique for tsunami finite element model using this method (McKenzie, 1993; de Lange, 1997):

- The use of linear interpolating functions.

  The error can be reduced by using higher order interpolating functions but it would greatly increase the complexity of the numerical model. The best approach (de Lange, 1997) is to ensure that elements adequately define the domain.
- The numerical integration with *lumping* of matrices.

  The error is small as long as the elements in the leading diagonal are dominate the matrices.
- Time stepping using the Lax-Wendroff Method.

  This numerical scheme introduces numerical diffusion into the system, limiting the size of the time step that can be used (de Lange, 1997). If numerical diffusion is significant, the model will predict wave propagation velocities that are too fast. It is necessary to check the predicted tsunami travel time by manual calculation to ensure that they are realistic. If they are not, the time step should be increased (de Lange, 1997). The upper bound on the time step which is based on stability condition of the Lax-Wendroff method is given by

$$\Delta t < \frac{d}{|v|}$$

where d is typical grid spacing, and v is information propagation speed which is simply the wave speed in tsunami model ($v = \sqrt{gh}$). The lower limit for the time step depends on the goal of the simulation results.

- The boundary conditions

  There are two main boundaries in the model: land boundaries, and open (ocean) boundaries. If we have an open (ocean) boundaries, ideally all waves should be transmitted fully through the boundary. However, with this model the presence of more than one wave at a boundary can cause reflections (de Lange, 1997). This problem can be solved by clamping the boundaries. For land boundaries, the non-linear problem arises if we apply moving boundaries to simulate an inundation area. For this model, the wetting and drying capability are included but using a linear approach.

- The size and shape of elements.

  The size and shape of elements will create problem such as artificial reflections if the area of adjacent elements varies by more than 10%, and interpolation errors if triangular elements are not close to equilateral (de Lange, 1997).

4.5.The Tsunami Finite Element Computer Program

The simulation program used in this research was used previosly by Mckenzie (1993) and modified by de Lange (1997). These tsunami simulation model has been implemented as two computer programs (de Lange,1997): TSUGRID and TSUNAMI.

The TSUGRID software.

This software takes the finite element grid files generated by the TRIGRID software package. The program determines the interpolation functions for the elements, and set up a binary file containing the necessary grid information for the simulation program.

The TSUNAMI software.

The TSUNAMI program implements the tsunami finite element model in section 4.4. It uses the finite element grid and boundary node data from the *.bin file created by TSUGRID, and additional boundary information provided by the user to

simulate tsunami behaviour. TSUNAMI requires up to five input files (de Lange, 1997):

- Command file.

  This file specified the parameters controlling the execution of the TSUNAMI program, including the names of the other input files.

- Grid data file.

  This is the *.bin file produced by TSUGRID that defines the finite element grid and the grid dependent constants.

- Hot start file.

  This contains a full set of data specifying the complete state of the numerical model. It is used to restart the simulation at some point during the evolution of the tsunami after time zero.

- Specified boundary file.

  This contain user defined boundary conditions. These may include known wave elevations or water velocities for ocean boundary nodes, nodes at which a fixed sinusoidal wave form will be applied, and displacement data for generating a tsunami.

- Time history node file.

  This contains the node numbers for the nodes where tsunami elevation time histories are required.

The results of the tsunami model are output in five ways (de Lange, 1997):

- A graphical display of the tsunami elevations is displayed on the computer screen as the model runs.
- A summary of all the nodal values is written to a text file at user specified intervals. These data are not in suitable form for input into other programs. The data are appended to the end of the file.
- A summary of the tsunami elevation at user specified nodes is written to a history file at the end of each time step. The data are appended to the end of the file.
- A summary of all the nodal elevation values is written to a text file at user specified intervals. The file is in the required format for the DISPLOT program in the TRIGRID package. This allows the tsunami elevation data to be combined

with the grid data for the generation of contours and profile plots. The file can also be input into many other software packages such as MATLAB. The program generates a new file extension of the form *.nnn each time the information is output. The first file *.000 consists of the initial depth data. The subsequent files (*.001, *.002,....) contain tsunami elevation data.

- The complete state of the model domain is written to a text file at user specified intervals. These data can be used for a hot restart of the model, allowing the use of different time steps for the generation and propagation phases of the tsunami. Each time data are sent to this file, the existing file is replaced so that the file only contains the most recent state of the model.

The simulation of wetting and drying nodes for inundation and to allow for the possibility of drying during generation processes are included in TSUNAMI program. However, it is not recommended to use it, as inundation behavior is best handled by non-linear numerical models.

In chapter six, the structure of the program and their implementation for events simulated in Auckland Volcanic field will be discussed.

4.6. References

Babuska, I., and Aziz, A.K., (1972), Preliminary Remarks in The Mathematical Foundations of the Finite Element Method with applications to partial Differential Equations., Aziz, A.K.,(ed), 797 p.

Connor, J.J., and Brebbia, C.A., (1976) Finite Element Techniques for Fluid Flow., Newnes-Butterworths., Boston, 310 p.

de Lange, W.P.,(1997), Tsunami Manual., Dept. of Earth Sciences., University of Waikato. New Zealand.

McKenzie, D.D.J.,(1993), Numerical modelling of Tsunamis in the Bay of Plenty. M.Sc. Theses. Department of Earth Science. University of Waikato., New Zealand.

Smith, M.S., and Shepherd, J.B., (1995) Potential Cauchy-Poisson Waves Generated by Submarine Eruptions of Kick'em Jenny Volcano., Journal of Natural Hazards, Vol.11. No.1. p. 75-94.

Smith, M.S., and Shepherd, J.B., (1993) Preliminary Investigations of the Tsunami Hazard of Kick'em Jenny Submarine Volcano., Journal of Natural Hazards, Vol.7 No.3. p. 257-276.

Tinti, S., and Gavagni, I., (1995), A Smoothing Algorithm to Enhance Finite-Element Tsunami Modelling: An Application to the 5 February 1783 Calabrian Case, Italy., Journal of Natural Hazards, Vol.12. No.2. p.161-197

Chapter Five

PHYSICAL MODELLING OF VOLCANOGENIC TSUNAMIS

5.1. Introduction

In parallel to the mathematical modelling is the physical modelling, which is a reproduction of a physical system at a laboratory scale. The major dominant forces acting on the system are represented in the model in correct proportion to the actual physical system. This method allowing reproduction of complex boundary and initial conditions beyond the accuracy of finite difference models.

In the field of tsunami research, physical models were used widely to evaluate the influence of protective barriers and to determine inundation zones. Only a few experiments have been undertaken to examine the generation of tsunamis, most of these have considered tsunami generation by a fault mechanism.

This chapter presents the results of scale models of volcanogenic tsunamis with special emphasis on submarine explosion, caldera formation and pyroclastic flow mechanism based on the Krakatau event of 1883.

5.2. Overview of Krakatau Event

The Krakatau volcanic complex lay between the Indonesian island of Java and Sumatera in the Sunda Straits (Figure.5.1). Before the 1883 eruption, the complex consisted of three main islands: Krakatau in the south, Sertung to the west, and Panjang in the east. Krakatau, the largest island, was formed from three overlapping volcanic cones - Perboewatan, Danan, and Rakata - aligned along northwest-southeast trend and increasing in altitude to 830 m at the southern peak of Rakata.

The 1883 eruption of Krakatau has been very well documented (Simkin and Fiske, 1983). A large part of Krakatau island disappeared and a ~7 km diameter

caldera was formed in its place. The eruption column reached the stratosphere and produced a volcanic cloud that spread rapidly around the globe in the equatorial region while expanding northward at a rate of ~70 km/day (Sigudsson et al., 1991). The runup heights along the coasts of Java and Sumatera were determined from both eye-witness accounts and a field survey immediately after the eruption and they exceeded 35 m in height. Four main mechanisms have been proposed for the largest tsunami generated by the Krakatau event; viz. submarine explosion, large scale caldera collapse of the northern sector of Krakatau island, emplacement of pyroclastic flow deposit, and lateral blast. Most interpretations of the Krakatau event rest on the work of Verbeek (in Simkin and Fiske, 1983), although geological and geophysical studies of this volcano are continuing (Sigurdsson et al., 1991; Deplus et al., 1995; Carey et al., 1996; Mandeville et al., 1996; Sigurdsson, 1997., pers.com.).

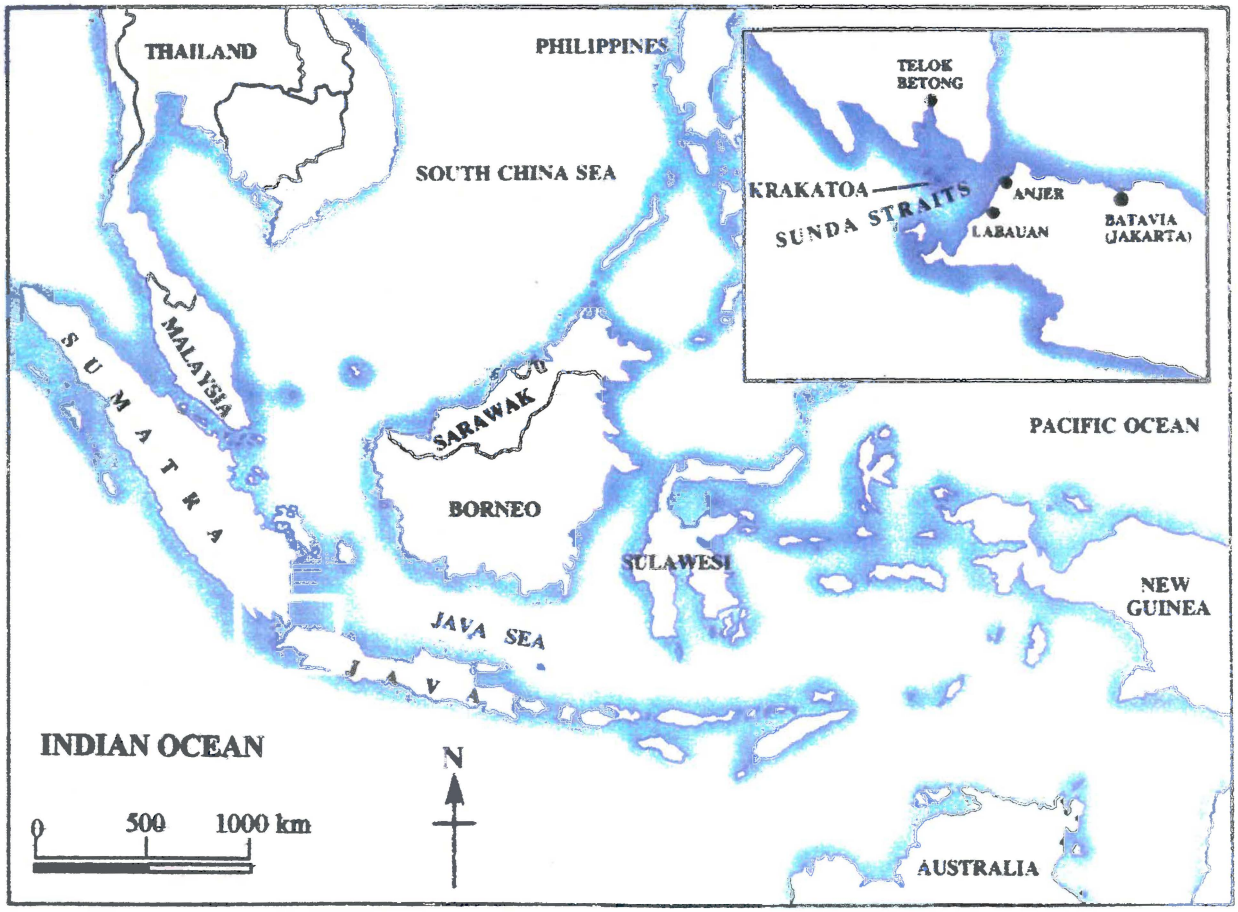

Figure 5.1. The Krakatau volcanic complex lay between the Indonesian island of Java and Sumatera in the Sunda Straits (modified from Matthew, 1988).

5.3. Overview of The Physical Model

The basis of all physical modelling is the concept that the model behaves in a manner similar to the prototype it is intended to emulate. Therefore, physical modelling is performed by designing, constructing, verifying and testing a scale model of the prototype situation. There is a possibility that physical model results may not be indicative of prototype behaviour. Thus, it is important to minimize this possibility by careful model design and validation, careful testing of the model, and careful interpretation of model predictions.

Similitude and Similarity

The physical basis of justification for conducting hydraulic models at reduced scale are the principles of similitude, and the requirements of similarity. It provides the necessary background for deriving appropriate scaling relationships for hydraulic physical models. Similitude is achieved when all major factors influencing reactions are in proportion between prototype and model , while those factors that are in proportion throughout the model domain are so small as to be insignificant to the process. Requirements for similarity can be either criteria of similitude, or conditions of similarity which are established on the basis of dynamical considerations, dimensional analysis, and differential equations. The difference between criteria of similitude and conditions of similarity is significant. Following Hughes (1993) the explanation of these two terms follow :

- Criteria of Similitude (Scale Laws)

  Criteria of similitude are imposed by physical relationships between parameters. The mathematical condition must be met by the ratios of certain parameters between prototype and model, and can not be altered without altering the underlying assumptions.
- Condition of Similarity

  Conditions of similarity are conditions that the experimenter chooses in order to make the physical model reproduce satisfactory results. These conditions may include one or more similitude criteria (scale laws) along with several conditions determined by observation or intuition.

Requirements of similitude will vary with the problem being studied and the degree of accuracy desired for the model reproduction of prototype behaviour. Meanwhile, the prerequisite for complete similarity is that the model be geometrically similar to the prototype. Therefore the requirements and prerequisites consist of scale factors (scale ratios), geometric similarity, kinematic similarity, and dynamic similarity.

Scale Ratios

The correspondence between prototype and model parameters is denoted by the scale ratio. The ratio of a parameter in the prototype to the value of the same parameter in the model is represented as :

$$N_X = \frac{X_p}{X_m} = \frac{\text{value of X in prototype}}{\text{value of X in model}} \tag{5.1}$$

where N_x is the prototype-to-model scale ratio of the parameter X, and the subscripts *p* and *m* represent prototype and model, respectively. The scale ratio can be expressed as the product of other scale ratios as determined from the dimensional units of the variable in question (Hughes, 1993).

Geometric Similarity

Geometric similarity exists between two objects or systems if the ratios of all the corresponding linear dimensions are equal. This relationship is independent of motion of any kind and involves only similarity in form (Warnock, 1950 in Hughes, 1993). There are two kinds of geometric similarity which cnbe represented in the model. These are geometrically undistorted models and distorted models. The geometrically undistorted models are those where the vertical and horizontal scales are the same and they represent the true geometric reproduction of the prototype. The distorted models are models in which the vertical and horizontal length scales are different.

Kinematic Similarity

Kinematic similarity indicates a similarity of motion between particles in model and prototype. In a geometrically similar model, kinematic similarity gives particle paths that are geometrically similar to the prototype.

Dynamic Similarity

Dynamic similarity between two geometrically and kinematically similar system requires that the ratios of all vectorial forces in the two system be the same (Warnock, 1950 in Hughes, 1993). The requirement for dynamic similarity arises from Newton' s second law that equates the vector sum of the external forces acting on element to the element's mass reaction to those forces. There is no known fluid that will satisfy force requirements with perfect similitude requirements; ie.

$$N_{Fi} = N_{Fg} = N_{F\mu} = N_{F\sigma} = N_{Fe} = N_{Fpr}\,, \tag{5.2}$$

where F_i : inertial force, F_g : gravitational force, F_μ = viscous force, F_σ = surface tension force, F_e = elastic compression force, F_{pr} = pressure force. Therefore, an important task in scale model design is to relate the important force ratios, and to provide justification for neglecting the others (Hudson, et al.1979; Hughes, 1993).

Hydraulic Similitude

The degree of accuracy that must be sought from a physical model is governed by the objective of the study. If the model is intended to examine the general trends rather than precise details, some variable can be neglected if they are though to be unimportant relative to the primary physical mechanism involved in the problem (Hughes, 1993). A scale effect can occur because of the appearance of forces in the model, that are negligible in the prototype, such as bottom roughness and surface tension, or when the scale ratio of physical parameter does not maintain the same value over the entire domain of the model. The best guard against scale effects is to build the scale model as large as possible.

Hydraulic similitude criteria

There are several hydraulic criteria for the flow problem in physical modelling that can be used. For practical hydraulic flow problems, the Froude Criterion and Reynolds Criterion as the main criteria to be considered, particularly when designing a coastal scale model.

- Froude Criterion

The Froude number is a parameter that expresses the relative influence of inertia and gravity forces in a hydraulic flow. It is given by :

$$\sqrt{\frac{\text{inertial force}}{\text{gravity force}}} = \sqrt{\frac{\rho L^2 V^2}{\rho L^3 g}} = \frac{V}{\sqrt{gL}} \tag{5.3}$$

where ρ is fluid density, L is length, V is velocity and g is gravitational acceleration.

The Froude number in the model and prototype must be the same to achieve similitude. This can be expressed by scale ratios as :

$$\frac{N_V}{\sqrt{N_g N_L}} = 1 \quad \text{or} \quad N_{Fr} = 1 \tag{5.4}$$

This formula is known as the Froude model criterion for modelling flows in which the inertial forces are balanced primarily by the gravitational forces. It is valid for most flows with a free surface (Hughes, 1993). A physical interpretation of the Froude number is that it gives the relative importance of inertial forces acting on a fluid particle to the weight of the particle (Munson et al., 1990 in Hughes, 1993).

- Reynolds Criterion

The Reynolds number is an important parameter when viscous forces dominate in a hydraulic flow. It is given by the ratio of inertial to viscous forces as :

$$\frac{\text{inertial force}}{\text{viscous force}} = \frac{\rho L^2 V^2}{\mu VL} = \frac{\rho LV}{\mu} \tag{5.5}$$

where μ is dynamic viscosity.

Similitude is achieved when the Reynolds number is the same in the model and prototype, and in term of scale ratios is given as :

$$\frac{N_V N_L N_\rho}{N_\mu} = 1 \quad \text{or} \quad N_{Re} = 1 \tag{5.6}$$

This formula is known as Reynolds model criterion. The Reynolds scale law is intended for modelling flows where viscous forces predominate (Hughes, 1993). A physical interpretation of the Reynolds number is that it gives the relative importance of the inertial force on a fluid particle to the viscous force on the particle. It also distinguish between laminar and turbulent flow.

5.4. Test Facility

The physical modelling of volcanogenic tsunamis were performed in the wave basin and glass-walled flume at the Tsunami Research Center of Coastal Engineering Laboratory BPP Teknologi at Yogyakarta (Indonesia). The wave basin in which 3 Dimensional (3 D) tests were conducted possessed the following dimension :

- Length : 30.00 m
- Width : 22.00 m
- Height (water depth) : 1.00 m

The glass-walled flume in which the 2 Dimensional (2D) tests were performed had dimensions of :

- Length : 30.00 m
- Width : 0.30 m
- Depth : 0.60 m.

This facilities are illustrated in Figure.5.2.

5.5. Background of Events Simulated

The events simulated by this physical modelling are based on the main mechanism which was believed by researchers as a process for tsunami generation at Krakatau.

Caldera Formation

This mechanism has been proposed by several researchers. A large part of Krakatau Island disappeared during the 1883 eruption and an approximately 7 km diameter caldera was formed with a depth 270 m; the collapse of Rakata would have followed the boundary of the prehistoric caldera (Sigurdsson et al., 1991; Deplus et al., 1995; Mandeville et al., 1996; Carey et al., 1996). The associated events included emission of huge volumes of ignimbrite that covered the island and the surrounding sea-floor, and changed the bathymetry of this region considerably (Figure 5.3).

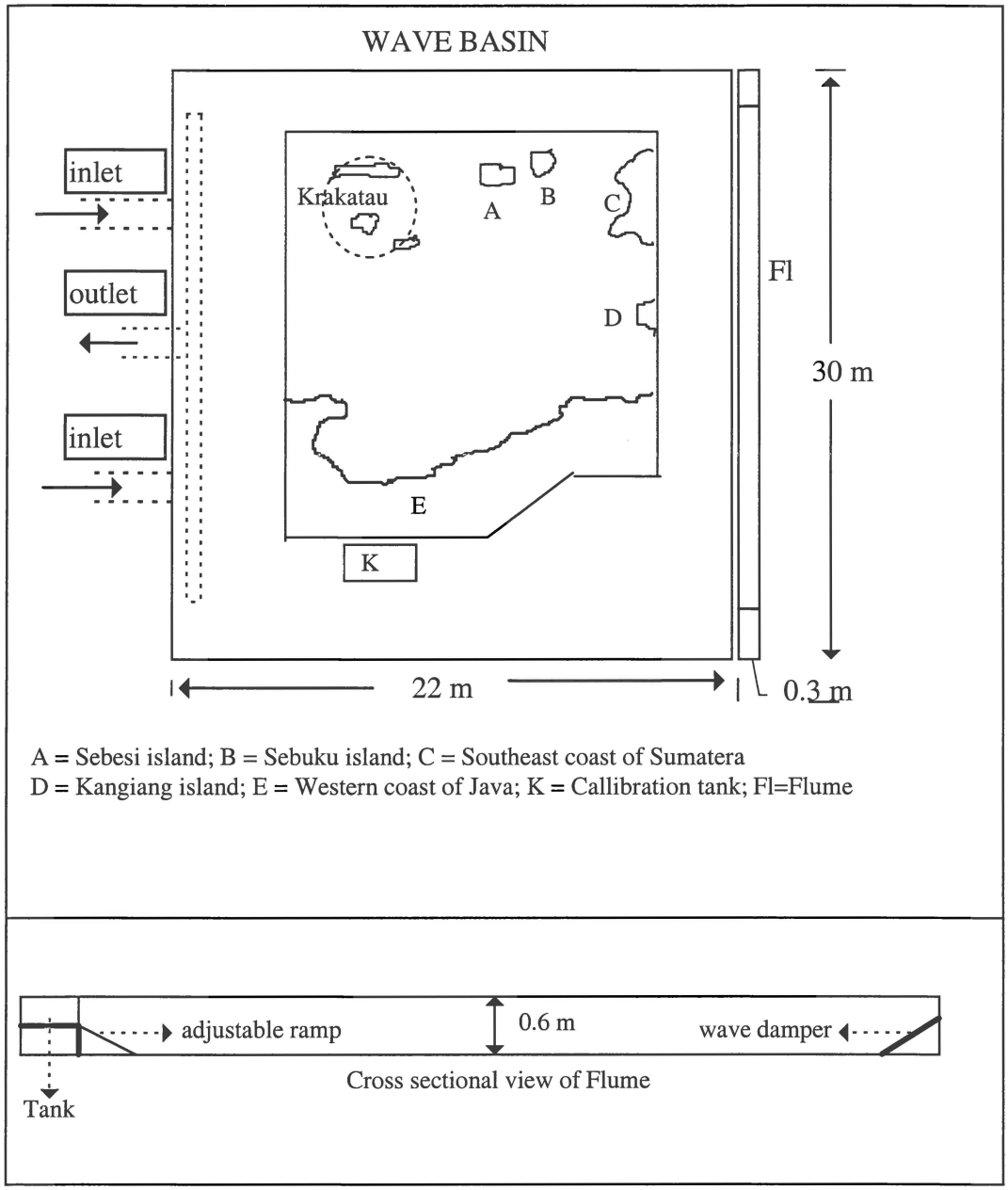

Figure 5.2. Lay out of laboratory facilities at the Tsunami Research Center

Pyroclastic Flow

Recently it has been suggested that pyroclastic flows provided the main forces which generated the catastrophic wave in the 1883 Krakatau events (Self and Rampino, 1981; Francis and Self, 1983; Sigurdsson et al., 1991; Deplus et al., 1995; Monaghan et al., 1997; Mandeville et al., 1996; Carey et al., 1996). They generally agree that the culminating event was the generation of pyroclastic flows by gravitational collapse of the eruption column. Most of the Krakatau island then

disappeared into the sea when the roof of the magma chamber collapsed. Before the major collapse of the volcano, a vast volume of ignimbrite had been erupted and this caused the tsunami.

Submarine Explosion

In chapter 2, it was mentioned that a submarine explosion could a generate tsunami. In the case of Krakatau event, some consider that a submarine explosion mechanism is the main force of tsunami generation (Nomanbhoy and Satake, 1995).

There is still debate on which mechanism is appropriate as the main cause of tsunami generation during the Krakatau 1883 event. However, the physical modelling will examine each proposed mechanism.

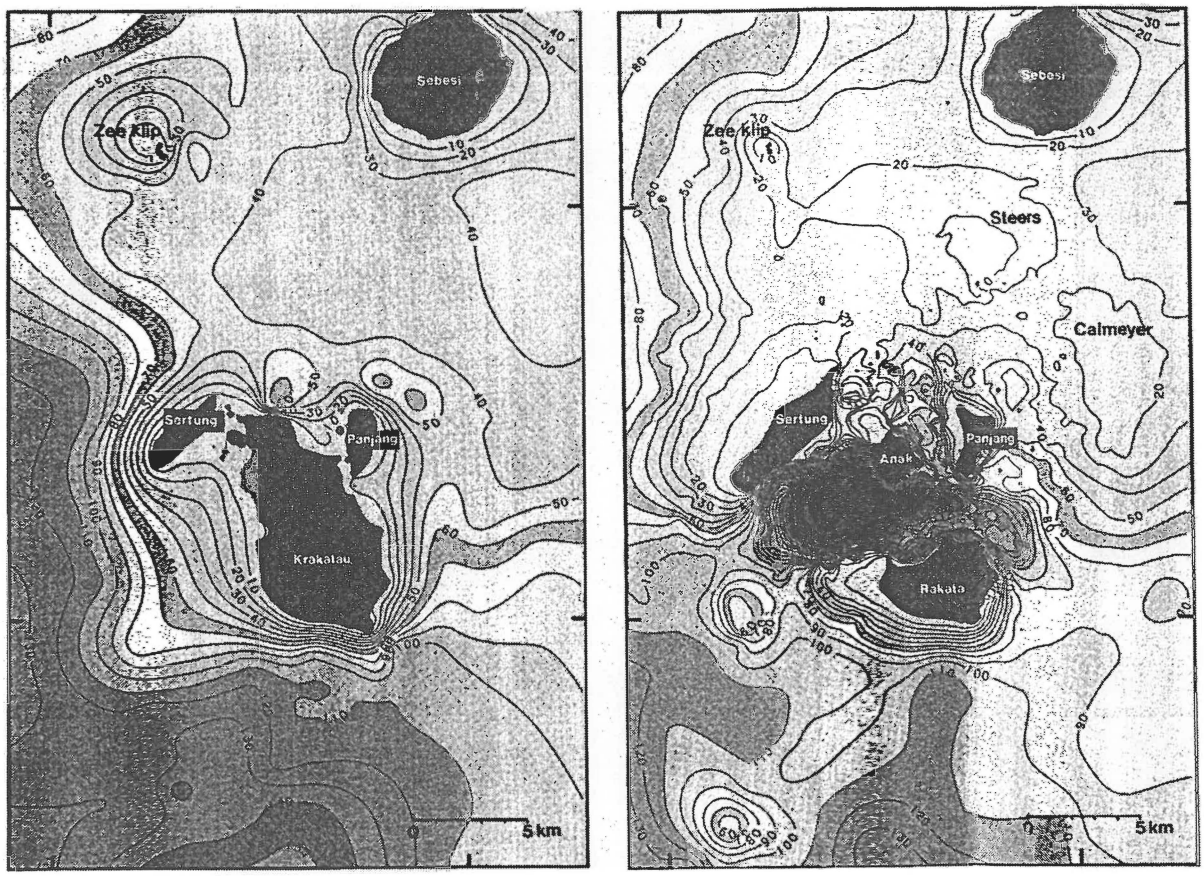

Figure 5.3. The bathymetry changed surrounding the Krakatau before and after 1883 event (source : Sigurdsson et al.1991).

5.6. Model Test

5.6.1. Two Dimensional (2D) Model Test

A two dimensional model test was carried out in the glass-walled flume to examine the pyroclastic flow mechanism. The lay-out of the facilities is illustrated on Figure 5.4.

In modelling pyroclastic flows, the experiments were carried out by using an adjustable inclined ramp (which could be removed). This ramp extended from the reservoir where the flow materials are stored to the bottom of the flume. The reservoir was located above the flume and was designed to model the flow of pyroclastic materials through two media (air and water). The materials that we used for flows were mixtures of sand, mud and water. A coloured dye was used to ease identification of the flow materials and their interaction with the water in the flume.

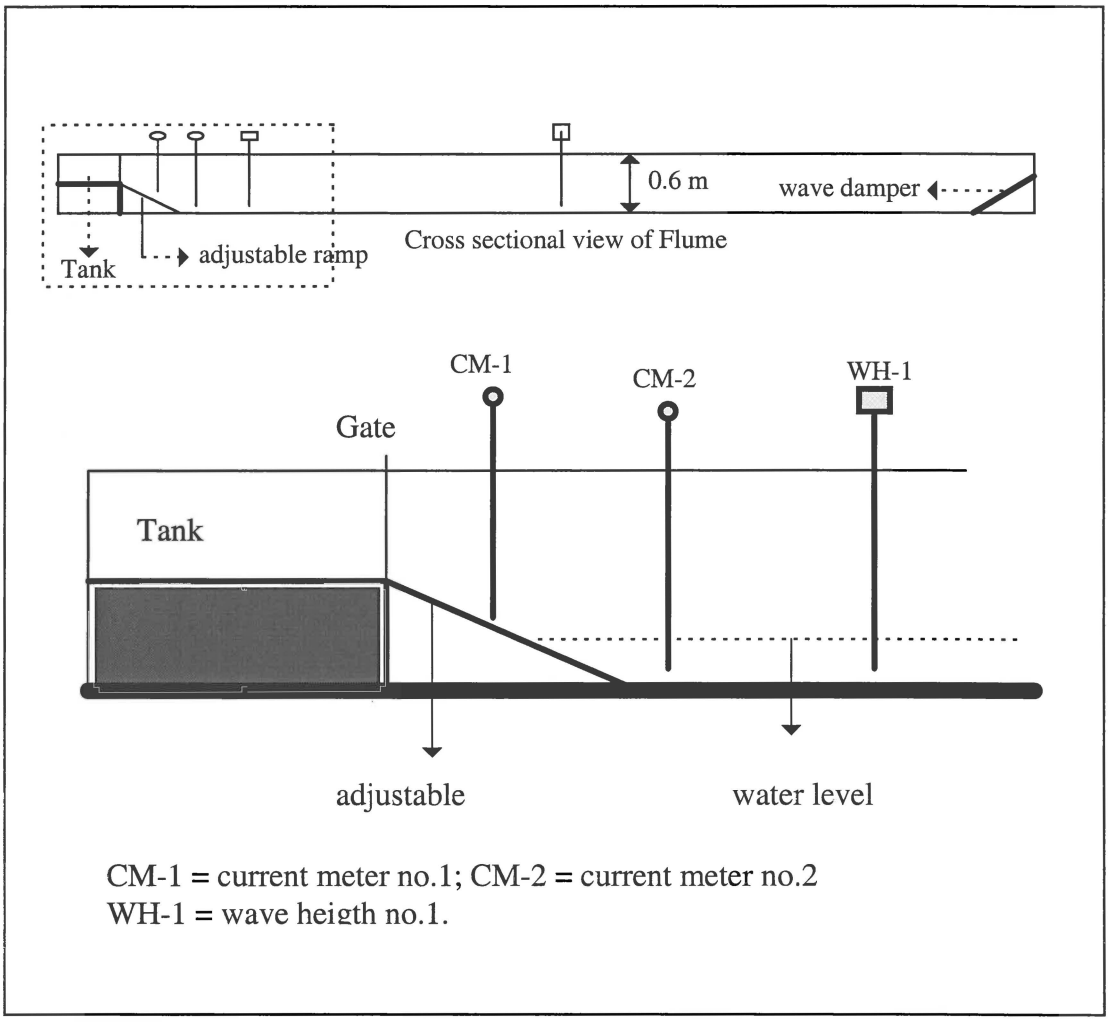

Figure 5.4. Lay-out of 2-dimensional (2D) test facility

Eight (8) experiments were undertaken by using 2 different flow mixtures and various combination of ramp angle as follows (Table 5.1) :

- Test 1. Material in storage is dyed fresh water, the freshwater deep in flume is 20 cm and angle of ramp is 20°, 30°, 60° and 90° (or without ramp).
- Test 2. Material in storage are mixtures of mud, sand and fresh waters, the depth of freshwater in flume is 20 cm and angle of ramp is 20°, 30°, 60° and 90° (or without ramp).

Table 5.1. A combination of experiments

Angle (α)	20°	30°	60°	90°
Fresh water	experiment 1	experiment 2	experiment 3	experiment 4
Mud sand + water	experiment 5	experiment 6	experiment 7	experiment 8

The depth of water in flume is 20 cm

When the gate of the reservoir was opened, the materials slid down the ramp. The following observations were made: speed of the flow down the ramp and after reaching the flume waters; the dimension of flow that had been generated including the head of flow; the amplitude and speed of any waves initiated at the interface and at some distance from the source; and the nature of any deposition of materials. The observations were made by using a high speed camera, video, current meters, wave height meters, and a bottom profiler. For the high speed camera and video, the wall of the glass flume was gridded with 10 cm squares as scales.

5.6.2. Three Dimensional (3D) Model Test

Three dimensional model tests were carried out in wave basin for volcanogenic tsunamis with different source mechanism, viz., caldera formation, pyroclastic flow and submarine explosion.

Model Scale

The horizontal and vertical scale of the model were selected as 1:5000 and 1:500 respectively. The scale was selected, to meet the requirement to reproduce all

relevant phenomena as accurately as possible, and allowing for limitations of the test facilities and the available materials.

The similarity of the physical and dynamical processes within a wave during the generation, propagation and runup is of importance for the investigation. Gravity forces dominate the type of process in situ, hence, the model should be designed in such a way that gravity forces are correctly reproduced. This requirement implies the application of the Froude Law to formulate scale relationships.

The Froude Model Law requires that the Froude number in both model and prototype must be the same to achieve similitude, and it gives following scale relationships:

- Horizontal Length (nL) = 5000
- Vertical Length (nD) = 500
- Time (nT) = $\frac{nL}{\sqrt{nH}}$
- Tsunami Height (nH) = nD

Model Construction

The lay-out of the model (Figure 5.1) was decided after taking into consideration the area to be reproduced inside the wave basin. This area was based on the availability of documented tsunami records during the 1883 events, ease of installation, methodology and direction of data acquisition, and access into basin for constructing the scenario of the event simulated.

With a scale of 1:5000 horizontal and 1:500 vertical, the model was setup and constructed to represent the area which covers all of the western coast of Java, and the tip of Sumatera behind Sebuku and Sebesi Island, as shown in Figure 5.5. Construction of the model commenced by first drawing the coordinates in the basin. The geographical outline and contour lines were then marked. A quantity of sand and/or aggregate was spread around up to the desired level. The level of each contour was achieved using small wooden piles and thin wooden plates with additional aggregates placed between the plates. The surface was covered with approximately 5 cm of cement. For the purpose of caldera formation test, the caldera formed by the eruptions was created first. The caldera diameter in the model was 1.2 m and the water inside the caldera was 0.55 m deep relative to mean sea level.

The experiments

The experiments were conducted in the wave basin and the sequences of a typical experiment are illustrated in Appendix 2.



Figure 5.5. The photograph of 3-dimensional (3D) model in wave basin

Caldera Formation

For this test a conical cylinder was placed in the basin, fully covering the caldera so that the caldera remained dry when the basin was filled by the water (Figure 5.6.). The waves were simulated by lifting the conical cylinder suddenly. After the conical cylinder was lifted, the water surrounding the caldera surged into the caldera, and generated a tsunami.

Pyroclastic Flow

For modelling this event, experiments were carried out by using an adjustable inclined ramp. The experimental approach was an extension of the two dimensional pyroclastic flow experiments in a glass-walled flume with the same materials. The pyroclastic flow were directed towards the Sebuku, Sebesi and Sumatera coastline fronting Rajabasa as these areas were damaged by pyroclastic flows during the 1883 eruptions (Verbeek in Simkin and Fiske, 1983).

Submarine Explosion

Two models were used for this experiment: firstly using explosives; and secondly by dropping a circular plate. For the explosive tests, two types of test were performed, i.e., with and without a chamber where the chamber represented the shape of Krakatau before the eruption.The explosive tests were also used to demonstrated the characteristic of the explosion causing wave generation. The amount of explosive material used was scaled by tube units, where 1 tube was equal to 2.10 gram of explosive. Nine (9) experiments were carried out, with varying scale of explosive from 1 tube to 9 tubes. During these experiments, there are no measurements of the sound or explosive forces from the explosion, but there were recorded on video. For the plate experiments, the plate was released (free fall) from various levels above the target area (Krakatau Volcanic complex).

Data Collection & Processing

Data collection for all experiments used 16 wave height meters and 8 current meters to obtain all of the important data relating to the generating mechanism and propagation of waves and currents. All of the instruments operated simultaneously and were connected to a HP6000 Data Logger for further processing. Processing of wave and current data were done with HP Signal software packages and MATLAB. The output format can be seen in Appendix 3.

5.7. Results and Discussions

5.7.1. Two Dimensional (2D) Pyroclastic Flow Experiments

Eight (8) experiments were arranged by using 2 different flow materials and 4 combination of ramp angle (section 5.5.2.) as follows :

- Test 1. Material in storage is dyed fresh water, the freshwater deep in flume is 20 cm, and angle of ramp is 20°, 30°, 60° and 90° (or without ramp),
- Test 2. Material in storage is mud and coarse sand, the freshwater depth in flume is 20 cm, and angle of ramp is 20°, 30°, 60° and 90° (or without ramp).

Table 5.2. A number of experiments

Angle (α)	20 °	30 °	60 °	90 °
Fresh water	experiment 1 (3 test)	experiment 2 (3 test)	experiment 3 (3 test)	experiment 4 (3 test)
Mud sand + water	experiment 5 (3 test)	experiment 6 (3 test)	experiment 7 (3 test)	experiment 8 (3 test)

The depth of water in Flume is 20 m.

Results of 2-dimensional (2D) Model

From these experiments, we consider the flow down the ramp acted like the gravity currents, and we examined the interaction of the head of gravity currents and the water in flume, and the generation of the waves.

Gravity Currents and Wave Generation

In examining the gravity currents and wave generation from the experiment, we first consider the general effects of the flow and their interaction when they met a water in Flume in both cases viz., the dyed freshwater material and the mixed of mud and sand.

General Effects

Test 1. Experiments with Dyed Fresh Water.

In this experiment the pyroclastic flow was represented by dyed freshwater and the fluid in the flume was freshwater. Therefore the density of the reservoir fluid(ρ_r)

equaled the density of the fluid in the flume (ρ_f), allowing us to examine the interaction of two fluids with almost equal density ($\rho_r \sim \rho_f \sim 1001$ kg/m^3).

The ramp surface was very smooth to minimize the friction between the flow and ramp surface. Two current meters were installed in the flume to measure the velocity of the flow. The first current meter measured the current velocity flowing down the ramp, and the second current meter was located at the base of the ramp and measured the velocity of the current when the flow enter the water in flume on each test. When the gate is opened and the material was flowing down the ramp, the flow is turbulent. The head of the gravity current is larger than the flow behind the head.

When the head of flow met the surface of water in flume, the mixing process was started and the head of flow was reduced. However the flow continued on to reach the bottom of the flume. The less dense portion of the flow are dispersed as buoyant fluid and rise to the top and flow faster at the surface. The first wave is generated as a Solitary wave with a steep slope. A small second wave with a low slope followed the first wave. The second wave was generated due to the turbulence and the force of buoyant fluid which pushed the water up. With these experiments, generally, only one Solitary was generated, even if the pyroclastic flow continued to flow down the ramp for a long period (Figure.5.6).

The variation of wave height with variation of ramp angle is nearly independent as demonstrated by Monaghan et al. (1997). However, there is a tendency for decreasing of the wave height with increasing angle of ramp from 20° to 60°. The decrease of the wave height is relatively small, from 6.8 cm to 5.0 cm with error readings 0.4 ($\pm$ 0.4 cm). Of interest is when the angle of ramp was 90°, the wave height increased again, and it measured 6.3 cm (Figure.5.7).

The turbulence and mixing became more intense when the angle of ramp steepened. The head of pyroclastic flow showed more intense vortex motion, which was related to the current velocity which increased with steeper ramp slopes.

Test 2. Experiments with Mixed Mud and Sand

The same procedure as test 1 was used to carry out the experiments. The material used to represent the pyroclastic flow was a mixture of freshwater, mud and sand. The density (ρ_m) of this material was 1346 kg/m^3 .

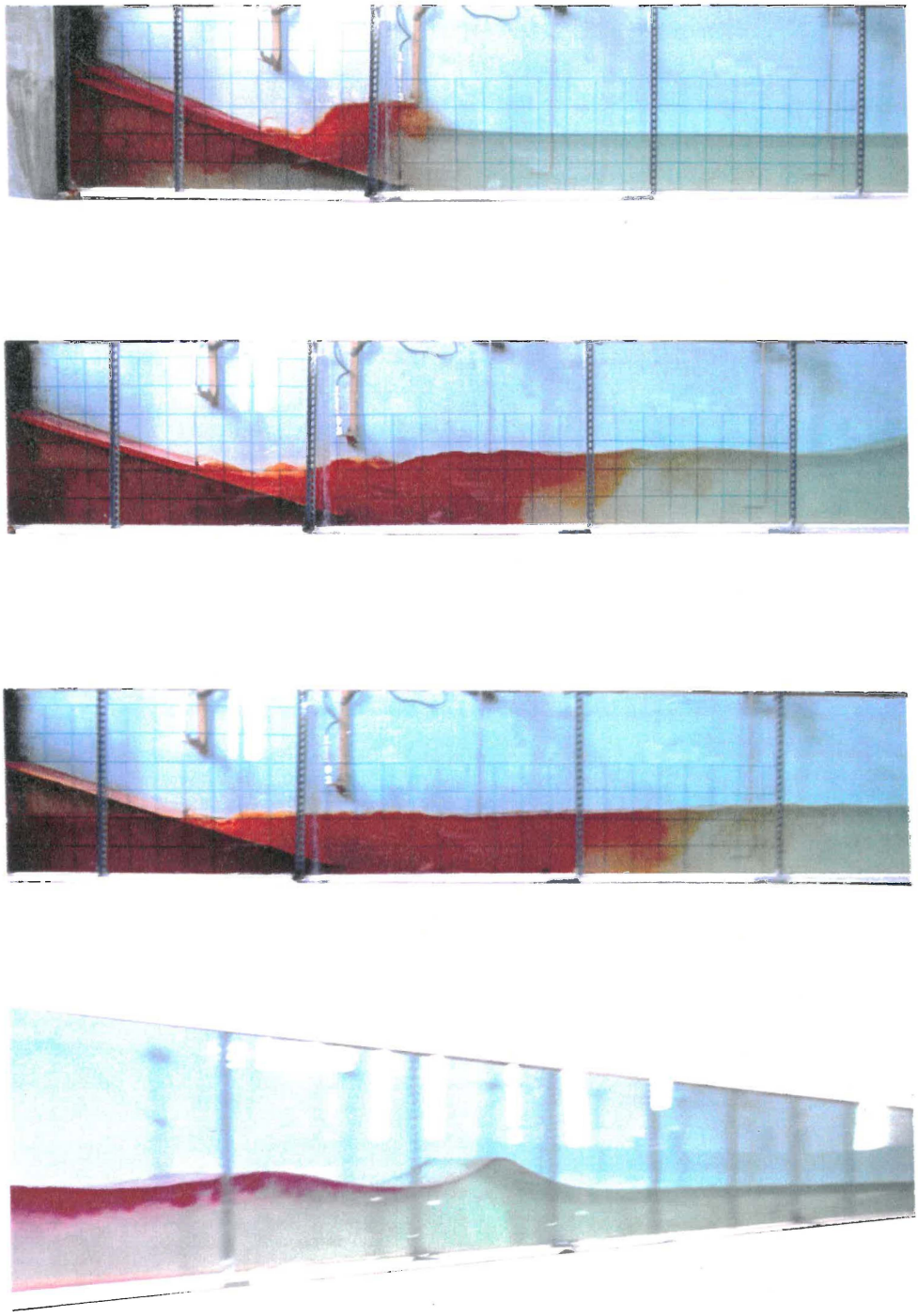

Figure 5.6. The sequences dynamic of pyroclastic flow shows the turbulent and well mixed flow and the first stage of wave initiation and its propagation.

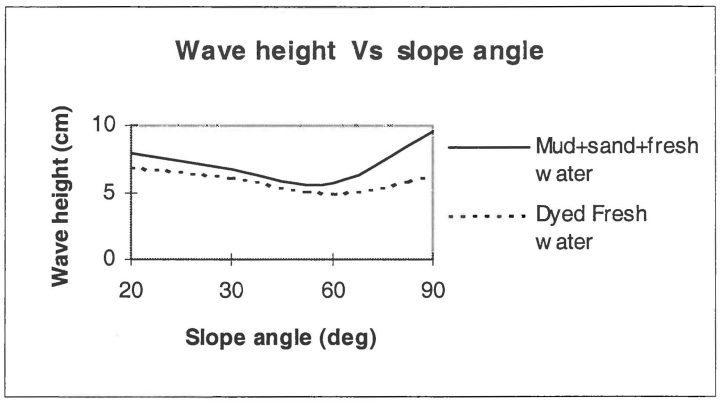

Figure 5.7. The changes of wave height with slope angle shows the tendency of decreasing of the wave height from 20° - 60° and increased after 60°. It also shows that the denser material of flow generated higher wave.

When the gate was opened, the material flowed down the ramp as a turbulent and well mixed flow. However, the coarser material remained at the base of the turbulent flow. When the head of the pyroclastic flow hit the water surface, the mixing processes started. At this stage, the flow divided into two; a buoyancy flow with light material in suspension, and a denser flow consisting of heavier materials which kept flowing at the bottom of flume as a bore phenomena as indicated by Bonnecaze et al. (1993). At first, the denser bottom flow moved faster than the material moving in suspension. However it settled out rapidly at the bottom bringing the flow to a stop. The upper suspension continued to move forward and settled out at greater distance from the ramp than the coarse material.

The deposition of sediment was dependant on the angle of the ramp. For low ramp angles (20° and 30°), the coarse sediments are deposited at the base of the ramp and extend away for a significant distance with a thinning upwards trend. When the angle is 60° the sediments were deposited further from the base of ramp but were spread over a smaller area (Figure 5.8).Therefore the energy of the flow of this angle can transport and deposit sediment as a coherent unit at some distance from ramp. For angle 90° (or free fall), some of sediments still remain in the base of ramp.

- **Ramp angle (α) = 20°**

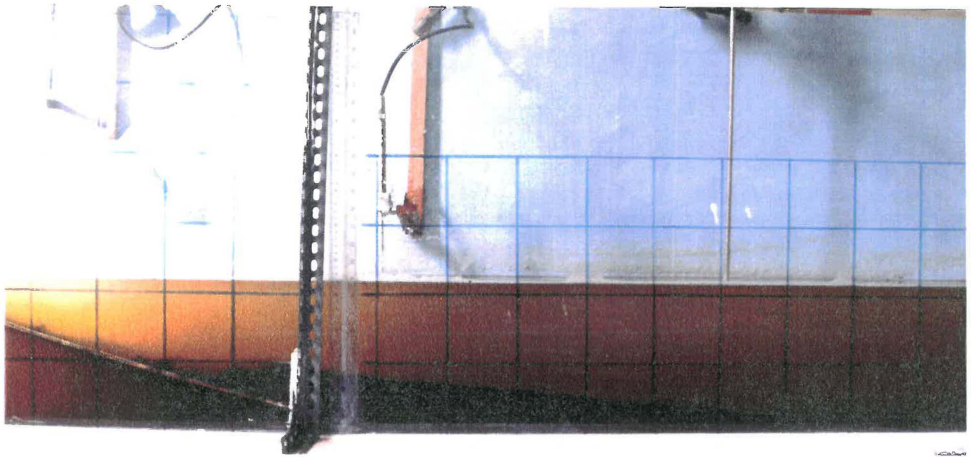

- **Ramp angle (α) = 60°**

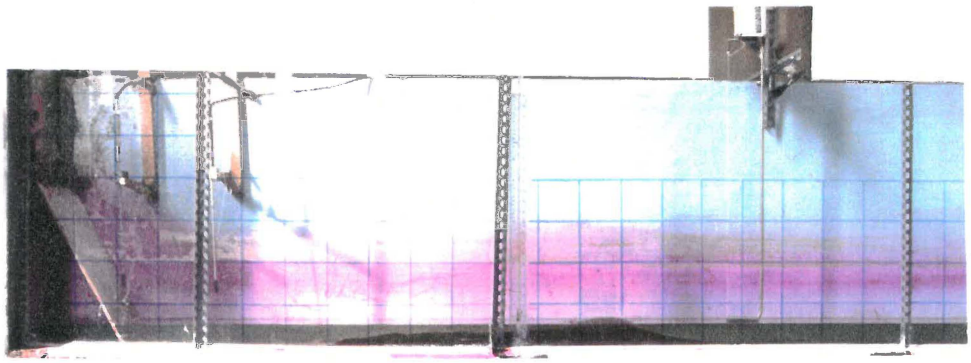

- **Ramp angle (α) = 90°**

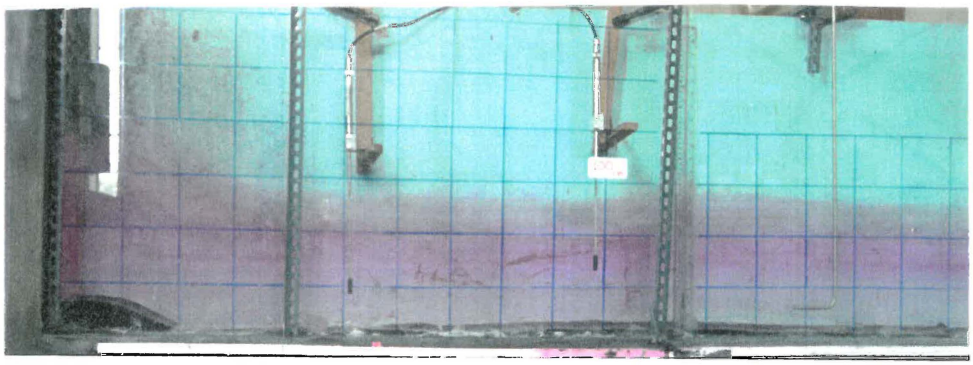

Figure 5.8. The sediments were deposited further from the base of ramp for angle > 30°.

A Solitary wave was generated, with the mechanism being almost the same with as test 1. Compared to test 1, the wave is higher and steeper and the flow velocity is stronger. This is due to the increased density of the pyroclastic flow and the rapid deposition of coarse sediment (sand). The second wave was generated with low angle of slope following the first wave after certain period of time due to the bouyancy forces which lifted the water up, together with the backrush of the waters that went up the ramp. Monaghan et al. (1997) showed that the denser the material of pyroclastic flow, the bigger the wave that can be generated. This is consistent with of our results.

Properties of the Waves

From the experiments, it was clear that the wave generated by the entry of the pyroclastic flow is a Solitary wave. The form of the wave is defined by (Bousinessq solution) :

$$\eta = H \operatorname{sech}^2\left[\left(\frac{3H}{4d^3}\right)^{1/2}(x - ct)\right] \tag{5.7}$$

and the velocity (c):

$$c = \left[gd\left(1+\frac{H}{d}\right)\right]^{1/2} \tag{5.8}$$

where H is the wave height, η is the height of the water surface above the static level, x is the origin of the horizontal coordinate measured from the position of the peak of the wave , g is gravitational acceleration, and d is the depth of water in flume .

Geologic significance

The experiments show that a tsunami wave can easily be generated by gravity flows entering the water, regardless of the slope. The wave properties depend on the relative densities of the flow and the receiving body, and the velocity of the flow. The angle of entry of the flow into the water determines the deposition pattern of sediment.

These results can be applied to explain the observed characteristics of tsunamis and deposits cause by the volcanic activities. It suggests that tsunamis can be generated by the entrance of a pyroclastic flow into the sea. The occurrence of the Calmeyer and Steers shallow produced by the 1883 Krakatau event was reproduced by

the pyroclastic flow experiment with coarse sand and mud and an entry angle is 60°. This produced a compact deposit some distance from the ramp. This experiment also is consistent with the most deposits preserved close to the original Krakatau shore (Figure 5.3).

A more dilute upper component of the pyroclastic flow, including the hot gas and ash, travelled along the sea surface for up to 45 km and killed more than 1000 people at Katimbang, Sumatera Island (Sigurdsson et al., 1991). This can be explained by the experiments which showed the propagation of less dense material from the pyroclastic flow near the water surface. These experiments did not include the influence of high temperature (~ 600° C) of the material, which can enhance the ability of the flows to travel.

5.7.2. Three Dimensional (3D) Model Test Results

Caldera Formation

For this model test, the tsunami began with a fall of water surface elevation, then the water surface in the caldera rose higher than the still water level and waves propagated out of the caldera. The measurement results of the surface wave elevation close to Carita Bay shows that initially, the water surface fell. Unfortunately, the wave sensor which was dedicated to measure wave formation inside the caldera did not work properly due to its lack of sensitivity. A sensor with high accuracy and sensitivity is required to measure the phenomena inside the caldera. A high resolution transducer is proposed as a better approach.

The highest model wave recorded outside the caldera was approximately 20 m and the horizontal runup along Carita Bay was about 1.5 km (prototype units). Meanwhile the arrival time of the first tsunami wave was about 5 - 12 second along the western coast of Java.

Pyroclastic Flow

With these experiments, we found that the same scale flows that were used in the flume tests could not be applied in the wave basin. The pyroclastic flow could not generate the expected wave by flowing or releasing material down the inclined ramp with the flow source at the same elevation as before. This result shows that more energy required to generate waves in the wave basin. Based on geological and

geophysical studies (Sigurdsson and Carey, 1997) for the 1883 eruption, the pyroclastic flow had velocities in excess of 160 km/hour (4444.5 cm/sec). The flume model velocities were only 115.5 cm/sec. This behaviour has to be taken into account for future experiments.

Submarine Explosion

Experiments without Chamber

Using only explosive material without a chamber, which assumes that the caldera had already formed, produced a typical shallow water explosion phenomena. Initially at the center of the explosion, a crater was formed instead of a water dome, which is consistent with the findings of Le Mehaute and Wang (1996). This mechanism also can be categorized as a point source mechanism. The typical wave formation produced by this mechanism is consistent with the aerial photograph of Eruption 1929 of Anak Krakatau (Figure 5.9). There are clear concentric eruption-waves emanating from the eruption point (Simkin and Fiske, 1983).

Paradoxically, increasing the scale of the explosion did not produce larger waves. Large explosions produced a crater and a single large radial waves was generated at some distance from the crater. This was followed at some distance by 2 - 3 waves produced by the crater formation. The first wave was stable and propagated as a Soliton, but the following waves were easily dispersed. The first wave was generated by the changing atmospheric pressure caused affecting the water surface. Larger explosions produced dry craters, and the wave decreased in size.

This experiment, with a point source and crater formation, can be approximated by using closed form analytical solutions for the initial disturbances. There are three cases consistant with these experiments, where the solutions of mathematical formulation of explosion generated water waves follow an exponential form. In these cases, the wave decreases monotically, there is no beating, and the maximum wave is the leading wave which dominates over all the trailing waves. All these solutions represent the case of explosions in shallow water. The form of the initial disturbance and the analytical solutions (Le Mehaute and Wang, 1996), are illustrated in Table 5.3.

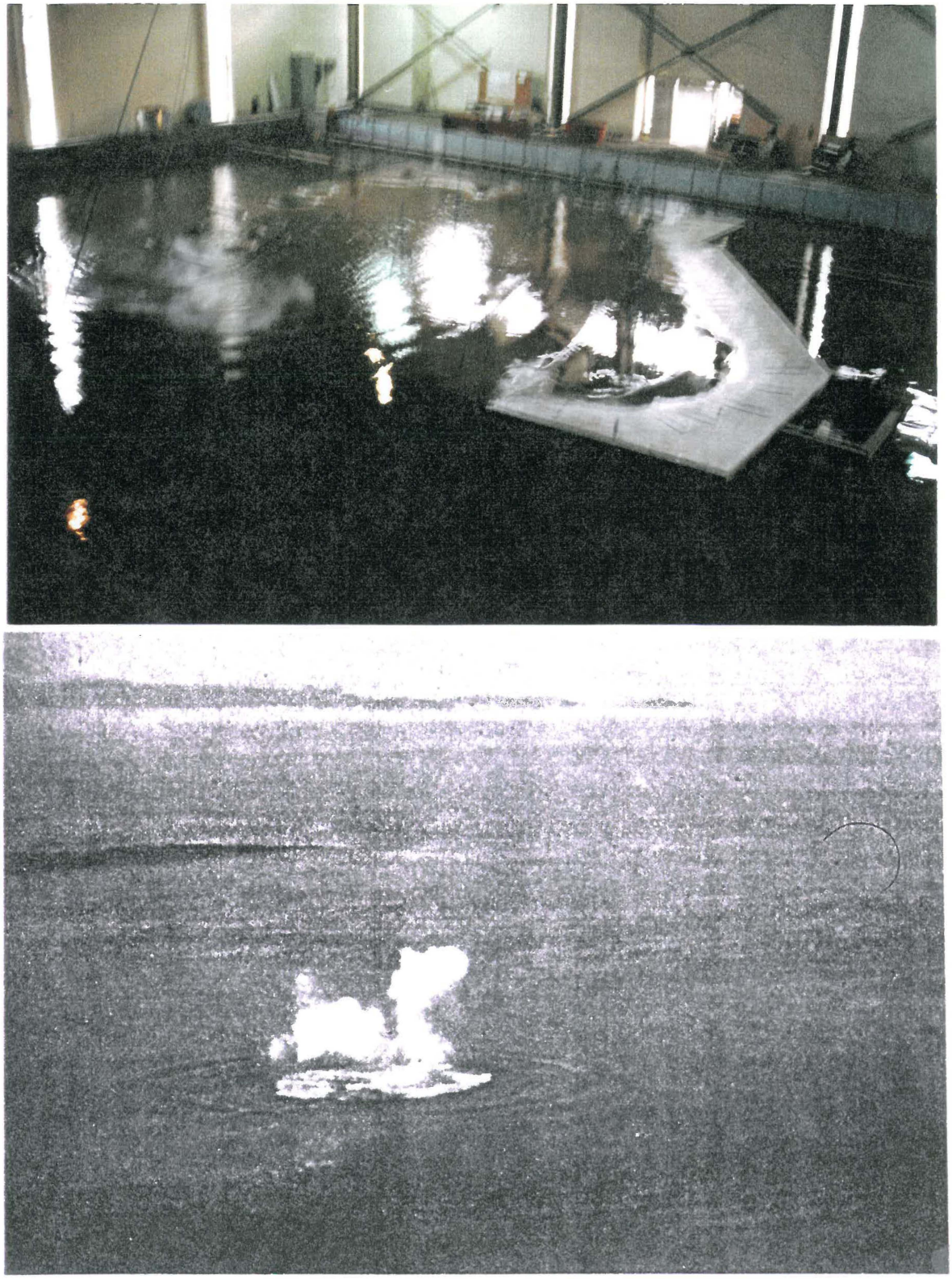

Figure 5.9. The typical wave formation produced by a point source mechanism is consistent with the aerial photograph of Eruption 1929 of Anak Krakatau. There are clear concentric eruption-waves emanating from the eruption point (Simkin and Fiske, 1983).

Experiments with Chamber

The function of chamber for these experiments was to represent the body of the volcano. The explosive was put in the center of the chamber which was then destroyed by the explosion. This method formed larger craters than the point source explosion. The intensity of the explosion (in decibels) was also much higher. We found from this experiment that as the scale of explosion increased, the force of the explosion was not the main mechanism generating the waves. Instead the caldera formation due to destruction of chamber plus the explosion generated crater became the main mechanism. Increasing the explosion scale, increased the explosive force blowing the chamber to pieces radially, but this extra energy was not transferred directly into the water to generate the waves. Further, when pieces of chamber fell into the water, they generated secondary waves which disturbed and reduced the main wave field.

During these experiments, the atmospheric pressure forces from the larger explosions (7 - 9 tubes) did not produce the main single wave as observed with lower intensity explosion. This suggests that the whole water surface of the wave basin was within the influence of the pressure forces. The waves were generated mainly by the crater formation, as occurred with the point source mechanism, but the craters were larger. In this situation, the water surged into the crater and then rushed back to generate the first wave, followed by the second and third waves. Non-linearity phenomena were obvious and recorded by the video.

Free Fall Circular Plate

Nonlinear shallow water waves were also generated by dropping a circular plate to simulate waves like those produced in an explosion (Le Mehaute and Wang, 1996). For these experiments, the dropping a circular plate into the caldera simulated the waves produced by the collapsing of a rising ash column when it loses upward momentum. Several experiments were performed by changing the initial height of the circular plate to represent different ash column heights.

Results from these experiments shows that, very high waves can be generated by this mechanism. The first waves generated have longer periods than the second, third and fourth waves. A part from the initial wave, the waves generated were non-linear and easily dispersed.

Table 5.3. The form of initial disturbance with analytical solution (Le Mehaute and Wang, 1996)

Cases	Initial disturbance η_0, w_s, I	Initial conditions η_0, w_s, I	Hankel transform $\bar{\eta}_0, \bar{w}_s, I$	Vol.* πR^2	Energy* $2\pi\varrho g R^2$
1	uniform 	$r_0 \leqq R_0 = R \quad -1$ $r_0 > R_0 = R \quad 0$	$-\frac{R}{k} J_1(kR)$	1	$\frac{1}{4}$
2	parabolic 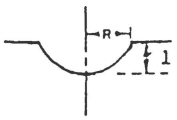	$r_0 \leqq R_0 = R \quad \left(\frac{r_0}{R}\right)^2 - 1$ $r_0 > R_0 = R \quad 0$	$-\frac{2}{k^2} J_2(kR)$	$\frac{1}{2}$	$\frac{1}{12}$
3	parabolic zero volume 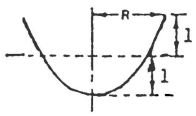	$r_0 \leqq R_0 = R \quad 2\left(\frac{r_0}{R}\right)^2 - 1$ $r_0 > R_0 = R \quad 0$	$-\frac{R}{k} J_3(kR)$	0	$\frac{1}{12}$
4	quadric zero volume 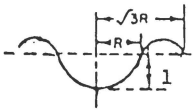	$r_0 \leqq R_0 = \sqrt{3}R$ $-\frac{1}{3}\left(\frac{r_0}{R}\right)^4 + \frac{4}{3}\left(\frac{r_0}{R}\right)^2 - 1$ $r_0 > R_0 = \sqrt{3}R \quad 0$	$-\frac{4}{k^2} J_4(kR)$	0	$\frac{1}{10}$
5	hyperbolic 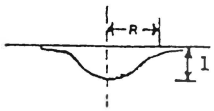	$-\frac{R^3}{(R^2 + r_0^2)^{3/2}}$	$-R^2 e^{-kR}$	2	$\frac{1}{8}$
6	Gaussian 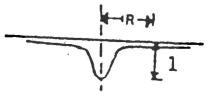	$-\exp\left[-\left(\frac{r_0}{R}\right)^2\right]$	$-\frac{R^2}{2}\exp\left[-\left(\frac{kR}{2}\right)^2\right]$	1	$\frac{1}{8}$
7	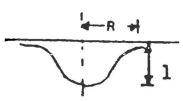	$-\frac{n! R^{n+1}}{(R^2 + r_0^2)^{\frac{n+1}{2}}} \times P_n\left[\frac{R}{(R^2 + r_0^2)^{1/2}}\right]$	$(kR)^{n-1}\exp(-kR)R^2$		

* These two columns are for free-surface elevation η_0 only.

Geological Significance,

A single large explosion could not produce the observed waves from the Krakatau 1883 event. If a super violent explosion did occur during Krakatau event, then the water waves (tsunamis) that caused devastating effects on the surrounding coastal land were not caused by direct transfer explosive forces. Instead a sequence of one or more pyroclastic flows, or a collapsing column in and arround the Krakatau island complex are the most likely mechanism causing the largest tsunami. The occurrence of the Calmeyer and Steers shallow area on Krakatau event 1883 can be explained by pyroclastic flow experiments with coarse sand and mud with steep entry angle ($\geq 60^{o}$). These experiments produced a most close to source and a compact deposit containing much of the flow material at a distance.

5.8. References

Bonnecaze, R.T., Huppert, H.E., and Lister, J.R.,(1993), Particle-driven gravity currents. Journal of Fluid Mechanics. Vol.250.p. 339-369.

Cas, R.A.F., and Wright, J.W.,(1991), Subaqueous pyroclastic flows and ignimbrites: an assessment, Bulletin Volcanology. Vol.53. p.357-380.

Camus, G., and Vincent, P.M.,(1983), Discussion of a new hypothesis for the Krakatau volcanic eruption in 1883., Journal of Volcanology and Geothermal Research. Vol.19. p. 167-173.

Camus, G., and Vincent, P.M.,(1986), Discussion : The origin of the 1883 Krakatau tsunamis by P.W. Francis., Journal of Volcanology and Geothermal Research. Vol.30. p. 169-177.

Carey, S., Sigurdsson., Mandeville, C.,and Bronto, S.,(1996), Pyroclastic flows and surges over water: an example from the 1883 Krakatau eruption, Bulletin Volcanology.Vol.57.p.493-511.

Deplus, C., Bonvalot, S.,Dahrin, D., Diament, M., Harjono, H., and Dubois, J.,(1995), Inner structure of the Krakatau volcanic complex (Indonesia) from gravity and bathymetry data, Journal of Volcanology and Geothermal Research. Vol.64.p.23-52.

Duffy, D.G.,(1992), On the generation of oceanic surface waves by underwater volcanic explosions, Journal of Volcanology and Geothermal Research. Vol.50. p.323-344.

Francis, P.W.,(1985), The origin of the 1883 Krakatau tsunamis. Journal of Volcanology and Geothermal Research. Vol.25., p.349-363.

Hudson, R.Y., Herrman, F.A., Sager, R.A., Whalin, R.A., Keulegan, G.H., Chatham, C.E., and Hales, L.Z., (1979), Coastal Hydraulic Models. Special Report No.5, US Army Engineer Waterways Experiment Station, Vicksburg, Mississippi.

Hughes, S.A.,(1993), Physical Models and Laboratory Techniques in Coastal Enginnering. Advanced series in Ocean Engineering. Vol.7. 568 p.

Le Mehaute, B., and Wang, S.(1996), Water waves generated by underwater explosion. Advanced series in Ocean Engineering. Vol. 10. 367 p.

Mandeville, C.W., Carey, S., and Sigurdsson, H.,(1996), Sedimentology of the Krakatau 1883 submarine pyroclastic deposits. Bulletin Volcanology. Vol.57.p.512-529.

Matthews, S.R.,(1988), The eruption of Krakatau, Wayland., Australia.

Monaghan, J.D., Cas, R.A.F., Kos, A.M., and Hallworth, M.,(1997), Tsunami generation by pyroclastic flows, Applied Mathematics Report and Preprints, Department of Mathematics, Monash University, Australia, 47 p.

Nomambhoy, N. and Satake, K.,(1995), Generation mechanism of tsunamis from the 1883 Krakatau eruption, Geophysical Research Letters.Vol.22.No.4.p. 509-512.

Sigurdsson, H., Carey, S., Mandeville, C., and Bronto, S.,(1991), Pyroclastic flows of the 1883 Krakatau eruption., EOS, Transaction, American Geophysical Union, Vol.72.No.3., p.377-392.

Sigurdsson, H., and Carey, S.,(1997), comments in article : Wave of destruction., Earth Magazine. p.28-29.

Simkin, T., and Fiske, R.,(1983), Krakatau, 1883 - the volcanic eruption and its effects. 464p. Smithsonian institution Press, Washington D.C.

Self, S., and Rampino, M.R.,(1981), The 1883 eruption of Krakatau., Nature.Vo.294.p. 699-704.

Self, S., and Rampino, M.R.,(1982), Discussion : Comments on 'A geophyisical interpretation of the 1883 Krakatau eruption.by I. Yokoyama, Journal of Volcanology and Geothermal Research. Vol.13.p. 379-386.

Sigurdsson, H., Carey, S., and Mandeville, C.,(1991), Krakatau., National Geographic Research & Exploration.Vol.7(3).p.310-327

Tinti, S., and Saraceno, A.(1993), Tsunamis related to volcanic activity in Italy, in : Tinti.S, (eds) : Tsunamis in the world, Kluwer Academic Publ.p.43-63.

Valentine, G.A.,(1987), Stratified flow in pyroclastic surges, Bulletin Volcanology.Vol.49. p.616-630

Chapter Six

MATHEMATICAL MODELLING OF VOLCANOGENIC TSUNAMIS

6.1. Introduction

In accordance with the main aim of this research, the mathematical model established earlier was applied to evaluate the possibility of tsunami generated by volcanic activity in the Auckland Volcanic Field. The results can be used as for tsunami hazard assessment in Auckland region.

The activity of Auckland Volcanic Field is elaborated in section 6.2. These results are used to define the tsunamigenic events simulated. The simulations results are then presented.

6.2. Overview of Auckland Volcanic Field.

The Auckland Volcanic Field has been active for over 140,000 years and has formed 49 small basaltic volcanoes within an area of about 360 km^2 centred on Auckland City (Figure 6.1). This field contains predominantly monogenitic volcanoes which comprise the Auckland intraplate volcanic province (Smith, 1989). The most recent eruption in the field (Allen and Smith, 1994), Rangitoto Island, occured within the last 800 years. However, there is no clear oral history or written record of the type and effects of eruptions. An understanding of the type of eruption and associated hazard are based on detailed studies and interpretation of volcanic deposits.

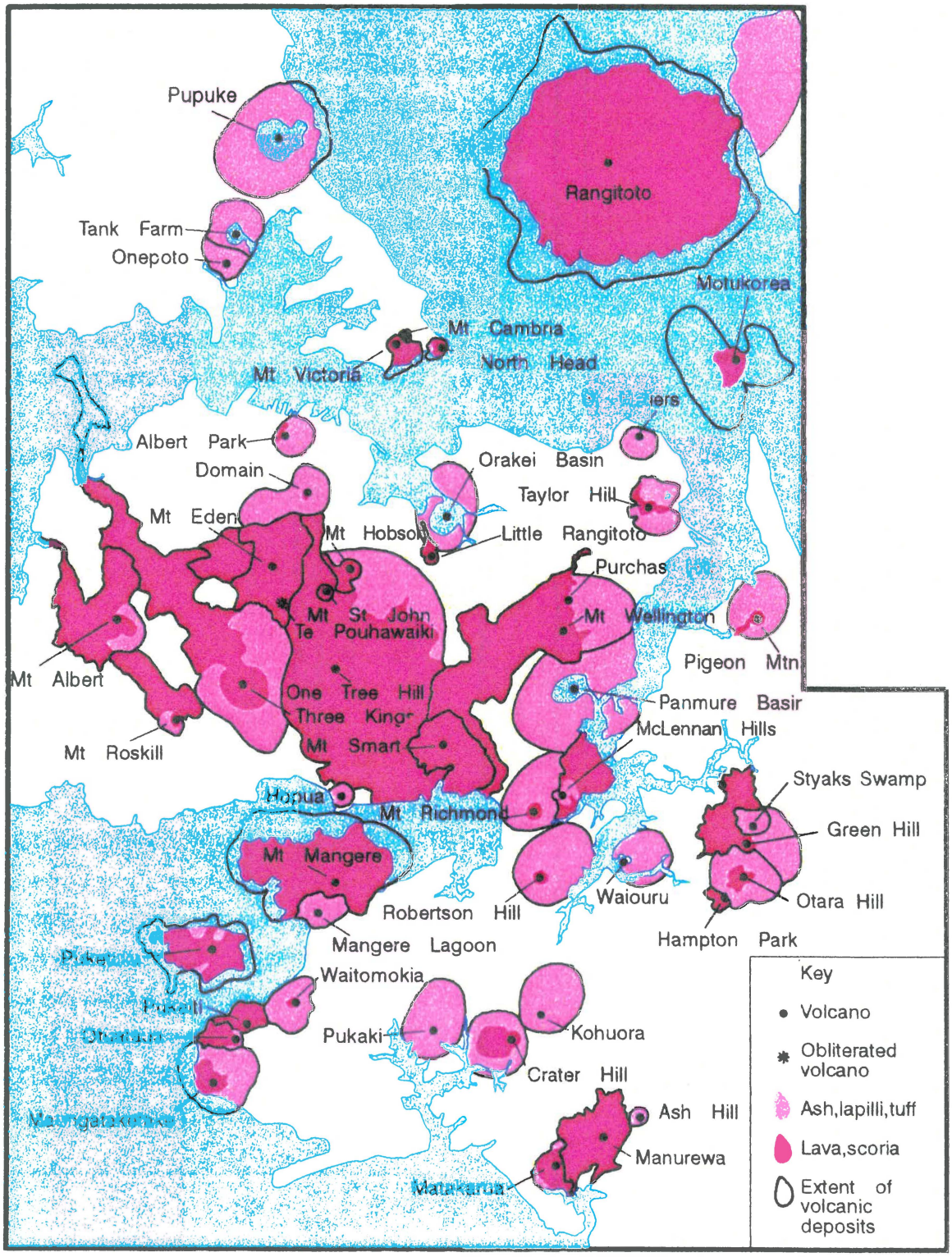

Figure 6.1. The Auckland Volcanic Field has been active for over 140,000 years and has formed 49 small basaltic volcanoes within an area of about 360 km^2 centre on Auckland (source: Nairn et al.,1996)

Eruption History

Eruptions of the Auckland Volcanic Field have occured at intervals of hundreds to thousand of years. Of the 49 eruptions, 20 have occured within the last 20,000 years and 18 of these were between 20,000 and 10,000 years ago. About 9 eruptions occured earlier than 100,000 years ago. Therefore there is no reason to believe that activity has ceased with the recent arrival of humanity (Nairn et al.,1996).

The average size of eruption can be divided into small, medium and large-sized events based on the total volume of erupted material (Smith and Allen, 1993). Five of the volcanoes (Mt Mangere, One Three Hill, Three Kings, Mt Eden and Mt Wellington) are of medium size. The largest, Rangitoto, represents 58% of the total volume of erupted material. The rest of the volcanoes are generally localised (less then a kilometre across) and the total of erupted material is small (Allen and Smith, 1993; 1994).

There are appears to be a trend towards an increase in the size of the average eruption (Figure 6.2). The medium -sized eruptions occurred between 20,000 to 10,000 years ago and the largest eruption was 600 - 800 years ago (Smith and Allen, 1993).

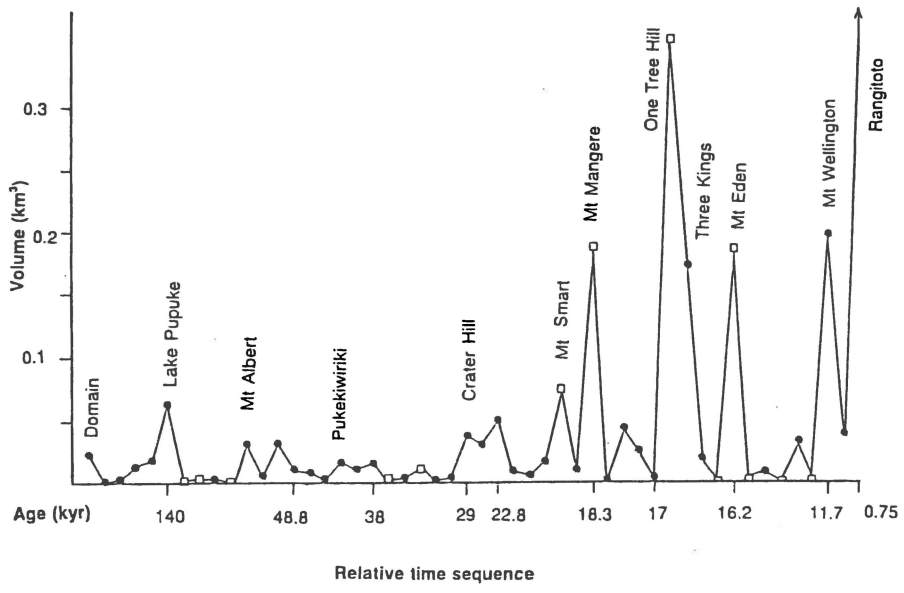

Figure 6.2. The trend towards an increase in the size of the average eruption at Auckland Volcanic Field (source: Smith and Allen, 1993).

Eruption style

Based on detailed studies and interpretation of volcanic deposits, the style of eruptions in the Auckland Volcanic Field is largely controlled by whether the vent is on land or within the sea, and by the near-surface occurrence of water -saturated sediments (Nairn et al. 1996). Past eruptions have covered a range from phreatomagmatic, caused by explosive interaction of magma and external water, to purely magmatic (involvement of external water is not siginificant). Phreatomagmatic activity occurred during 73% of the eruptions in the Auckland Field (Allen and Smith, 1993). However, evidence of changes to the eruption style during the course of an eruption is seen in many volcanic deposits (Houghton et al., 1996).

Phreatomagmatic eruptions in the Auckland Volcanic Field involve the interaction of high temperature basaltic magma and external water (surface water or groundwater) (Nairn et al., 1996). Explosive phreatomagmatic eruptions blast out pyroclastic material in the form of vertical eruption column, and a basal horizontally directed flow (base surge). The base surge is the most hazardous of all possible volcanic products from a future Auckland eruption, because it is extremely violent and moves very quickly with speeds from 15-30 m/s to 100 m/s. Examination of tephra deposits in Auckland show that surges from Auckland's volcanoes have travelled up to distances of 1.5 km or more (Allen and Smith, 1993). However, the travel distance of the surge depends on the local topography and eruption energy of the volcano.

6.3. Events Simulated

In developing simulated events for volcanogenic tsunamis in the Auckland Volcanic Field, a number of assumptions have been made. These relate to the vent location and the tsunami generation mechanism. The events are based on the previous activity in Auckland Volcanic Field and overseas (Krakatau). The generation mechanisms are pyroclastic flow, submarine explosion and maar formation.

There are 4 locations considered as having the potential to generate the tsunamis that affect the Auckland region (Figure 6.3). The scenarios developed by Nairn et al.(1996) are used for the source areas under the sea and close to the shoreline: Rangitoto Channel, and Tamaki Estuary. Another 2 areas have also been added to examine the influence of vent location: Rangitoto Volcano, and Browns (Motukorea) Island.

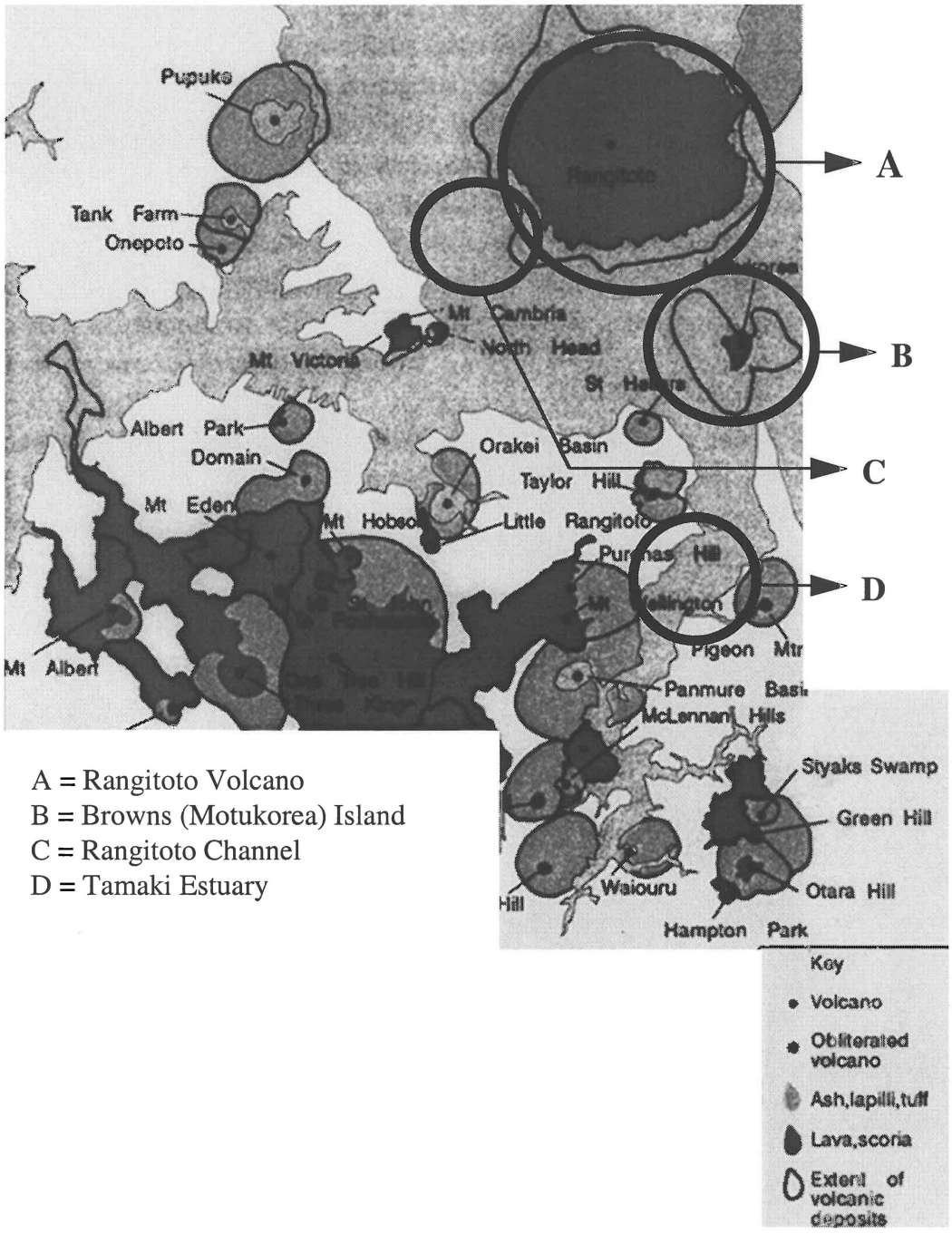

A = Rangitoto Volcano
B = Browns (Motukorea) Island
C = Rangitoto Channel
D = Tamaki Estuary

Figure 6.3. The 4 locations (A, B, C, D) considered as having the potential to generate the tsunamis and affect the Auckland region (modified from Nairn et al, 1996)

The Scenarios

- Rangitoto Channel

Vent location :	Offshore in Rangitoto Channel
Underlying country rock :	Seafloor sediments over Waitemata Group Flysch (Sandstones and mudstones)
Magma type :	Basalt
Water depth :	< 20 m
Erupted volumes:	Tehpra - 10^7 m^3; lava -10^8 m^3
Generation mechanism :	Submarine explosion, maar formation and pyroclastic flow.

- Tamaki Estuary

Vent location:	Tamaki Estuary
Magma Type :	Basalt
Underlying country rock:	Micaceous sand of tidal mudflats, over Waitemata Group Flysch (sandstones and mudstones)
Erupted Volume:	Tephra fall - 10^7 m^3, base surge deposits - $5x10^7$ m^3
Water depth :	< 5m
Generation mechanism :	Submarine explosion and maar formation

- Motukorea

Vent location :	Motukorea Island
Magma type :	Basalt
Underlying country rock :	Waitemata Group Flysch (sandstone and mudstone)
Generation mechanism :	Pyroclastic flow

- Rangitoto Volcano

Vent location :	Rangitoto Island
Magma Type :	Basalt
Underlying country rock:	Waitemata Group Flysch (sandstone and mudstone)
Generation mechanism:	Pyroclastic flow

6.4. Numerical Simulation

The TSUNAMI numerical program was applied for the events specified in section 6.3. Each simulation has different input values that depend on the local characteristics and generation mechanism. The bathymetry of the Auckland region was digitized and converted into a finite element grid mesh for the simulation using TRIGRID and TSUGRID software packages.

6.4.1. Construction of the Finite Element Grid

Bathymetry map NZ 532 was used to generate a finite element grid mesh for the Auckland region covering Waitemata Harbour, and Rangitoto Channel, including the Tamaki Estuary. The TRIGRID software package generated the finite element grid mesh automatically for this area and minimized the interpolation errors which could occur if triangular elements were not close to equilateral. The finite element grid mesh produced is illustrated in Figure 6.4 for Auckland Region, and the procedure to produce the finite element grid by using this software package is given through the following sub-section.

Preparation of Depth and Model Grids

The TRIGRID programs were needed for production of depth and model grids for generating the initial triangular finite element grid mesh for modelling use (Walters and Henry, 1995). The depth grid was developed first; its boundary nodes were obtained by sampling digitised coastlines; its internal nodes were soundings or contour samples; the spacing of the nodes was such that the surface formed by the triangular facets of the depth grid constituted a good fit to the coastlines and bathymetry of the basin to be modelled. The model grid was developed subsequently to the depth grid; it used the same boundary nodes as the depth grid, but its interior nodes are entirely different from those of the depth grid, their spacing being governed by quite different criteria.

The Depth Grid

The bathymetric information for developing depth grid is taken from bathymety map NZ 532 as both discrete form (soundings) and semi-discrete form

(contours). The digitized coastline (including islands) was used as the boundary nodes of the depth grid. Either depth soundings and /or points from digitized depth contours can be used as interior nodes for the depth grid. Therefore, the water depth is known at every vertex of the depth grid, and positive water depths are always obtained at 'wet' points.

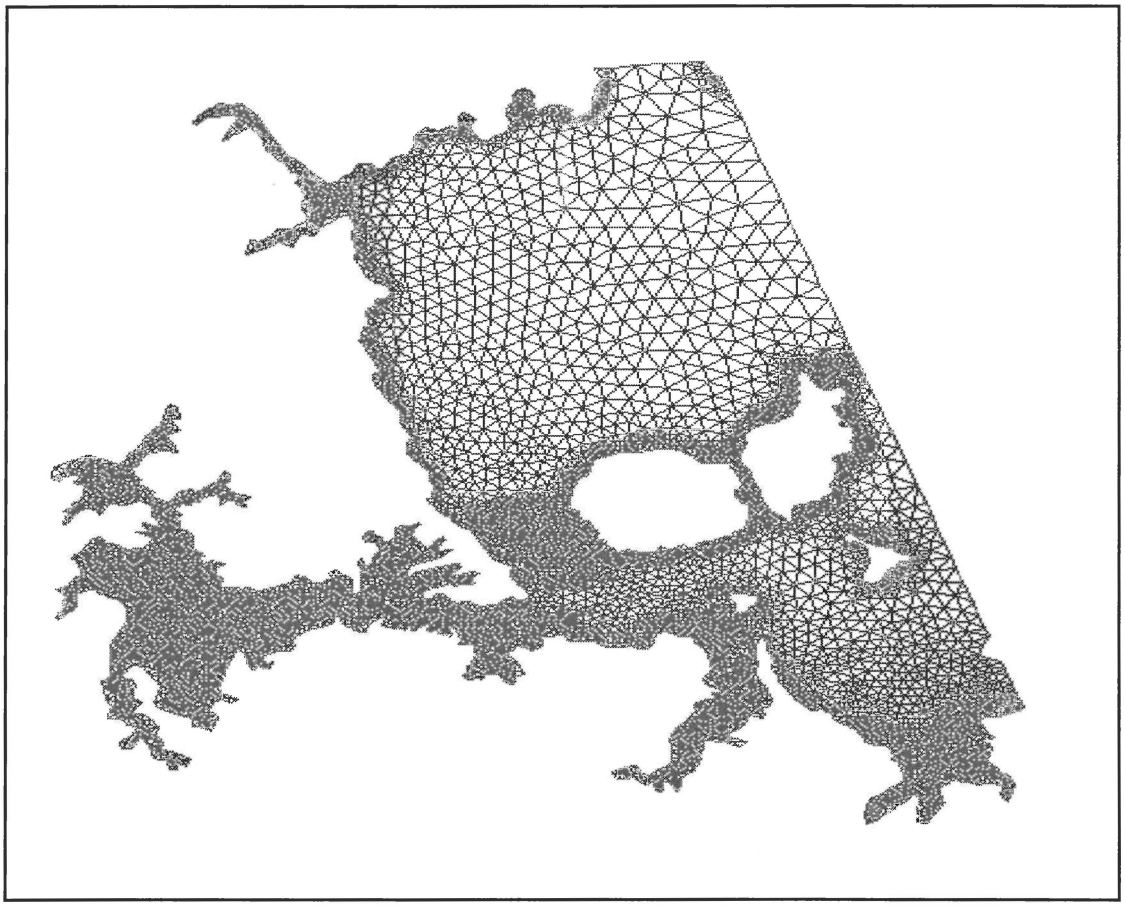

Figure 6.4. The finite element grid mesh produced by TRIGRID for the Auckland region consists of 6383 nodes, with maximum of 11 neighbours.

TRIGRID uses linear interpolation to find water depth within each triangle of the depth grid, node chosen as the basis for a depth grid should not be far apart in regions where depth is varying rapidly. Spacing of the depth grid where depth is varying rapidly, can be controlled by making sure at the digitizing stage that more contours are included in these areas and by sampling these contours at smaller intervals.

To summarise, the stages for preparing a depth grid are :

- **DIGITIZING STAGE:** any digitizing software packages can be used. For this study the TECHBASE digitizing software package was used to digitize the NZ 532 bathymetry map with output: boundaries and contours data in DIGIT format and soundings data in NODE format. The diagram can be seen below :

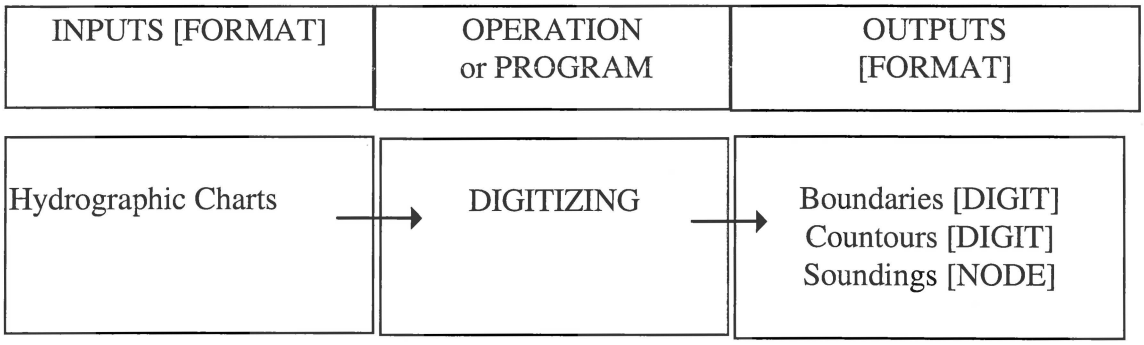

All boundaries are digitized counterclockwise and if possible, boundaries are digitized at several times the resolution required eventually for the depth or model grid boundaries (Walters and Henry, 1995). The outer boundary of the domain, made up alternately of stretches of land and open sea boundary, is digitised as an entity, so that the digitized locations of all points on the outer boundary appear in consecutive data blocks in the digitized boundary data file with the first block corresponding to a stretch of land boundary.

- **DEPTH GRID STAGE:** in this stage, all of output from digitizing stage are input to the TRIGRID program which consist of five principal programs for preparing depth grids as follows (Walters and Henry, 1995):

  SAMPLER Program:

  is used for interactive graphical selection of points from boundary and depth contour data files, in DIGIT (.dig) format, for uses as depth grid nodes. It can also accept a file of depth soundings in NODE (.nod) format for use as interior nodes. Output from SAMPLER is in NODE (.nod) format.

NODER Program:

is used for interactive graphical checking and editing of the depth nodes output by SAMPLER. Input and output are in NODE (.nod) format.

GRIDIT Program: creates a depth grid from the set of nodes output by SAMPLER or NODER, using Renka's triangulation algorithm. Output consist of an optional triangle list, in TRIANG (.tri) format, and a triangulated grid in NEIGH (.ngh) format.

EDITOR Program:

is used for interactive graphical checking and editing of the depth grid. In particular, the Editor option RETRONODE should be used to check the integrity of grid boundaries; any errors detected can be corrected using editing functions available in the Editor. Input and output are in NEIGH (.ngh) format.

DISPLOT Program:

is used occasionally for producing hardcopy plots of NODE (.nod) or NEIGH (.ngh) format files if required at any stage of depth grid production. The program is useful for checking the representation of scalar variable (usually depth) in the depth grid by using the Contour option.

In summary, the flowchart of depth grid preparation is illustrated on Figure 6.5.

The Model Grid

An irregular triangulated depth grid covering the model domain to be modelled is used to produce a model grid that suitable for use in model computation. The triangular elements of the model have the following properties (Walters and Henry, 1995):

- Elements areas should be approximately proportional to local mean water depth. This means that the Courant number and hence the computational efficiency of model calculations is roughly uniform throughout the grid. In physical terms, it means that roughly the same number of samples points per-wavelength is used everywhere.
- The shape of every element should be as close to equilateral as possible, to minimse interpolation error when functions are evaluated within triangles.

To form appropriately sized grid elements, the TRIGRID package employs a novel method of creating variably-spaced points to form the basis for triangulation.

The principal programs used for preparing the model grid are (Walters and Henry, 1995):

- ***NODER:*** extracts boundary nodes from the depth grid for further use in the model grid; creates a fine rectangular grid over the model domain and evaluates depths; groups the squares of the fine regular grid into clusters whose area is dependent on local water depth; calculates the centres of area of the clusters; and outputs these together with boundary nodes as a set of nodes for the model grid.
- ***GRIDIT:*** triangulates the set of boundary and interior nodes produced with the NODER to create a model grid, using the Renka triangulation algorithm; and outputs a grid file in NEIGH (.ngh) format and a triangle list in TRIANG (.tri) format.
- ***EDITOR:*** permits interactive monitoring and editing of the model grid; provides an option (RETRONODE) for checking the integrity of grid boundaries and editing functions for correcting any errors detected; and outputs an edited grid in NEIGH (.ngh) format.
- ***SPLITTER:*** permits interactive positioning of open boundaries and simultaneously removing unwanted portions of the model grid.
- ***REDEP:*** re-evaluates water depths at all nodes of the edited model grid by interpolation from depth grid.

In summary, the flowchart of Model Grid preparation is illustrated in Figure 6.6.

The final model grid produced consisted of 6383 nodes, with a maximum 11 neighbours (Figure 6.4). This model grid fulfills the requirement of Courant number for stability of numerical computation. The local Courant ratio cT/L (where T = the time step, L is some linear measure of element size (length or width), and c = wave speed) is keep fairly uniform over the whole grid. An example of the model grid which is covered the whole Hauraki Gulf can be seen in Figure 6.7.

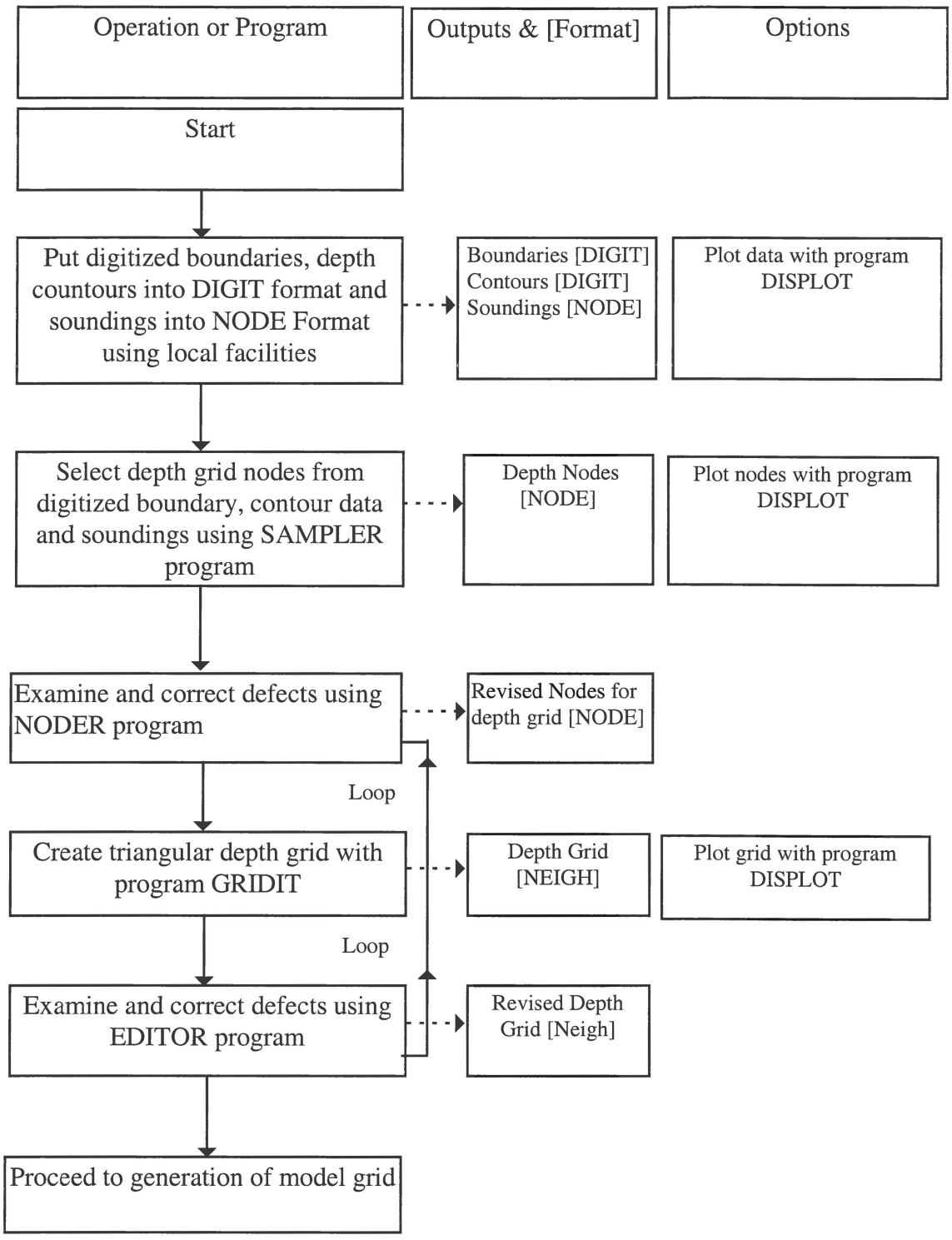

Figure 6.5. The flowchart of depth grid preparation

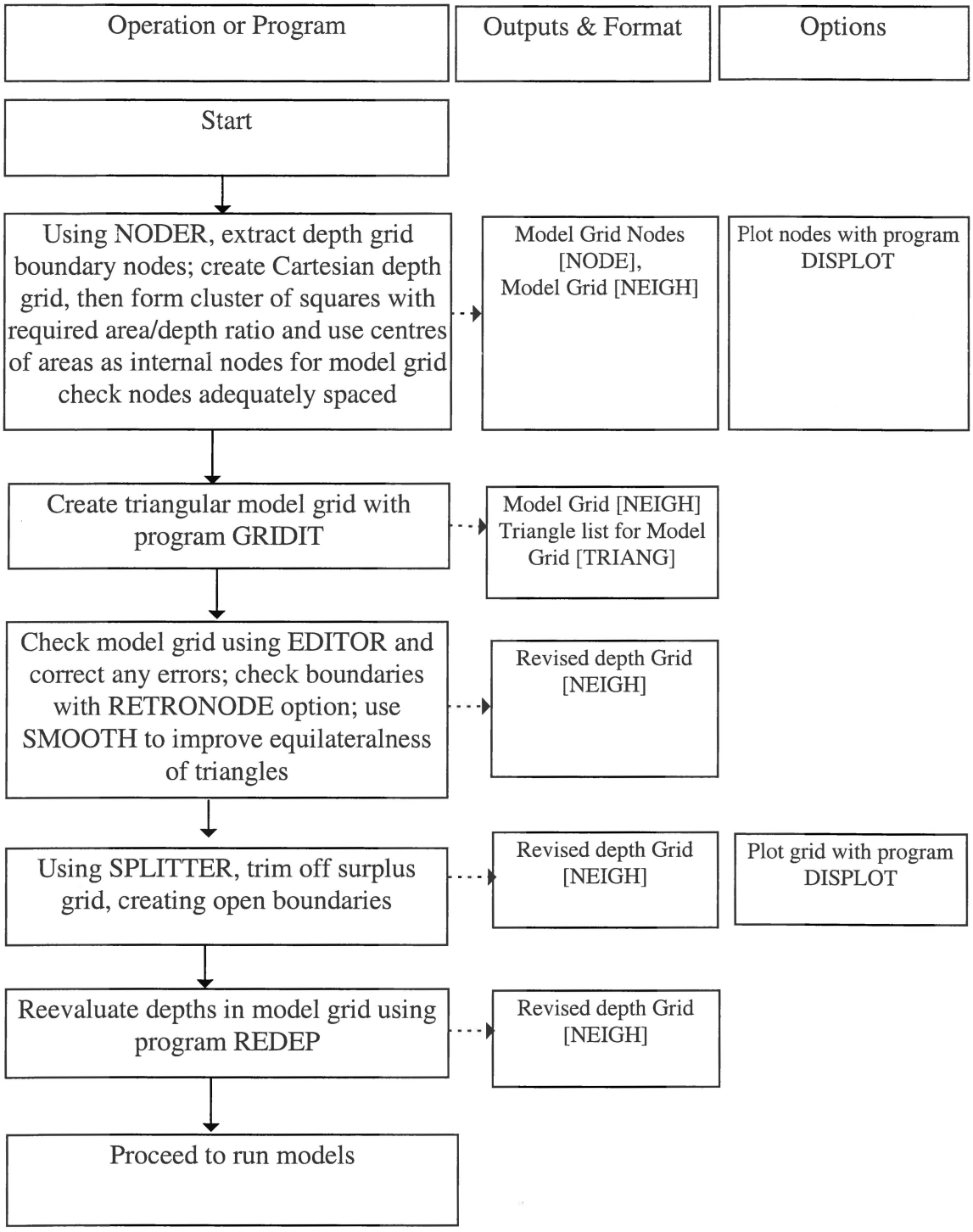

Figure 6.6. The flowchart of model grid preparation.

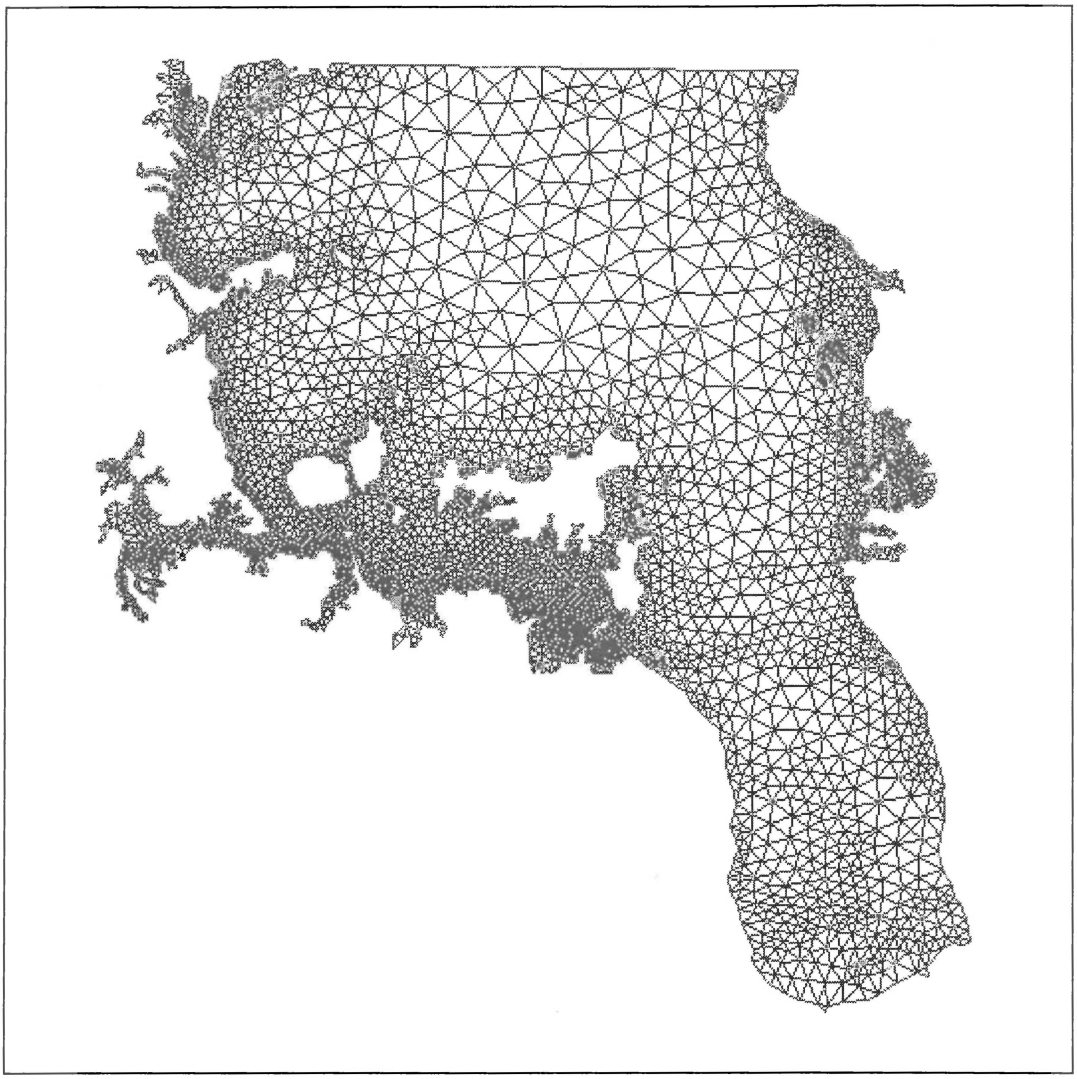

Figure 6.7. The finite element grid for the Hauraki Gulf showing that for the area with rapid change of contour bathymetry are represented by fine elements.

The TSUGRID software takes the finite element grid files generated by the TRIGRID software package. It determines the interpolation functions for the elements, and sets up a binary file containing the necessary grid information for TSUNAMI software to run the simulation. The main difference between the two grids is that TRIGRID normally defines x and y distances in kilometres and TSUNAMI requires them as metres. The TSUGRID allow the user to select an allowable error to define how similar elements must be before TRIGRID assigns them the same interpolating functions (de Lange, 1997).

6.4.2. Boundary and Initial Conditions

There are two boundaries for these simulations, land (island) boundaries and ocean boundaries. Land (coastline and island) boundaries were set up as fixed (reflective) boundaries and the ocean boundaries used the clamp method to suppress possible reflections.

The ability of TSUNAMI software to allow wetting and drying conditions was not applied to the land boundaries. Inundation is best handled by a non-linear numerical model (de Lange, 1997).

Three initial conditions of tsunami generation mechanism were used; initial condition for maar formation, pyroclastic flow and submarine explosions. Each initial condition has different characteristic as follow:

- Maar Formation

  The formation of a maar was considered to behave in a similar manner to caldera formation as modelled for Krakatau. For this simulation, the tsunami began with a fall of water surface elevations into the maar which is formed after explosion. The sea surface in the maar was set to zero or deeper than original average sea bottom on this area or the initial water displacement is downwards (negative).

- Pyroclastic flow

  For this simulation, the pyroclastic flow is treated as a horizontal piston which is represented by a sequence of wedge-shaped displacements of the seabed to include both lateral and vertical displacements (de Lange, 1983; de Lange et al., 1997). At each time step, the sea bed moves up or down as necessary to replicate the passage of the flow as on Figure 6.8 .

- Underwater explosion

  There are two initial conditions for this simulation that relate to the explosion process. First, the initial displacements are positive (upwards), forming a dome shape, and the second initial condition represents a shallow water or high energy explosion where the initial displacements will be negative or downwards in the crater and positive (upwards) around the crater.

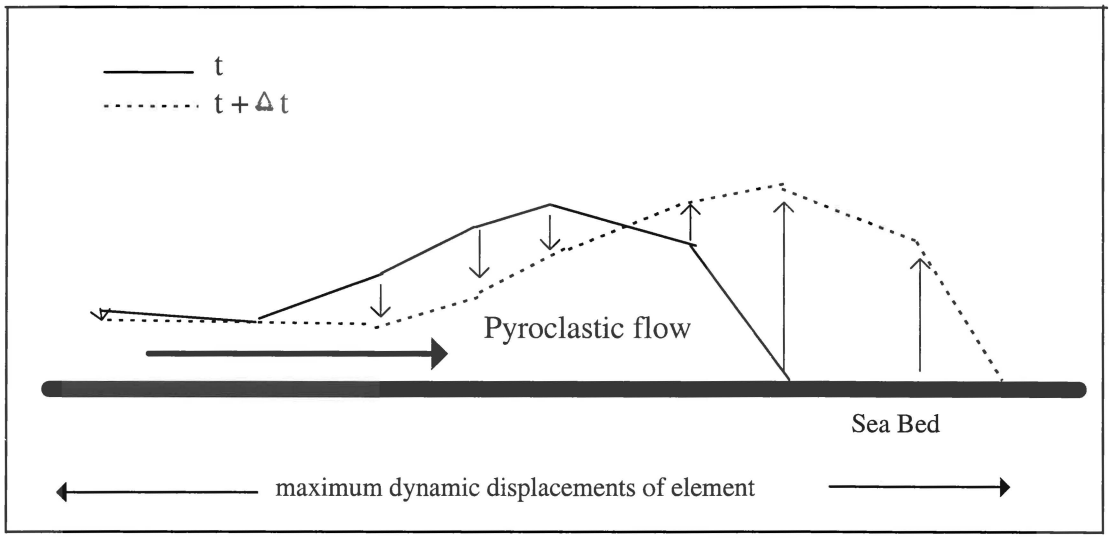

Figure 6.8. The schematic diagram of dynamic initial condition of the pyroclastic flow.

The generating of the initial conditions are defined by three parameters (de Lange et al, in press):

- The time when movement starts;
- The vertical velocity; and
- The time when movement stops.

These initial conditions are specified as a boundary condition file for TSUNAMI software. Three types of boundary conditions can be entered with this file (de Lange, 1997):

- Specified x and y velocities. The x and y velocity is fixed at various nodes. The value applies for the whole simulation. This mainly used to specify river flows entering the model. The x and y velocities are specified separately so that it is not necessary to have paired values.
- Specified elevations. This defines the nodes at which a fixed forcing period and amplitude are applied.
- Displacements. This defines the sea bed deformation responsible for generating a tsunami. TSUNAMI assumes that the sea bed deformation is directly transmitted to the sea surface.

The format of boundary file can be seen in appendix 1.

6.5. Results

6.5.1.The Initial Test

The initial tests of all three mechanism were undertaken to examine the validity of the numerical model for the generation mechanism involved. The mechanisms are submarine explosion that generates dome with single and multiple explosion, maar formation, and pyroclastic flow. A summary of the major findings is as follows:

Submarine Explosion Mechanism

The displacements of sea bottom representing a submarine explosion were assumed to generate a dome at the sea surface. The maximum height of displacement used for the Rangitoto channel was 6 m in 7.8 m water depth. The resulting dome at the water surface for single explosion reached up to 7.5 m height. The height of water surface at the center of dome decreased quickly, and became 2.4 m after 1 minute's simulation. These results showed that a single explosion with dome formation generates concentric waves that easily disperse. Figures 7 and 8 (Appendix.1) shows the waves one and five minutes after explosion. The leading waves for this mechanism are known as a positive waves.

Multiple explosions produce a higher wave compared to a single explosion (Appendix.1. Figures 1-20). The time gaps between explosions are critical and give a different effect on the waves generated near to the source and shoreline (Appendix.1. Figures 19-20). Two explosions with the same dome dimension were used. A shorter time gap had more influence on wave characteristic close to the source. As the dome height at the source became higher, waves around the generating area were absorbeb by the rising up of the water. A longer time gap gaves sufficient time for waves to move away from the generation area and propagate into the shoreline. Resonance occurred if there was sufficient time for the wave reflected back from the shore to interact with the wave generated by the last explosion.

Since the model is governed by the linear shallow water equation, the non-linear phenomenon of the generation processes are not represented very well. The model cannot produce highly non-linear motion in the very short time that usually occurs at the initial stage of a shallow submarine explosion.

Maar Formation

Maar formation is represented by inputting a negative displacement of the sea surface. The location and dimensions of the maar was assumed to be the same as the submarine explosion test, where maximum displacement was - 6.0 m. The results of the model run showed that the water surged into the maar formation and only a small part of the water rushed back out from generation area. The model failed to generate water jet above the sea level as shown on physical modelling test (Appendix.2.), which is important as an additional force for wave generation. However, there was a concentric sequence of negative sea surface disturbances generated. Using - 6 m initial displacement, the maximum of sea recession along the coastline were 10 cm and disappeared in 5 minutes (Appendix.1. Figures 21-28). With these results, the model only shows the effect of maar formation on the coastline as recession of water levels.

Pyroclastic Flow Mechanism

The dynamic initial condition based on physical mechanism of pyroclastic flow (de Lange, 1983; de Lange et al., in press) was used in modelling. The methodology is intended to simulate the flows that cause an initial upward displacement with variable uplift velocity. These dynamic displacements followed the physical modeling results.

The finite element grid close to the coastline starts with rapid negative displacements, followed by the positive displacements. The vertical velocity involved in the positive displacements for these elements is slower than the negative displacements. Velocities were determined by using the duration time of the pyroclastic flow entering the sea. In general, the highest uplift velocity is applied at the distal margins of the flow, and the lowest velocities close to the coastline (or the source).

The simulation results showed that the dynamic initial condition produced larger waves compare to the static water surface displacement, and also it propagated at higher speed. Directionality of the flow is clearly evident (Appendix.1. Figures 29-30 and Figures 59 - 63) and is a function of water depth, wave height and the dynamic uplift velocity. In general, the main direction of the flows is along the semi-major axis of the flows where the flow had the maximum thickness. The numerical model results

showed that to produce a real 'high speed flow' of pyroclastic flows, the horisontal component of dynamic uplift velocity will have to be considered, and finer grid elements sizes are needed for generation area to have a reasonable dynamic uplift velocity distribution of the flows.

The physical modelling results (chapter 5) showed the effects of horizontal force along the flows. These horizontal forces speed up the flows and propagation of the waves and were not included in this numerical model.

6.5.2. Events Simulated Results

Four locations were considered as having the potential to generate tsunamis and affect the Auckland region. The results of numerical modelling are explained as follow:

RANGITOTO CHANNEL

Submarine Explosion Scenario

For submarine explosion in the Rangitoto channel, the maximum water depth at the source of explosion is 11 m. Two explosions were used with time gaps between explosions of 5 minutes. The first explosions consist of two overlapping explosion within 5 seconds. First explosion used maximum initial sea bottom displacement with dome shape of 6 m at the center. Start time from 0 to 3 seconds. Second explosion used 6 m with start time 0 to 5 seconds. This overlapping explosion generated a dome shape at the sea surface in the Channel with maximum height at the center of dome of 21.2 m

Five minutes after the first explosion, a second overlapping explosion is initiated 30 seconds after the collapsing of 'caldera' at the sea bottom. The collapsing of caldera takes 3 seconds with maximum depth - 6 m. The vertical displacement of the first explosion takes 4 seconds to reach 5 m maximum dome height at the sea bottom and second explosion start at the same time with 5 seconds duration to reach 7 m of sea bottom displacement. This explosion formed a dome at the sea surface in the Channel with maximum height at the center of dome of 21.0 m. The time history of the submarine explosion is illustrated in Figure 6.9.

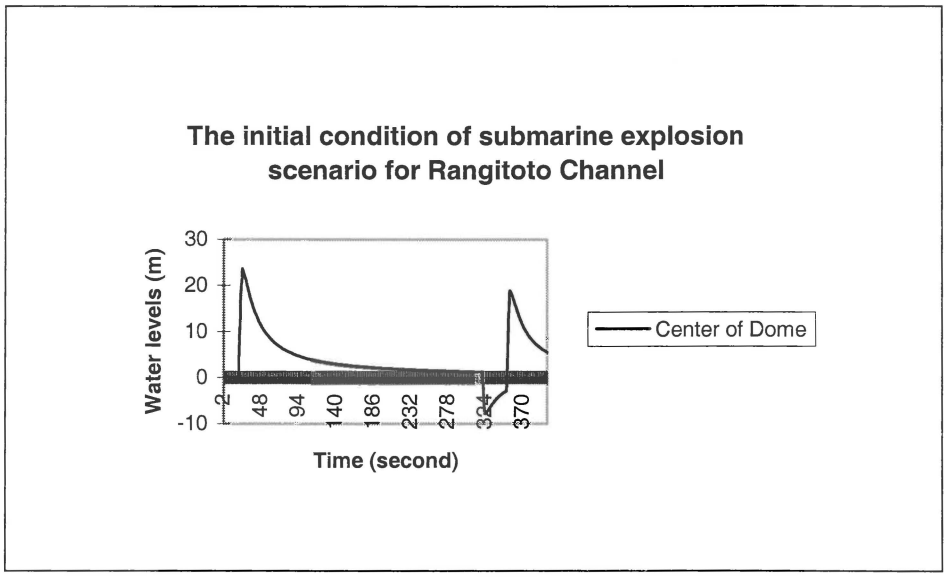

Figure 6.9. The time history of the submarine explosion with multiple explosion and collapsing of caldera.

Waves

One minute after the first explosion (Appendix.1. Figure 33), the first wave propagated radially from the source and hit both sides of the channel. Within one minute, the coast from North Head to Takapuna Beach are flooded with waves whose height varies from 0.4 m to 2.7 m. At the same time the wave height along the west coast of Rangitoto island varies from 0.4 m to 1 m.

Within three minutes (Appendix.1. Figure 34) the waves reach the South coast from St.Heliers Bay to Okahu Bay with waves from 0.29 m to 0.57 m, and at Devonport Beach to North Head from 0.29 m to 1.7 m. Narrow Neck Beach, Takapuna Head and Cheltenham Beach are still affected by high waves from 1.2 m to 2 m. Large waves are also present at Coastguard Bay, Rangitoto Island.

Five minutes after the first explosion (Appendix.1.Figure 34), the sea surface dropped at the center of the explosion due to caldera collapse. At this time, 1 m waves height at the areas from Narrow Neck to Cheltenham Beach, and 0.12 m at Milford Beach, Hobson Point, Devonport Beach and Browns Island.

One minute after the last explosion (Appendix.1. Figure 36) the highest waves hit both sides of the Channel varying from 1 m to 3 m. At Mechanics Bay the wave heights reach 0.1 m. After 10 minutes, the waves reach the mouth of Tamaki Estuary and Wharf area in Auckland with 0.1 m heights (Appendix.1.Figure 39).

The maximum extents of the tsunami occurs 30 minutes after the last explosion (Appendix.1. Figure 40). The water level varies from 0.27 m in the mouth of Waitemata Harbour to 0.4 m close to the Auckland Harbour Bridge. Tamaki Estuary has also flooded and it is evident from Figures 41 to 44 in Appendix.1., the seiching occurs in Shoal Bay and Tamaki Estuary.

The pattern of waves propagation suggests that edge waves (Mach stem waves) occurred along the eastern coast and propagated up to the north. The current patterns also suggest edge waves with strong currents flowing along the coastline. Through the pattern of current propagation, bore formation possibly occured in Waitemata Harbour and Tamaki Estuary, although the model cannot handle non-linear bores.

Currents

Strong currents are generated during the initial stage of the explosion. One minute after the explosion the current speeds reach 1 m/s at Takapuna Head (Appendix.1. Figure 45). Due to the geometry of the region, the current flow is divided into two main directions; to the south and to the north. To the north, the currents flow faster along the coastline from Takapuna Head up to Torbay and also around Rangitoto Island (Appendix.1.Figures 46-53). To the south, the main direction of the flow heads towards St.Heliers Bay, and only a small part of the water mass flows into the mouth of Waitemata Harbour.

The existance of Browns (Motukorea) Island is significant for the flow pattern in this region. This island diverts the flow into the Tamaki Estuary (Appendix.1. Figure 50) and protects the area behind the island. This results in possible flooding of areas around the Estuaries and oscillation of the water level, (seiching).

Maar Formation

The initial test results showed that the numerical model cannot adequately reproduce this mechanism. However, the model does show some of the effects of maar formation in terms of the changing of water levels along the coastline. Current patterns also showed that for the first three minutes there were strong currents directed to the center of the maar (Appendix.1.Figures 26 and 27).

RANGITOTO VOLCANO

- **Pyroclastic Flow Scenario**

For the pyroclastic flow scenario the flow was directed towards the mouth of Waitemata Harbour. Dynamic initial displacement was used as the initial condition for the pyroclastic flow. The maximum vertical displacement of the sea bottom in the generation area was 9 m, and duration time of the displacement was 5 seconds.

After one minute simulation, the radial distribution of the flow is evident. At this time a 0.05 m wave reached North Head and and St. Heliers Bay. The current pattern in Figure 65 (Appendix.1) shows that after 5 minutes, the wave propagated mainly to the northwest through the Rangitoto Channel, and to the southeast to Tamaki Estuary. The bathymetry in the mouth of Waitemata Harbour bends the flow towards those regions. With this pattern of propagation, bore formation most likely occurs and bores will propagate through Rangitoto Channel to the north, and to Tamaki Estuary in the south.

Within 10 minutes the leading waves (0,1 m height) reach Milford Beach, Devonport, Orakei Bay and Bucklands Beach in Tamaki Estuary (Appendix.1. Figure 66). Strong currents flow along the coastline. The distribution of the flow is almost uniform. The current speed reduced after 20 minutes, and 0.1 m waves reached Auckland Harbour and Half Moon Bay in Tamaki Estuary (Figure 67. Appendix.1.).

BROWNS (MOTUKOREA) ISLAND

- **Pyroclastic Flow Scenario**

For this scenario the main direction of the pyroclastic flow is to the west. The duration to reach the maximum displacement of 7 m at the sea surface was 2 seconds. The pattern and direction of the flow (waves and currents) generated by this mechanism can be seen on Figure 59- 63 (Appendix.1). It is clear that the radial distribution of the flow to the west has been influenced by the shallow bathymetry condition of this area.

Fast moving waves and currents enter Tamaki Estuary and Rangitoto Channel after one minute as shown in Figure 60 (Appendix.1). At the mouth of Tamaki Estuary there is a concentration of the flow, and after 5 minutes 0.4 m waves hit the area from the mouth of the Estuary up to Sandy Point. To the north the waves started to enter the

Rangitoto Channel and mouth of Waitemata Harbour, and to the south the waves propagate with almost the same speed. Of interest is that after 60 minutes, the waves travel most of the way to the north of the grid with height 0.02 m, as well as to the head of Waitemata Harbour (Figure 63 Appendix.1). In Tamaki Estuary seiches occurred with water levels reaching 0.3 m.

TAMAKI ESTUARY

- **Submarine Explosion Scenario**

For a submarine explosion in Tamaki Estuary, the maximum water depth at the center of the explosion is 5.2 m. An overlapping explosion used sea bottom displacements with a dome height of 1.8 m in 3 s for first explosion, and 2.8 m in 5 s for second explosion. The explosions start at the same time. This overlapping explosion generates a dome at the sea surface in the Estuary with a maximum height at the center of dome of 5.5. m. Because of the geometry of the Estuary, waves and currents generated by the explosion propagate into two directions: upstream and downstream.

After one minute from the explosion the dome height at the center decreased and became 1.4 m. In the Half Moon Bay the wave height was 0.8 m to 1.1 m and at the Buckland Beach and Sandy Point Beach it was 0.2 m. In the upstream areas the waves propagate and reach Wakarunga Creek area with 0.2 m height. After five minutes, waves with height 0.1 m reach the end and the mouth of the estuary. Currents flow faster in downstream direction, but at the upstream end slack water occurs when the water levels become 0.32 m after 15 minutes. After 20 minutes from the explosion, flow in the Estuary is all directed toward the mouth of the Estuary (downstream).

6.6. References

Allen, S.R., and Smith, I.E.M., (1994), Eruption styles and volcanic hazard in the Auckland Volcanic Field, New Zealand., Geoscience reports of Shizuoka University 20:p.5-14.

de Lange, W.P.(1983), Tsunami Hazard: an investigation into the potential tsunami hazards of the Bay of Plenty Region using numerical models. M.Sc., University of Waikato, Hamilton. 275 p.

de Lange, W.P.,(1997), Tsunami Manual., Dept. of Earth Sciences.,University of Waikato. New Zealand.

de Lange, W.P., Prasetya, G.S. and Healy, T.R.(in Press), Modelling of Tsunamis generated by pyroclastic flows (Ignimbrites).

Houghton, B.F., Wilson, C.J.N., Rosenberg, M.D., Smith, I.E.M.,Parkes, R.J.,(1996), Mixed deposits of complex magmatic and phreatomagamtic volcanism: an example from Crater Hill, Auckland, New Zealand. Bulletin of Volcanology 58. p. 59-66.

Nairn, I.A., Johnston, D.M.,and Thordarson, T.,(1996), Eruption scenarions for auckland Volcanic Field, Institute of Geological and Nuclear Sciences.

Smith, I.E.M, (1989), North Island., in : Johnson, R.W.,Knutson J.,and Taylor S.R.(eds.), Intraplate volcanism in eastern Australia and New Zealand, p. 157-162, Cambridge University Press, Cambridge, UK.

Smith, I.E.M., and Allen, S.R., (1993), Volcanic Hazards at The Auckland Volcanic Field: Volcanic Hazards Information series, No. 5, CD 304., Ministry of Civil Defence.25.p.

Tinti, S., and Saraceno, A.(1993), Tsunamis related to volcanic activity in Italy, in : Tinti.S, (eds) : Tsunamis in the world, Kluwer Academic Publ.p.43-63.

Walters, R.A., and Henry, R.F.,(1995), TRIGRID Users Manual GKS version, 121 p.

Weir, G.J., and White, S.P.,(1982), Mathematical modelling of volcanic tsunamis. New Zealand Journal of Marine and Freshwater. Vol.16. p. 373-382.

Chapter Seven

CONCLUSIONS

7.1. Introduction

Tsunamis generated by volcanic eruptions are much less frequent than tsunamis produced by submarine earthquakes. A review of volcanic tsunamis with particular reference to the Krakatau event 1883 identified 10 main mechanisms may account for tsunami generation. Four of these - caldera collapse, debris avalanches, submarine explosions and pyroclastic flows- have been suggested as the mechanisms that produce the largest tsunamis.

Physical (scale) and numerical modelling approaches provided the methodology to understand the physical processes of volcanogenic tsunamis. The results can be used to develop predictive tools for volcanogenic tsunami hazard assessment.

7.2. Major Findings

Previous studies have suggested several alternative mechanisms to account for the largest tsunamis formed during the 1883 Krakatau eruption (caldera collapse, debris avalanches, submarine explosions and pyroclastic flows). Physical and numerical modelling have provided useful insights into the actual mechanisms and the characteristics of the tsunami waves produced. The findings support the hypothesis developed by Sigurdsson et al. (1991) from geological evidence that the largest Krakatau tsunamis were generated by pyroclastic flows.

The findings on tsunami generation processes made by this study are as follows:

- **Submarine explosion mechanism**

A single explosion cannot produce a high wave. As the size of the explosion increased, the efficiency decreased markedly once the radius of the explosion bubble exceeded the water depth. The maximum wave height produced was less than that observed at Krakatau in 1883. The efficiency of the submarine explosion mechanism is increased by using a sequence of smaller explosions, instead of one large explosion. However the timing between explosions is critical; if the explosion are too close together or too far apart, the efficiency decreases. Based on the numerical modelling it is considered that the optimal timing will vary with water depth and explosive yield.

- **Pyroclastic flow**

Waves can easily be generated by gravity flows entering the water, regardless of the slope. The wave properties depend on the relative densities of the flow and the receiving body, and the velocity of the flow. The angle of entry of the flow into the water determines the deposition pattern of sediment: at low angles the nexus of deposition is at the base of the slope; and this moves further away from the shore as the slope angle increases. This behaviour accounts for both the moat evident around the base of the former Krakatau volcano, and the shallow Steers and Calmeyer shoals. In the physical tests, the less dense material from the pyroclastic flow propagates near the water surface for long distance. This is consistent with evidence from Krakatau. Although the tests were not performed, it is probable that multiple smaller pyroclastic flows will produce larger waves than a single large one. Numerical modelling of single pyroclastic flows demonstrates that the resulting tsunami is highly directional, with the largest wave heights along the axis of the flow. Physical modelling of column collapse using a free-falling circular flat plate produced a radially uniform 'flow'. The distribution of ignimbrite produced by Krakatau in 1883 is fairly uniformly distributed around the source, although there is some indication of thicker flows being directed towards the northeast and west. This suggests multiple pyroclastic flows flowing radially from the eruption column, with possibly large late phase flows (occuring just before caldera collapse) being preferentially directed towards the northeast and west. These late flows were responsible for forming the largest tsunami waves.

- **Caldera collapse**

The efficiency of this mechanism to generate a wave is dependent on the 'collapsing time' and the volume of the caldera. A very sudden collapse with appropriate caldera dimensions could produce significant waves. This mechanism starts with the dropping of sea level around the area, producing an initial negative wave displacement.

From these findings, if a super violent explosion did occur during the 1883 Krakatau eruption as suggested by reports in the historical record, then the water waves (tsunamis) that caused the devastating effect on the surrounding island were not caused by the direct transfer of explosive forces. Instead a sequence of one or more pyroclastic flows, resulting from a collapsing eruption column, in and around the Krakatau complex are the most likely mechanism causing the largest tsunami. The formation of the Steers and Calmeyer shoals by the 1883 Krakatau event was reproduced by the pyroclastic flow experiments using coarse sand and mud with steep entry angle ($\geq 60^{o}$). This simulation also left the moat evident in the present bathymetry.

The numerical modelling of volcanogenic tsunamis from the Auckland Volcanic Field showed that volcanic tsunamis are not a major threat to Auckland. However under suitable conditions a volcanic eruption could produce moderately large tsunamis that generate strong currents. The maximum impact occurs along shores close to the source of the tsunami. The modelling presented in the preceding chapters represent the worst possible scenarios. Therefore it is unlikely that any coastal region will experience wave heights much larger than 1 m.

Of interest was the consistent development of trapped waves (edge waves) along the North Shore beaches, and the seiching within Tamaki Estuary. Tamaki Estuary has shown an amplified response to historic teletsunami, so this may be a fundamental behaviour of the estuary.

7.3. Implications for Civil Defence

The numerical modelling of volcanogenic tsunamis for the Auckland Volcanic Field has some implications for the local Civil Defence:

- Phreatomagmatic eruptions are the most common eruptive style. These typically form maars by a series of explosions as evidenced by the layering in the surrounding tuff rings. The modelling shows that a series of explosions is the most efficient explosion mechanism. If the timing between eruptions is optimal then quite large tsunamis can be generated (up to 20 m at source) that can have a significant impact on nearby shores.
- Modelling for pyroclastic flows from Browns Island shows that an eruption in shallow water will have a bigger impact than a deeper water site, such as Rangitoto Channel.
- The tsunamis produced will reach the shore within minutes of the eruption, but can persist for up to an hour. The tsunami travel further along the deeper water open coasts, than within the shallow Waitemata Harbour.
- Tamaki Estuary was affected by all the sources considered. The Estuary seiched readily, which amplified the tsunami waves at antinodal points. Therefore the Tamaki Estuary is likely to show a significant response to any tsunami.
- Overall the hazard associated with volcanogenic tsunami in Auckland is low.

7.4. Further Research

There are some obvious directions for further research suggested by the findings of this study. These include:

- There is a need to develop a three-dimensional pyroclastic physical model that can replicate the observed behaviour of pyroclastic flows. In particular field observations demonstrate that column collapse produces multiple flows that may head in different directions (ie. pulsed gravity flows). The best this study could achieve was a uniform radial flow.
- The physical model results should be used to improve the numerical model approach to pyroclastic flow simulation. The dynamic vertical displacement

approach used does not adequately account for the horizontal impulse forces evident in the physical model.

- There is a need to develop a numerical approach to account for the central jet observed in the physical submarine explosion and caldera collapse results. This is a non-linear phenomenon which is not well represented by the linear numerical model.
- The numerical model should be applied to the Krakatau 1883 eruption.

7.5. Reference

Sigurdsson, H., Carey, S., Mandeville, C., and Bronto, S.,(1991), Pyroclastic flows of the 1883 Krakatau Eruption., EOS, Transactions, American Geophysical Union., Vol.72.,No.36. p.377-392.

APPENDIX.1.

File Desription and Simulation Results

TRIGRID File descriptions:

Digit (.dig)
Node (.nod)
Neighbour (Neigh) (.ngh)
Triangle (.tri)

TSUNAMI files:

Command File
Boundary Condition File
Time History File

Simulation Results

(All plot Contours in meter)

TRIGRID FILES:

DIGIT (.dig)

A digit file consists of a set of lines representing either boundaries or contours. Digit files are used as input to the Sampler program, which support subsampling of the digitized files.

The digit file format is an historical format, closely matched to the output of a particular digitizing system. This imposes several constraints:

- The length of each segment is unknown at the time it is started.
- There are only x, y values associated with each point.

For a boundary file, each boundary is represented by one line. The first segment of each boundary line is considered to be a digitized coastline. If there is a second segment, it is a water (open) boundary. Each subsequent segment in the boundary is part of an alternating sequence of coastline and water boundaries.

For contour files, the contour number must be distinctive from the contour numbers used in the accompanying boundary file. Examples of these file types follow:

- **Boundary file**

This file has two boundaries. The outer boundary has several segments of digitized coastline, and several of digitized open water boundaries. The inner boundary is a single segment of digitized coastline.

```
1       0.00            !start of first boundary, depth 0.00
  1.570         13.470          !x,  y for point 1
  1.560         13.450          !x,  y for point 2
  1.540         13.440
.
.
.
  3.760         0.430
  3.750         0.410
  3.760         0.390           !x, y for point 666
667   -9999           !end of first block, which had 666 points
88      88.00         ! start of 1st boundary, 2nd block, open
  3.750         0.370
  3.770         0.370
  3.790         0.370
.
.
.
  9.710         3.100
  9.700         3.120
  9.690         3.140
350   -9999           !349 points in 2nd boundary block - end
```

```
 88      88.00          !start of 1st boundary, 3rd block,  closed
  9.670          3.140
  9.660  3.160
  .
  .
  .
  1.620          13.470
  1.600          13.470
 100     -9999  !end of 1st boundary, nth block
2        0.00   !start of 2nd boundary, depth 0.00
  4.190          7.970
  4.190          7.950
  4.210          7.920
  .
  .
  .
  4.120          8.030
  4.140          8.020
 450     -9999  !end of 2nd boundary, 449 points.
```

- **Contours File**

This file has a set of 12 contours. For some depths, there is more than one contour.

```
101     5.00                   !first contour number, depth
  4.290          0.610         !x(1)  y(1)
  4.260          0.660         !x(2)  y(2)
  4.240          0.710
  4.230          0.760
.
.
.
  3.890          3.510
  3.890          3.560
  3.890          3.610
  54          -9999      !end of line 101, which has 63 points
102     10.00          !start of line 102, depth 10.0
  4.800          0.560
  4.800          0.610
  4.790          0.660
.
.
.
  1.921          12.456
  1.920          12.456
  1.922          12.457
  157       -9999       !end of line 102, which has 156 points
124     20.00
```

```
  2.921        10.345
  2.920        10.345
  2.919        10.346
.
.
.
  3.002        5.234
  3.001        5.235
  3.001        5.236
  40      -9999        !end of line 124, 39 points.
```

NODE (.nod)

This format is used to describe a set of points in three dimensions. The points include sets of connected boundary points, and unconnected interior points. Files of this format are edited and/or created by the NODER program, and are used as input to the GRIDIT program.

The format is:

Line 1: total number of nodes in the files - an integer NTOT
Line 2: total number of boundaries in the file - an integer NBTOT
Line 3: Number of points in the first boundary - an integer NBTHIS
Line 4 - 4+NBTHIS-1: x,y,z values for one point on current boundary

Lines 3 and 4 ..are repeated NBTOT times for the boundaries, and then one additional time for the unconnected interior points. The value of NBTHIS for the interior points may be zero.

```
347                                  !NTOT
  2                                  !NBTOT
156                                  !NBTHIS - 1st boundary has 156 points
        1.570  13.470  0.00  !x y z - point 1
        1.430  13.180  0.00  !x y z - point 2
        1.423  13.324  0.00
.....
        1.231  12.123  0.00
        1.121  12.007  0.00  !x y z - point 156 - last in first boundary
       23                            !NBTHIS - 2nd boundary has 33 points
        2.043  10.223  0.00
        2.041  10.225  0.00
...
        1.001  8.345   0.00
        1.002  8.346   0.00
    245                                  !NBTHIS - interior points - there are 245 of
them
        7.895  4.456   0.00
        7.896  4.457   0.00
```

....

```
      3.123  6.243    0.00
      3.124  6.242    0.00
```

NEIGHBOUR (NEIGH) (.NGH)

The format of this file is:

Line 1: NREC - the number of nodes in the file - integer
Line 2: MAXNGH - maximum number of non-zero neighbours in this grid
Line 3: RANGES - four values, which are XHIGH,YHIGH,XLOW,YLOW - floating point numbers
Lines 4..4+NREC-1: NREC lines containing information about each node (NODENO, X, Y, depth, compuational code, and a list of its neighbouring node numbers)

```
344                                    !NREC - number of nodes file
  9                                    !MAXNGH - maximum number of neighbours
 10.480      13.470      0.440      0.350  !RANGES -
  1   1.570  13.470  1   0.00   2   204   126   0     0     0     0

  2   1.430  13.670  1   0.00   1   204     3   0     0     0     0
....
342   2.160  12.300  0   30.00  246 247   473   475   454   455   0
343   2.660  12.700  0   30.00  123 124   248   457   247   456   0
344   4.133   6.324  0   15.00  170 234   276   207   453   109   0
```

TRIANGLE (.tri)

These files are produced by the GRIDIT program and by the EDITOR
They exist in two forms: The first has three columns per triangle, containing the node numbers. The second has an additional column, containing the element number.

TRIANGLE - 3 column

```
      1     2     3    !NODE1  NODE2  NODE3 - the three node numbers for triangle
1
      1   204   126    !NODE1  NODE2  NODE3 - the three node numbers for triangle
2
      2     3   204
...
    466   468   472
    468   469   471
```

TRIANGLE - 4 column

```
1   1     2    204  !Element-No NODE1 NODE2 NODE3 - the three node for triangle 1
2   1   204    126  ! Element-No NODE1 NODE2 NODE3 - the three node for triangle 2
3   2     3    204
```

TSUNAMI FILES:

Command File

The command file controls the running of the tsunami program. It is a 17 line text file containing the following information:

- Title: line used to described the simulation.
- Binfile: the name of the *.bin file produced by TSUGRID.
- Hotfile: the name of file containing data on the state of the model need for a hot start.
- Specfile: the name of file containing boundary information not included in the *.bin file
- Timdfile: the name of the file containing the numbers of the nodes at which time histories of the tsunami elevation are required.
- Outfile: the name of text file containing a summary of the nodal values at user specified intervals.
- TRIfile: the root name for the files produced in the DISPLOT format. The file name must include an extension. However the TSUNAMI program will ignore the extension and replace it with numbers from 000 to 999. DISPLOT is a program in the TRIGRID suite that can plot the model results as contour maps.
- Backfile: the file name for a dump of the entire state of the model at user specified intervals. This file can be used for a subsequent hot start.
- Timhfile: the file name for the tsunami elevation time history output.
- Max: number of iterations or time steps required. Must be a positive integer greater than zero.
- Iout: number of iterations between the output of nodal values to outfile.
- Imout: number of iterations between output of nodal tsunami elevation data to TRIfile.
- Isout: number of iterations between output of the tsunami model state to backfile. Must be a positive integer greater than zero.
- Delt: model time step (s). Must be a positive non-zero value.
- Ruw: weighting factor in the matrix lumping scheme. This can be used to correct for the errors arising from the matrix lumping required by the Lax-Wendroff two step method. It is normally set at 1.0.

The following listing represents a command file used to simulate the tsunamis generated by submarine explosion.

Boundary Condition File

The boundary condition file (specfile) contains the boundary condition that can be varied between simulations. There are three types of boundary conditions that can be entered with this file:

- Specified x and y velocities. The x and y velocities are fixed at various nodes. The value applies for the whole simulation. This mainly used to specify river flows entering the model. The x and y velocities are specified separately so that it is not necessary to have pairs value.
- Specified elevations. This defines the nodes at which the forcing period and amplitude defined in the command file are applied.
- Displacements. This defines the sea bed deformation responsible for generating a tsunami. TSUNAMI assumes that the sea bed deformation is directly transmitted to the sea surface.

The format of the boundary file is

iix
iux_1,tux_1
iux_2,tux_2
iux_3,tux_3
.
.
.
iiy
ivy_1,tvy_1
ivy_2,tvy_2
ivy_3,tvy_3
.
.
.
iie
iet_1,tet_1,pet_1
iet_2,tet_2,pet_2
iet_3,tet_3,pet_3
.
.
.
jdc
idc_1,str_1,vel_1,sto_1
idc_2,str_2,vel_2,sto_2
idc_3,str_3,vel_3,sto_3
.
.
.

The variables are explained below:

- iix: number of nodes with specified x velocity values.
- iux,tux: node number(iux) and the associated specified x velocity value (tux).If iix is zero these lines are omitted, otherwise there are iix lines of values with one pair of values per line. The separators can be tabs, commas or spaces.
- iiy: number of nodes with specified y velocity values. Normally this will be the same as iix, but this is not essential.

- ivy, tvy: node number (ivy) and the associated specified y velocity value (tvy). If iiy is zero these lines are omitted, otherwise there are iiy lines value with one pair of values per line.
- iie: number of nodes with specified elevations. The elevations are defined by the forcing period, amplitude and phase.
- iet, tet, fet, pet: node number (iet) at which specified sinusoidal wave is to applied. tet is the initial wave elevation to be applied. fet is associated with the forcing period to be applied and pet is the phase of sinusoidal wave to be applied. This enables a submarine explosion to be simulated by defining an initial sea surface displacement, and setting the forcing amplitude to zero.
- jdc: number of nodes at which sea floor displacements are defined.
- idc, str, vel, sto: node number (idc) at which the displacement occurs. The displacement is defined by a starting time (str), a vertical velocity (vel) and stop time (sto). The stop time must be after the start time. The velocity is assumed to be positive upwards and the program accepts positive and negative velocities. Any given node may appear more than once, so that complex deformation time histories can be defined. TSUNAMI converts the velocity into a displacement by determining the deformation duration for the current time step. The start and stop times for repeated nodes can overlap, in which case the final result is the sum of the displacements.

Listing of boundary file:

Time History File

The time history file specifies the nodes at which a time series of the tsunami elevation should be saved. This provides more complete data than the other forms of output from the TSUNAMI program. The format of this file is as follows

iop
nop1
nop2
nop3
.
.
.

The variables are explained below:
iop: the number of nodes for which time histories are required.
nop: node number. One node number per line.

Comments can be added after the node numbers. The separators can be tabs, commas or spaces.

The Boundary Condition File of Rangitoto Volcano Pyroclastic Modelling

0			
0			
68			
1	0	0	0
1823	0	0	0
1991	0	0	0
1992	0	0	0
1994	0	0	0
2119	0	0	0
2120	0	0	0
2261	0	0	0
2262	0	0	0
2263	0	0	0
2438	0	0	0
2439	0	0	0
2696	0	0	0
2697	0	0	0
3011	0	0	0
3395	0	0	0
3687	0	0	0
3688	0	0	0
3948	0	0	0
4206	0	0	0
4429	0	0	0
4609	0	0	0
4764	0	0	0
4921	0	0	0
5016	0	0	0
5122	0	0	0
5205	0	0	0
5335	0	0	0
5410	0	0	0
5480	0	0	0
5538	0	0	0
5614	0	0	0
5613	0	0	0
5612	0	0	0
5617	0	0	0
5615	0	0	0
5684	0	0	0
5685	0	0	0
5686	0	0	0
5738	0	0	0
5737	0	0	0
5739	0	0	0
5774	0	0	0
5775	0	0	0
5806	0	0	0
5833	0	0	0
5857	0	0	0

5887	0	0	0
5956	0	0	0
5997	0	0	0
6034	0	0	0
6136	0	0	0
6168	0	0	0
6199	0	0	0
6292	0	0	0
1003	0	0	0
6345	0	0	0
6346	0	0	0
1004	0	0	0
1008	0	0	0
1009	0	0	0
1010	0	0	0
1011	0	0	0
1012	0	0	0
1013	0	0	0
1014	0	0	0
1015	0	0	0
1016	0	0	0
104			
4392	1	-1	3
4393	1	-1	3
4395	1	-1	3
4238	1	-1	3
4236	1	-1	3
4237	1	-1	3
4234	1	-1	3
4235	1	-1	3
4394	1	2	2
4391	1	2	2
4240	1	2	2
4239	1	2	2
4163	1	2	2
4159	1	2	2
4160	1	2	2
4167	1	2	2
4164	1	2	2
4169	1	2	2
4171	1	2	2
4233	1	2	2
4244	1	2	2
4242	1	2	2
4157	1	2	2
4158	1	2	2
4161	1	2	2
4162	1	2	2
4166	1	2	2
4165	1	2	2
4168	1	2	2
4170	1	2	2
4172	1	2	2
4241	1	5	2
4156	1	5	2
4155	1	5	2

3981	1	5	2
3978	1	5	2
3979	1	5	2
3974	1	5	2
3973	1	5	2
3977	1	5	2
3975	1	5	2
4154	1	5	2
3985	1	5	2
3984	1	1	2
3983	1	1	2
3980	1	1	2
3976	1	1	2
3918	1	1	2
3982	1	1	2
3912	1	1	2
3914	1	1	2
3917	1	1	2
4392	3	2	5
4393	3	2	5
4395	3	2	5
4238	3	2	5
4236	3	2	5
4237	3	2	5
4234	3	2	5
4235	3	2	5
4394	0	3	5
4391	0	3	5
4240	0	3	5
4239	0	3	5
4163	0	3	5
4159	0	3	5
4160	0	3	5
4167	0	3	5
4164	0	3	5
4169	0	3	5
4171	0	3	5
4233	0	3	5
4244	0	3	5
4242	0	3	5
4157	0	3	5
4158	0	3	5
4161	0	3	5
4162	0	3	5
4166	0	3	5
4165	0	3	5
4168	0	3	5
4170	0	3	5
4172	0	3	5
4241	0	7	5
4156	0	7	5
4155	0	7	5
3981	0	7	5
3978	0	7	5
3979	0	7	5
3974	0	7	5

3973	0	7	5
3977	0	7	5
3975	0	7	5
4154	0	7	5
3985	0	7	5
3984	0	7	5
3983	0	9	5
3980	0	9	5
3976	0	9	5
3918	0	9	5
3982	0	9	5
3912	0	9	5
3914	0	9	5
3917	0	9	5

The Boundary Condition File for Rangitoto Channel Submarine Explosion Modelling.

0			
0			
68			
1	0	0	0
1823	0	0	0
1991	0	0	0
1992	0	0	0
1994	0	0	0
2119	0	0	0
2120	0	0	0
2261	0	0	0
2262	0	0	0
2263	0	0	0
2438	0	0	0
2439	0	0	0
2696	0	0	0
2697	0	0	0
3011	0	0	0
3395	0	0	0
3687	0	0	0
3688	0	0	0
3948	0	0	0
4206	0	0	0
4429	0	0	0
4609	0	0	0
4764	0	0	0
4921	0	0	0
5016	0	0	0
5122	0	0	0
5205	0	0	0
5335	0	0	0
5410	0	0	0
5480	0	0	0
5538	0	0	0
5614	0	0	0
5613	0	0	0
5612	0	0	0
5617	0	0	0
5615	0	0	0
5684	0	0	0
5685	0	0	0
5686	0	0	0
5738	0	0	0
5737	0	0	0
5739	0	0	0
5774	0	0	0
5775	0	0	0
5806	0	0	0
5833	0	0	0

5857	0	0	0
5887	0	0	0
5956	0	0	0
5997	0	0	0
6034	0	0	0
6136	0	0	0
6168	0	0	0
6199	0	0	0
6292	0	0	0
1003	0	0	0
6345	0	0	0
6346	0	0	0
1004	0	0	0
1008	0	0	0
1009	0	0	0
1010	0	0	0
1011	0	0	0
1012	0	0	0
1013	0	0	0
1014	0	0	0
1015	0	0	0
1016	0	0	0
205			
4141	20	6	23
4144	20	6	23
4143	20	6	23
4146	20	6	23
4145	20	6	23
3995	20	6	23
3994	20	6	23
3999	20	6	23
4140	20	6	23
4142	20	6	23
4256	20	5	23
4251	20	5	23
4147	20	5	23
4148	20	5	23
3991	20	5	23
3993	20	5	23
3992	20	5	23
3997	20	5	23
3998	20	5	23
4138	20	5	23
4139	20	5	23
4255	20	5	23
4256	20	5	23
4258	20	3	23
4253	20	3	23
4252	20	3	23
4249	20	3	23
4149	20	3	23
4150	20	3	23
3988	20	3	23
3990	20	3	23
3902	20	3	23
3901	20	3	23

3898	20	3	23
3996	20	3	23
4000	20	3	23
4001	20	3	23
4135	20	3	23
4137	20	3	23
4259	20	3	23
4257	20	3	23
4141	20	6	25
4144	20	6	25
4143	20	6	25
4146	20	6	25
4145	20	6	25
3995	20	6	25
3994	20	6	25
3999	20	6	25
4140	20	6	25
4142	20	6	25
4256	20	6	25
4251	20	5	25
4147	20	5	25
4148	20	5	25
3991	20	5	25
3993	20	5	25
3992	20	5	25
3997	20	5	25
3998	20	5	25
4138	20	5	25
4139	20	5	25
4255	20	5	25
4256	20	5	25
4258	20	3	25
4253	20	3	25
4252	20	3	25
4249	20	3	25
4149	20	3	25
4150	20	3	25
3988	20	3	25
3990	20	3	25
3902	20	3	25
3901	20	3	25
3898	20	3	25
3996	20	3	25
4000	20	3	25
4001	20	3	25
4135	20	3	25
4137	20	3	25
4259	20	3	25
4257	20	3	25
4141	320	-6	323
4144	320	-6	323
4143	320	-6	323
4146	320	-6	323
4145	320	-6	323
3995	320	-6	323
3994	320	-6	323

3999	320	-6	323
4140	320	-6	323
4142	320	-6	323
4256	320	-6	323
4251	320	-5	323
4147	320	-5	323
4148	320	-5	323
3991	320	-5	323
3993	320	-5	323
3992	320	-5	323
3997	320	-5	323
3998	320	-5	323
4138	320	-5	323
4139	320	-5	323
4255	320	-5	323
4256	320	-5	323
4258	320	-3	323
4253	320	-3	323
4252	320	-3	323
4249	320	-3	323
4149	320	-3	323
4150	320	-3	323
3988	320	-3	323
3990	320	-3	323
3902	320	-3	323
3901	320	-3	323
3898	320	-3	323
3996	320	-3	323
4000	320	-3	323
4001	320	-3	323
4135	320	-3	323
4137	320	-3	323
4259	320	-3	323
4257	320	-3	323
4141	350	5	353
4144	350	5	353
4143	350	5	353
4146	350	5	353
4145	350	5	353
3995	350	5	353
3994	350	5	353
3999	350	5	353
4140	350	5	353
4142	350	5	353
4256	350	4	353
4251	350	4	353
4147	350	4	353
4148	350	4	353
3991	350	4	353
3993	350	4	353
3992	350	4	353
3997	350	4	353
3998	350	4	353
4138	350	4	353
4139	350	4	353
4255	350	4	353

4256	350	4	353
4258	350	2	353
4253	350	2	353
4252	350	2	353
4249	350	2	353
4149	350	2	353
4150	350	2	353
3988	350	2	353
3990	350	2	353
3902	350	2	353
3901	350	2	353
3898	350	2	353
3996	350	2	353
4000	350	2	353
4001	350	2	353
4135	350	2	353
4137	350	2	353
4259	350	2	353
4257	350	2	353
4141	350	7	354
4144	350	7	354
4143	350	7	354
4146	350	7	354
4145	350	7	354
3995	350	7	354
3994	350	7	354
3999	350	7	354
4140	350	7	354
4142	350	7	354
4256	350	7	354
4251	350	6	354
4147	350	6	354
4148	350	6	354
3991	350	6	354
3993	350	6	354
3992	350	6	354
3997	350	6	354
3998	350	6	354
4138	350	6	354
4139	350	6	354
4255	350	6	354
4256	350	6	354
4258	350	4	354
4253	350	4	354
4252	350	4	354
4249	350	4	354
4149	350	4	354
4150	350	4	354
3988	350	4	354
3990	350	4	354
3902	350	4	354
3901	350	4	354
3898	350	4	354
3996	350	4	354
4000	350	4	354
4001	350	4	354

4135	350	4	354
4137	350	4	354
4259	350	4	354
4257	350	4	354

The Boundary Condition File for Browns Island Pyroclastic Flow Modelling

0			
0			
68			
1	0	0	0
1823	0	0	0
1991	0	0	0
1992	0	0	0
1994	0	0	0
2119	0	0	0
2120	0	0	0
2261	0	0	0
2262	0	0	0
2263	0	0	0
2438	0	0	0
2439	0	0	0
2696	0	0	0
2697	0	0	0
3011	0	0	0
3395	0	0	0
3687	0	0	0
3688	0	0	0
3948	0	0	0
4206	0	0	0
4429	0	0	0
4609	0	0	0
4764	0	0	0
4921	0	0	0
5016	0	0	0
5122	0	0	0
5205	0	0	0
5335	0	0	0
5410	0	0	0
5480	0	0	0
5538	0	0	0
5614	0	0	0
5613	0	0	0
5612	0	0	0
5617	0	0	0
5615	0	0	0
5684	0	0	0
5685	0	0	0
5686	0	0	0
5738	0	0	0
5737	0	0	0
5739	0	0	0
5774	0	0	0
5775	0	0	0
5806	0	0	0
5833	0	0	0
5857	0	0	0
5887	0	0	0

5956	0	0	0
5997	0	0	0
6034	0	0	0
6136	0	0	0
6168	0	0	0
6199	0	0	0
6292	0	0	0
1003	0	0	0
6345	0	0	0
6346	0	0	0
1004	0	0	0
1008	0	0	0
1009	0	0	0
1010	0	0	0
1011	0	0	0
1012	0	0	0
1013	0	0	0
1014	0	0	0
1015	0	0	0
1016	0	0	0
110			
3408	2	-1	3
3410	2	-1	3
3412	2	-1	3
3380	2	-1	3
3379	2	-1	3
3382	2	-1	3
3381	2	-1	3
3667	2	1	3
3666	2	1	3
3665	2	1	3
3411	2	1	3
3409	2	1	3
3378	2	1	3
3376	2	1	3
3377	2	1	3
3033	2	1	3
3031	2	1	3
3668	2	3	3
3712	2	3	3
3713	2	3	3
3716	2	3	3
3715	2	3	3
3663	2	3	3
3664	2	3	3
3413	2	3	3
3374	2	3	3
3375	2	3	3
3040	2	3	3
3036	2	3	3
3035	2	3	3
3032	2	3	3
3029	2	3	3
3030	2	3	3
2985	2	5	3
2986	2	5	3

3669	2	5	3
3711	2	5	3
3714	2	5	3
3717	2	5	3
3718	2	5	3
3719	2	5	3
3662	2	5	3
3414	2	5	3
3372	2	5	3
3373	2	5	3
3039	2	5	3
3038	2	5	3
3034	2	5	3
2982	2	5	3
2983	2	5	3
2984	2	5	3
2987	2	5	3
2988	2	5	3
2989	2	5	3
3028	2	5	3
3408	2	2	4
3410	2	2	4
3412	2	2	4
3380	2	2	4
3379	2	2	4
3382	2	2	4
3381	2	2	4
3667	2	3	4
3666	2	3	4
3665	2	3	4
3411	2	3	4
3409	2	3	4
3378	2	3	4
3376	2	3	4
3377	2	3	4
3033	2	3	4
3031	2	3	4
3668	2	5	4
3712	2	5	4
3713	2	5	4
3716	2	5	4
3715	2	5	4
3663	2	5	4
3664	2	5	4
3413	2	5	4
3374	2	5	4
3375	2	5	4
3040	2	5	4
3036	2	5	4
3035	2	5	4
3032	2	5	4
3029	2	5	4
3030	2	5	4
2985	2	7	4
2986	2	7	4
3669	2	7	4

3711	2	7	4
3714	2	7	4
3717	2	7	4
3718	2	7	4
3719	2	7	4
3662	2	7	4
3414	2	7	4
3372	2	7	4
3373	2	7	4
3039	2	7	4
3038	2	7	4
3034	2	7	4
2982	2	7	4
2983	2	7	4
2984	2	7	4
2987	2	7	4
2988	2	7	4
2989	2	7	4
3028	2	7	4

The Boundary Condition File for Tamaki Estuary Submarine Explosion Modelling

0			
0			
68			
1	0	0	0
1823	0	0	0
1991	0	0	0
1992	0	0	0
1994	0	0	0
2119	0	0	0
2120	0	0	0
2261	0	0	0
2262	0	0	0
2263	0	0	0
2438	0	0	0
2439	0	0	0
2696	0	0	0
2697	0	0	0
3011	0	0	0
3395	0	0	0
3687	0	0	0
3688	0	0	0
3948	0	0	0
4206	0	0	0
4429	0	0	0
4609	0	0	0
4764	0	0	0
4921	0	0	0
5016	0	0	0
5122	0	0	0
5205	0	0	0
5335	0	0	0
5410	0	0	0
5480	0	0	0
5538	0	0	0
5614	0	0	0
5613	0	0	0
5612	0	0	0
5617	0	0	0
5615	0	0	0
5684	0	0	0
5685	0	0	0
5686	0	0	0
5738	0	0	0
5737	0	0	0
5739	0	0	0
5774	0	0	0
5775	0	0	0
5806	0	0	0
5833	0	0	0
5857	0	0	0
5887	0	0	0

5956	0	0	0
5997	0	0	0
6034	0	0	0
6136	0	0	0
6168	0	0	0
6199	0	0	0
6292	0	0	0
1003	0	0	0
6345	0	0	0
6346	0	0	0
1004	0	0	0
1008	0	0	0
1009	0	0	0
1010	0	0	0
1011	0	0	0
1012	0	0	0
1013	0	0	0
1014	0	0	0
1015	0	0	0
1016	0	0	0
48			
1777	1	1.8	3
1881	1	1.8	3
1884	1	1.8	3
1887	1	1.8	3
1782	1	1.8	3
1780	1	1.8	3
1776	1	1.8	3
1778	1	1.8	3
1779	1	1.8	3
1734	1	0.8	3
1774	1	0.8	3
1775	1	0.8	3
1886	1	0.8	3
1885	1	0.8	3
1882	1	0.8	3
1883	1	0.8	3
1880	1	0.8	3
1878	1	0.8	3
1879	1	0.8	3
1781	1	0.8	3
1783	1	0.8	3
1731	1	0.8	3
1732	1	0.8	3
1736	1	0.8	3
1777	1	2.8	5
1881	1	2.8	5
1884	1	2.8	5
1887	1	2.8	5
1782	1	2.8	5
1780	1	2.8	5
1776	1	2.8	5
1778	1	2.8	5
1779	1	2.8	5
1734	1	1.8	5
1774	1	1.8	5

1775	1	1.8	5
1886	1	1.8	5
1885	1	1.8	5
1882	1	1.8	5
1883	1	1.8	5
1880	1	1.8	5
1878	1	1.8	5
1879	1	1.8	5
1781	1	1.8	5
1783	1	1.8	5
1731	1	1.8	5
1732	1	1.8	5
1736	1	1.8	5

COMMAND FILE :

- Example for Submarine Explosion with Hot Start file :

```
Test of Tsunami generated by Submarine Explosion
volc.bin
back.tmp
vent5b.dat
vhis2.dat
Bvent.tmp
Bplot.tmp
Aback.tmp
BVistes.out
      7200 number of iterations
         1 output of interval
         1 plot file output interval
         1 backup  interval
         1 Time step interval
         1 weighting factor
```

- Example for Pyroclastic Flow without Hot Strat file :

```
Test of Tsunami generated byPyroclastic Flow -
Motukorea
volc.bin

piro2.dat
vhis.dat
vent.tmp
Aplot.tmp
Aback.tmp
Vistes.out
      7200 number of iterations
         1 output of interval
         1 plot file output interval
         1 backup  interval
         1 Time step interval
         1 weighting factor
```

TIME HISTORY FILE

28
5045 Black Rock (Thorne Bay)(1)
4274 Narrow Neck Beach(4)
4007 Takapuna Head(5)
3885 Cheltenham Beach(6)
3430 North Head(7)
3433 Torpedo Bay(8)
3332 Devonport Beach(9)
2782 Mechanics Bay(32)
2162 Orakey Basin(37)
2483 Hobson Pt.(38)
2447 Okahu B(39)
2648 Mission Bay(41)
2467 St.Heliers B.(42)
2739 Ladies B.(43)
2662 West Tamaki Hd.(44)
2025 Sandy Pt.(48)
1787 Half Moon Bay.(60)
1956 Buckland Beach (up).(61)
2678 Music Pt.(64)
2452 Eastern Beach.(65)
5005 McKenzie Bay.(66)
4738 Coastguard Bay.(67)
4392 Fox Point.(70)
4236 Seawolf Rockers.(71)
4233 Wharf.(72)
4785 Islington Bay.(77)
4212 Motuihe Island.(78)
3404 Brown Island.(80)

Numerical Modelling Initial Test Results.
Submarine Explosion :

- Sea bottom deformation 6 meters, rising time 3 seconds

Single Explosion :

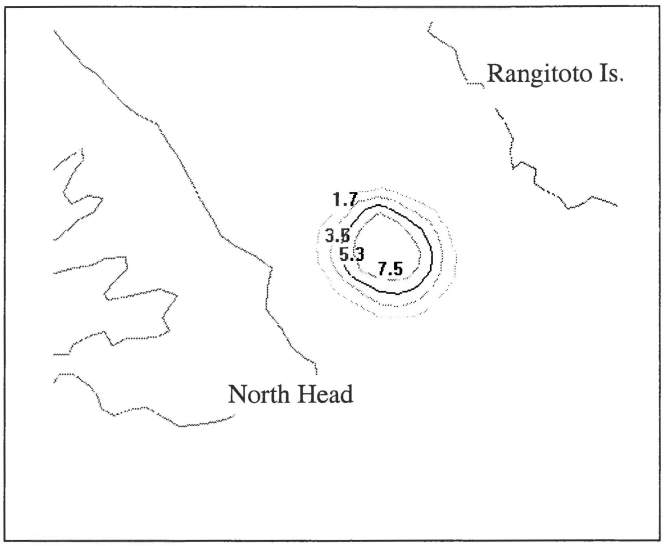

Figure 1. Dome shape at the sea surface one second after explosion completed.

Multiple Explosions (2 explosions) :

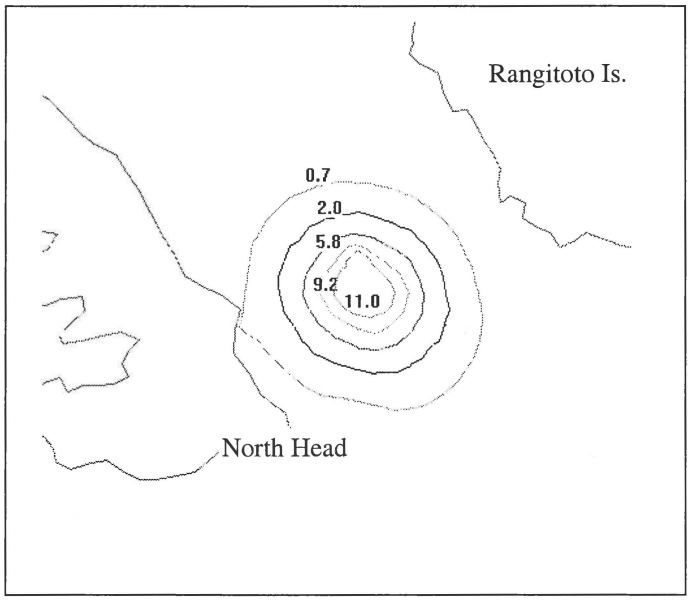

Figure 2. The dome one second after the last explosion. Time gap between explosion is 30 seconds

Multiple Explosions (2 explosions) :

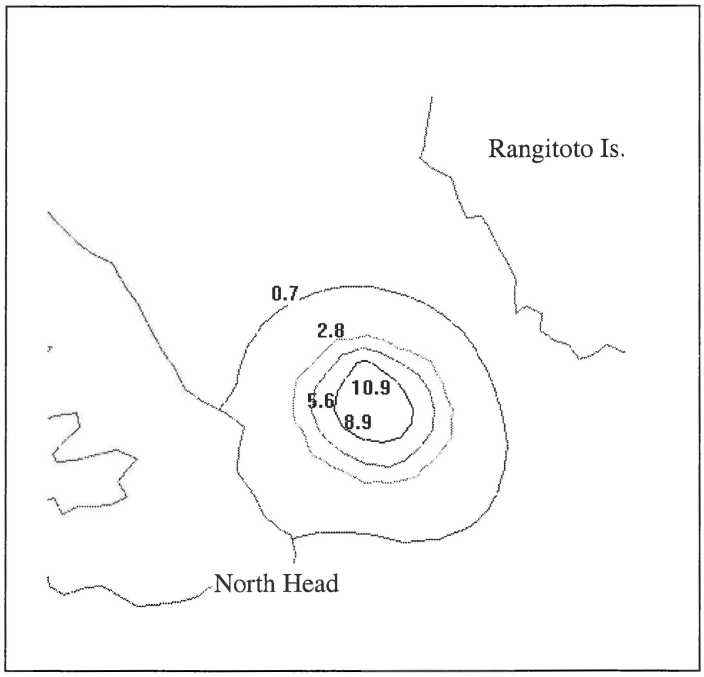

Figure 3. The dome one second after the last explosion. Time gap between explosion is 60 seconds

Multiple Explosions (2 explosions) :

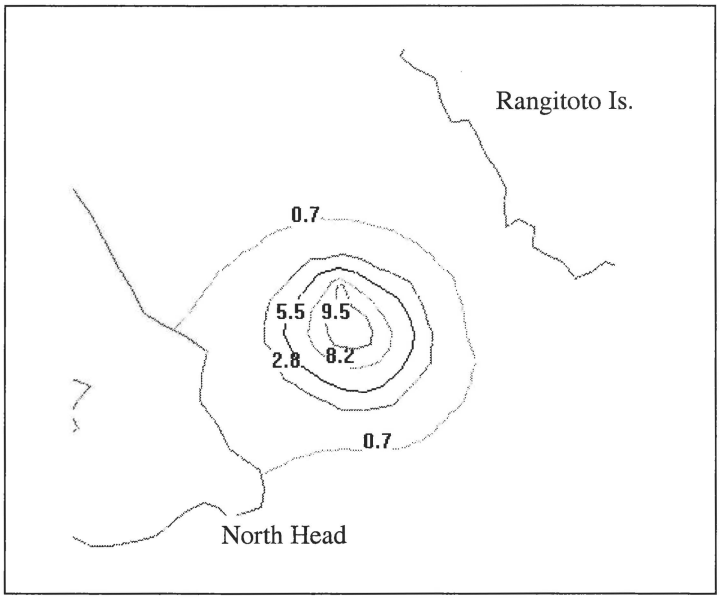

Figure 4. The dome one second after the last explosion. Time gap between explosion is 120 seconds

Multiple Explosions (2 explosions) :

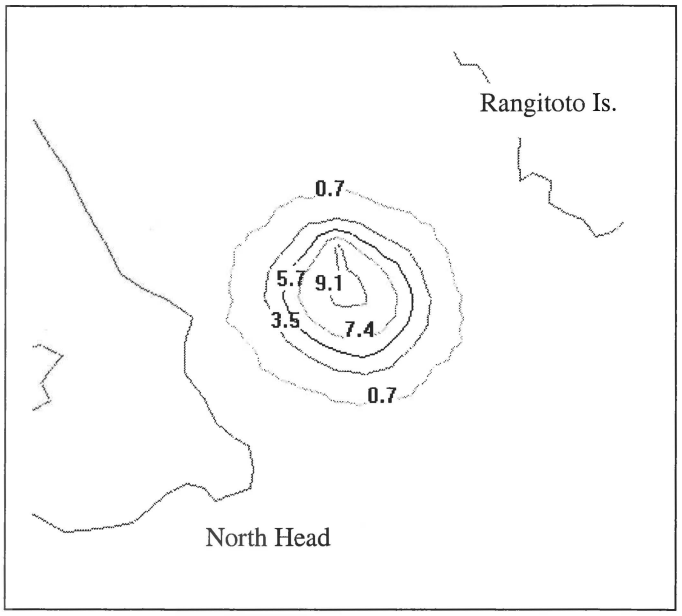

Figure 5. The dome one second after the last explosion. Time gap between explosion is 5 minutes

Multiple Explosions (2 explosions) :

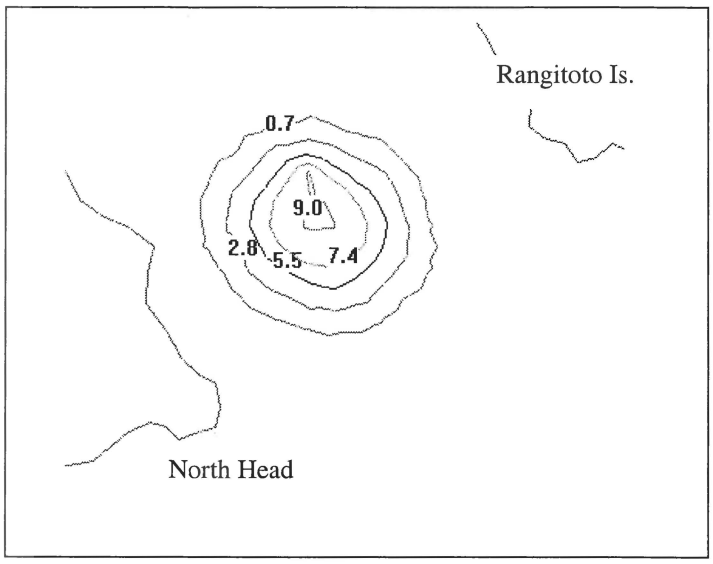

Figure 6. The dome one second after the last explosion. Time gap between explosion is 10 minutes

The wave dynamic :

Single explosion.

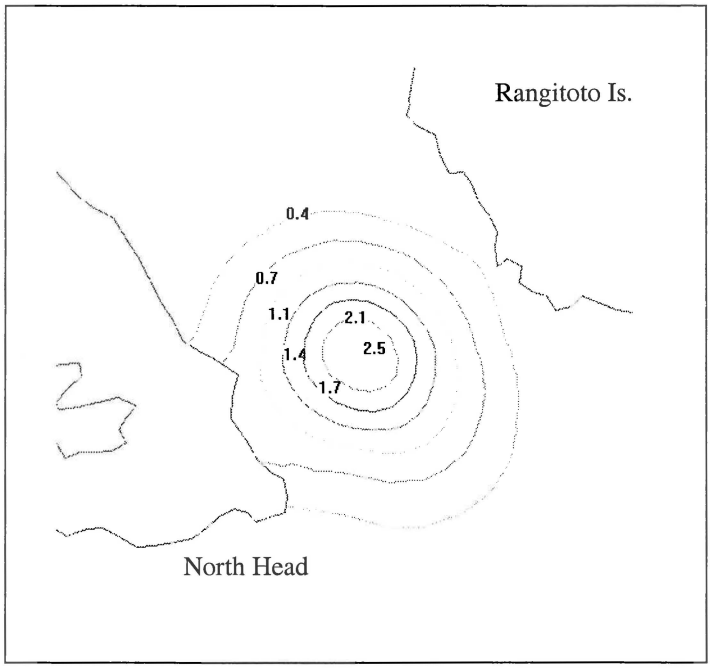

Figure 7. The patterns of wave propagation after 1 minute from explosion.

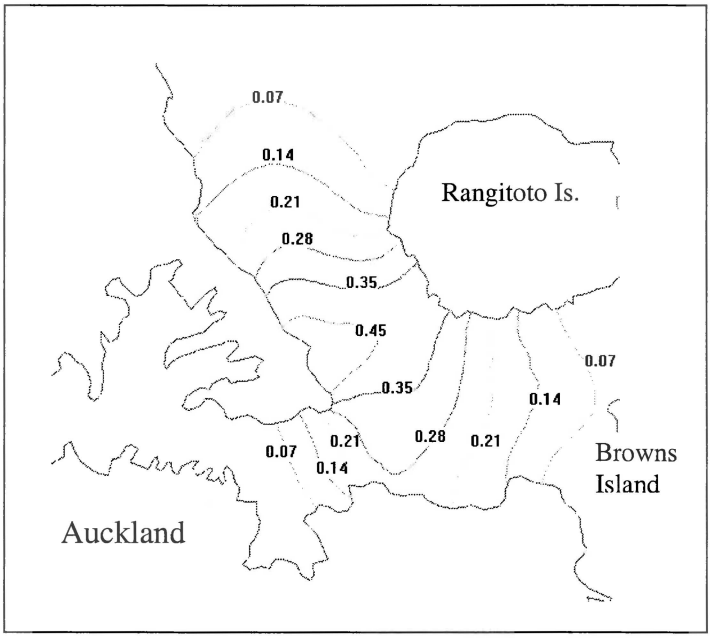

Figure 8. The patterns of wave propagation after 5 minutes from explosion.

Multiple Explosions (2 explosions) : Time gap 30 seconds

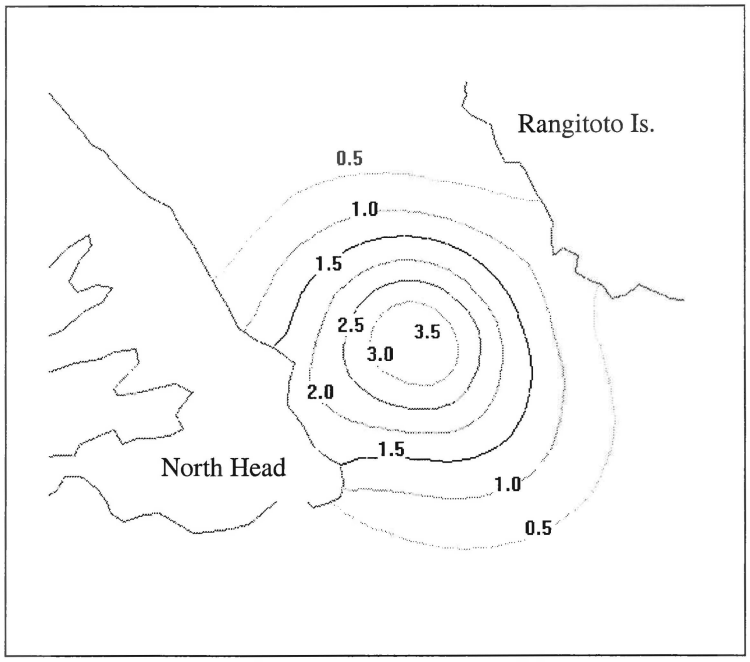

Figure 9. The patterns of wave propagation after 1 minute from the last explosion.

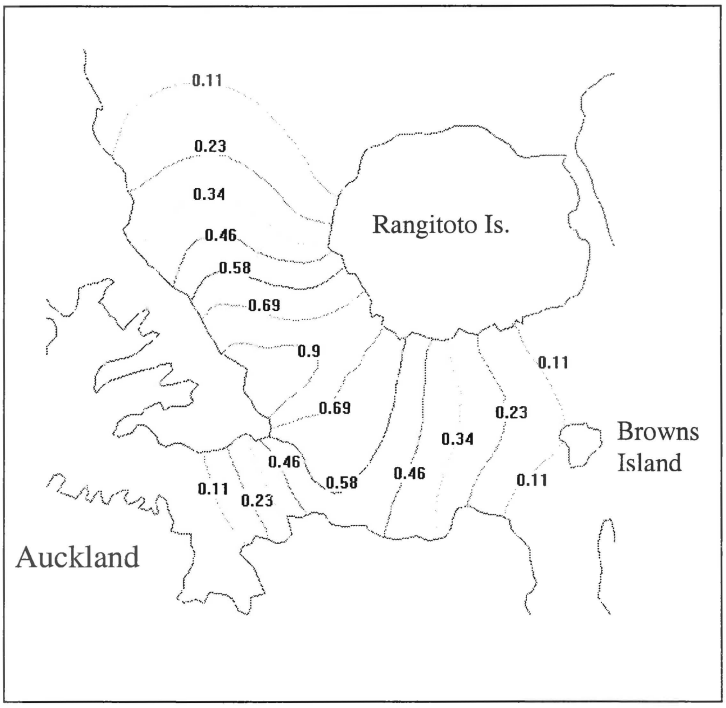

Figure 10. The patterns of wave propagation after 5 minutes from the last explosion.

Multiple Explosions (2 explosions) : Time gap 60 seconds

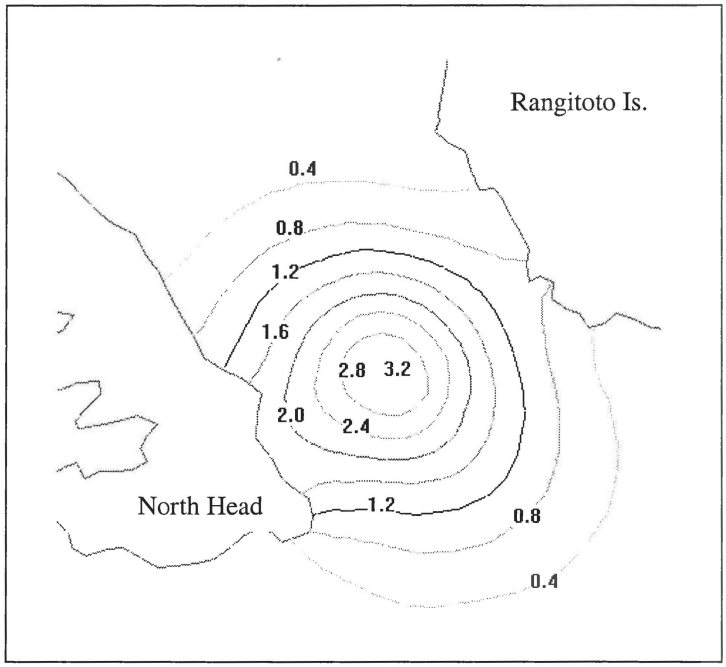

Figure 11. The patterns of wave propagation after 1 minute from the last explosion.

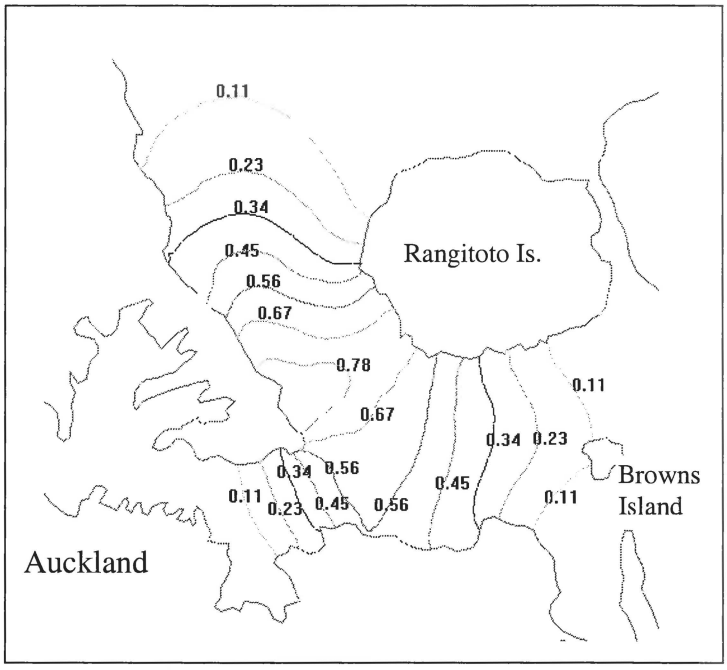

Figure 12. The patterns of wave propagation after 5 minutes from the last explosion.

Multiple Explosions (2 explosions) : Time gap 120 seconds

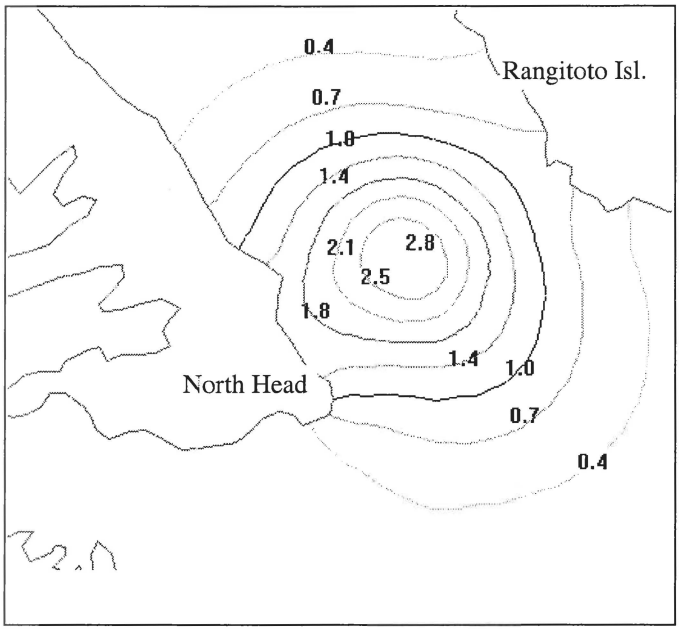

Figure 13. The patterns of wave propagation after 1 minute from the last explosion.

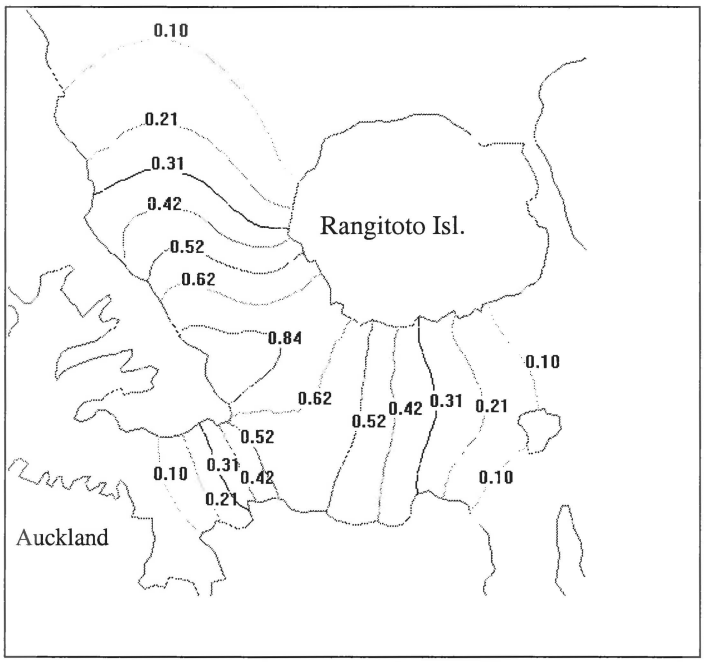

Figure 14. The patterns of wave propagation after 5 minutes from the last explosion.

Multiple Explosions (2 explosions) : Time gap 300 seconds

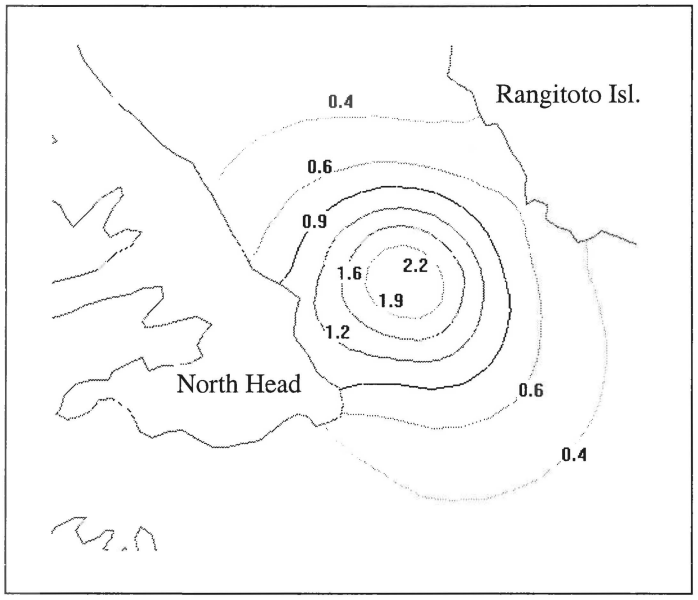

Figure 15. The patterns of wave propagation after 1 minute from the last explosion.

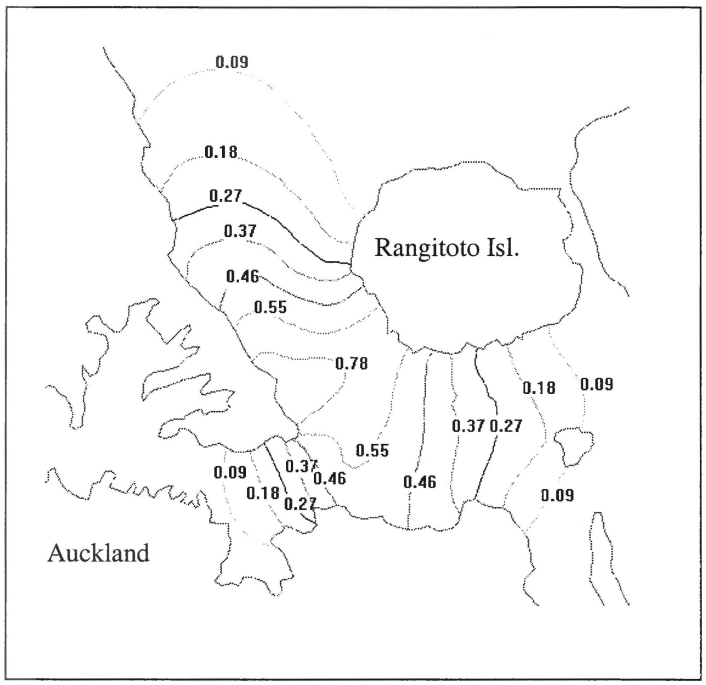

Figure 16. The patterns of wave propagation after 5 minutes from the last explosion.

Multiple Explosions (2 explosions) : Time gap 600 seconds

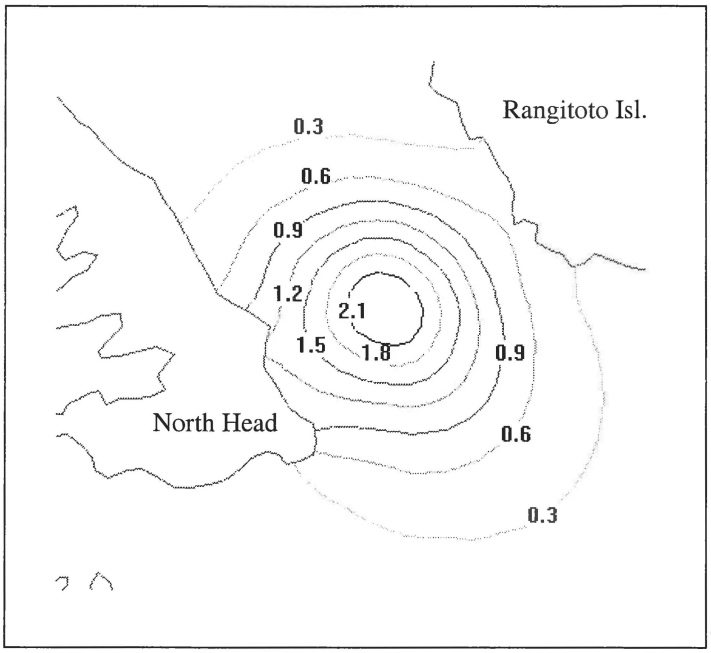

Figure 17. The patterns of wave propagation after 1 minute from the last explosion.

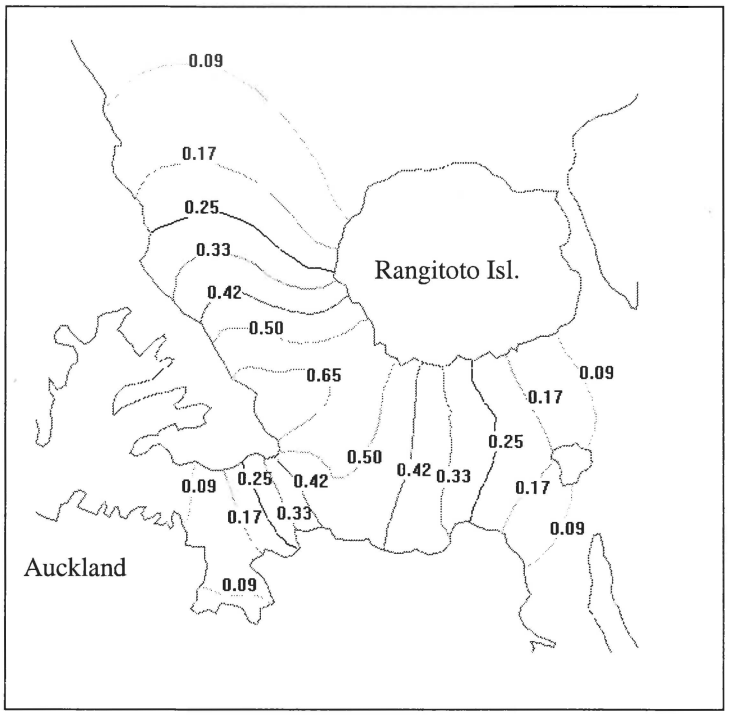

Figure 18. The patterns of wave propagation after 5 minutes from the last explosion.

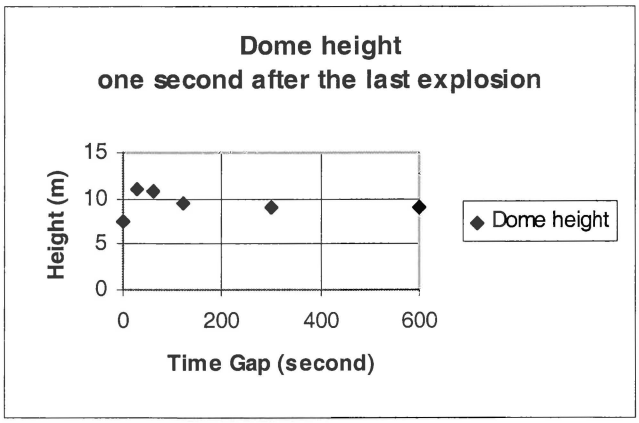

Figure 19. The variation of dome height produce by multiple explosion with variable time gaps at one second after the last explosion. Time gap 0 means a single explosion.

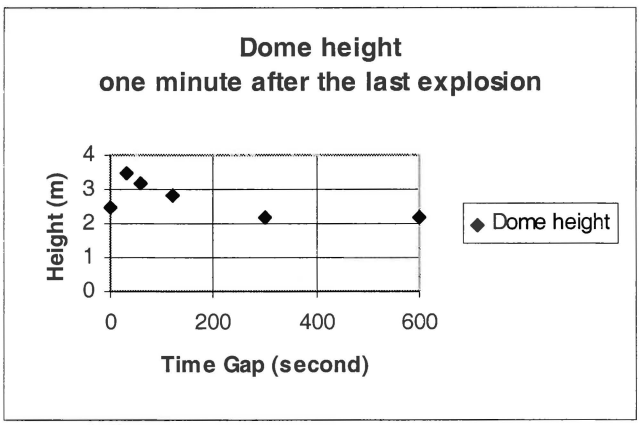

Figure 20. The variation of dome height produce by multiple explosion with variable time gaps at one one minute after the last explosion. Time gap 0 means a single explosion.

Maar Formation Test.

- Initial condition with maximum negative displecement -6 m.

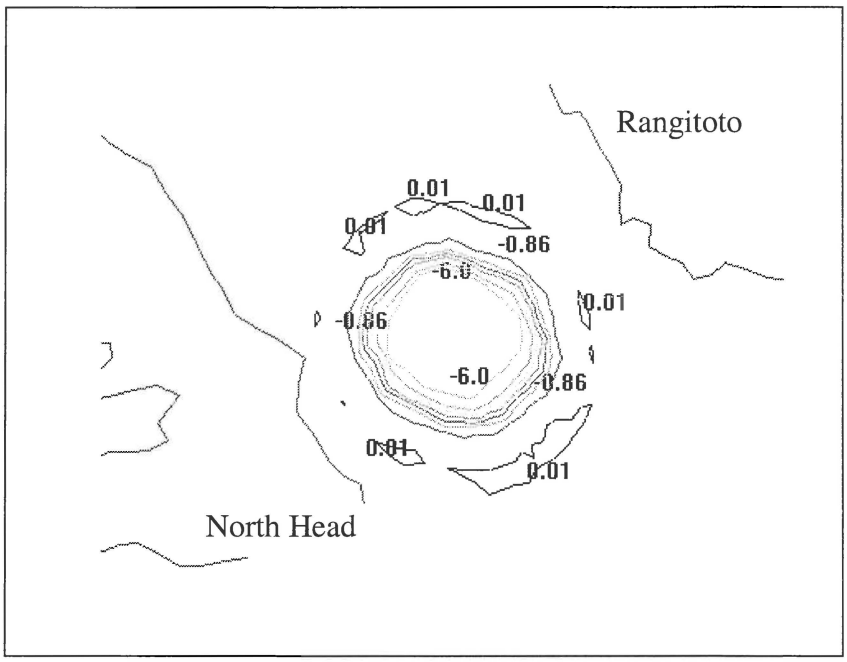

Figure 21. The initial condition of maar formation with negative displacement - 6 m.

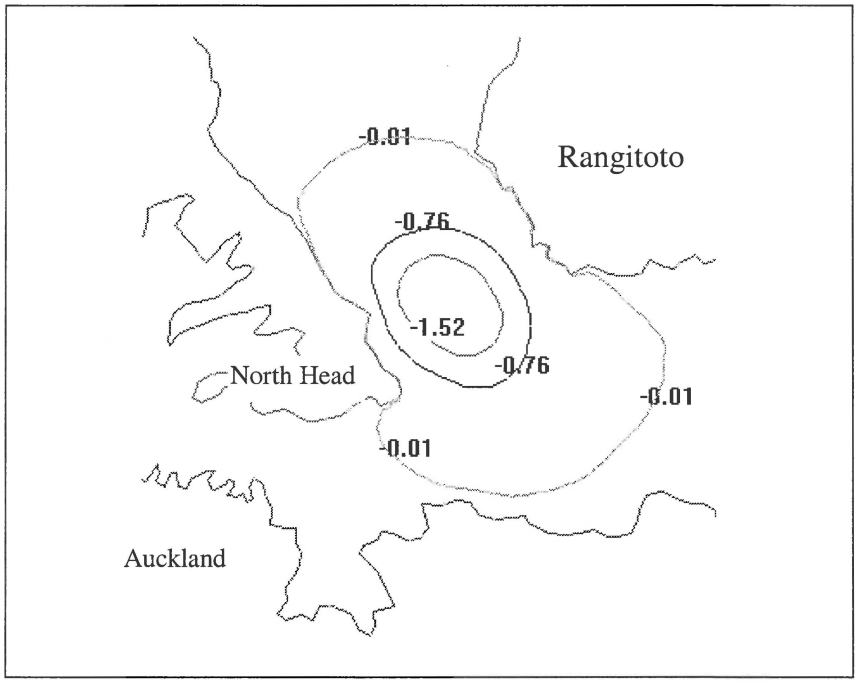

Figure 22. The pattern of sea disturbances one minute after the initial condition

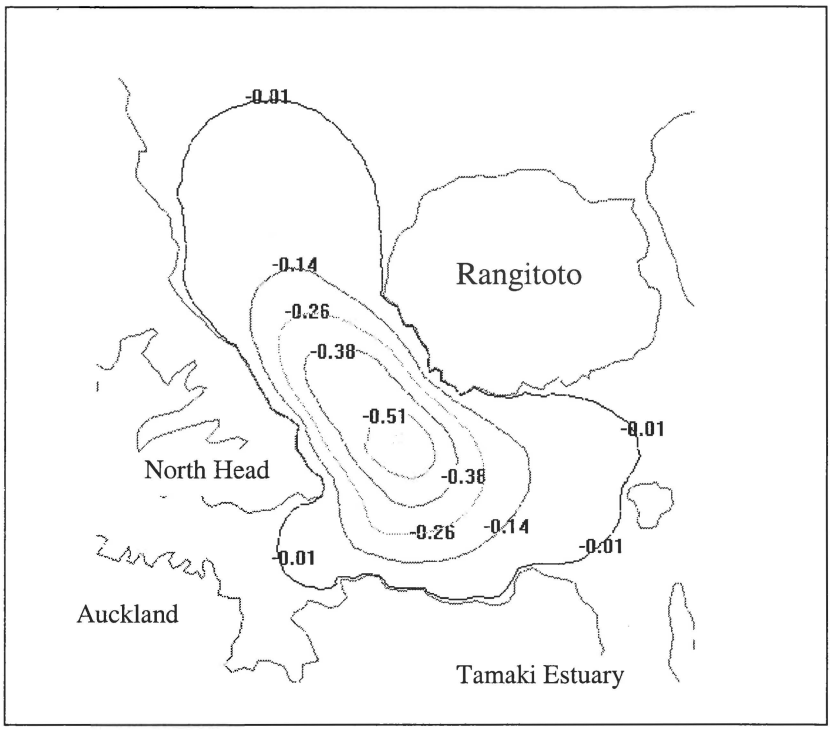

Figure 23. The sea elevations after 3 minutes from initial condition showing that the sea recession took place around the Rangitoto Channel.

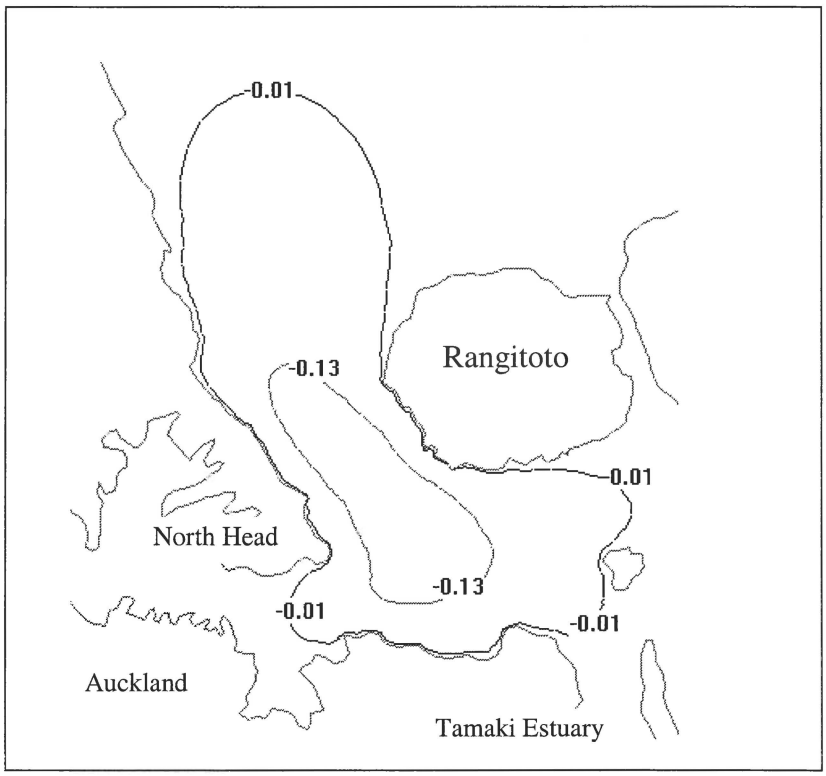

Figure 24. The pattern after 5 minutes showing that the center of disturbance has almost disappeared.

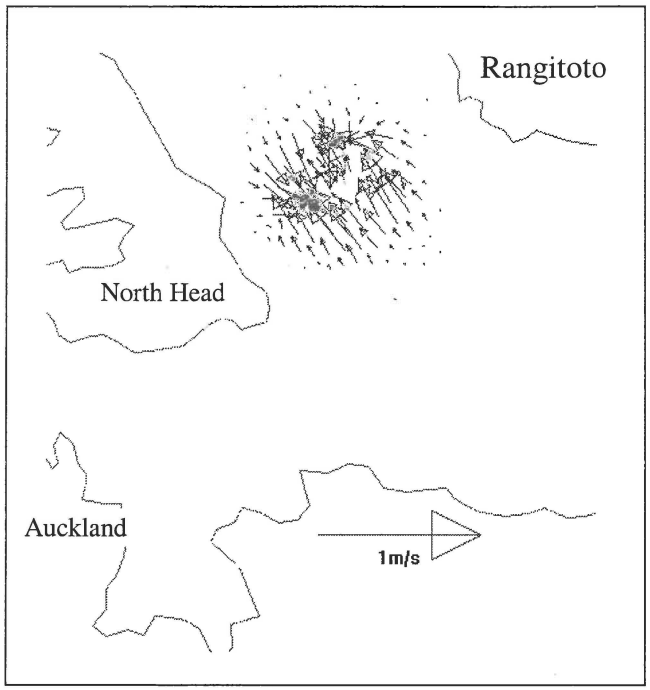

Figure 25. The current pattern for initial negative displacements for maar formation immediately after collapse.

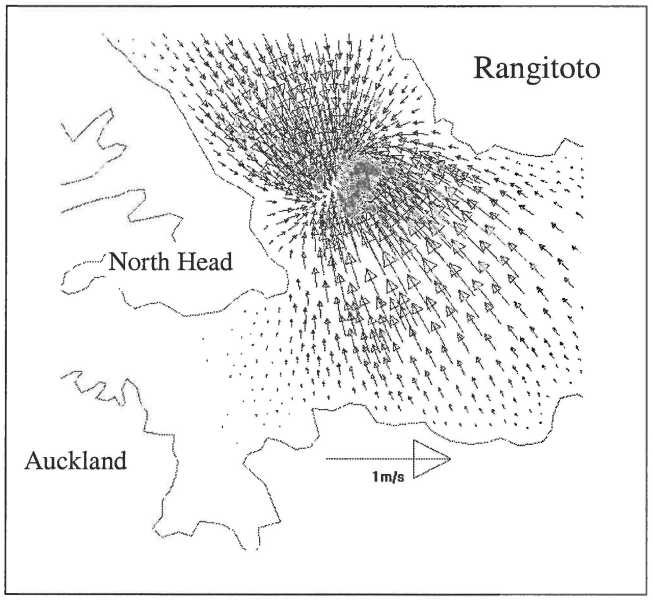

Figure 26. The current pattern for negative displacements after one minute from the initial condition.

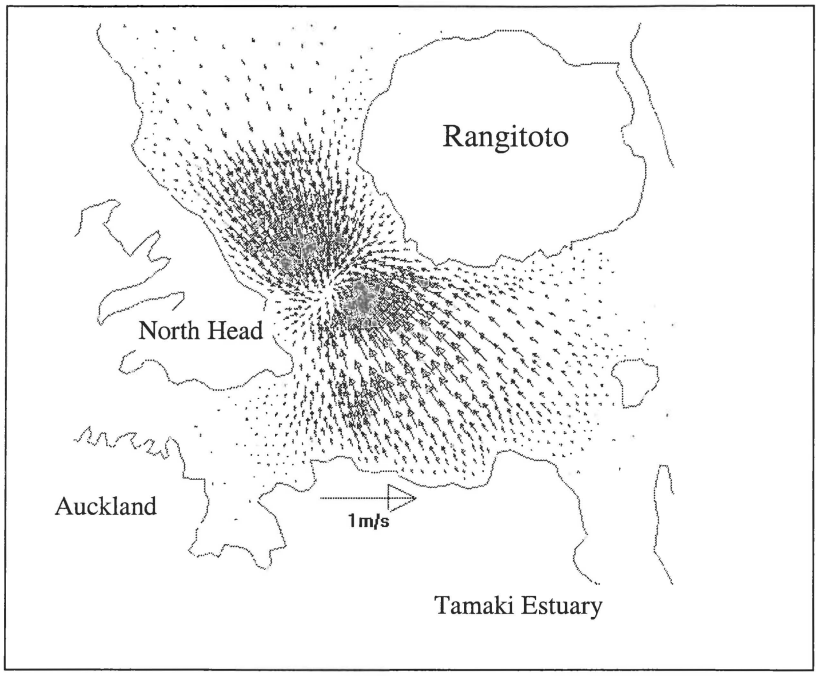

Figure 27. The current pattern for negative displacements after two minutes from the initial condition.

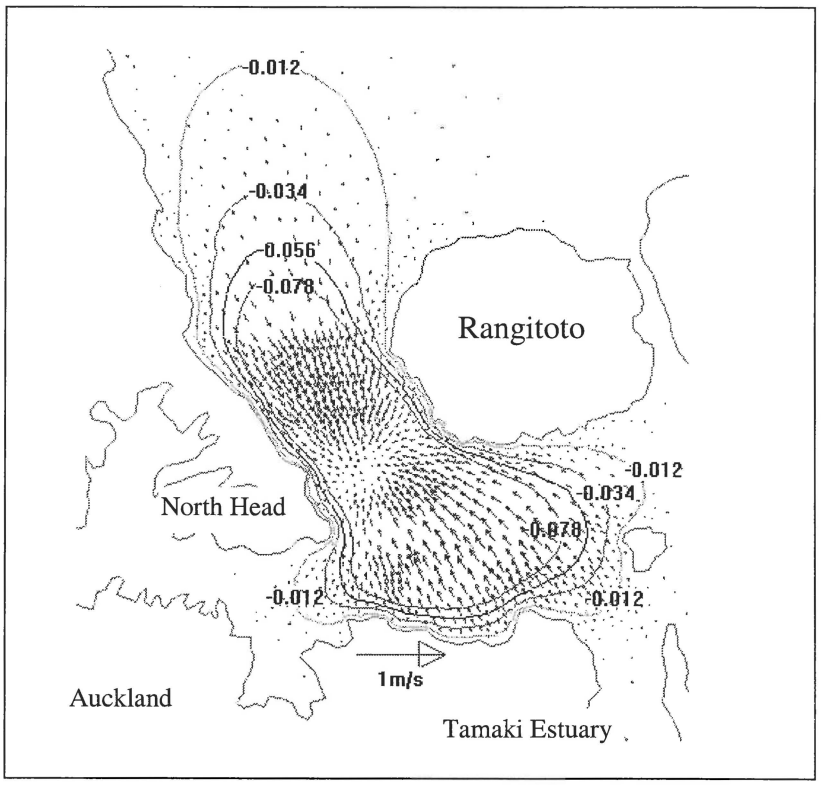

Figure 28. The current pattern for negative displacements after five minutes from the initial condition.

Pyroclastic Flow Initial Test

- Static initial condition with maximum displacement 7 m

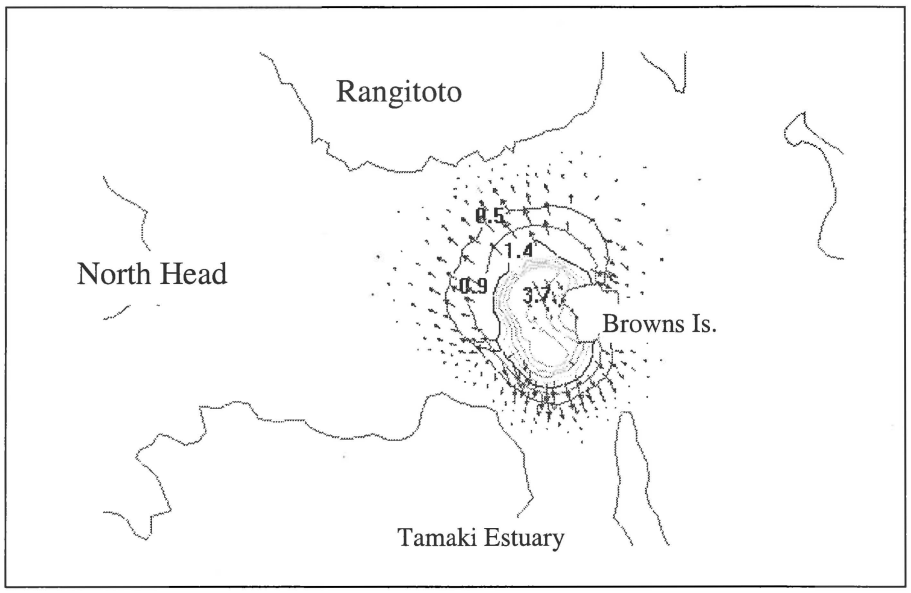

Figure 29. The result of static initial condition for pyroclastic flow test after 10 seconds from the initial condition where with maximum displacement is 7 m.

- Dynamic initial condition with displacement 7 m

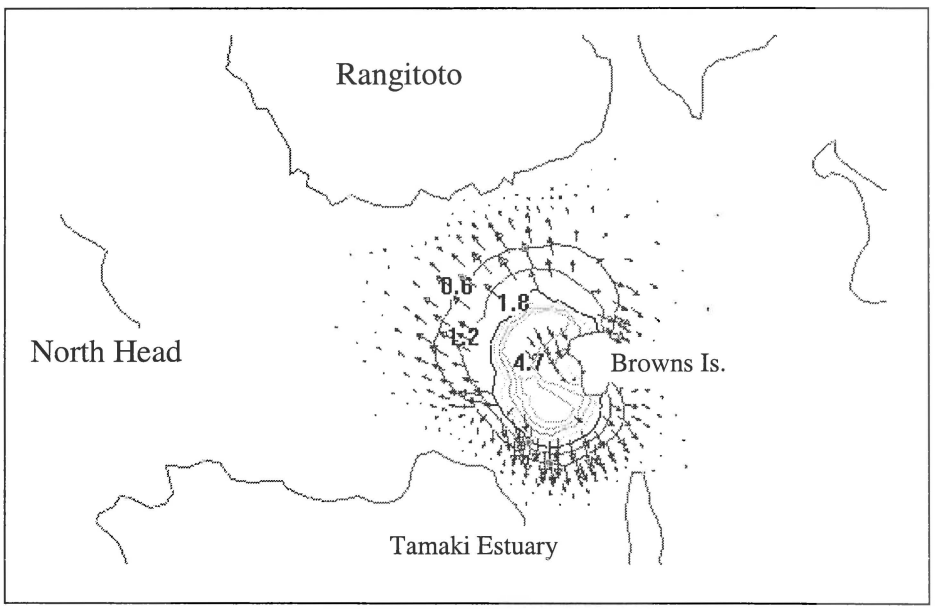

Figure 30. The results of dynamic initial condition after 10 seconds from the initial condition with maximum displacement 7 m.

RESULTS OF RANGITOTO CHANNEL EVENT

- **Submarine Explosion**

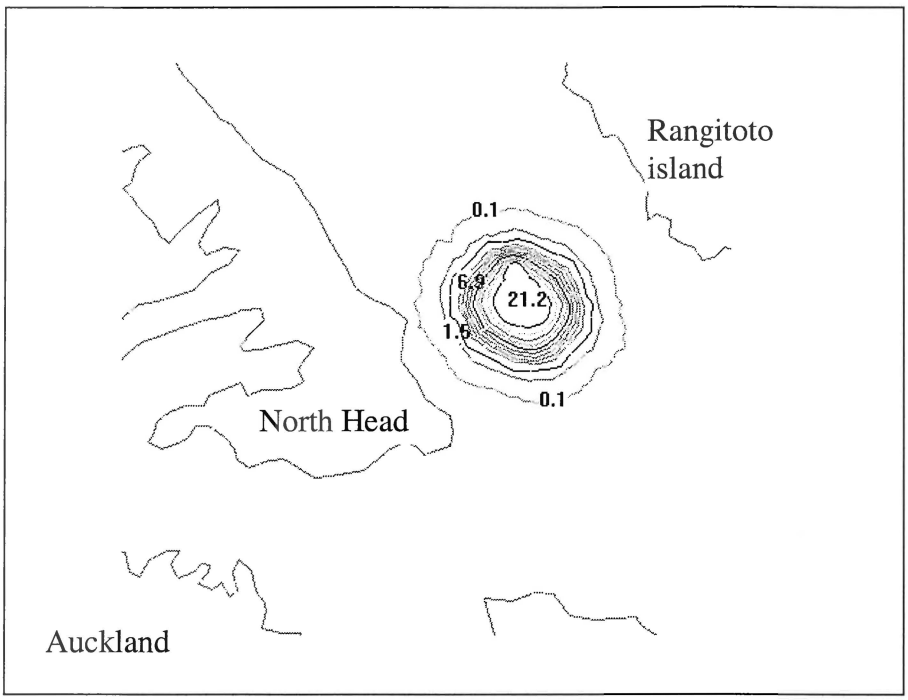

Figure 31. Initial condition of overlapping explosions at Rangitoto Channel.

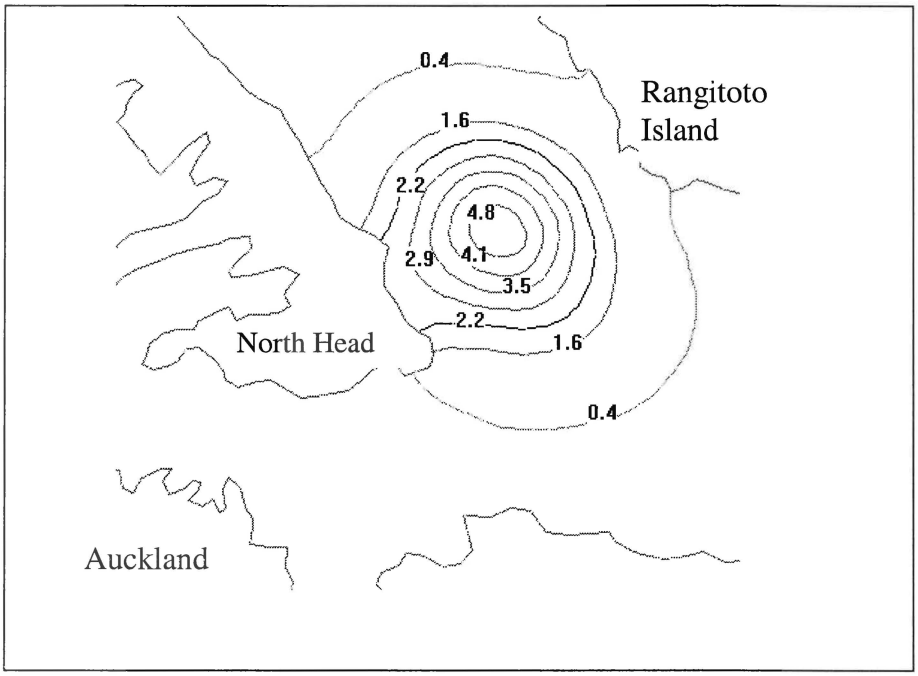

Figure 32. The pattern of waves one minute after 1st explosion.

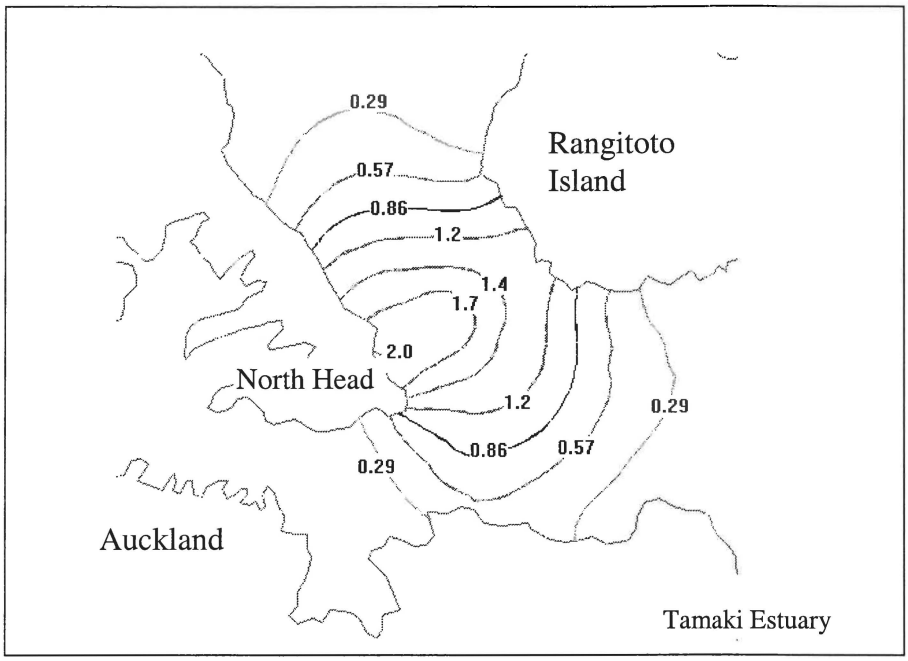

Figure 33. Three minutes after 1st explosion .

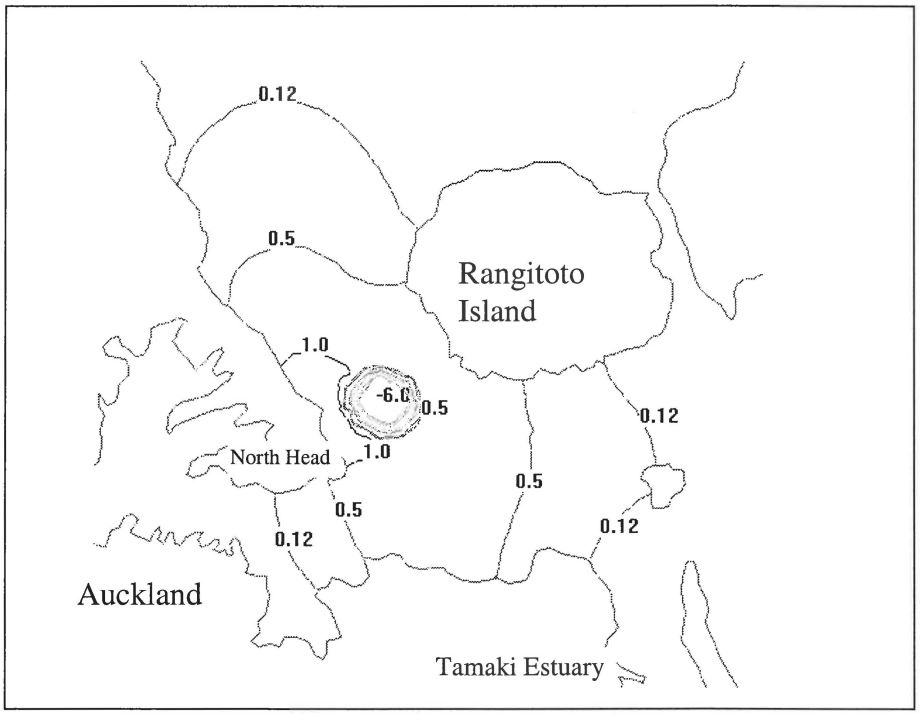

Figure 34. Five minutes from 1st explosion, collapsing of sea bottom is started 30 seconds before second explosion.

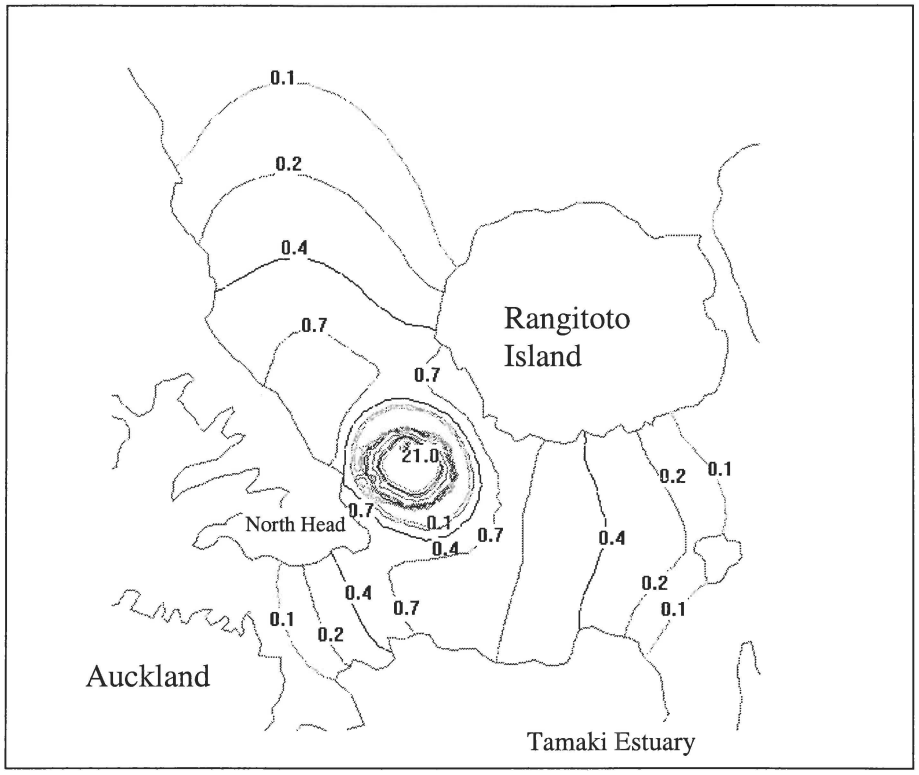

Figure 35. Second explosion is started with dome reaching 21.0 m height.

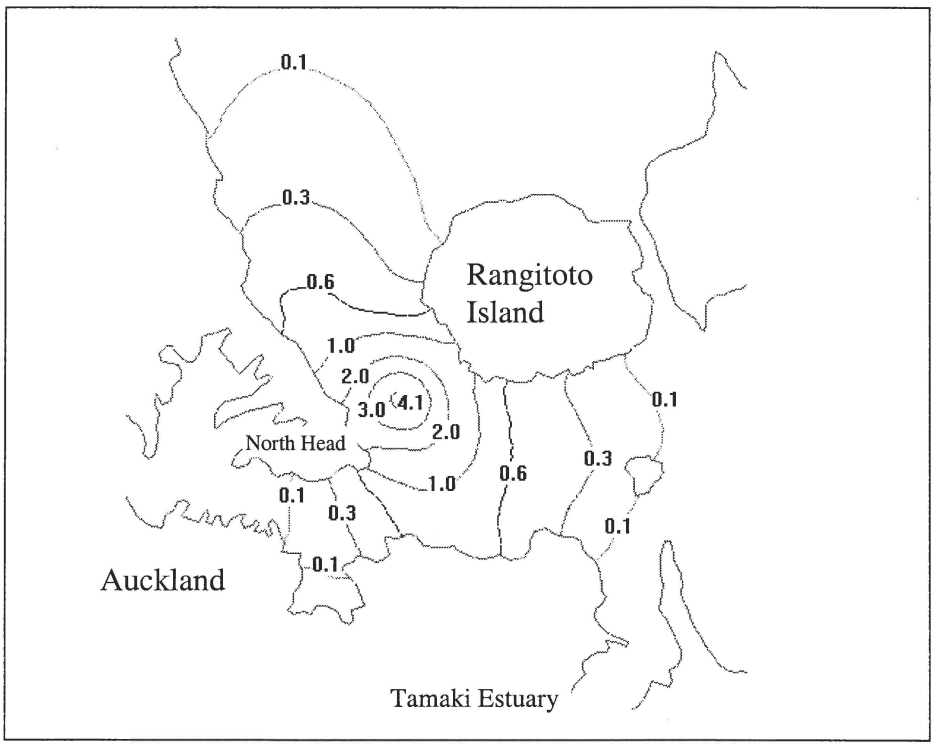

Figure 36. The waves pattern one minute after the last explosion.

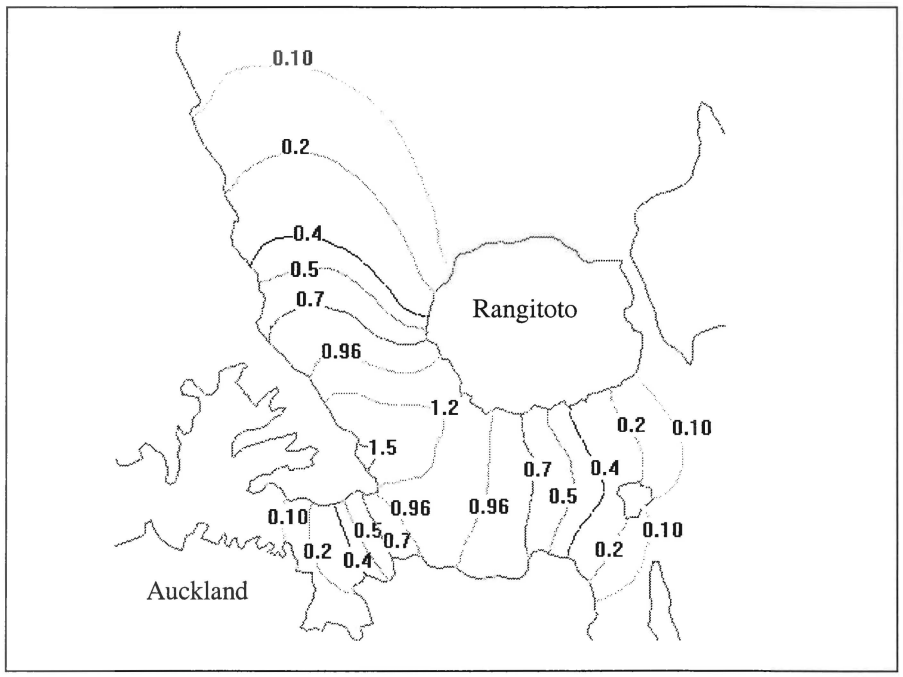

Figure 37. Five minutes after the last explosion.

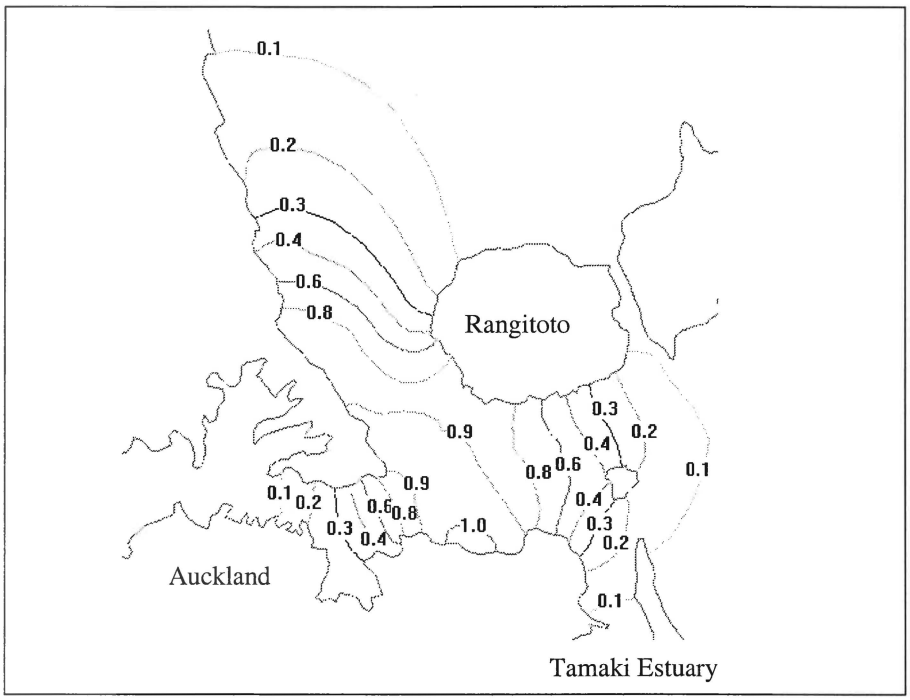

Figure 38. Ten minutes after the last explosion.

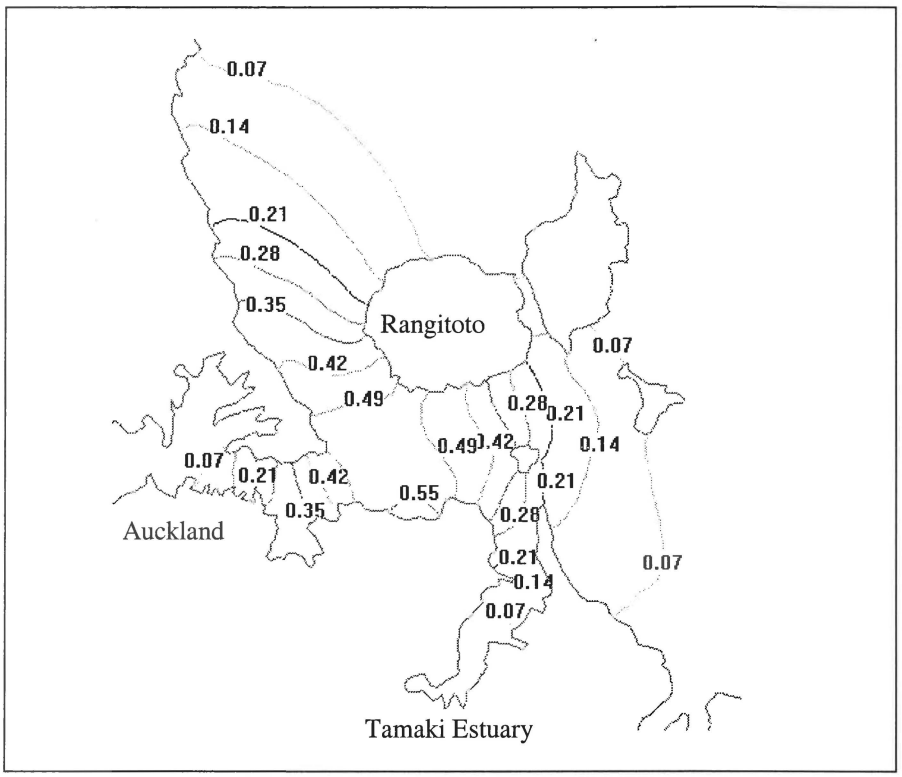

Figure 39. Twenty minutes after the last explosion.

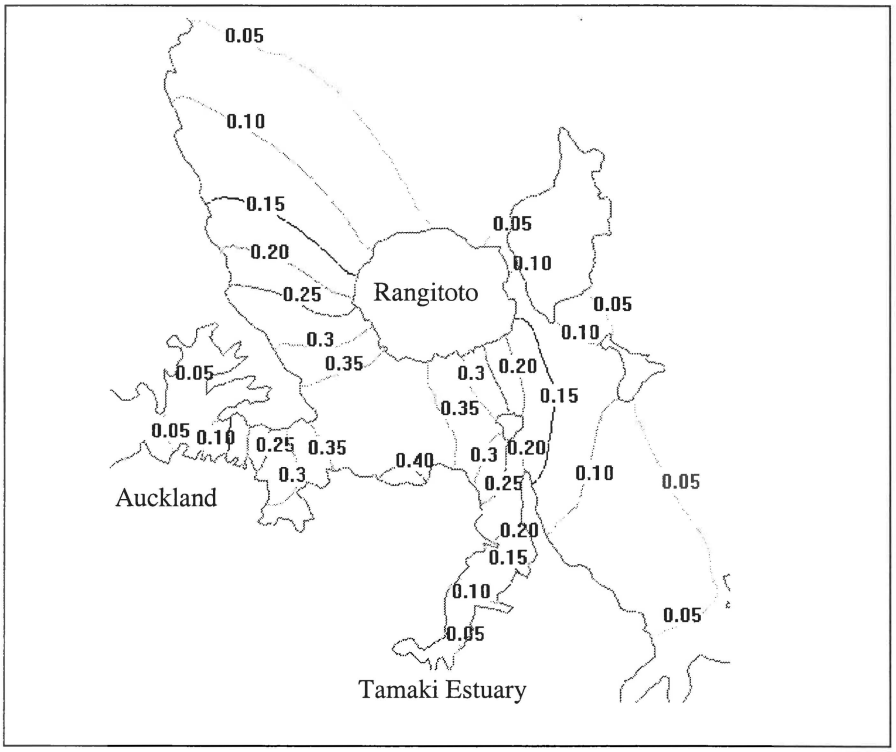

Figure 40. Thirty minutes after the last explosion.

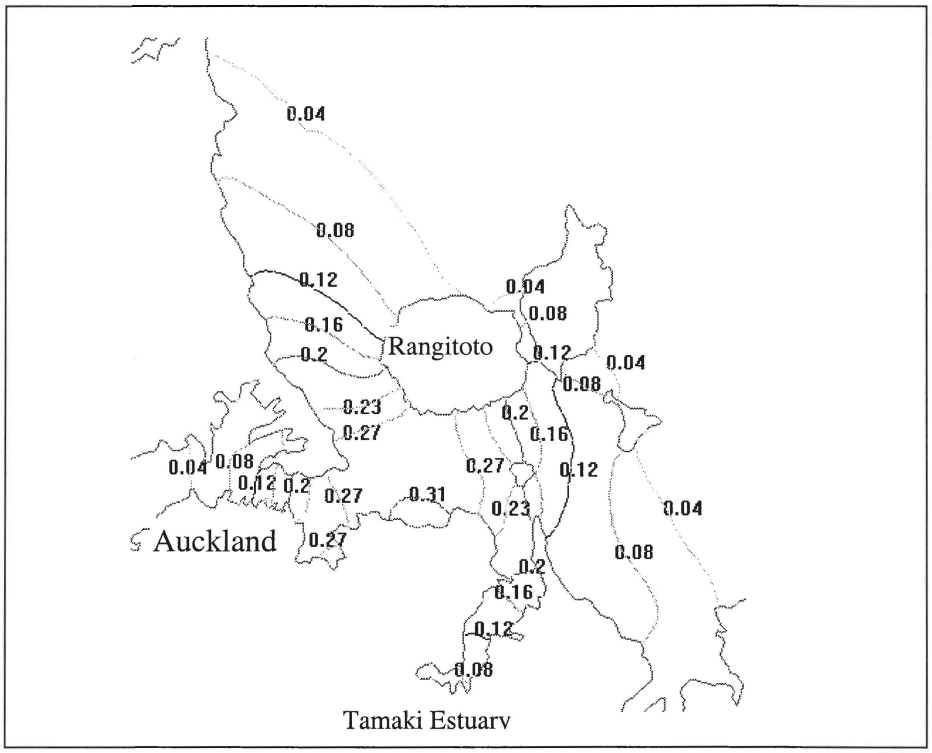

Figure 41. Forty minutes after the last explosion.

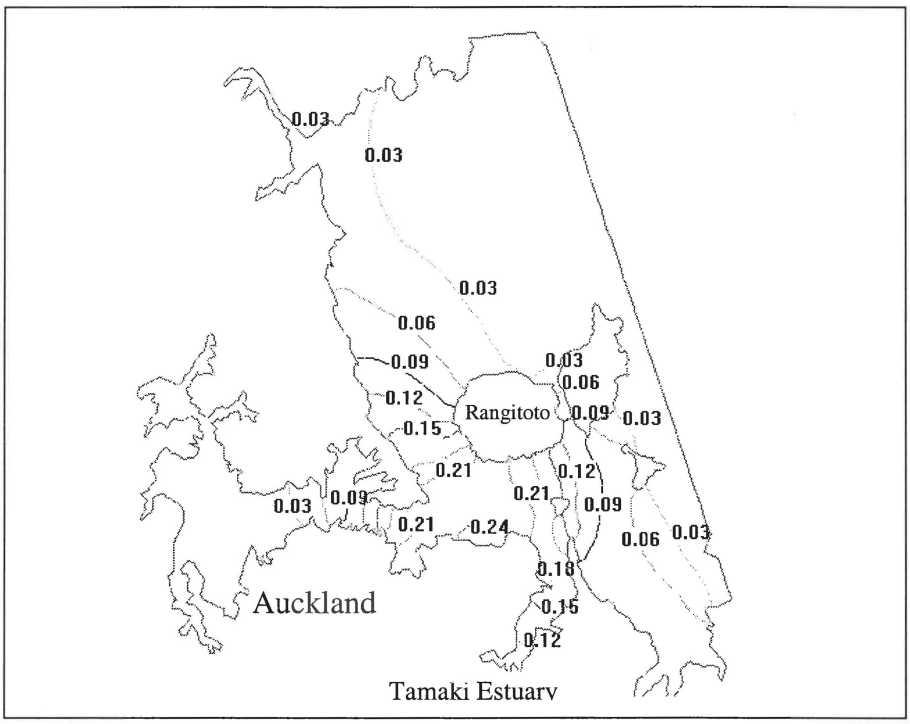

Figure 42. Fifty minutes after the last explosion.

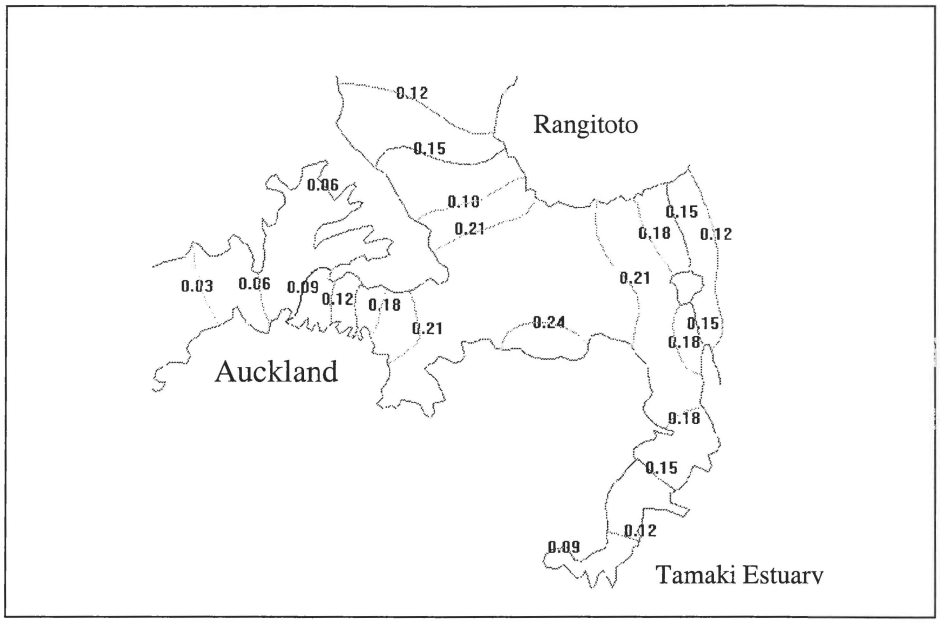

Figure 43. The water levels condition in Waitemata Harbour and its vicinity 50 minutes after the last explosion.

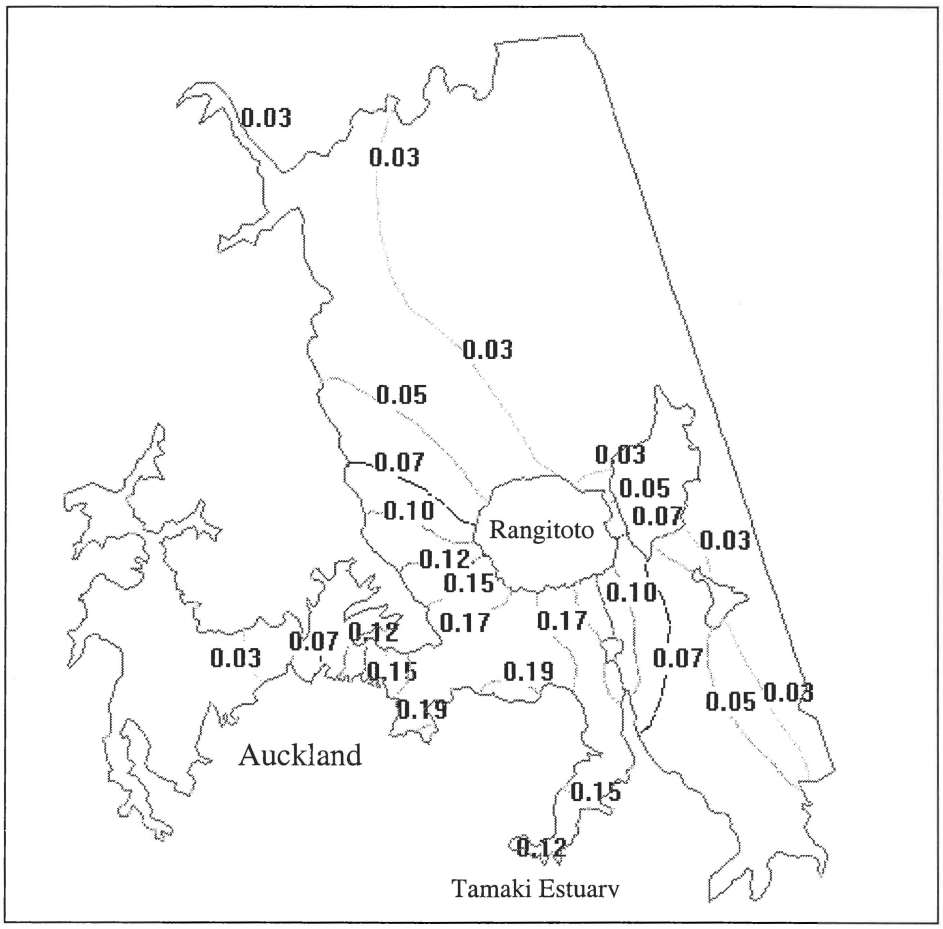

Figure 44. Sixty minutes after the last explosion.

CURRENT PATTERN

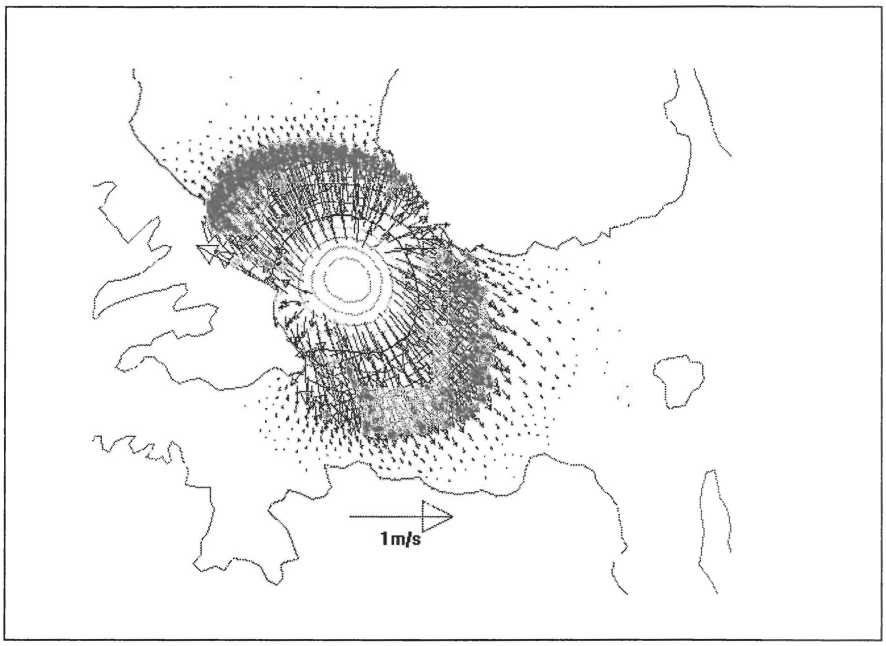

Figure 45. Current pattern one minute after 1st explosion

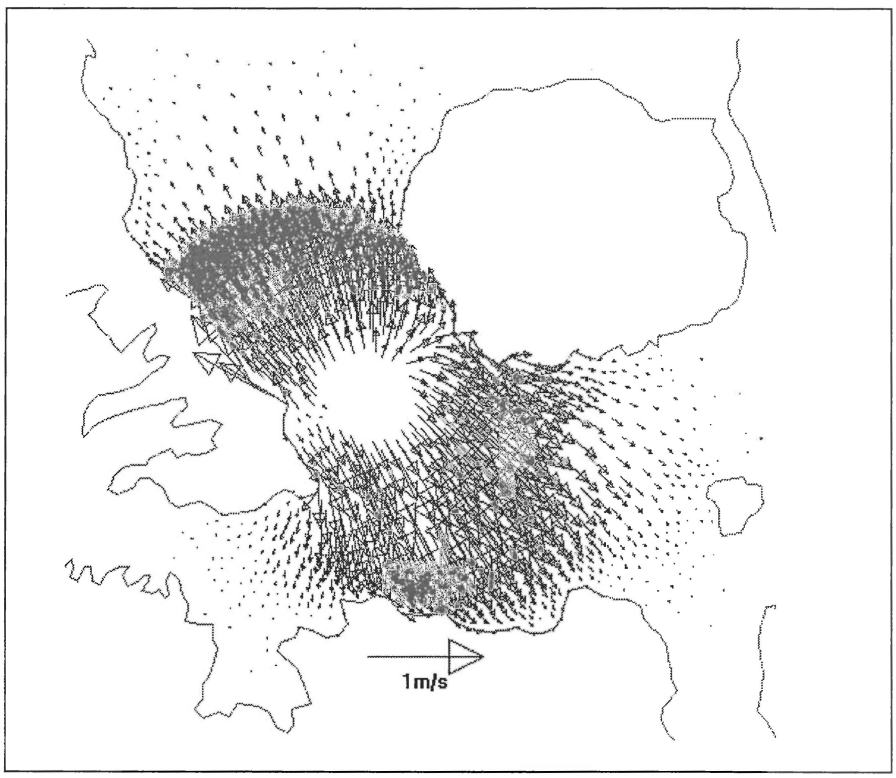

Figure 46. Three minutes after 1st explosion

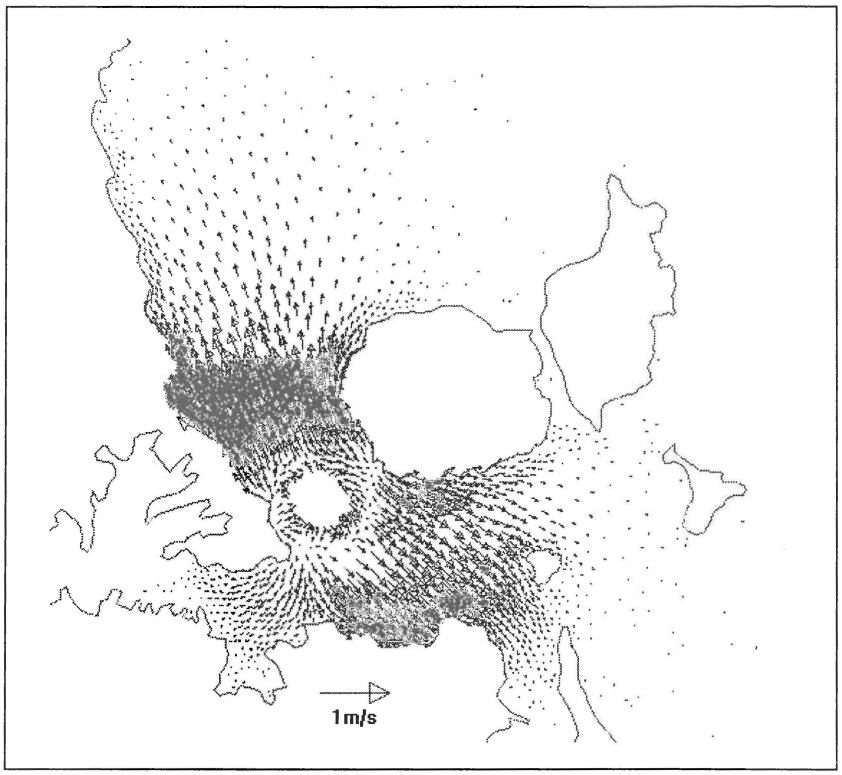

Figure 47. Current pattern at final stage of second explosion (five minutes after 1st explosion).

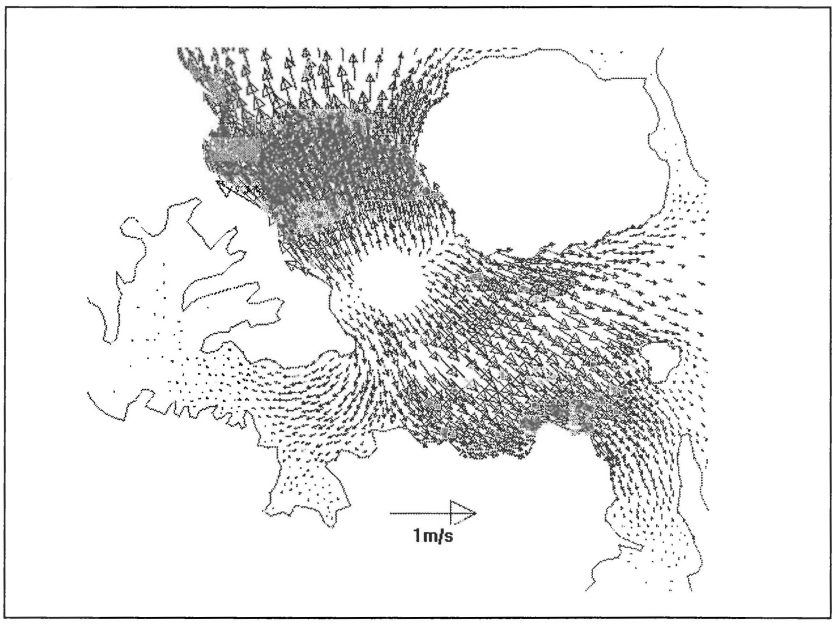

Figure 48. Five minutes after the last explosion strong currents enter the Tamaki Estuary.

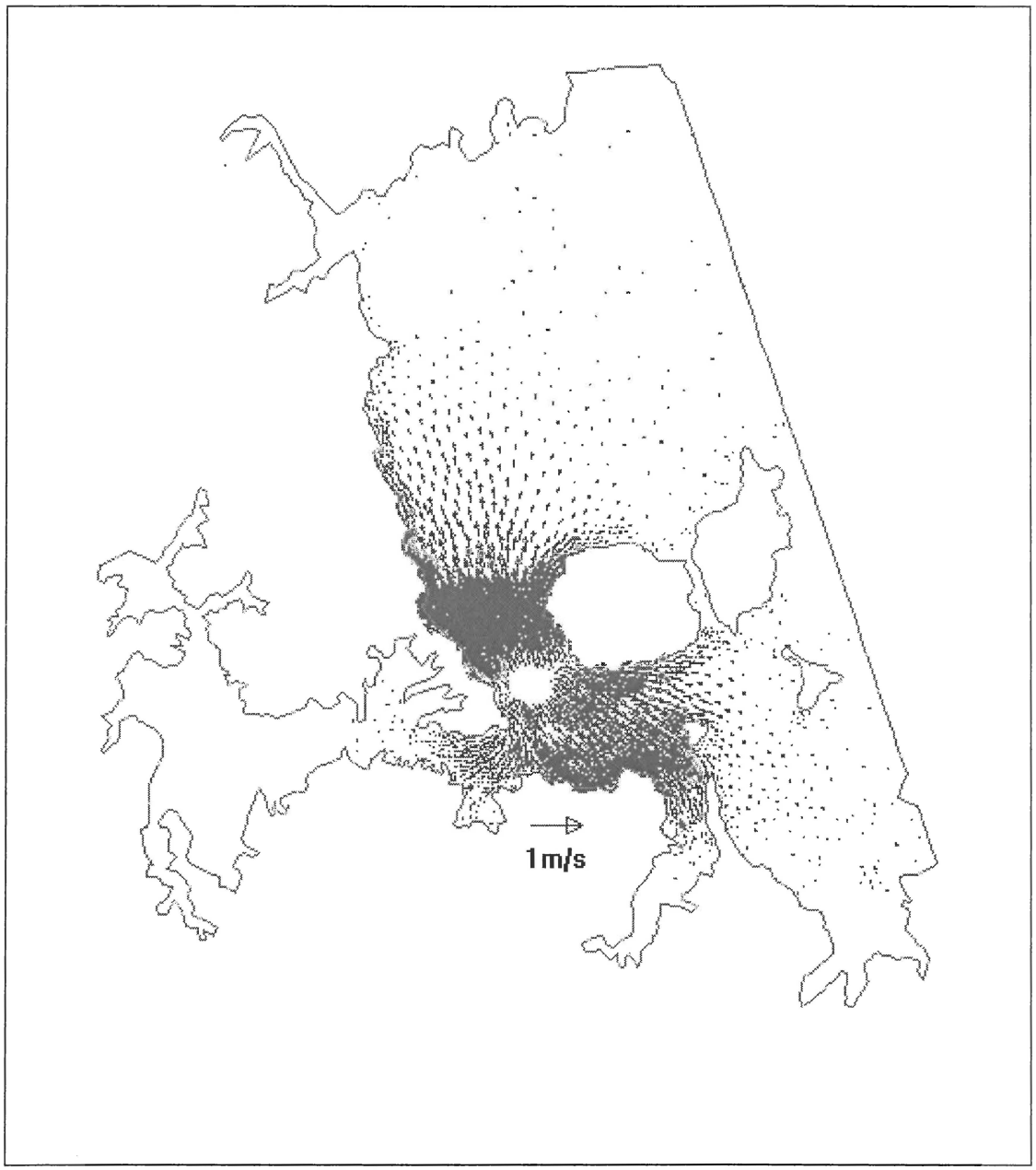

Figure 49. General view of current pattern 5 minutes after the last explosion. Strong current flows along the coastline to the north, around the Rangitoto Volcano and down to St.Heliers Bay and entrance of Waitemata Harbour. To the southeast the flow enter Tamaki Estuary.

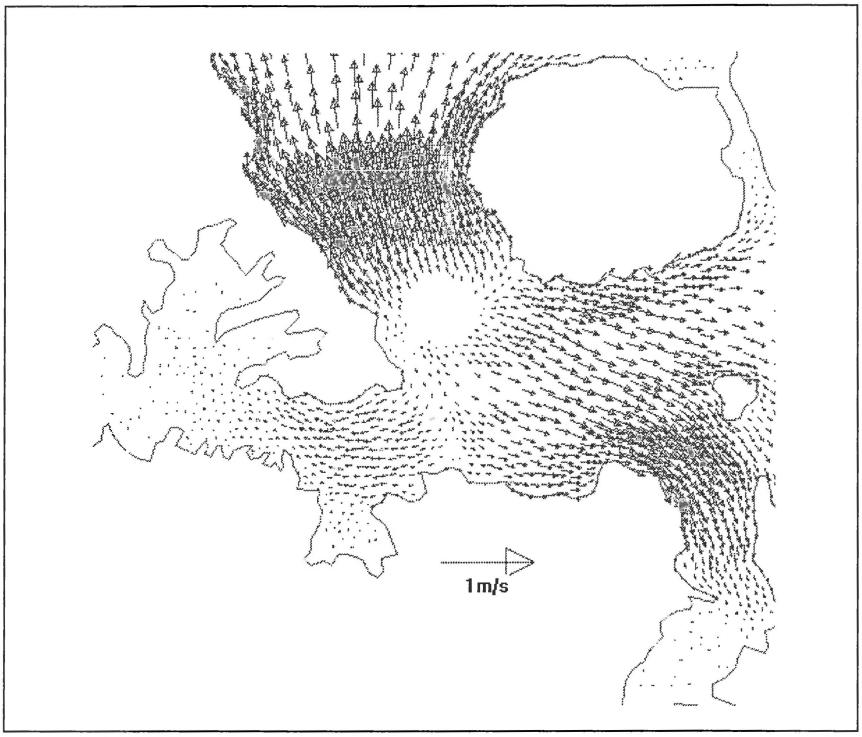

Figure 50. Current pattern 10 minutes after the last explosion. Strong current occured along the coastline move up to the north, along the northern and southern part of Rangitoto Volcano, and at the mouth of Tamaki Estuary. Browns Island blocked the flows and directed them toTamaki Estuary. In Waitemata Harbour current flows reach the Shoal Bay area and Auckland Harbour Bridge.

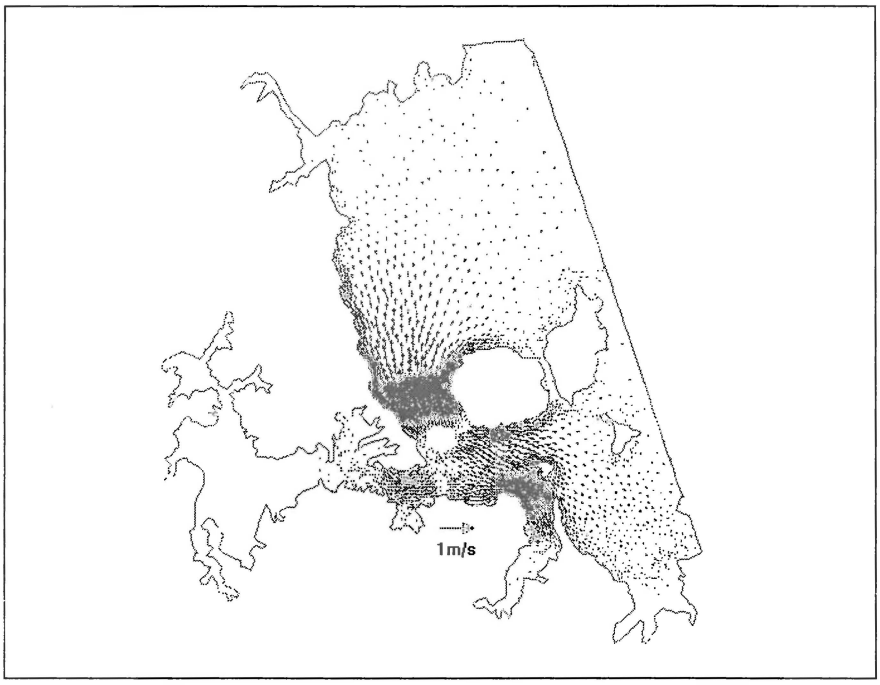

Figure 51. General view of current pattern after 10 minutes from the last explosion.

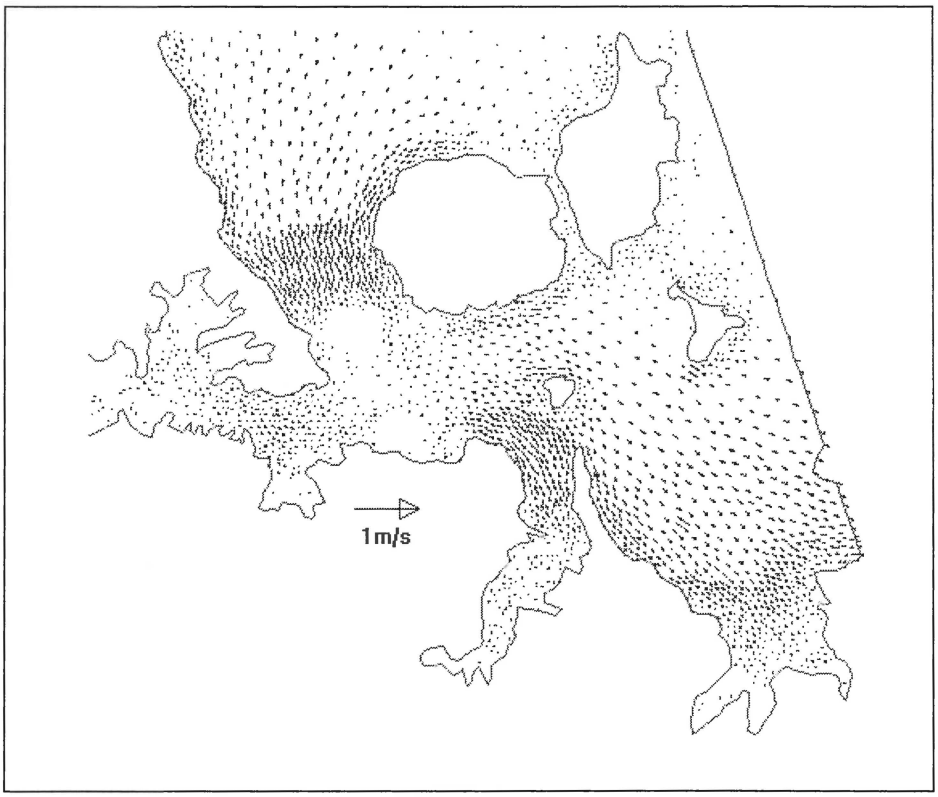

Figure 52. Current pattern after 40 minutes from the last explosion. The intensity of the flows are decreasing. However, rapid flow still occurs at the Rangitoto channel, mouth of Tamaki Estuary and Waitemata Harbour.

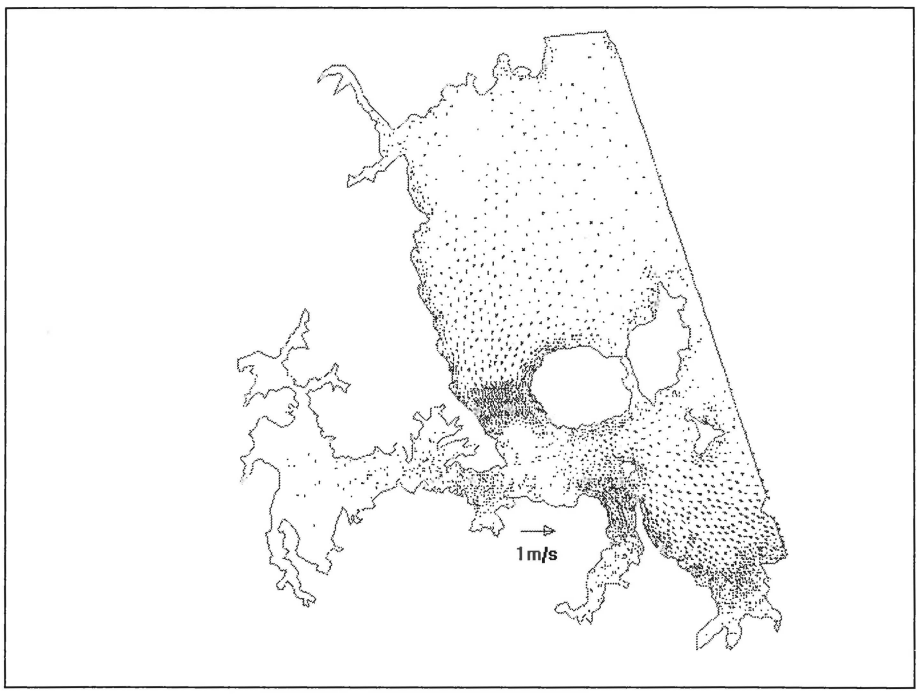

Figure 53. General view of current pattern after 40 minutes from the last explosion.

RESULTS OF TAMAKI ESTUARY EVENT

- **Submarine Explosion with maximum displacement at sea bottom 2.8 m**

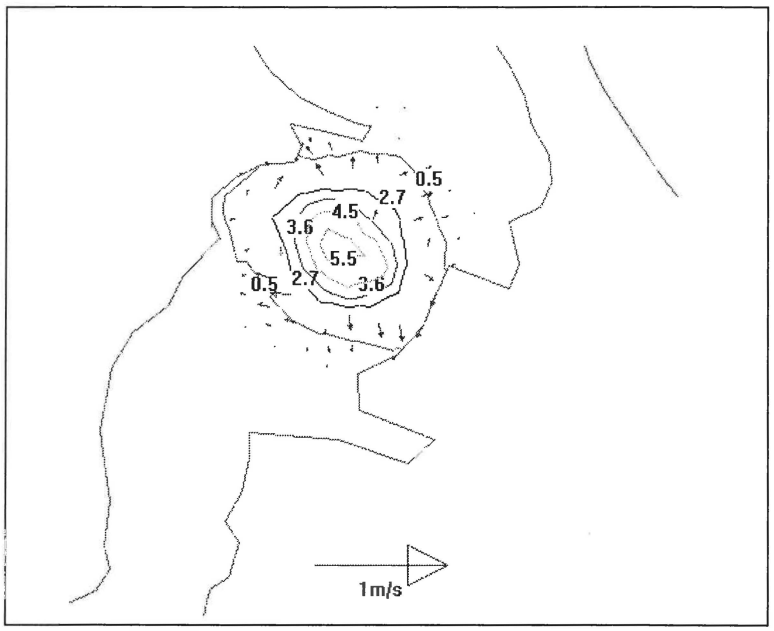

Figure 54. The initial condition of the submarine explosion for Tamaki Estuary.

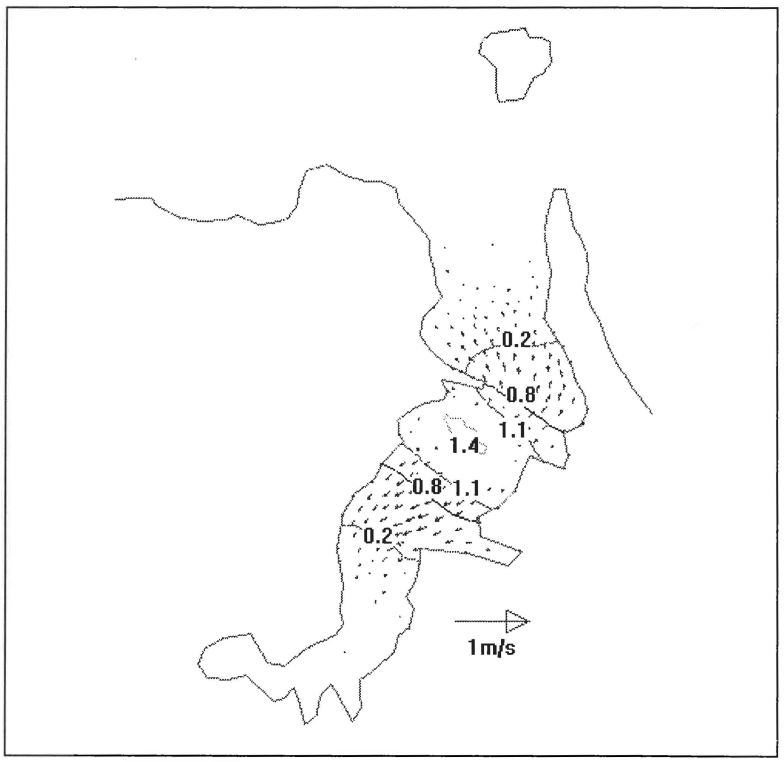

Figure 55. Wave and current pattern 1 minute after the explosion.

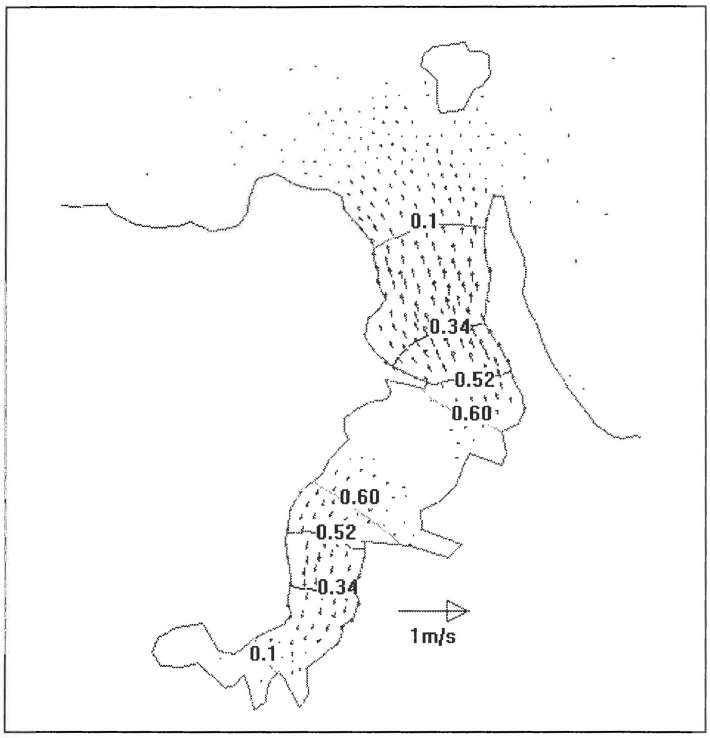

Figure 56. The condition of the estuary 5 minutes after explosion

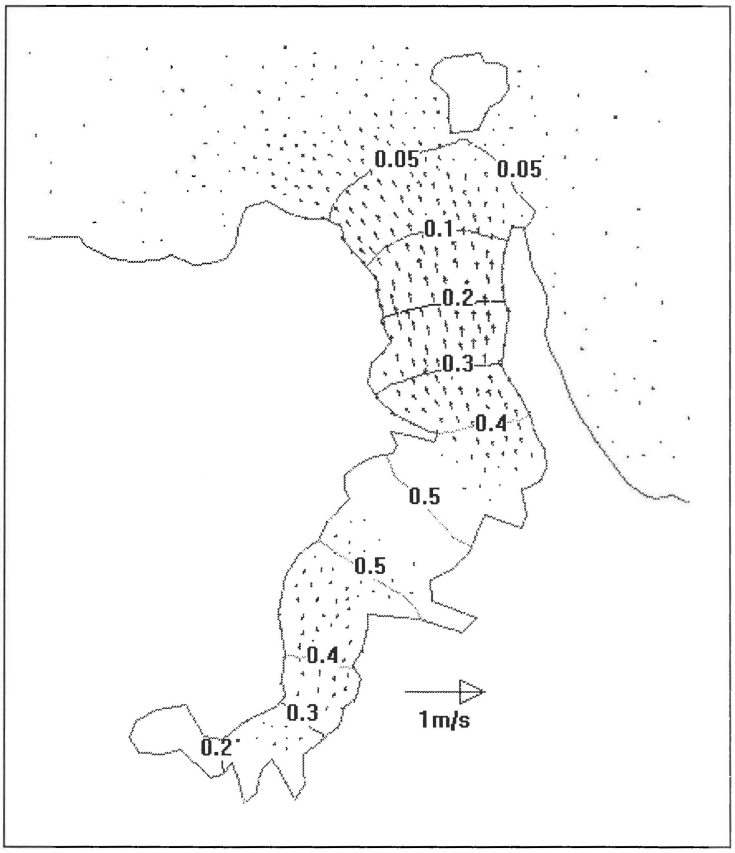

Figure 57. Ten minutes after explosion, at the end of estuary the wave height is 0.2 m

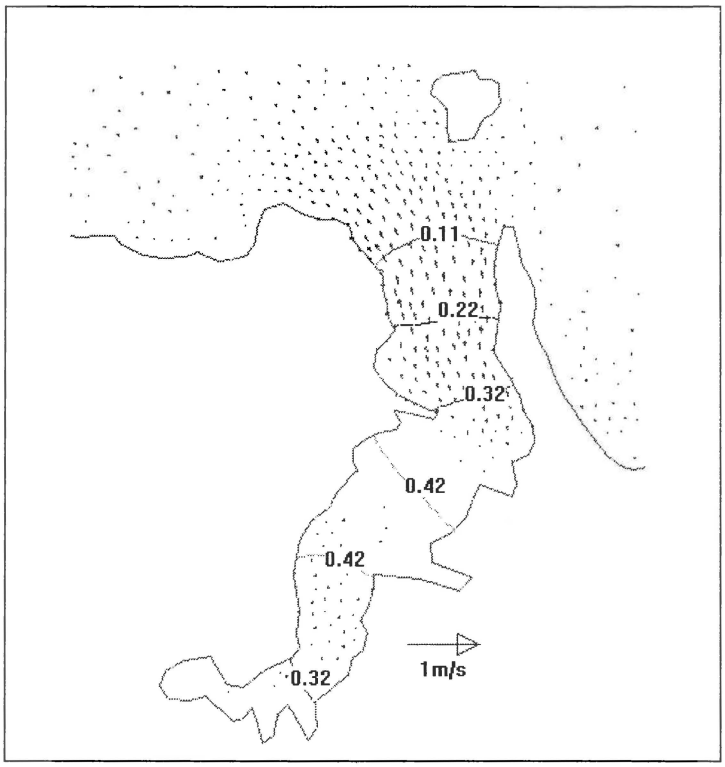

Figure 58. At 15 minutes after explosion the water level at end of eastuary (upstream) reaches 0.32 m and the current flow start to change direction to downstream. The slack water occurs.

RESULTS OF BROWNS (MOTUKOREA) ISLAND EVENT

- **Pyroclastic flow mechanism with dynamic initial condition**

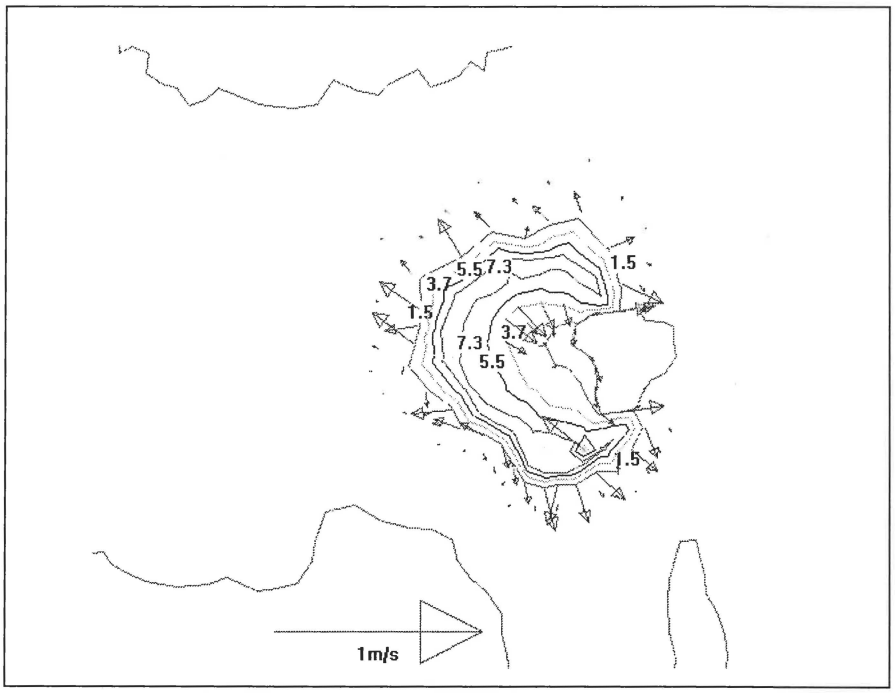

Figure 59. Initial condition of a pyroclastic flow entering the sea at Browns Island using dynamic initial condition.

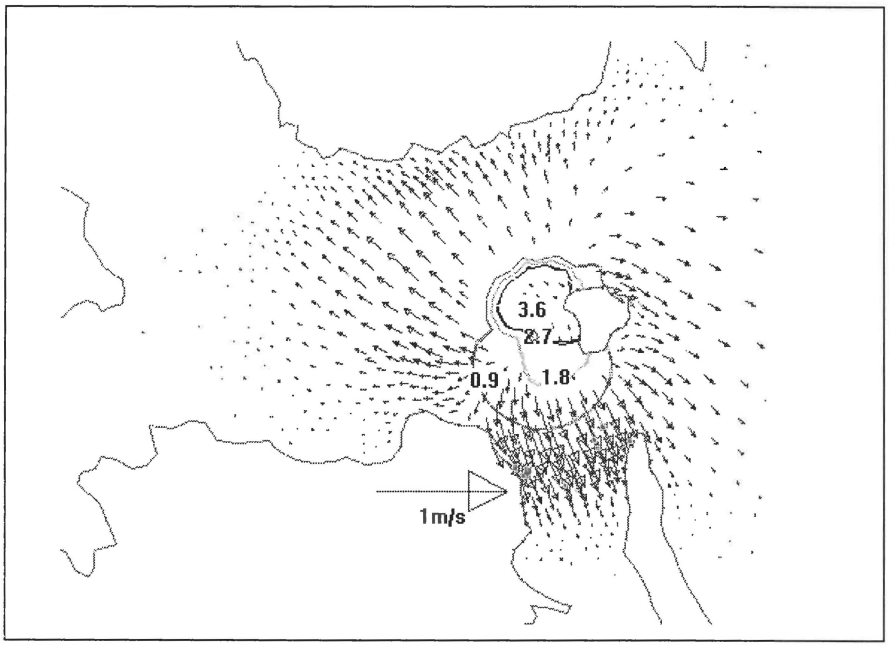

Figure 60. The pattern of waves and currents one minute after initial condition. Currents are rapidly flowing towards the mouth of Tamaki Estuary.

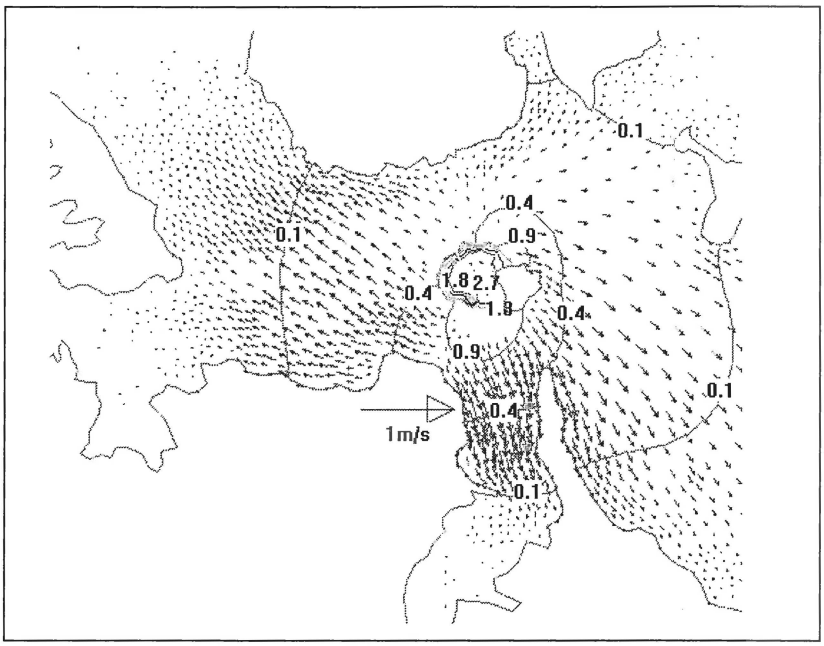

Figure 61. The pattern of waves and currents 5 minutes after the initial condition.

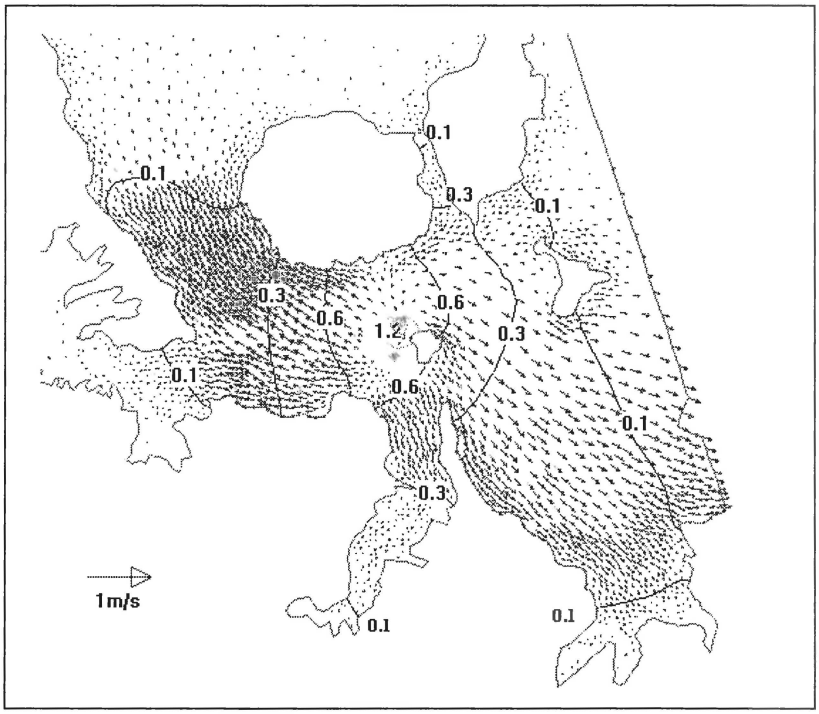

Figure 62. After 30 minutes from the initial condition, current flows into Tamaki Estuary are reduced and stronger current flows occur in Rangitoto Channel.

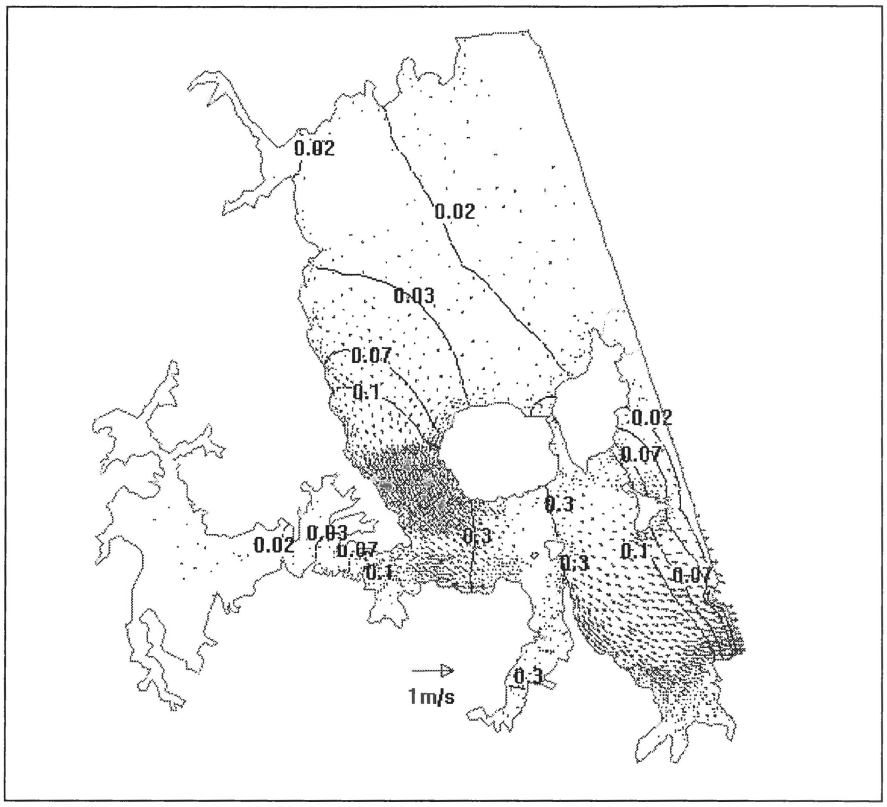

Figure 63. Sixty minutes from the initial condition, strong current still flows along the coastline from eastern beach of Musick Point down to Motukaraka Island and around the Rangitoto Island. The waves propagates up to the north with 0.02 m height. In Waitemata Harbour the wave varies from 0.02 m to 0.25 m.

RESULTS OF RANGITOTO VOLCANO EVENT

- **Pyroclastic flow mechanism with dynamic initial condition.**

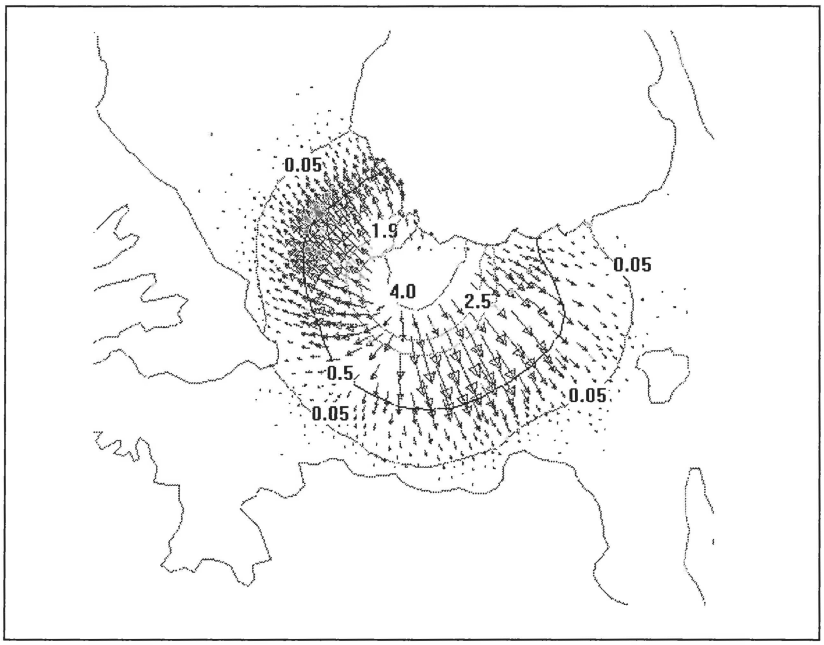

Figure 64. Initial condition of a pyroclastic flow entering the sea at Rangitoto Island using dynamic initial condition.

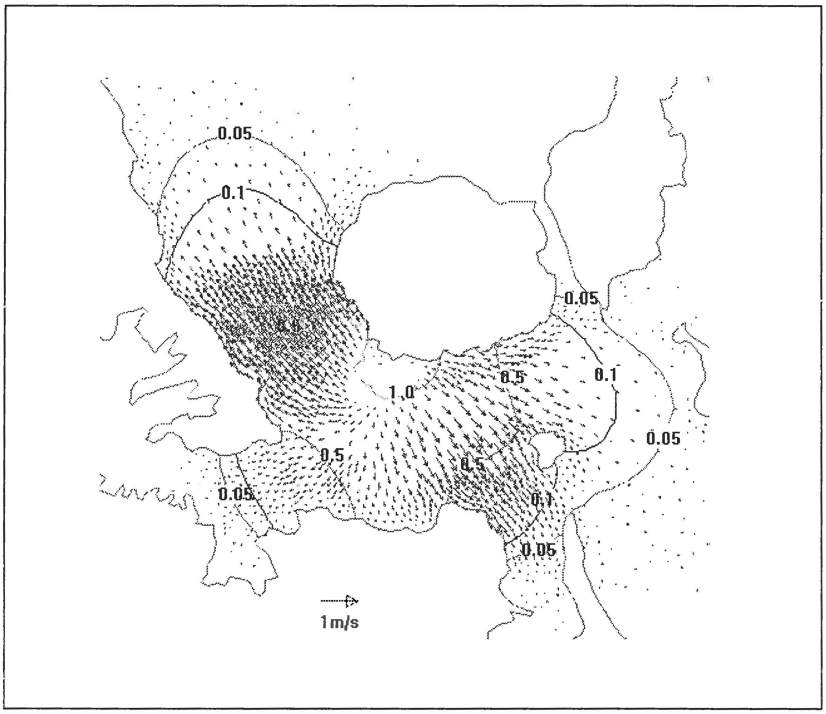

Figure 65. The pattern of currents and waves five minutes after initial condition.

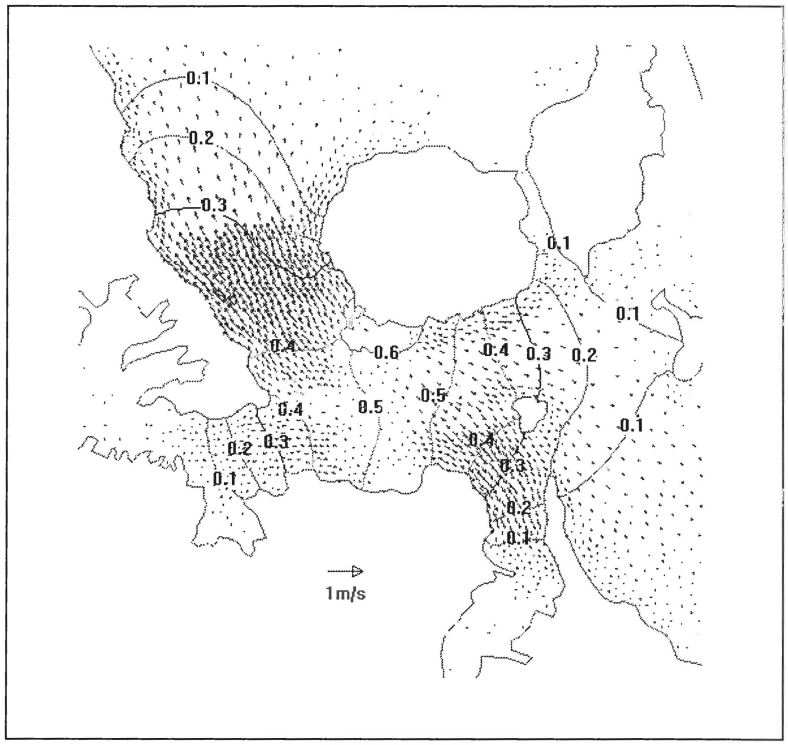

Figure 66. The waves and currents pattern after 10 minutes from initial condition.

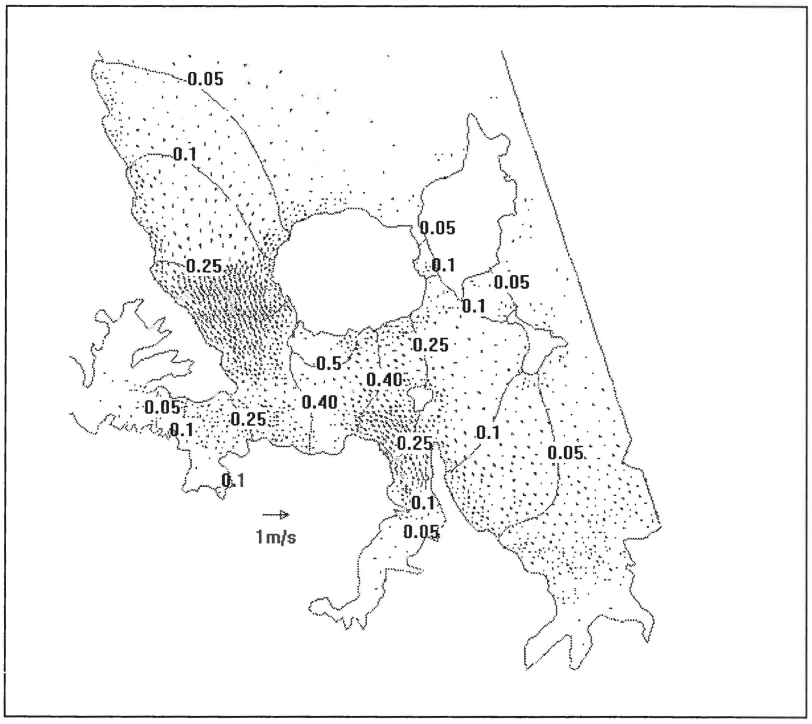

Figure 67. The waves and currents pattern after 20 minutes from initial condition. The current speed reduced and 0.1 m waves reached Auckland Harbour and Half Moon Bay in Tamaki Estuary.

APPENDIX.2.

Photographic Sequence of The Experiments

Preparation :

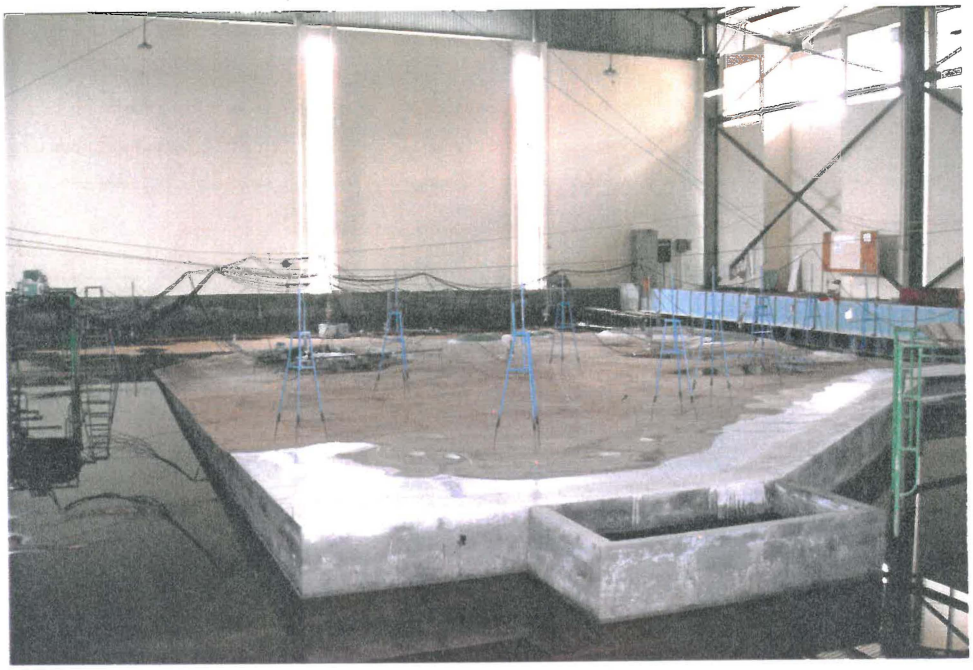

Figure Ap2.1. Overall view of wave basin and the three dimensional model. Sixteen wave sensors (blue tripods) and five current meters were installed and connected with HP data logger and computer for further processesing.



Figure Ap.2.2. The capacitance wave sensor (white colour) and tripod (blue colour) used to measure the tsunami waves in the model.

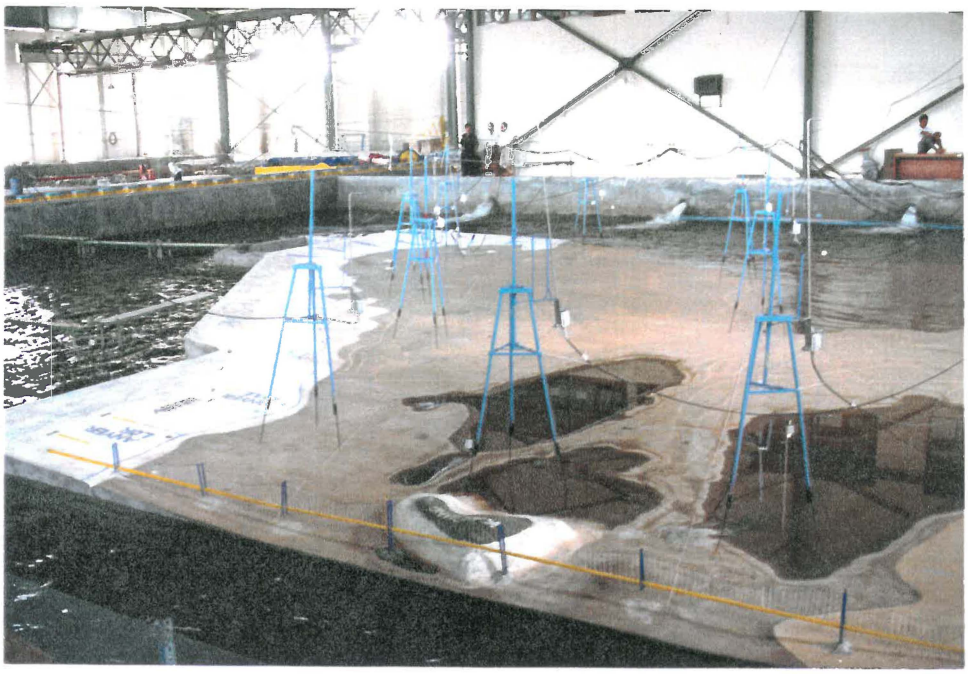

Figure Ap.2.3. Water from the reservoir starting to fill the wave basin

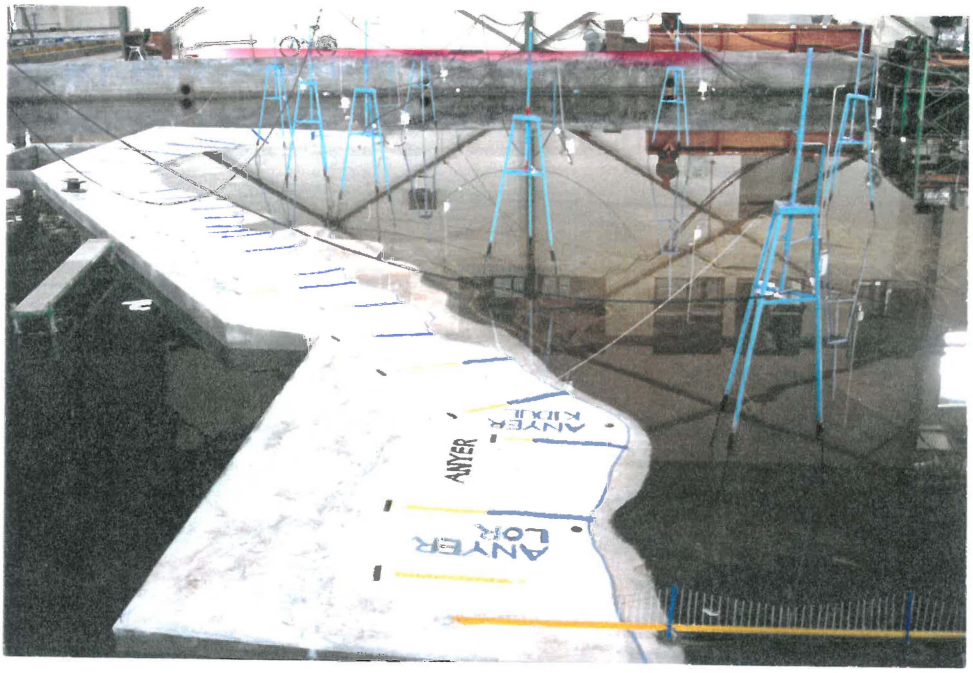

Figure Ap.2.4. The water level at the shoreline could be adjusted by controlling the outlet and intake pumps.



Figure Ap.2.5. The water surface in the wave basin before instrument calibration. It is necessary to keep the water surface calm to set the zero levels for measurement of wave height and current velocities.



Figure Ap.2.6. The computer and HP data logger before start the experiments.

Submarine Explosion :

- ***Experiments Without Chamber (point source).***
- ***Low Intensity of Explosion (2 tubes).***

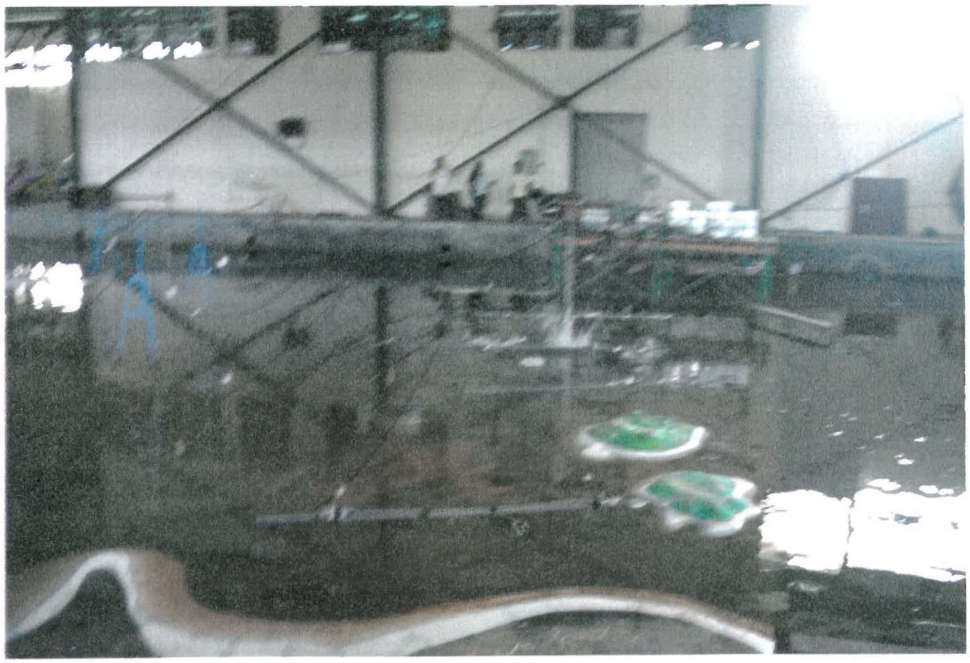

Figure Ap.2.7. The initial stage of submarine explosion test. The typical disruption of the water surface resulting from a point source mechanism can be seen at the source of explosion with the small quantity of explosive used, a dome formed in the water surface. This dome had just begin to break up when the photo was taken.



Figure Ap.2.8. Concentric eruption-waves emanating from the explosion point have propagated outside the Krakatau complex. The first three waves are evident.



Figure Ap.2.9. The initial waves reaching the main shores of the wave basin. The concentric pattern is still clearly evident.



Figure Ap.2.10. The first wave reaches the west coast of Java causing inundation of low lying areas.

- ***Experiments Without Chamber (point source).***
- ***High Intensity of Explosion (7 tubes).***



Figure Ap.2.11. With increasing the intensity of explosion, the water surface at the source of explosion no longer formed a dome shape, but developed a crater instead. The initial crater is showing in this photo.

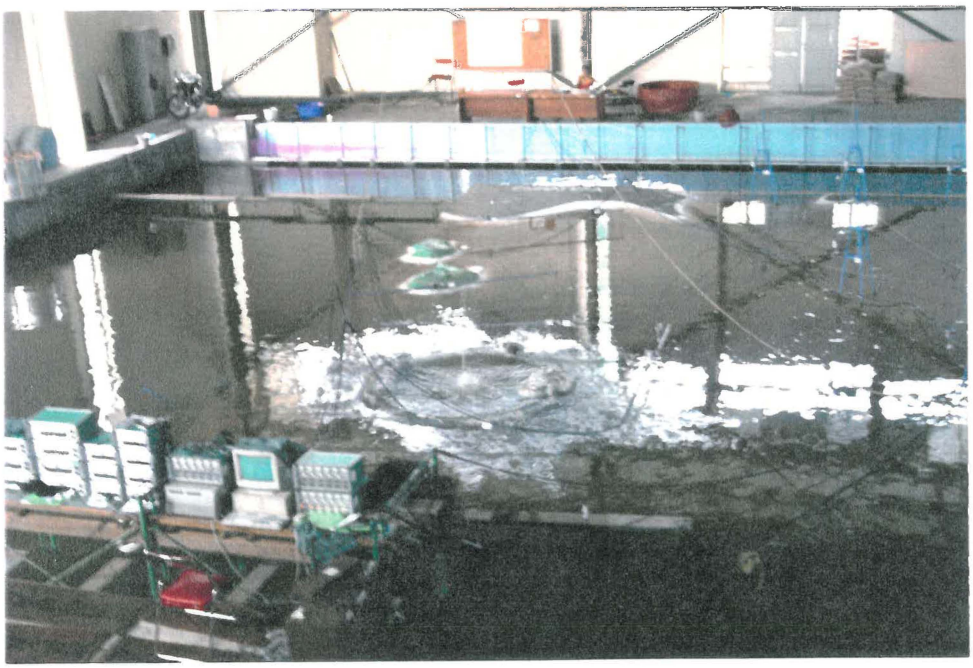

Figure Ap.2.12. Shortly after the explosion, the water surrounding the crater rush inwards and collide to form the jet shown in the centre of the crater. Waves then start to propagate outwards from the centre as the jet collapses.



Figure Ap.2.13. A few seconds after explosion, the bore and accompanying waves leave the vicinity of the crater at Krakatau.

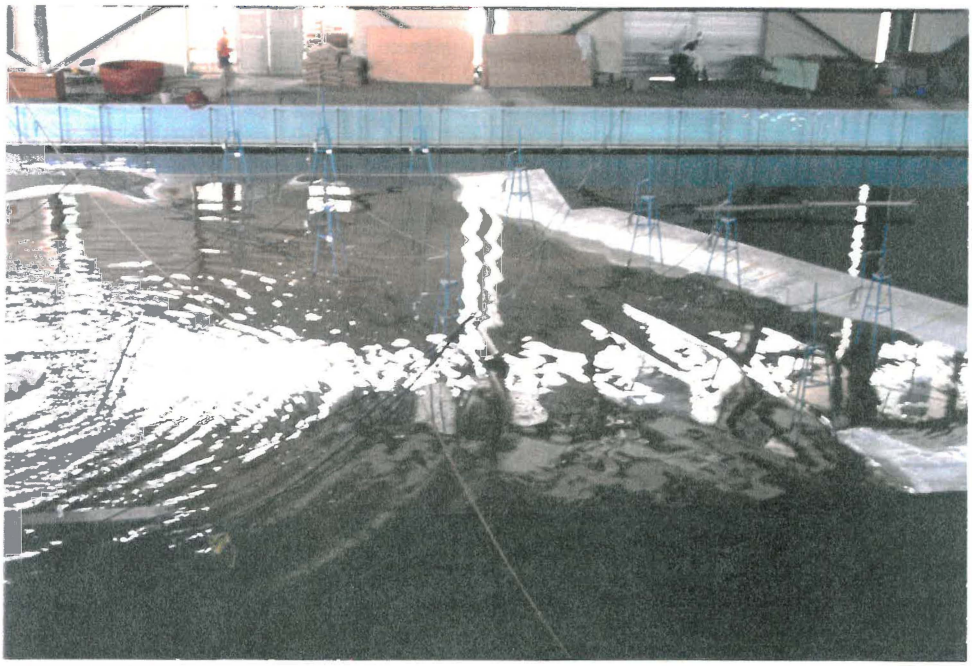

Figure Ap.2.14. The waves start approaching the west coast of Java.

- ***Experiments With Chamber.***
- ***Low Intensity of Explosion (2-3 tubes).***



Figure Ap.2.15. The preparation of explosion test with a confining chamber. The area around the chamber were infilled with sand to represent the Krakatau Island before it exploded.



Figure Ap.2.16. The initial stages of the explosion with a confining chamber. The white in the centre of the Krakatau complex was smoke from the explosion. The initial waves formed by the explosion were obscured.

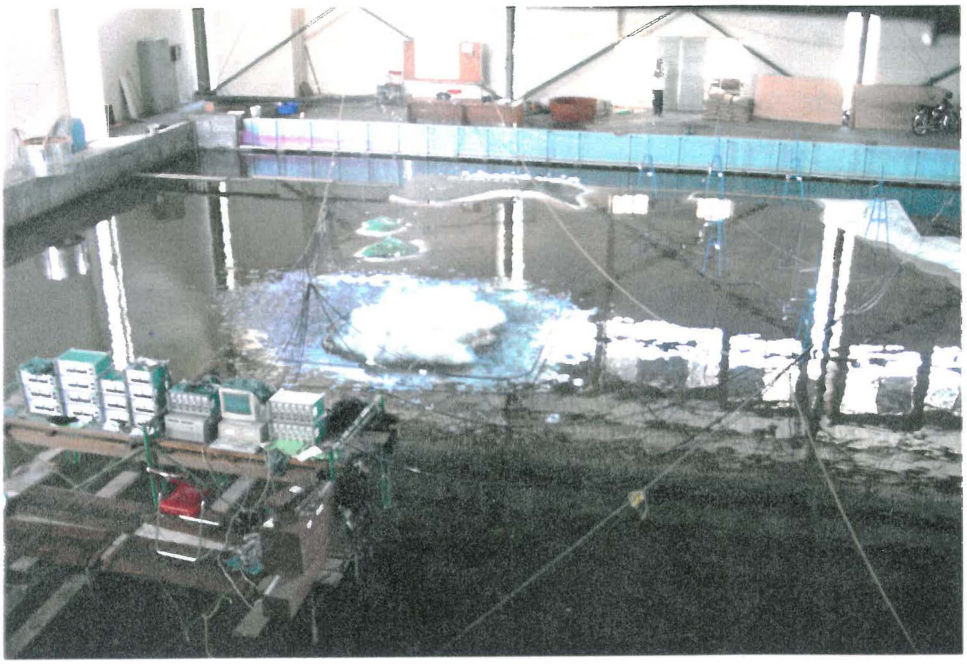

Figure Ap.2.17. A second after explosion, no waves have formed outside the Krakatau Island complex.

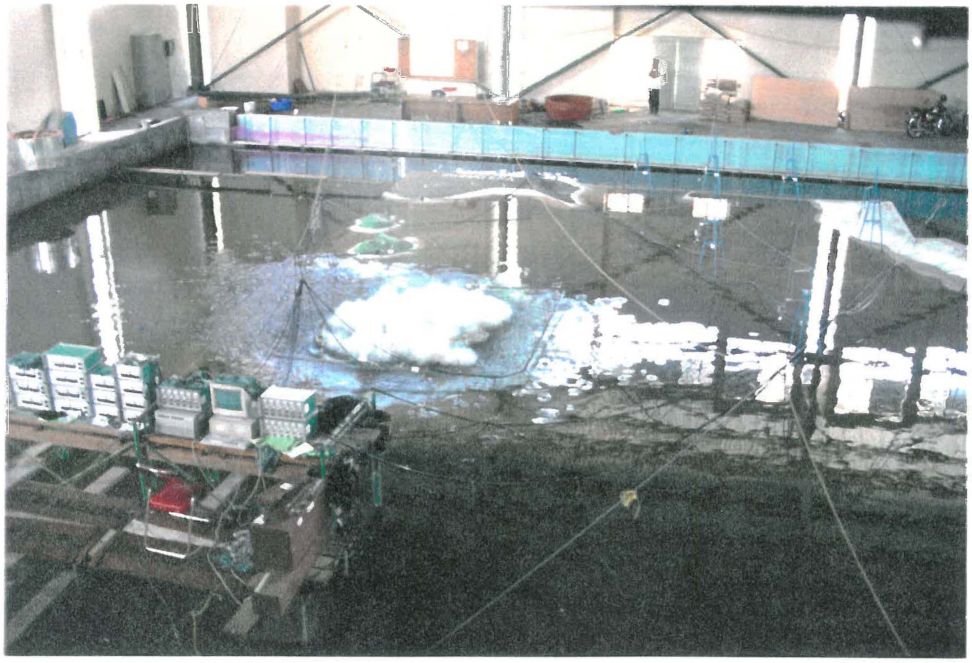

Figure Ap. 2.18. A few seconds after Figure Ap.2.17, the first wave starts to move towards the East, approaching the west coast of Java. The smoke still remains around the Krakatau complex.



Figure Ap.2.19. Shortly afterwards three to five leading waves are evident approaching the Sumatera coast and west coast of Java.

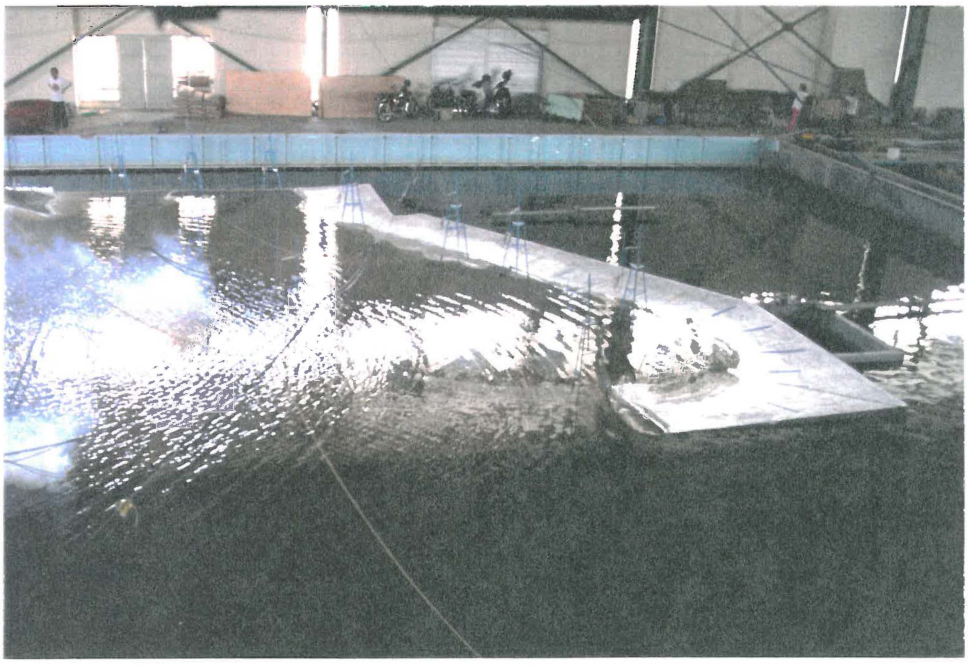

Figure Ap.2.20. The waves inundating the west coast of Java.

- ***Experiments With Chamber.***
- ***Medium Intensity of Explosion (4-6 tubes).***



Figure Ap.2.21. The medium intensity explosion test severely disrupted the water and formed a crater instead of forming a dome.



Figure Ap.2.22. A second after the explosion, the disrupted water dropped back into the crater. The white colour is the smoke from the explosion.

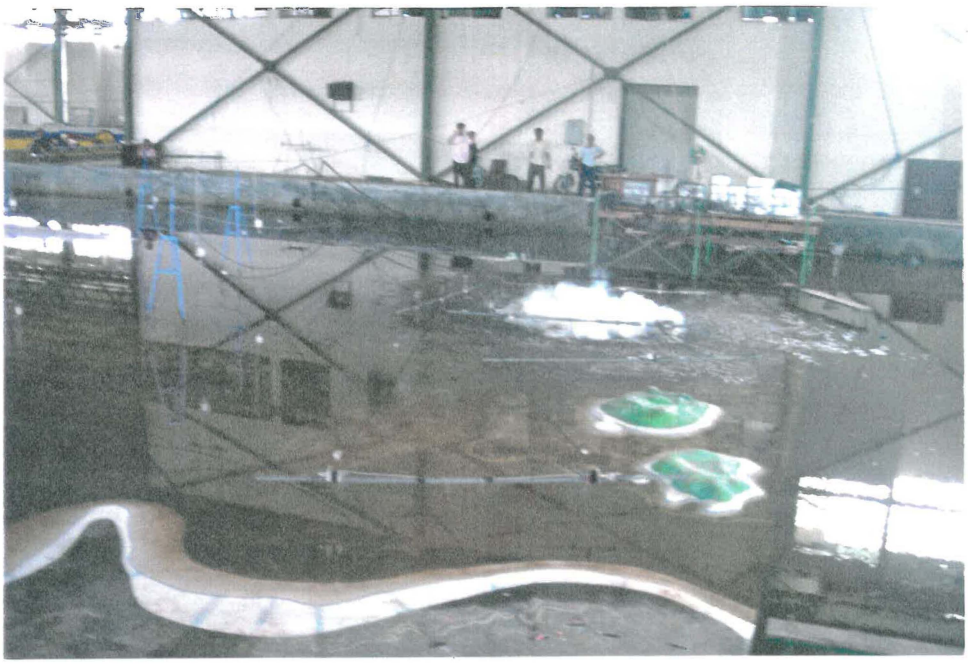

Figure Ap.2.23. Three seconds after explosion the initial wave has formed due to the expansion of the crater.

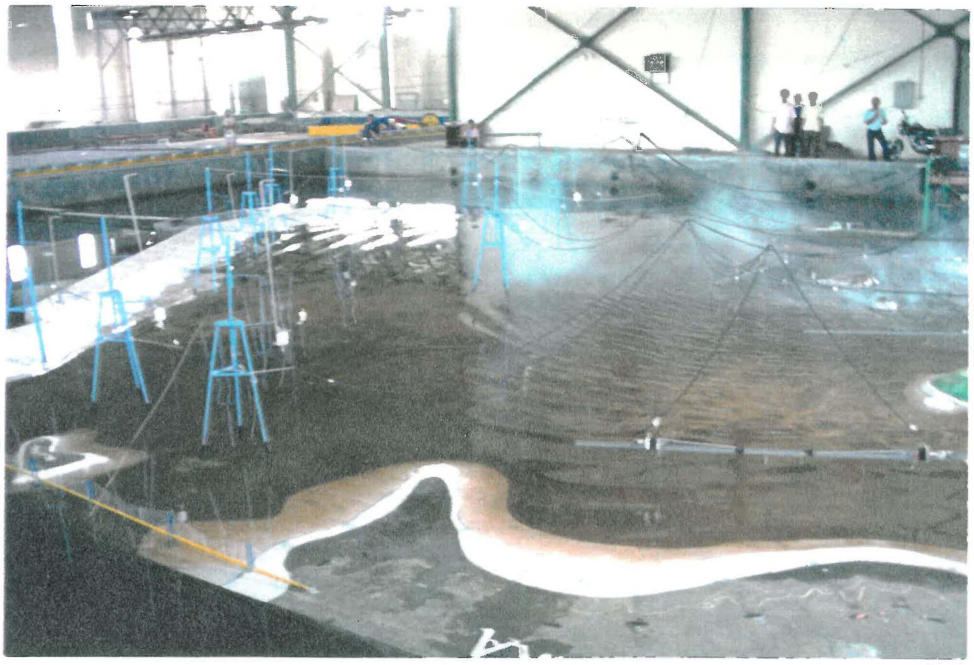

Figure Ap.2.24. The pattern of the waves approaching the west coast of Java and the Sumatera coast.

- ***Experiments With Chamber.***
- ***High Intensity of Explosion (7-9 tubes).***



Figure Ap.2.25. The high intensity explosion with a confining chamber showing the initial stage of the explosion (above) and the initial wave formation (below). The leading waves were generated mainly by the expansion of the crater.



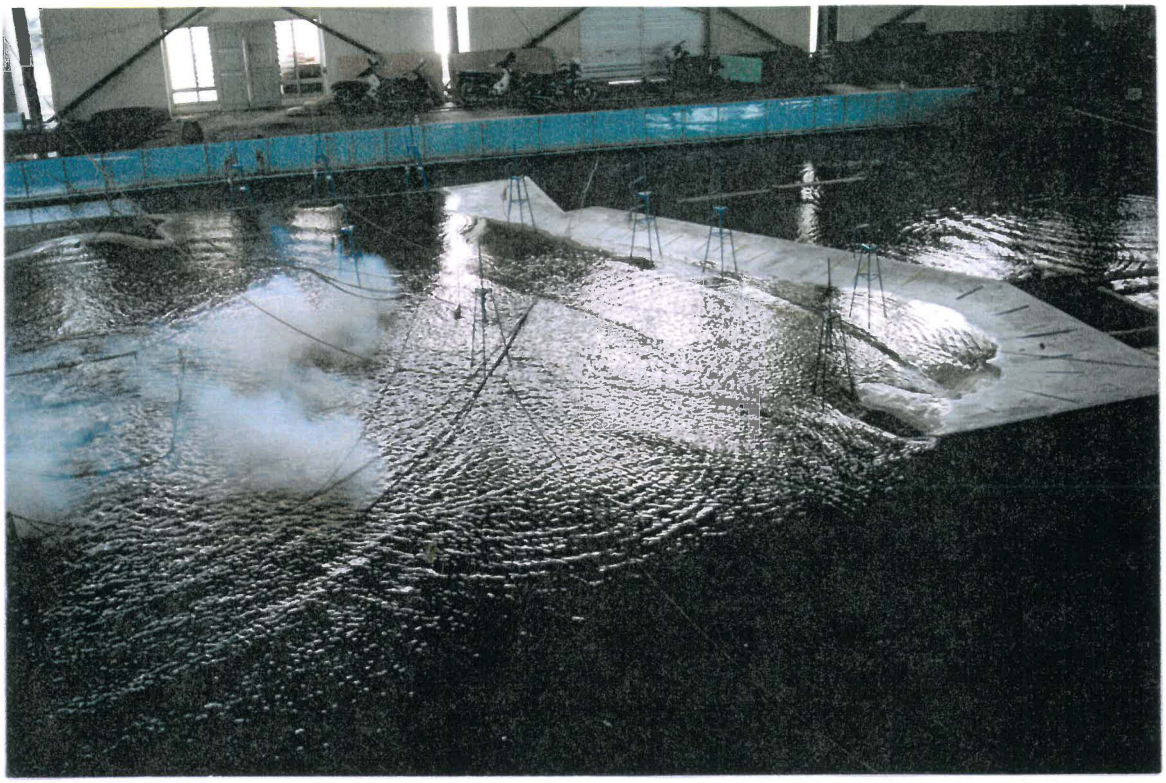

Figure Ap.2.26. The first wave reaches the west coast of Java and the Sumatera coast. There are obviously three 'large' waves generated by this mechanism.

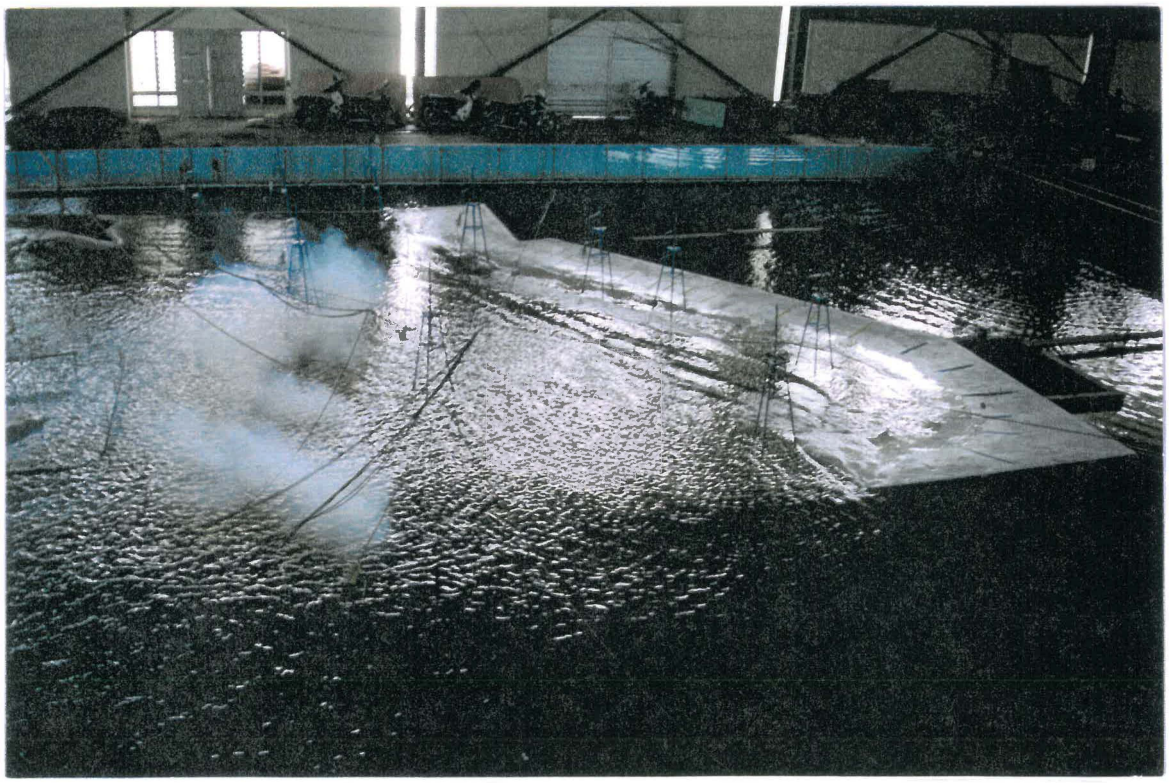

Figure Ap.2.27. The inundation of the shoreline after the arrival of the first wave.

Free Fall Circular Plate Experiments



Figure Ap.2.28. The initial condition for the free-fall circular plate experiments. The suspended plate was dropped into the water to simulate an explosion.



Figure Ap.2.29. Calibration of all instruments before dropping the circular plate.



Figure Ap.2.30. Immediately after the plate impacted the water surface. The crater and the first wave have formed.



Figure Ap.2.31. Shorthly after the water surged back into the crater to form a jet before collapsing to generate waves. Clearly,a single leading wave was formed.



Figure Ap.2.32. The waves have propagated outside the generation area.

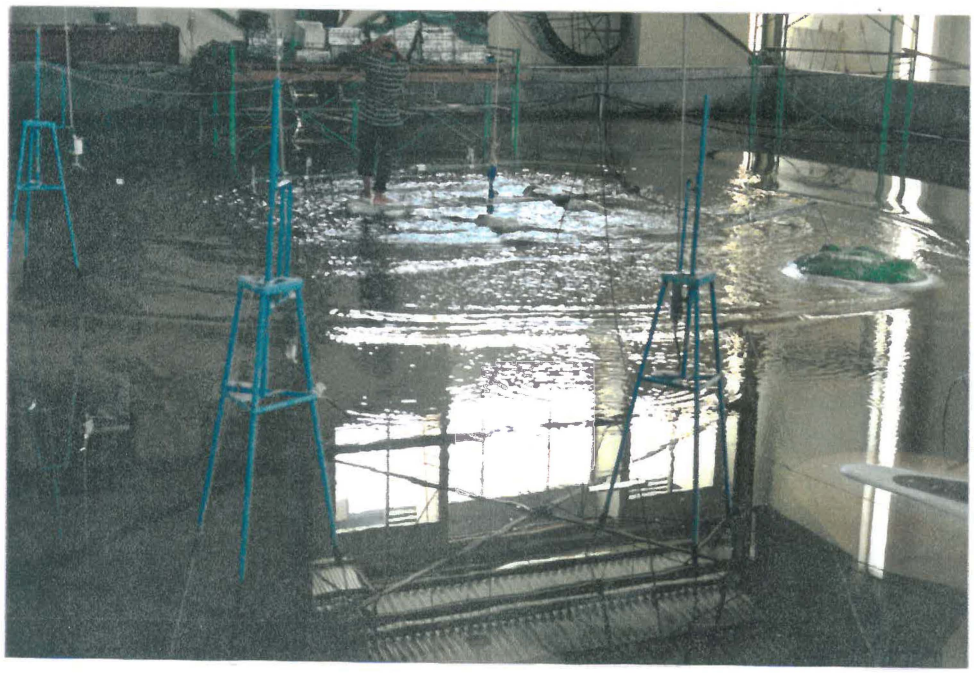

Figure Ap.2.33. There are clearly three main waves approaching the coast.

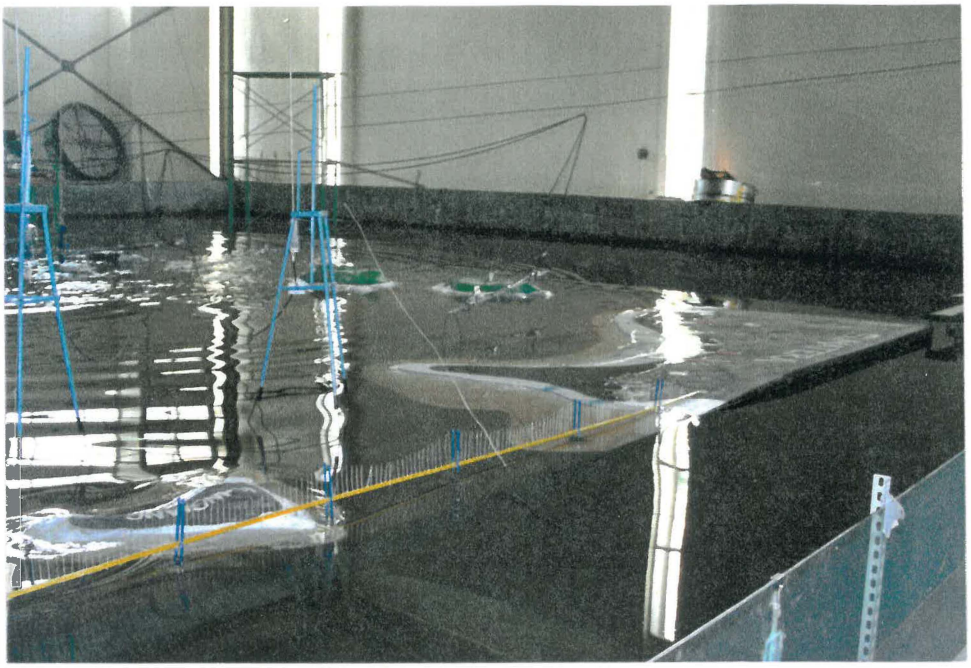

Figure Ap.2.34. The waves interacting with the Sumatera coast.

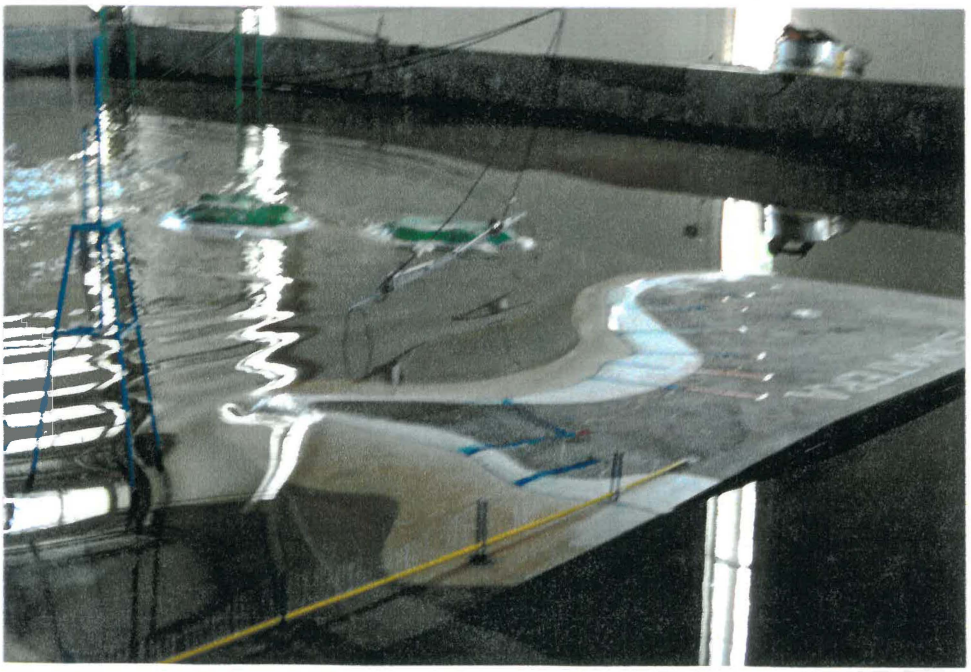

Figure Ap.2.35. Close-up of the first wave arriving at the Sumatera coast.

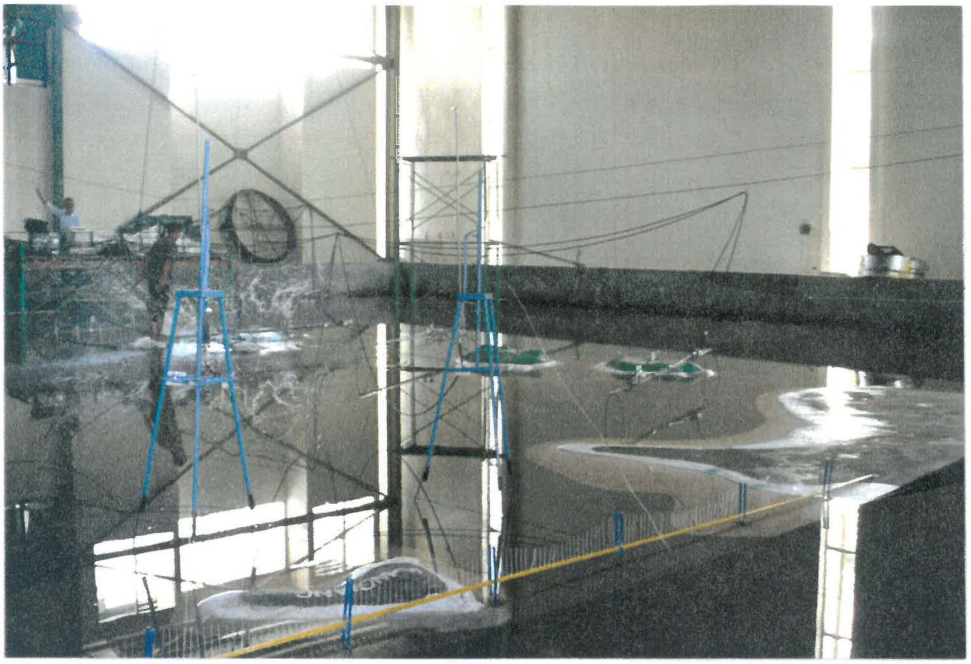

Figure Ap.2.36. Different view of the free-fall circular plate experiment at the initial stage when the circular plate has just dropped into the water.

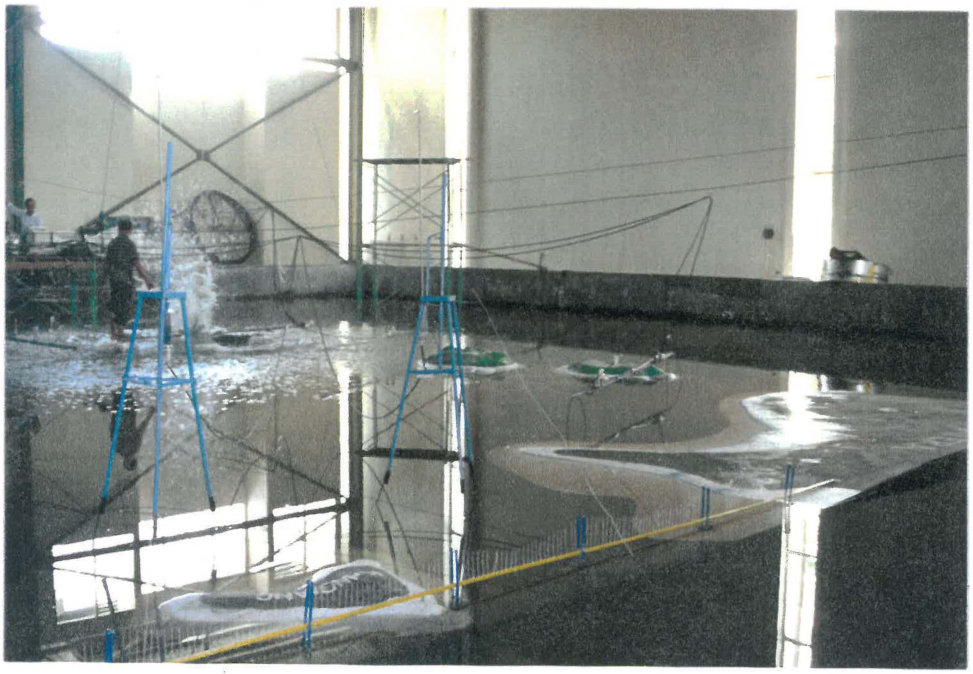

Figure Ap.2.37. The height of the jet of water formed the water surged back into the crater is clearly seen in this picture.

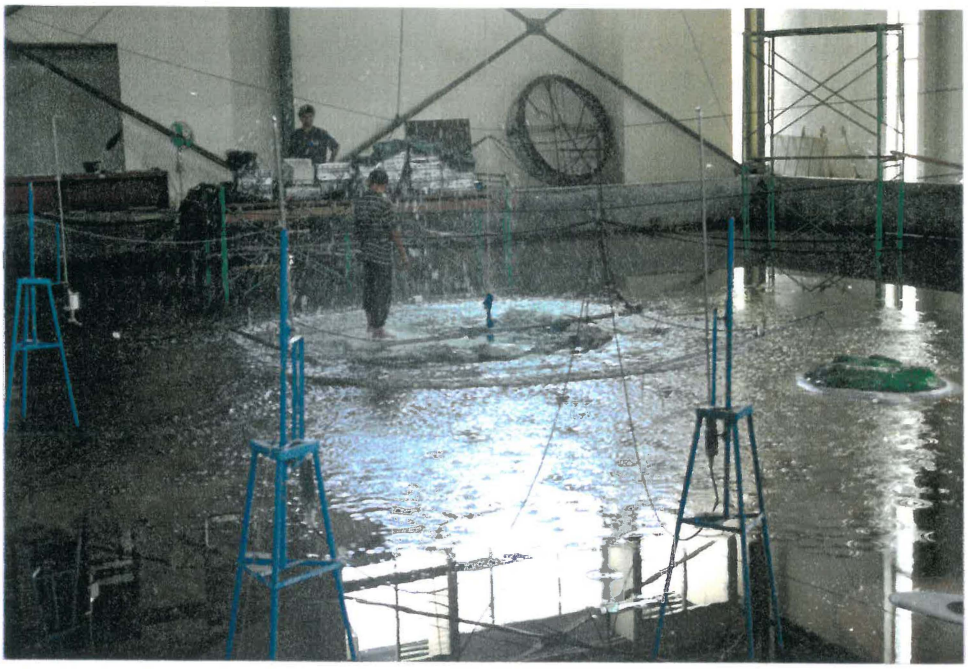

Figure Ap.2.38. The propagation of the leading solitary waves outside the generation area.

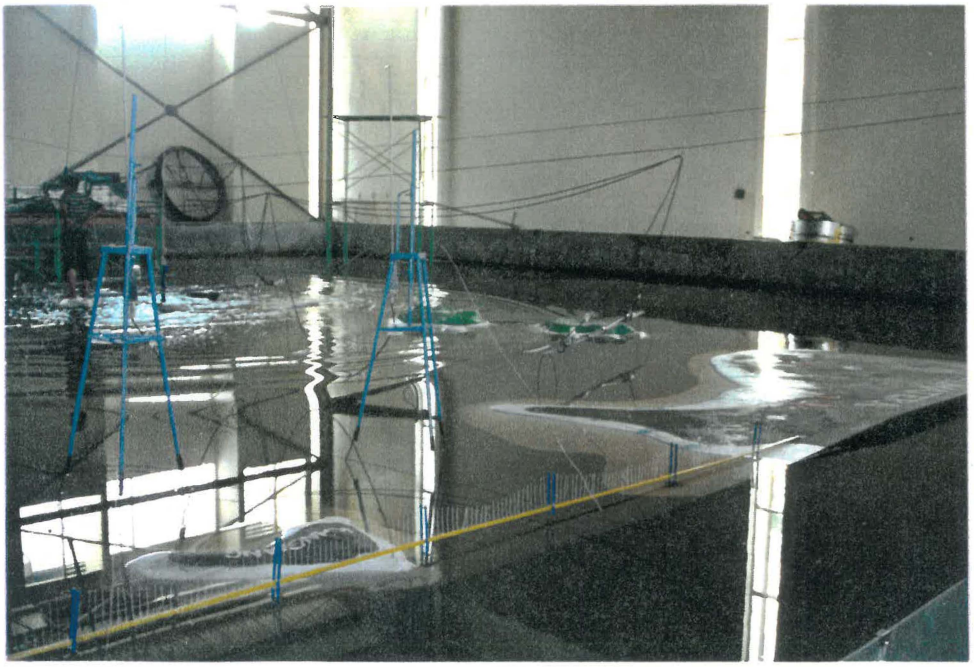

Figure Ap.2.39. The propagating waves approaching the coastline.

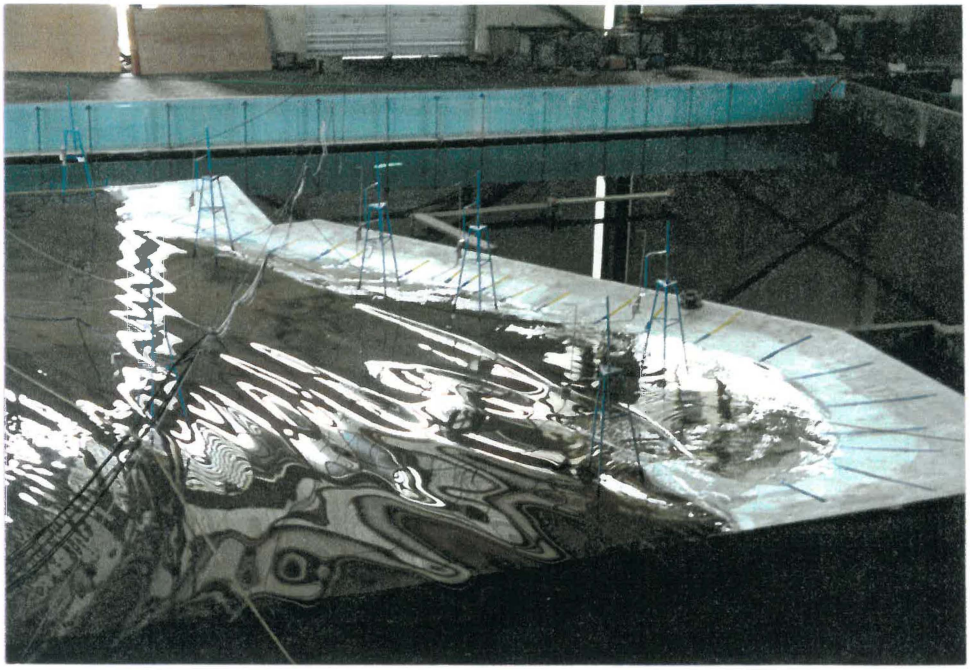

Figure Ap.2.40. The first wave hits the west coast of Java.

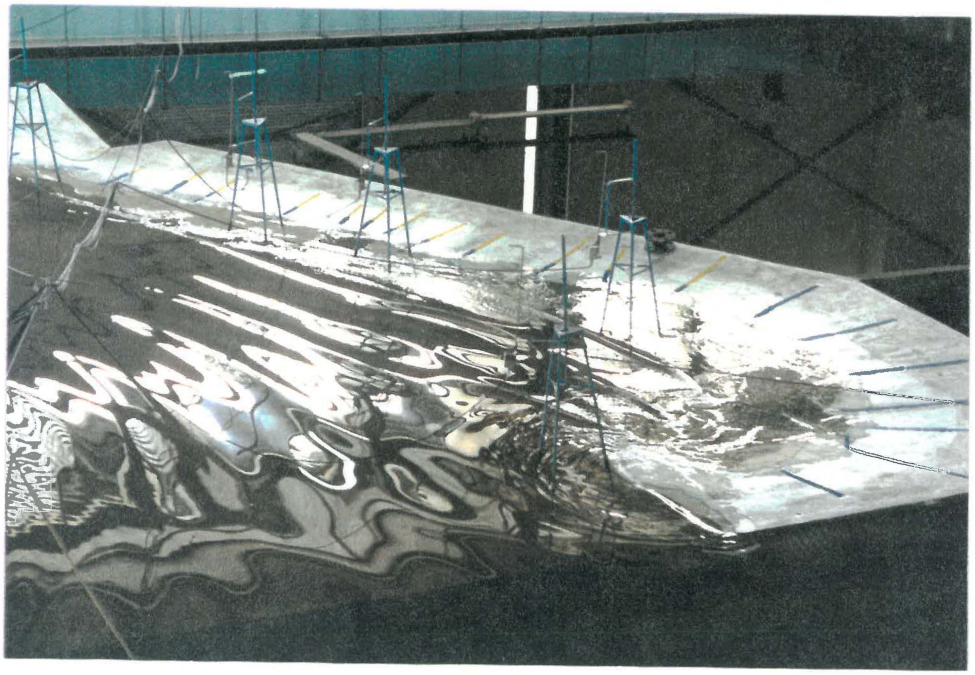

Figure Ap.2.41. The interaction of the first and second waves after they hit the tip of the west coast of Java.

Caldera Formation Test

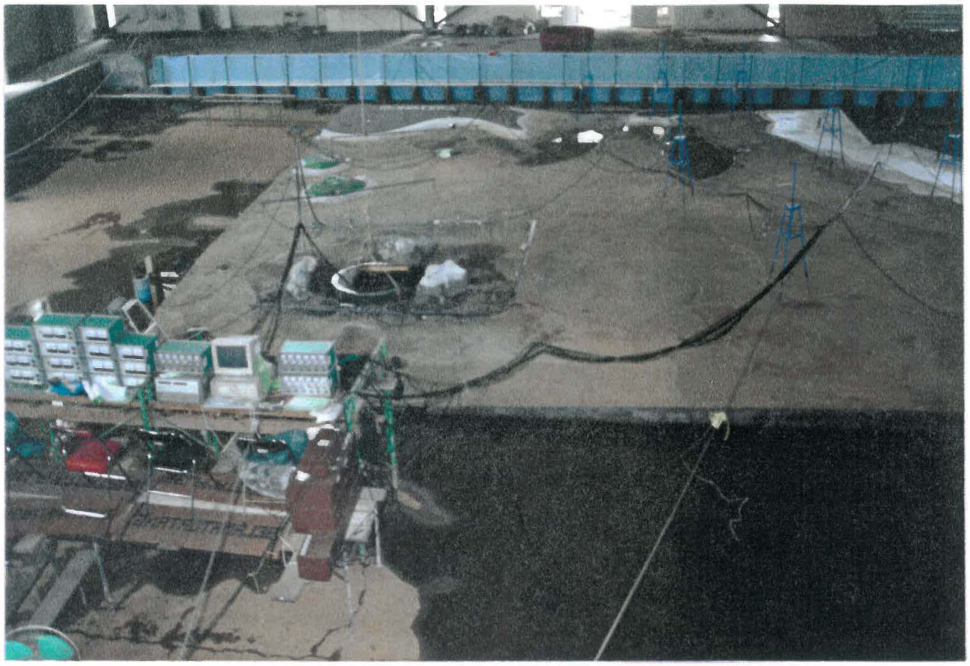

Figure Ap.2.42. The preparation for the caldera formation test showing the final caldera configuration.



Figure Ap.2.43. Filling of the wave basin with water and adjustment to the mean water level used for the tests.



Figure Ap.2.44. Calibration of instruments prior to caldera formation tests.

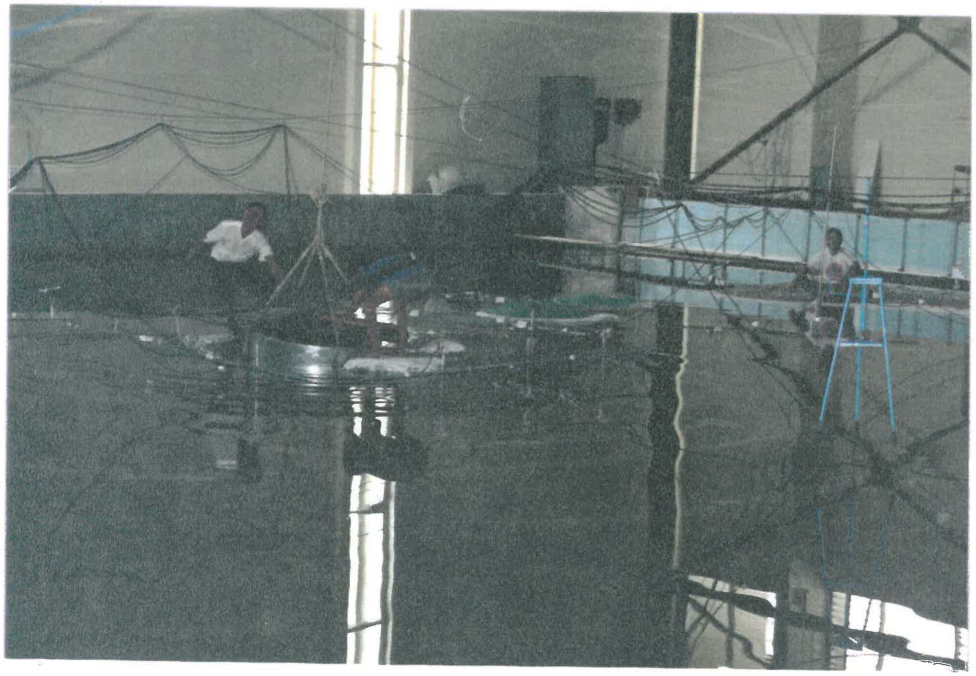

Figure Ap.2.45. The caldera plug has been uplifted and the first wave is starting to form.

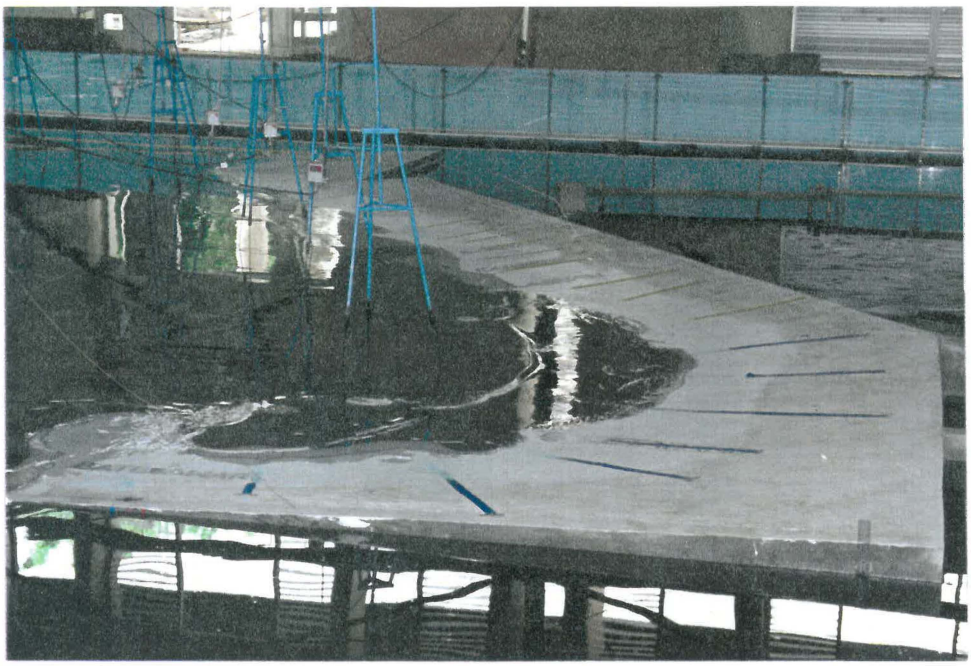

Figure Ap.2.46. The withdrawal of water along the west coast of Java before the first crest arrives.



Figure Ap.2.47. Inundation of the coast after the arrival of the first wave crest.

The Typical Wave Dynamic in the Coast.

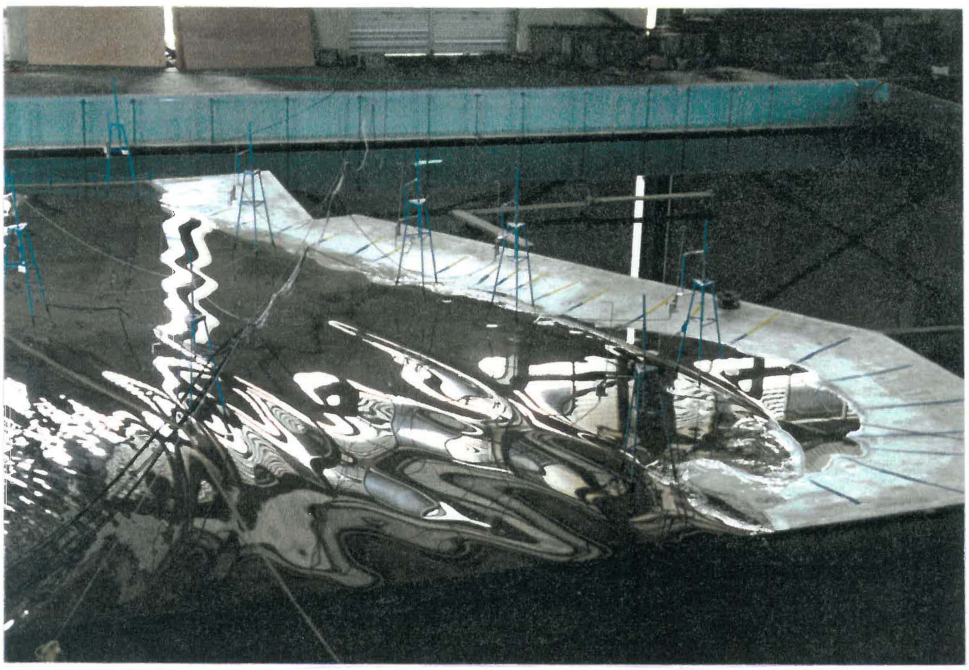

Figure Ap.2.48. A maximum of five waves were observed during the experiments as seen in this photograph.

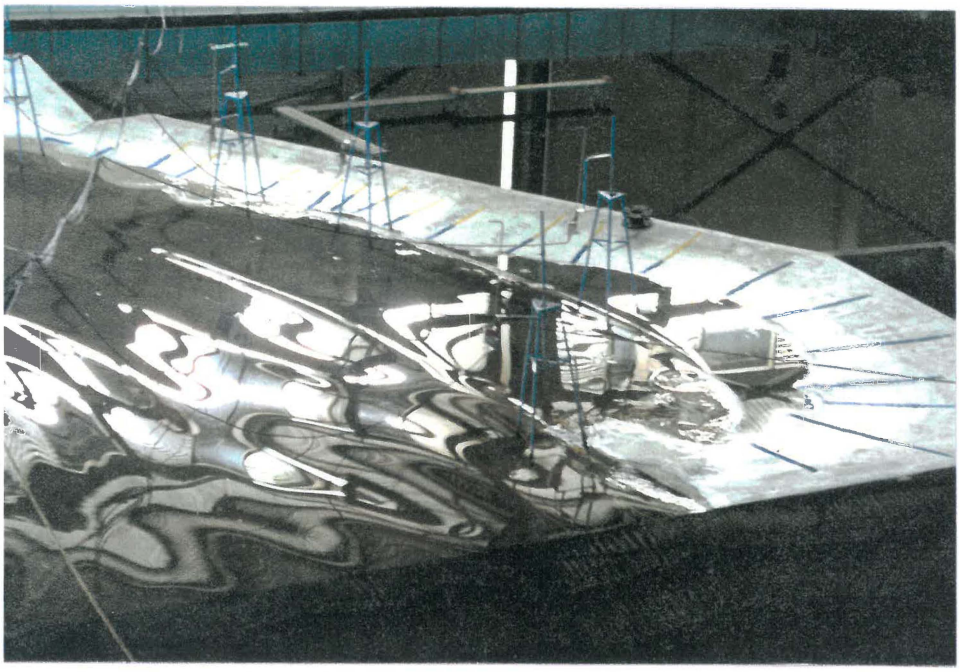

Figure Ap.2.49. Half of the first wave has inundated the northern part of the west coast of Java.

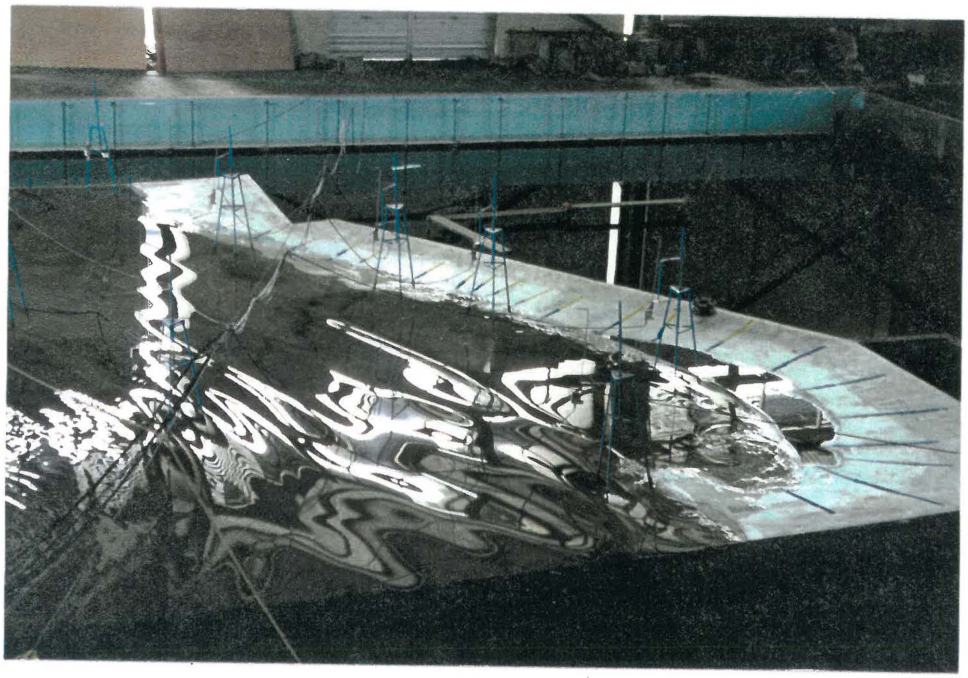

Figure Ap.2.50. The wave interaction at the coastline one second after Figure.Ap.2.49

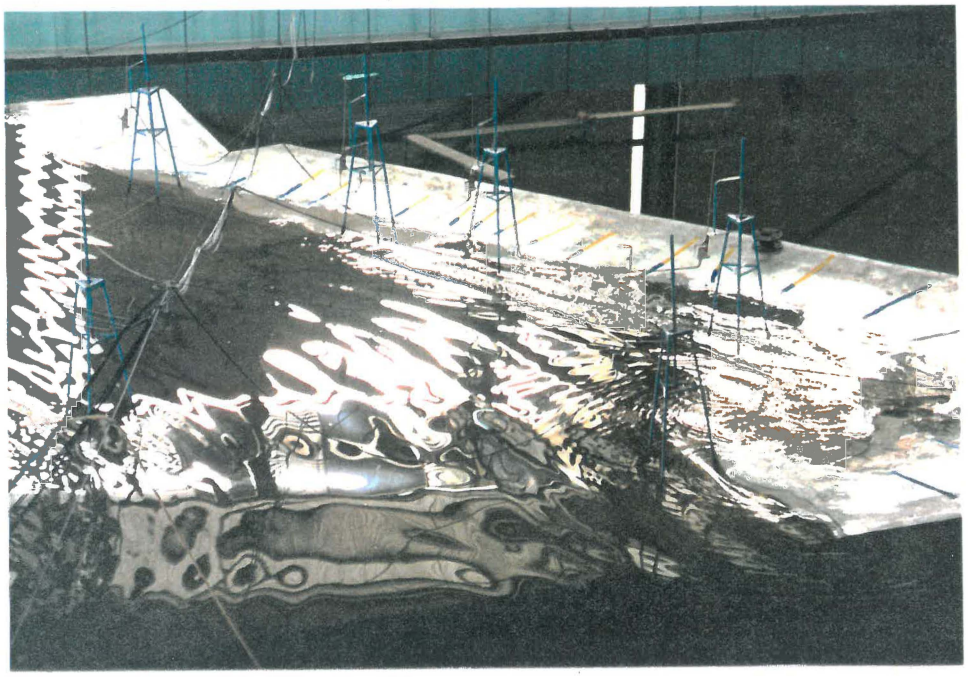

Figure Ap.2.51. The wave interaction at the coastline one second after Figure.Ap.2.50

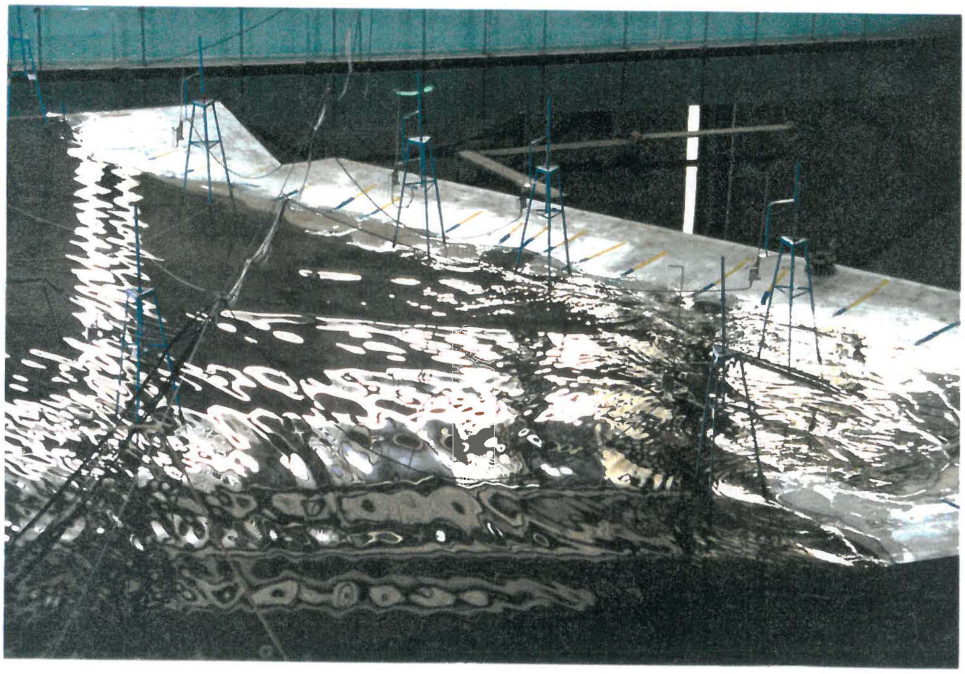

Figure Ap.2.52. The wave interaction at the coastline one second after Figure.Ap.2.51

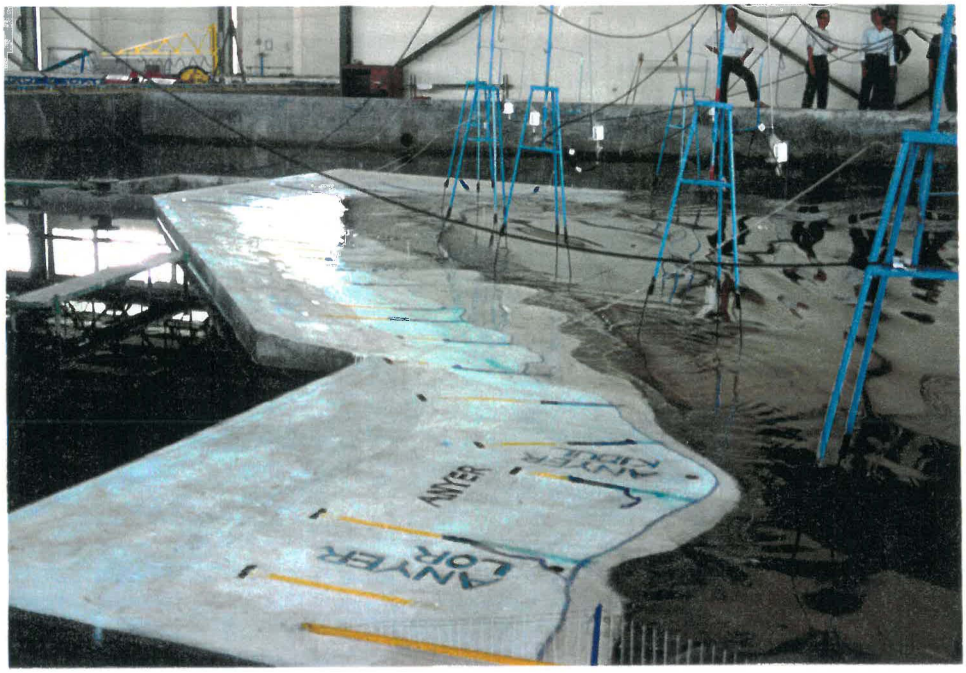

Figure Ap.2.53. Different view of waves approaching the west coast of Java. The first wave is clearly shown in the photograph.



Figure Ap.2.54. The first wave breaks and rushes up the coastline.

TWO DIMENSIONAL EXPERIMENTS

Dyed Fresh water :

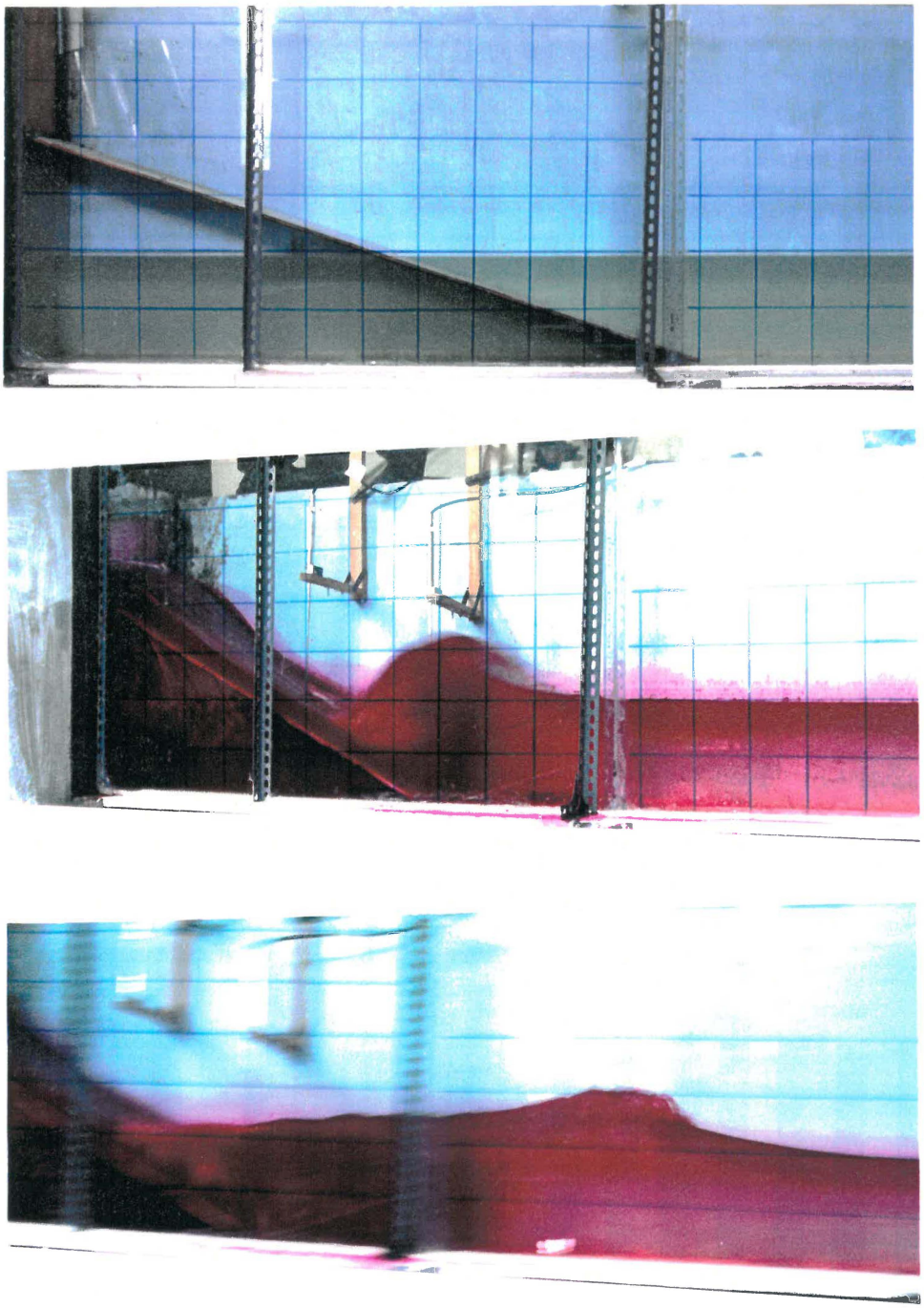

Figure Ap.2.55. This photographic sequence shows the main stages of the dyed freshwater water experiments in Flume. The initial condition (above) shows the calibration of the water level. Next is the initiation of the first wave (middle) when the pyroclastic flow hits the water surface in flume causing high turbulent and flow mixing. The waves propagate leaving the generation area. The dark red colour beneath the waves (photo in the middle) and behind the waves (below) in the water column shows the continuation of the pyroclastic flow.

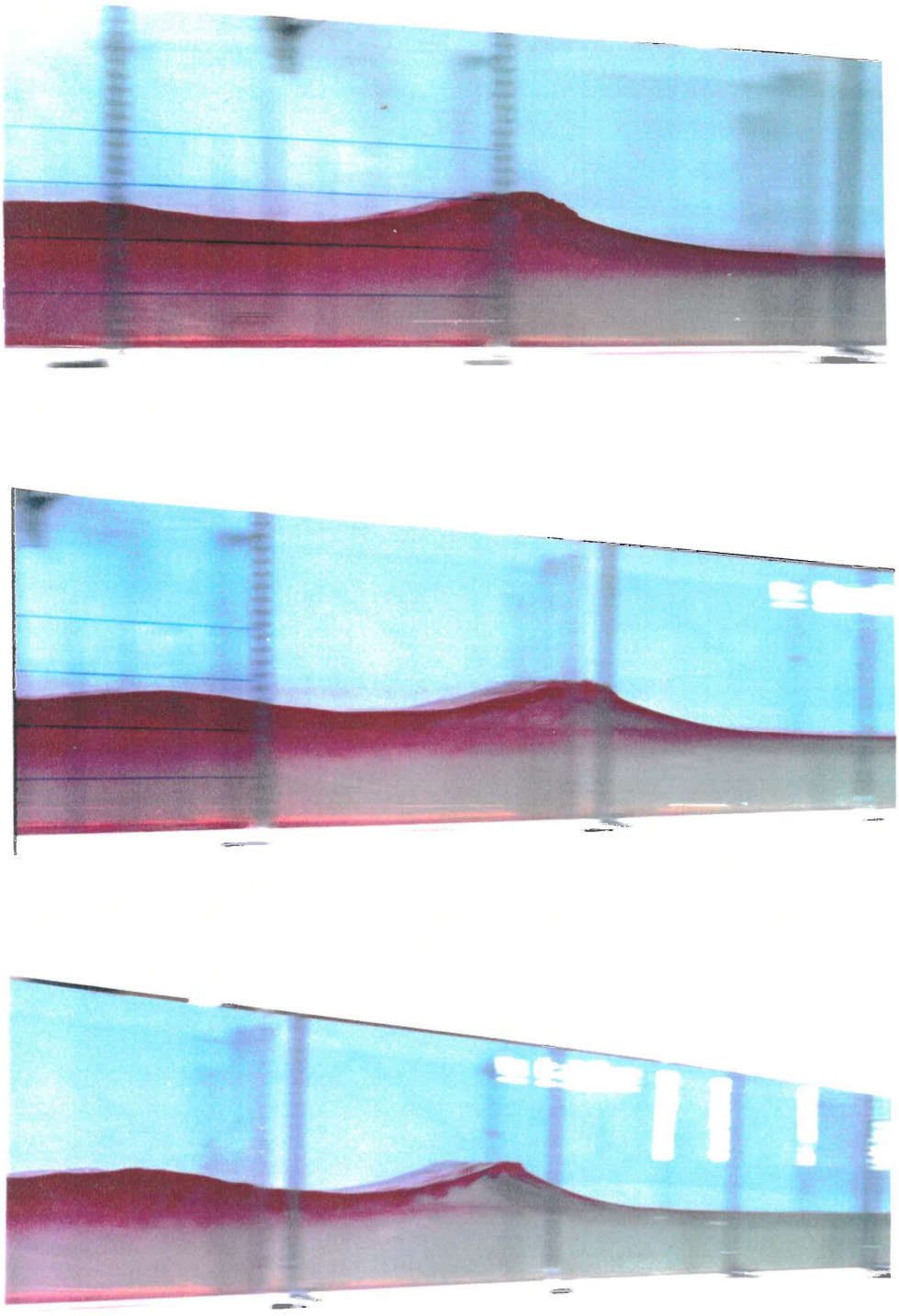

Figure Ap.2.56. The wave still maintains its shape and propagates at a speed of 1.85 m/sec. The lighter material of the pyroclastic flow propagates at the upper surface of the water column.

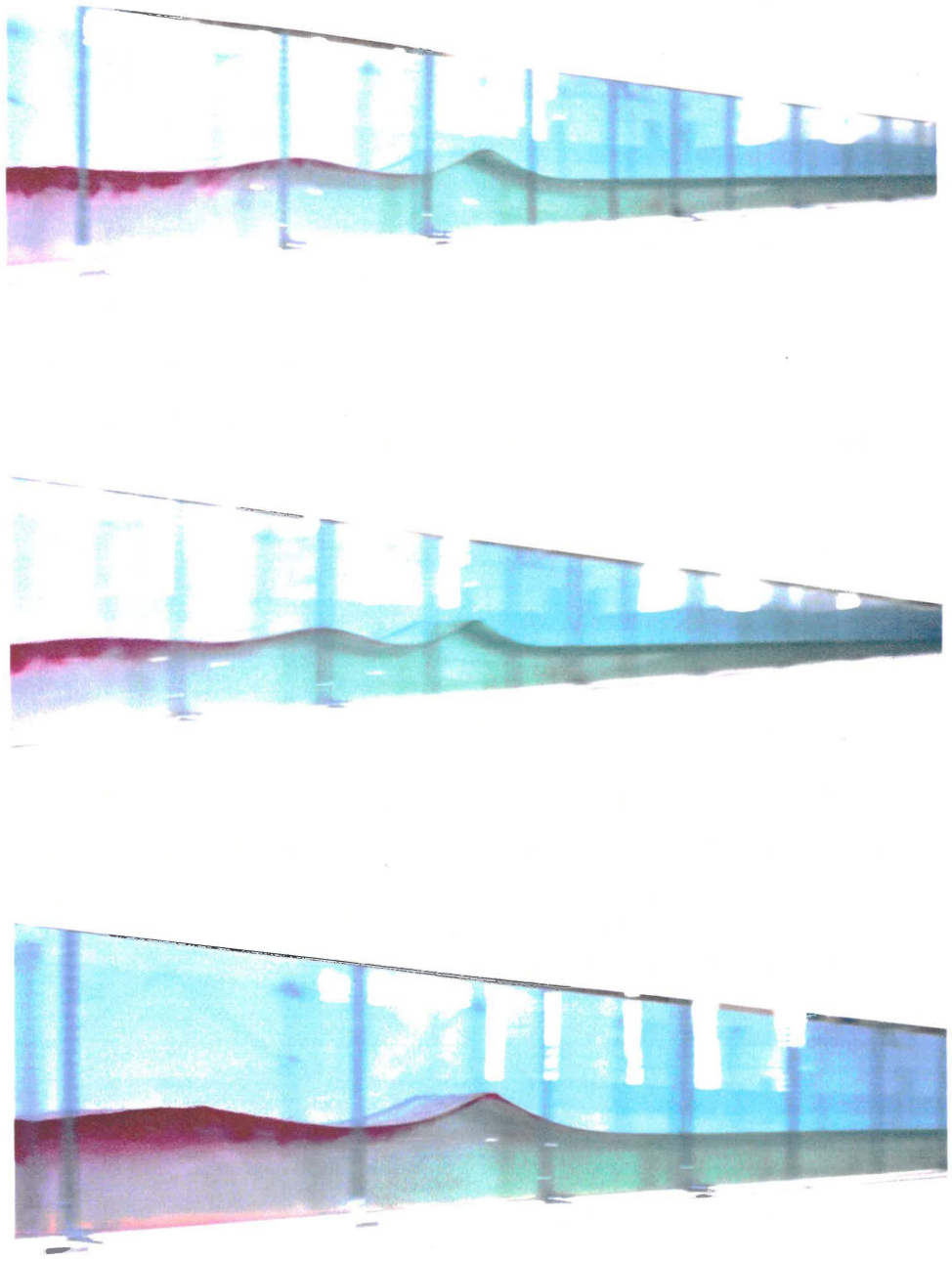

Figure Ap.2.57. Behind the first wave, there is a second low angle wave. This wave was generated due to the turbulence and the force of buoyant fluid which pushed the water up behind the flow.

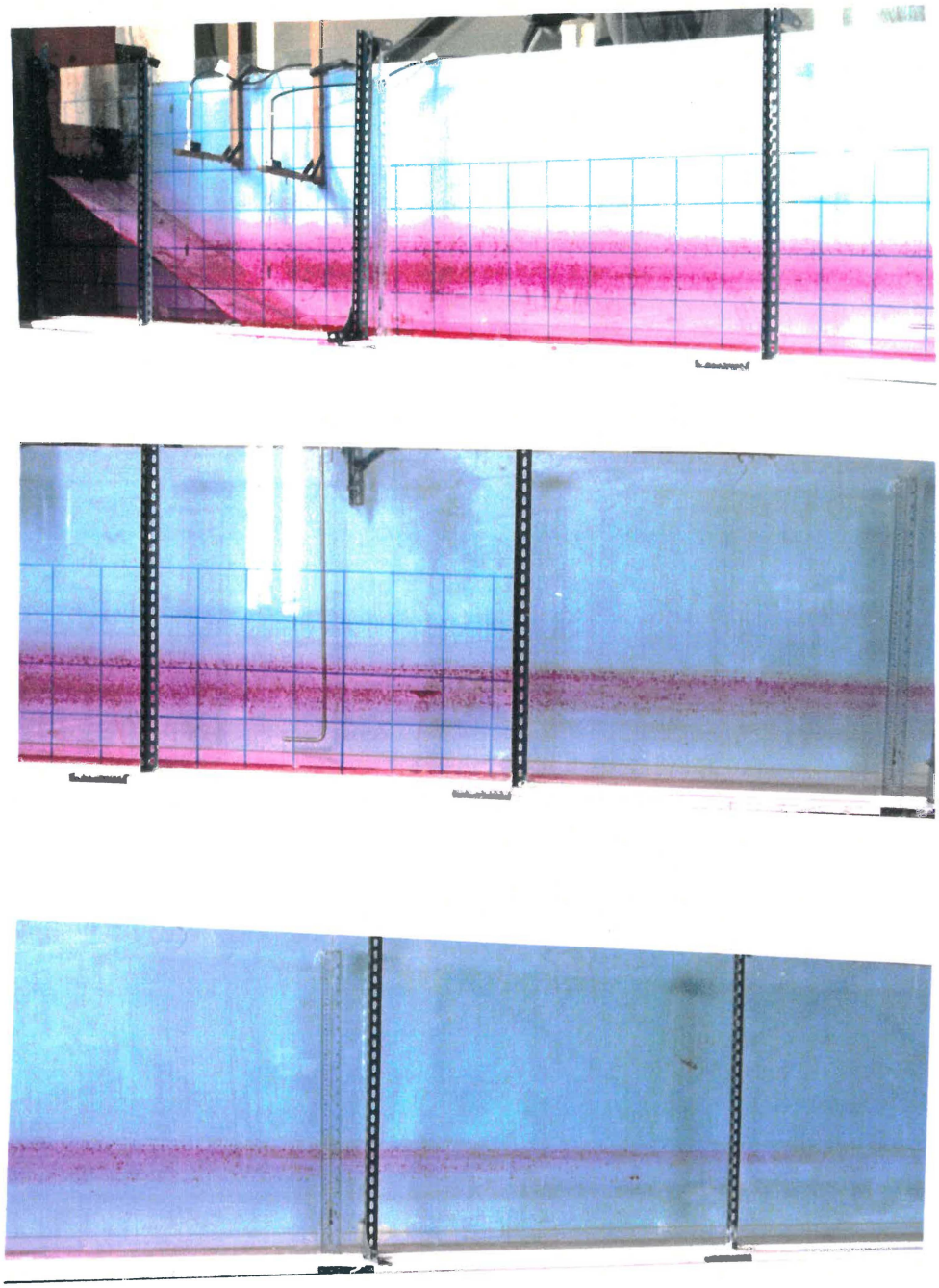

Figure Ap.2.58. A trace of light material remained on the glass-walls of the flume. A thick layer occured close to the source and it thinned along the flume indicating increased mixing and dispersion.

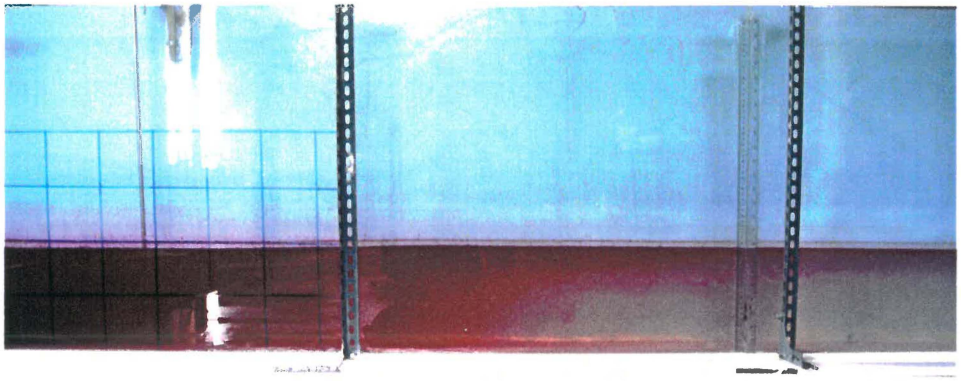

Figure Ap.2.59. The cross-sectional view of the dyed freshwater within the water column showing that close to the generation area the dyed freshwater was well mixed with the water in flume.

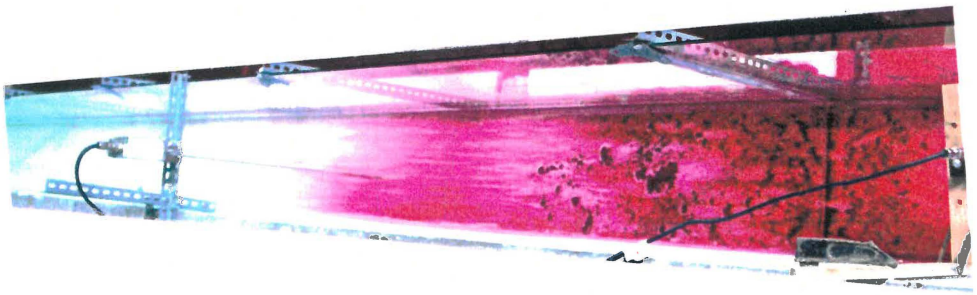

Figure Ap.2.60. Overhead photograph showing the trace of dyed freshwater which remained on the bottom of the glass-walled flume close to generation area. It shows the area where the flow material hit the bottom of the flume.

(Fresh Water + Mud + Sand) Experiments :

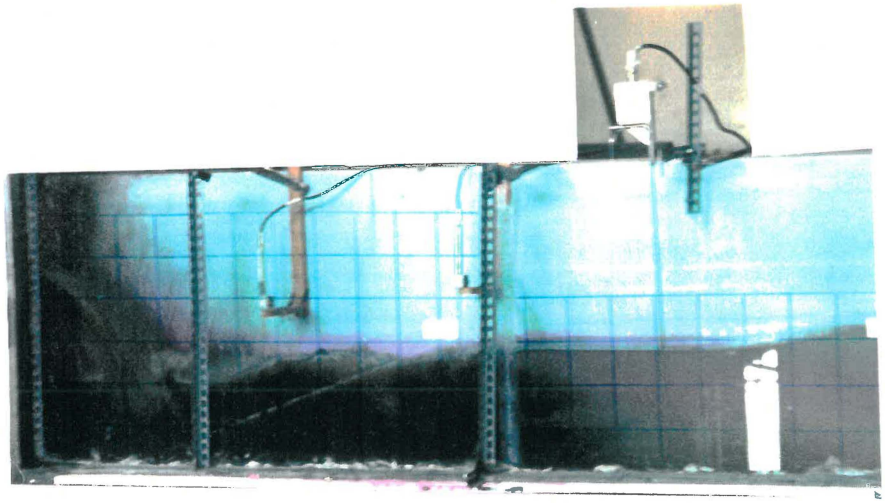

Figure Ap.2.61. The interaction of the mass flow and the water in flume is still in progress; the first wave has left the generation area. The water level behind the first wave remains calm and level.

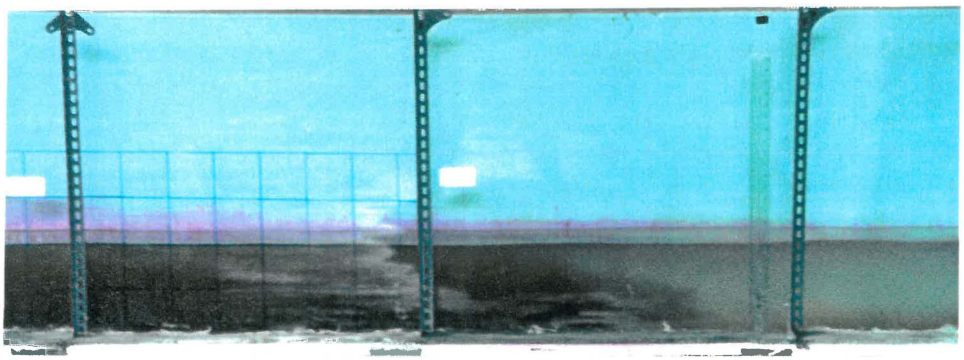

Figure Ap.2.62. The denser mass flow material flowing along the bottom of the flume without affecting the water surface.

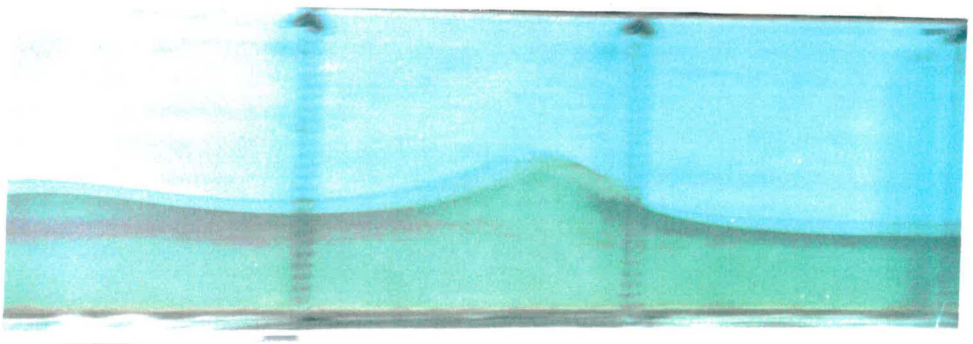

Figure Ap.2.63. The propagation of the first wave with a small surface roller formation.

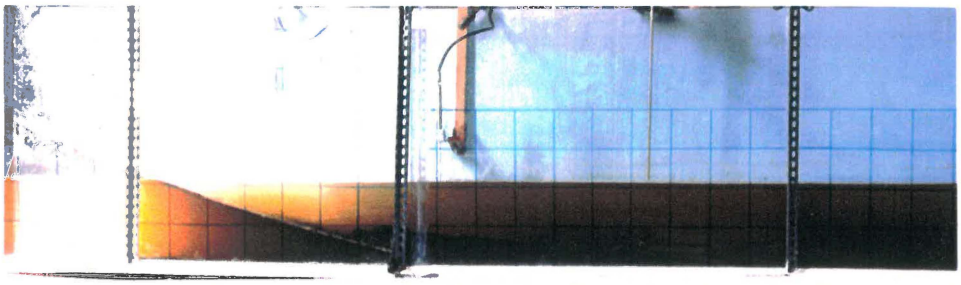

Figure Ap.2.64. The condition of the water in flume close to generation area after the test. The sediment in the flow was deposited at the base of the ramp.

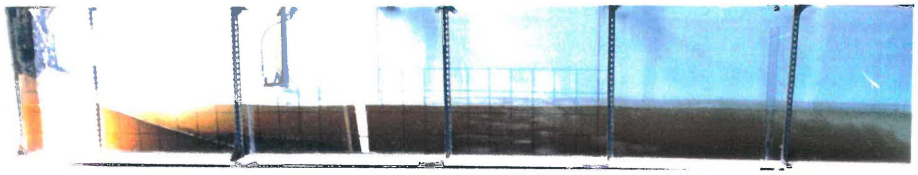

Figure Ap.2.65. The head of the flow is still flowing at the bottom of the flume, and some heavier sediment has deposited in the base of the ramp.

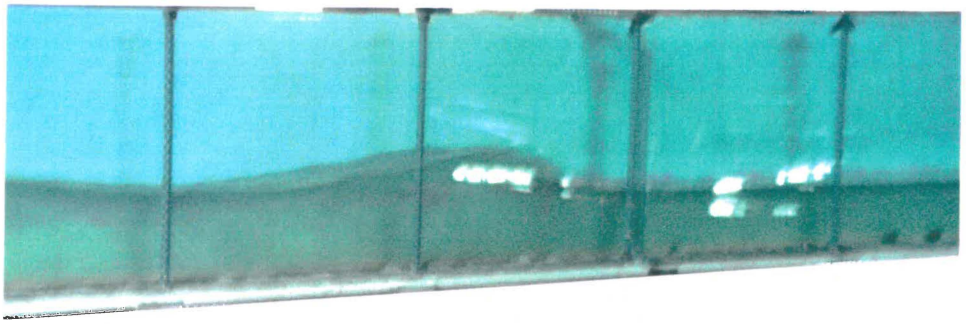

Figure Ap.2.66. The initial wave starts to change its shape; the roller in the wave crest becomes larger.

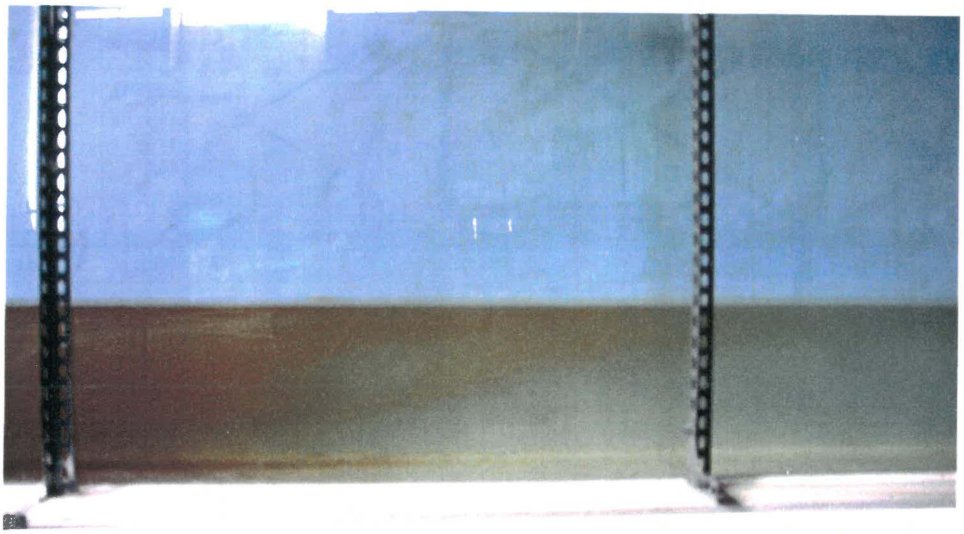

Figure Ap.2.67. A cross section of the flume showing the same characteristic distribution of material within the water column, with lighter material flowing at the top of water surface.

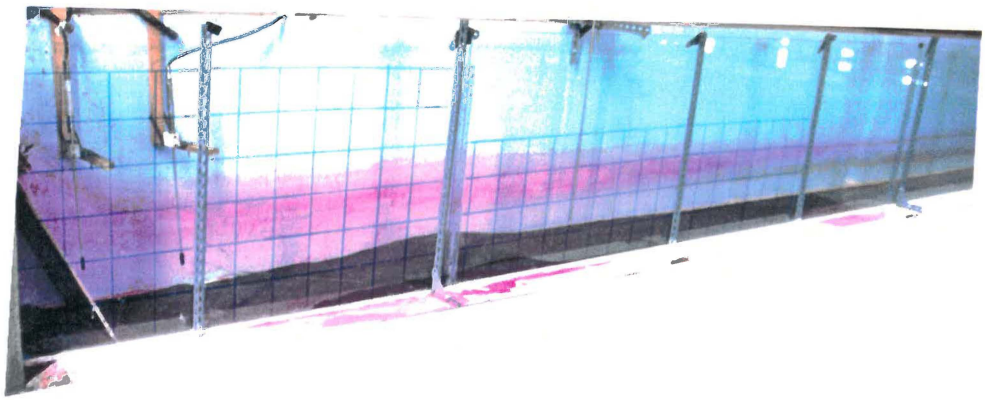

Figure Ap.2.68. The flow sediment material was deposited further away from the base of the ramp for the experiment with angle of ramp $\alpha = 60\ ^{o}$. This behaviour was evident during the 1883 eruption.

APPENDIX.3.

Resutls of Wave and Current Measurements

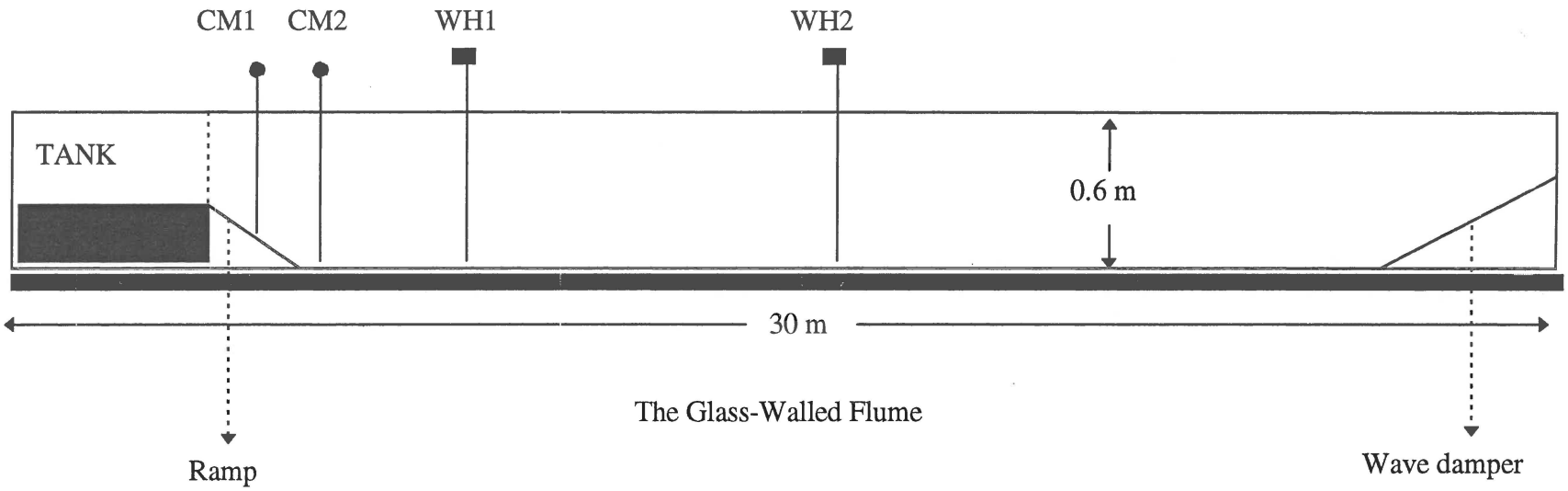

CURRENT METER :
CM1 = Electromagnetic current meter sensor 1
CM2 = Electromagnetic current meter sensor 2

WAVE HEIGHT :
WH1 = Capacitance wave height meter 1
WH2 = Capacitance wave height meter 2

Results in table :
Velocity 1, Direction 1 : CM1; Velocity 2, Direction 2 : CM2; Height 1 = WH1; Corr SL = final wave height after correction of Sea level and instrument; Inst. Corr = wave height after instrument correction

TEST 1.
Material in Tank : Dyed Fresh water
Angle of Ramp : 20 degree
Water depth in Flume : 20 cm

Time (second)	SL.Corr (mm)	Inst.Corr (mm)	Height 1 (mm)	Velocity 1 (cm/sec)	Direction 1 (deg)	Velocity 2 (cm/sec)	Direction 2 (deg)
52.32	0.00	10.64	8.98	0.12	-0.04	0.93	-9.07
53.22	-0.54	10.11	8.53	0.12	-0.04	0.38	-16.16
54.15	-0.86	9.79	8.26	0.13	-0.04	0.62	-16.84
55.12	-1.27	9.37	7.91	0.16	-0.04	0.67	-13.10
56.16	-1.66	8.98	7.58	0.16	-0.04	0.70	-14.81
57.19	-2.09	8.56	7.22	7.64	0.48	13.53	1.14
58.06	67.87	78.51	66.26	28.49	0.86	28.73	-15.73
59.09	31.61	42.25	35.66	28.86	10.75	28.69	44.98
60.05	4.05	14.69	12.40	28.83	-8.56	14.78	47.12
60.99	3.42	14.07	11.87	13.03	-167.23	2.51	-28.44
61.82	-0.82	9.82	8.29	5.00	113.37	10.29	-17.59
62.77	-8.76	1.89	1.59	1.23	-45.85	4.08	-62.71
63.61	-4.22	6.42	5.42	1.13	85.98	2.51	-159.18
64.51	-4.73	5.92	4.99	3.19	172.72	4.68	-129.48
65.35	-6.92	3.72	3.14	2.40	-167.45	4.47	-107.87
66.25	-5.22	5.42	4.58	1.83	-173.37	2.48	-131.12
67.22	-5.29	5.36	4.52	2.23	172.07	2.51	-121.95
68.1	-7.58	3.06	2.58	2.47	166.28	3.61	-104.89
68.94	-9.46	1.18	1.00	2.47	167.18	3.82	-96.78
69.84	-9.98	0.67	0.56	2.49	164.00	2.11	-99.93
70.74	-10.04	0.60	0.51	4.04	169.72	1.09	-174.64

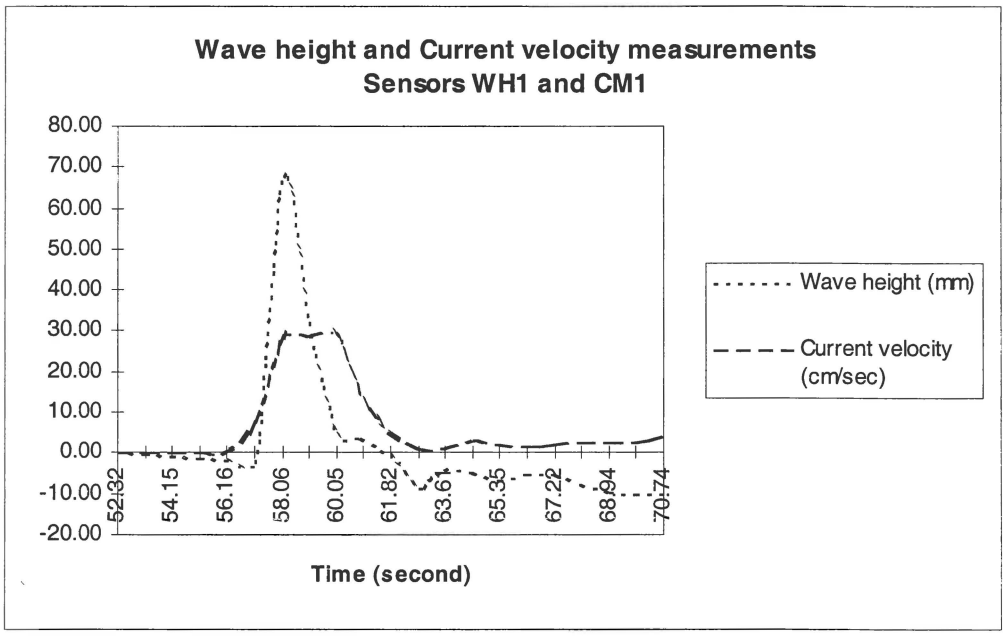

TEST 2.
Material in Tank : Mixed Mud & sand
Angle of Ramp : 20 degree
Water depth in flume : 20 cm

Time (second)	SL.Corr (mm)	Inst.Corr (mm)	Height 1 (mm)	Velocity 1 (cm/sec)	Direction 1 (deg)	Velocity 2 (cm/sec)	Direction 2 (deg)
34.28	0.00	-10.73	-8.83	1.48	165.85	1.50	-174.00
34.87	-0.07	-10.80	-8.89	4.23	-171.24	2.42	-166.77
35.53	0.77	-9.96	-8.20	110.33	-68.94	2.10	-5.36
36.19	2.80	-7.93	-6.52	115.40	14.92	89.26	28.23
36.9	24.25	13.52	11.13	110.08	-30.72	106.79	30.18
37.55	29.17	18.45	15.18	19.80	-26.66	38.59	17.34
38.22	8.91	-1.82	-1.49	8.14	76.59	39.21	49.57
38.83	22.98	12.25	10.08	11.76	-45.13	31.34	29.87
39.45	8.09	-2.64	-2.17	17.20	85.58	42.69	46.06
39.95	5.28	-5.45	-4.48	15.72	68.70	32.80	47.56
40.55	24.21	13.48	11.10	97.74	-96.48	39.41	5.70
41.21	4.65	-6.07	-5.00	11.05	-162.47	100.38	19.49
41.78	19.72	8.99	7.40	115.52	-117.19	50.65	44.32
42.43	53.26	42.54	35.01	2.32	94.13	7.68	87.21
43.06	79.34	68.62	56.47	115.21	133.42	4.64	-142.55
43.78	20.90	10.17	8.37	0.22	-0.05	3.45	-139.94
44.37	1.11	-9.61	-7.91	23.52	159.89	3.76	-155.55
45.04	35.59	24.86	20.46	30.21	-59.63	6.86	-122.49
45.76	1.96	-8.77	-7.22	65.60	78.24	3.23	-118.76
46.43	-9.74	-20.47	-16.85	3.22	50.94	3.91	-137.77

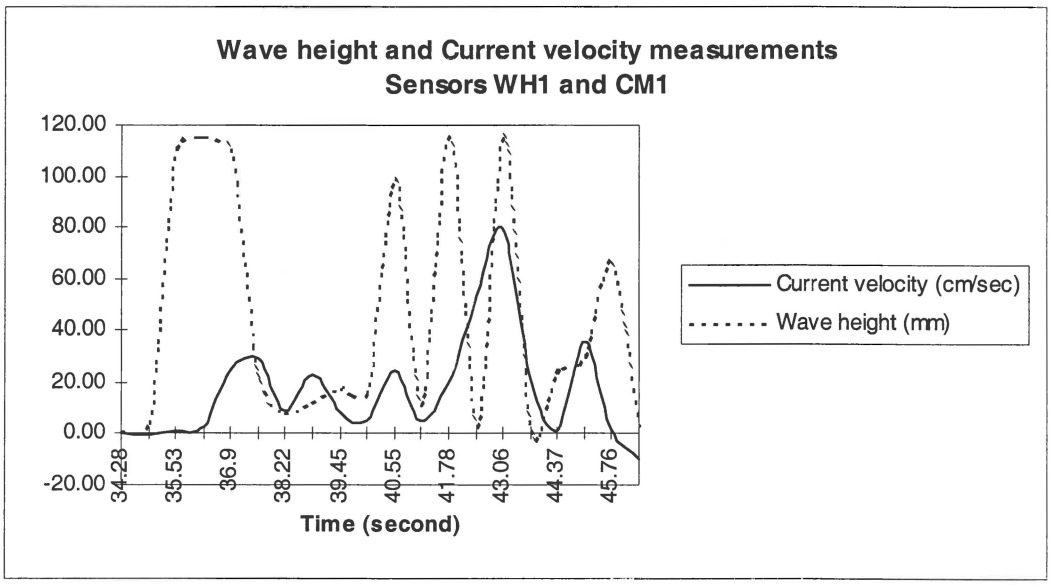

TEST 3.
Material in Tank : dyed fresh water
Angle of Ramp : 30 degree
Water depth in Flume : 20 cm

Time (second)	SL.Corr (mm)	Inst.Corr (mm)	Height 1 (mm)	Velocity 1 (cm/sec)	Direction 1 (deg)	Velocity 2 (cm/sec)	Direction 2 (deg)
30.68	0.00	-22.52	-18.53	0.58	-0.05	35.40	17.99
31.37	-0.18	-22.70	-18.68	42.15	-94.34	45.78	-167.98
31.98	28.79	6.27	5.16	35.56	-94.73	44.40	-161.90
32.58	54.51	32.00	26.33	115.40	-18.82	81.08	173.30
33.28	42.71	20.20	16.62	115.67	-133.86	37.24	-179.06
33.96	14.41	-8.10	-6.67	2.59	-65.15	32.47	-171.33
34.55	-1.14	-23.66	-19.47	8.63	-82.53	17.49	-146.89
35.10	0.42	-22.10	-18.19	0.16	-0.05	18.24	-109.88
35.75	-6.35	-28.87	-23.76	2.19	0.33	19.96	163.68
36.47	-3.90	-26.42	-21.74	0.20	-0.05	12.39	166.92
37.06	1.20	-21.31	-17.54	0.21	-0.05	10.03	-168.56
37.62	0.14	-22.38	-18.42	0.23	-0.05	14.34	-144.36
38.16	-0.56	-23.08	-19.00	0.24	-0.05	15.38	177.36
38.71	2.89	-19.63	-16.15	0.25	-0.05	14.87	177.48
39.25	1.47	-21.04	-17.32	0.26	-0.05	5.78	131.83
39.83	2.09	-20.43	-16.82	0.28	-0.05	5.34	178.77
40.42	8.59	-13.93	-11.47	0.29	-0.05	5.80	-160.45
41.03	9.35	-13.17	-10.84	0.30	-0.05	5.30	-121.38
41.68	4.25	-18.27	-15.03	0.31	-0.05	6.03	-121.78
42.31	6.72	-15.80	-13.00	0.32	-0.05	3.07	-154.36

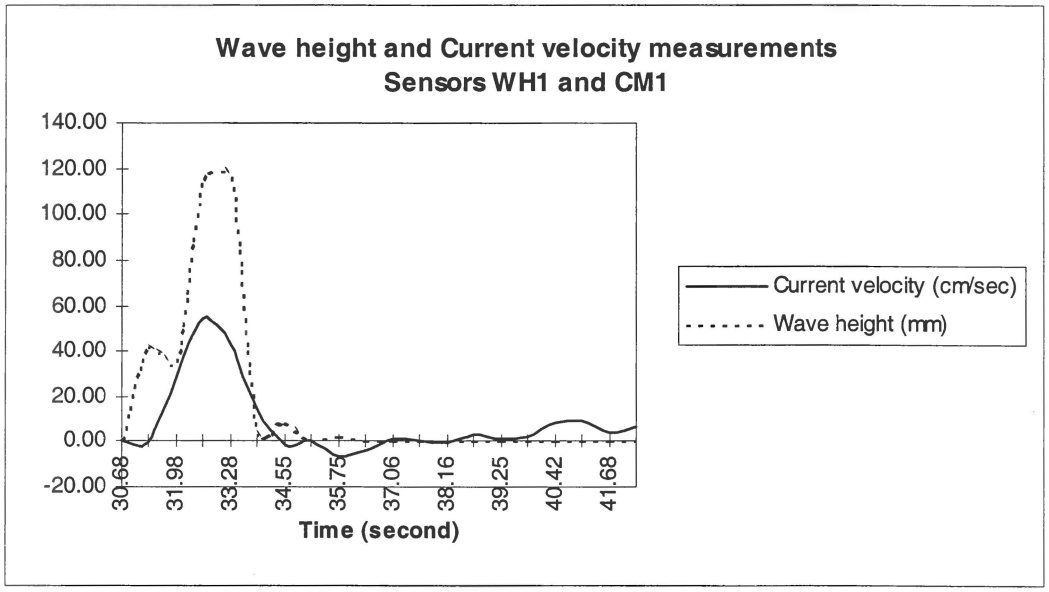

TEST 4.
Material in Tank : Mixed mud + sand
Angle of Ramp : 30 degree
Water depth in Flume : 20 cm

Time (second)	SL.Corr (mm)	Inst.Corr (mm)	Height 1 (mm)	Velocity 1 (cm/sec)	Direction 1 (deg)	Velocity 2 (cm/sec)	Direction 2 (deg)
31.09	0.00	-18.34	-15.10	0.60	-0.05	4.50	51.44
31.79	-0.01	-18.36	-15.11	93.00	-49.64	37.87	-54.35
32.35	0.00	-18.35	-15.10	91.28	115.11	113.73	-19.54
33.06	61.89	43.55	35.84	115.55	15.16	92.90	151.23
33.7	137.14	118.79	97.77	0.72	-84.57	57.65	-147.74
34.23	50.28	31.93	26.28	4.52	-91.61	87.95	52.32
34.85	21.96	3.61	2.97	0.20	-0.05	10.03	154.82
35.56	11.12	-7.22	-5.95	0.17	-0.05	10.00	174.86
36.28	0.73	-17.62	-14.50	0.19	-0.05	15.52	148.20
36.88	-6.24	-24.58	-20.23	0.21	-0.05	8.90	-176.22
37.44	1.20	-17.15	-14.11	0.22	-0.05	7.45	-117.74
37.98	-4.61	-22.95	-18.89	0.23	-0.05	6.64	-125.16
38.57	-0.24	-18.58	-15.29	0.25	-0.05	4.90	-166.69
39.16	-1.05	-19.40	-15.97	0.26	-0.05	6.01	-122.93
39.76	-0.13	-18.47	-15.20	0.28	-0.05	1.87	-140.02
40.31	-2.04	-20.38	-16.78	0.29	-0.05	0.54	-164.86
40.85	0.27	-18.07	-14.87	0.30	-0.05	0.39	-58.89
41.4	3.36	-14.98	-12.33	0.31	-0.05	1.92	-20.04
42.03	1.55	-16.80	-13.82	0.33	-0.05	1.55	-115.04
42.63	1.75	-16.59	-13.66	0.34	-0.05	2.07	-59.28

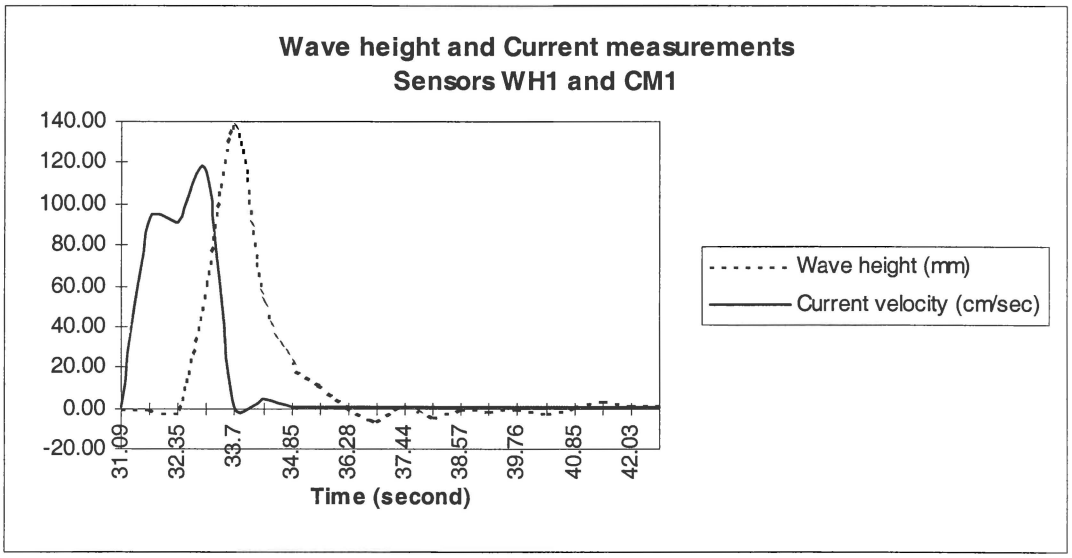

TEST 5.
Material in Tank : dyed fresh water
Angle of Ramp : 60 degree
Water depth in Flume : 20 cm

Time (second)	SL.Corr (mm)	Inst.Corr (mm)	Height 1 (mm)	Velocity 1 (cm/sec)	Direction 1 (deg)	Velocity 2 (cm/sec)	Direction 2 (deg)
27.91	0.00	-3.70	-3.05	0.44	-0.04	0.74	-151.51
28.57	0.55	-3.16	-2.60	0.94	-0.04	5.28	9.49
29.18	2.27	-1.43	-1.18	20.56	115.46	45.14	121.03
29.82	37.61	33.91	27.91	49.26	-64.24	30.90	114.72
30.4	46.55	42.84	35.26	45.05	-58.31	31.02	138.93
30.95	50.25	46.55	38.31	41.90	-143.88	55.99	177.83
31.6	29.82	26.12	21.50	46.40	38.66	23.78	144.66
32.14	7.75	4.05	3.33	24.25	-18.38	23.59	-172.60
32.77	2.85	-0.86	-0.71	28.42	-43.56	14.59	-149.88
33.31	-4.10	-7.81	-6.42	16.88	-16.82	17.60	-165.99
33.99	-3.58	-7.29	-6.00	16.15	-86.37	1.88	44.87
34.71	1.28	-2.42	-1.99	28.51	21.48	8.26	122.49
35.43	-0.75	-4.46	-3.67	19.11	-8.98	6.10	148.20
36.15	1.50	-2.21	-1.82	9.44	2.98	2.88	111.77
36.82	0.85	-2.86	-2.35	10.00	-42.34	6.32	105.53
37.42	-0.56	-4.27	-3.51	9.54	-42.53	4.17	72.25
38.12	2.40	-1.31	-1.08	5.87	-55.58	5.85	74.45
38.78	0.60	-3.10	-2.55	7.70	-60.46	3.73	131.54
39.45	-2.05	-5.75	-4.73	5.09	-71.17	3.07	131.25
40.13	-4.16	-7.87	-6.47	4.34	-62.70	4.21	72.32

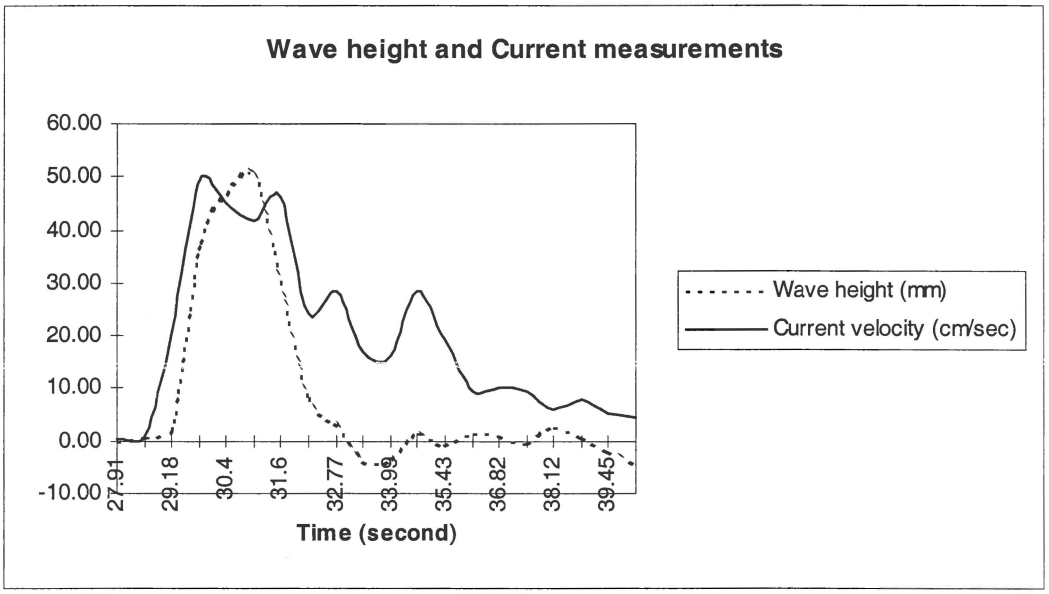

TEST 6.
Material in Tank : Mixed mud & Sand
Angle of Ramp : 60 degree
Water depth in Flume : 20 cm

Time (second)	SL.Corr (mm)	Inst.Corr (mm)	Height 1 (mm)	Velocity 1 (cm/sec)	Direction 1 (deg)	Velocity 2 (cm/sec)	Direction 2 (deg)
15.02	0.00	-25.01	-20.58	1.12	-0.04	0.48	-169.10
15.64	-1.12	-26.13	-21.50	0.33	-0.04	0.70	-158.88
16.28	-3.27	-28.28	-23.27	0.98	-31.61	0.31	28.42
16.93	-5.12	-30.13	-24.80	90.59	-180.10	58.49	84.93
17.59	53.39	28.38	23.36	93.40	-146.98	77.98	101.94
18.3	55.93	30.92	25.45	97.57	78.81	86.75	-164.57
18.95	21.95	-3.06	-2.52	99.87	-81.64	46.96	-175.05
19.56	14.74	-10.26	-8.45	115.53	-20.35	49.78	-61.49
20.28	-7.19	-32.20	-26.50	11.52	35.83	7.93	71.20
20.87	-3.98	-28.98	-23.86	36.42	-36.95	14.84	155.84
21.43	-4.34	-29.35	-24.15	8.11	166.74	5.23	137.31
22.13	-3.18	-28.19	-23.20	6.07	162.20	4.85	-118.70
22.81	-7.14	-32.15	-26.46	5.94	-66.72	2.03	126.96
23.42	-5.43	-30.44	-25.05	4.53	-145.19	6.38	121.68
23.96	-1.59	-26.60	-21.89	2.76	-156.62	1.35	118.32
24.55	-3.77	-28.78	-23.68	3.27	-161.73	3.66	138.03
25.19	-5.12	-30.13	-24.80	3.82	-80.40	4.37	116.96
25.79	-4.24	-29.25	-24.07	3.64	-112.01	3.87	105.36
26.44	3.35	-21.66	-17.83	4.87	-59.90	4.30	103.48
27.05	3.79	-21.22	-17.46	5.71	-119.81	5.75	141.61

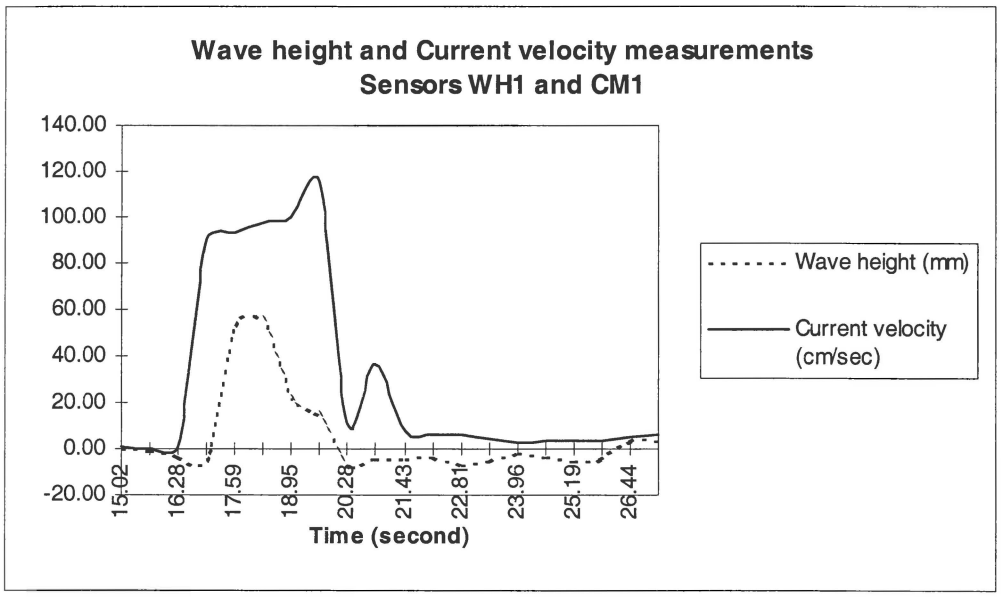

TEST 7.
Material in Tank : dyed fresh water
Angle of Ramp : 90 degree
Water depth in Flume : 20 cm

Time (second)	SL.Corr (mm)	Inst.Corr (mm)	Height 1 (mm)	Velocity 1 (cm/sec)	Direction 1 (deg)	Velocity 2 (cm/sec)	Direction 2 (deg)
40.31	0.00	2.82	2.32	2.77	52.95	1.69	61.55
40.95	-5.15	-2.33	-1.92	1.98	-64.40	1.82	-109.40
41.57	-1.84	0.97	0.80	49.55	-93.77	9.53	-105.36
42.17	13.66	16.48	13.56	38.42	133.98	37.01	-119.52
42.72	55.50	58.32	48.00	71.21	92.07	38.56	12.39
43.39	60.26	63.07	51.91	57.13	83.25	5.51	72.40
43.96	40.12	42.93	35.33	50.16	85.60	35.09	82.89
44.52	12.91	15.72	12.94	28.40	79.80	18.97	31.65
45.05	-9.54	-6.73	-5.54	31.87	123.68	25.23	32.62
45.59	-5.72	-2.90	-2.39	26.50	80.64	3.69	126.13
46.19	1.93	4.75	3.91	17.19	87.05	8.18	-104.18
46.78	-3.29	-0.48	-0.39	4.39	124.27	6.26	-27.34
47.38	0.38	3.20	2.63	6.04	115.11	3.68	-132.85
48.1	3.05	5.86	4.83	3.38	129.73	1.67	-88.57
48.69	1.00	3.81	3.14	5.29	-29.24	1.56	-173.71
49.29	1.26	4.08	3.36	7.42	-61.85	5.50	115.50
49.95	2.98	5.80	4.77	6.71	-69.09	4.71	139.63
50.61	4.93	7.74	6.37	7.84	-64.32	2.36	179.41
51.33	7.18	10.00	8.23	4.68	-47.78	1.42	103.68
52.05	6.59	9.40	7.74	5.46	-27.19	1.20	42.73

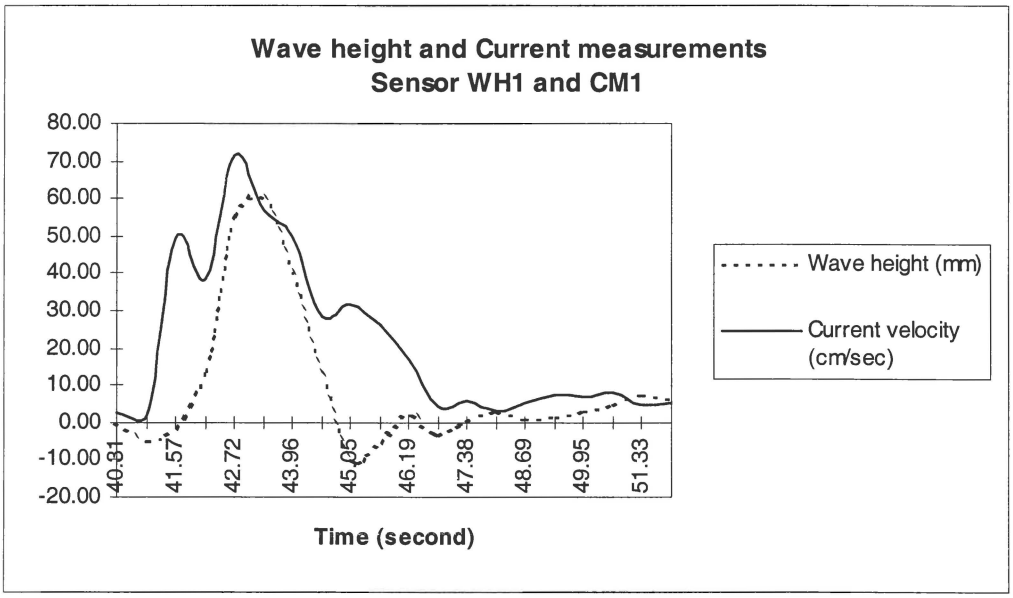

TEST 8.
Material in Tank : Mixed mud & sand
Angle of ramp : 90 degree
Water depth in Flume : 20 cm.

Time (second)	SL.Corr (mm)	Inst.Corr (mm)	Height 1 (mm)	Velocity 1 (cm/sec)	Direction 1 (deg)	Velocity 2 (cm/sec)	Direction 2 (deg)
43.54	0.00	-3.57	-2.94	1.61	-18.92	0.39	-71.57
44.21	0.20	-3.37	-2.77	1.52	-12.38	0.93	123.72
44.75	-0.07	-3.64	-2.99	42.38	109.69	53.59	-107.55
45.37	94.80	91.24	75.09	57.57	-100.18	45.07	-109.33
45.95	88.98	85.42	70.30	15.84	29.71	3.47	-27.83
46.55	66.21	62.64	51.56	32.51	-144.70	25.52	-129.25
47.1	22.06	18.49	15.22	22.70	75.52	5.47	-36.22
47.64	4.01	0.44	0.36	8.10	-148.89	7.95	-12.87
48.24	4.17	0.60	0.50	26.32	-33.03	6.26	-14.92
49	8.64	5.08	4.18	7.40	106.05	5.52	25.55
49.59	2.52	-1.04	-0.86	8.06	102.42	3.41	37.79
50.19	4.61	1.04	0.86	5.71	37.64	4.62	4.09
50.85	6.26	2.69	2.22	2.87	59.36	5.88	40.01
51.45	5.96	2.39	1.97	5.22	60.03	7.72	51.50
52.05	3.35	-0.22	-0.18	6.46	55.48	7.65	31.49
52.66	2.35	-1.22	-1.01	6.22	63.62	5.40	56.63
53.27	3.57	0.00	0.00	5.28	86.56	5.87	54.67
53.84	4.64	1.07	0.88	6.67	80.89	4.83	49.90
54.5	7.44	3.87	3.18	6.44	80.11	5.16	46.85
55.18	5.41	1.84	1.51	7.61	76.08	4.67	46.45
55.77	4.48	0.91	0.75	7.27	72.55	4.44	51.29

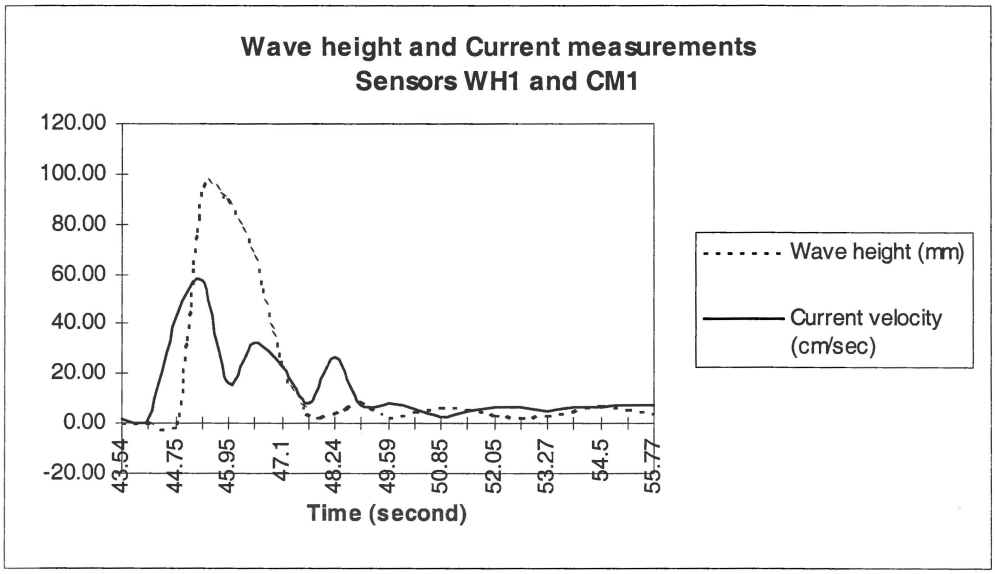

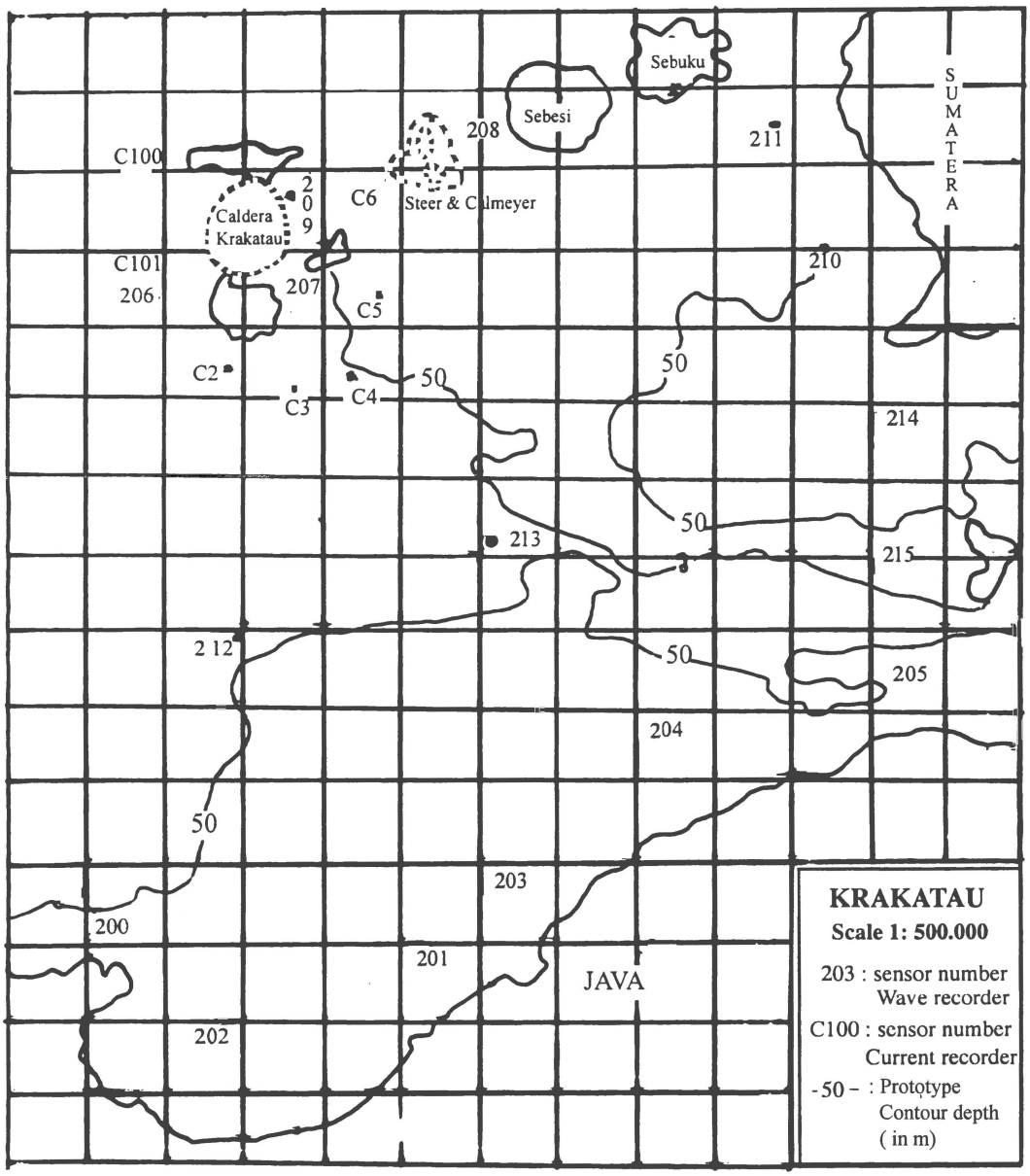

The physical modelling grid arrangement and the location of the sensors (wave sensor and current meter).

Sensor numbering and Table:

- Wave height:

Height 1, Height 2,.....Height 15: the wave height measurement number relate to sensor number 201 for Height 1, 202 for Height 2,.....215 for Height 15
For Sensor 200 it relate to Height 16.

- Current velocity:

Velocity 1, Velocity 2,.....Velocity 5 : the velocity measurement number relate to current sensor number C00, C01, C02, C03.....C05.
Direction 1, Direction 2,.....Direction 5 : the direction measurement number relate to current sensor number C100, C101, C2, C3.....C6

SUBMARINE EXPLOSION TEST.

- Wave height :

Submarine Explosion with Chamber
Intensity : 4 tubes

Time (Second)	Height 206 (cm)	Height 207 (cm)	Height 208 (cm)	Height 209 (cm)	Height 210 (cm)	Height 211 (cm)
0.00	0.00	0.00	0.00	0.00	0.00	0.00
1.57	0.01	-0.07	-0.01	-0.07	0.03	-0.09
3.09	0.04	0.12	0.01	0.12	-0.06	-0.51
4.63	0.06	-0.11	0.11	-0.11	-0.07	-0.11
6.12	0.06	-0.04	-0.09	-0.04	-0.12	-0.14
7.73	0.06	0.08	-0.02	0.08	-0.16	-0.53
9.39	0.05	0.06	-0.05	0.06	0.12	-0.17
11.01	0.04	0.14	0.04	0.14	0.41	-0.50
12.44	-0.01	0.02	-0.03	0.02	-0.05	-0.08
14.06	-0.01	0.24	-0.02	0.24	0.11	-0.08
15.58	-0.02	0.13	-0.03	0.13	0.11	-0.45
17.07	-0.02	-0.01	-0.01	-0.01	0.00	-0.08
18.51	-0.02	-0.13	-0.10	-0.13	-0.01	0.01
20.12	-0.02	0.21	-0.09	0.21	-0.05	-0.06
21.50	-2.58	1.47	-0.03	1.47	-0.17	-0.49
23.16	2.32	-4.25	1.01	-4.25	-0.40	-0.33
24.78	5.81	-0.19	3.84	-0.19	-0.41	-0.40
26.44	4.76	0.12	-1.87	0.12	-0.52	-0.12
27.84	1.91	7.01	-1.26	7.01	-0.17	-0.25
29.46	1.28	4.06	-1.74	4.06	-0.30	-0.16
31.01	3.36	5.77	2.77	5.77	1.22	-1.11
32.59	1.45	3.82	1.71	3.82	-0.63	-0.66
34.06	3.14	3.31	0.14	3.31	0.81	1.73
35.69	2.06	3.22	0.36	3.22	2.91	0.94
37.29	1.00	3.38	0.17	3.38	1.74	2.17
38.81	2.53	2.84	0.33	2.84	-1.47	-0.86
40.34	2.27	3.23	-0.42	3.23	-0.34	-0.94
42.14	2.03	3.71	1.89	3.71	-0.26	0.76
43.63	3.21	4.64	1.58	4.64	-0.45	-0.84
45.11	3.03	3.77	2.19	3.77	-0.16	-0.26
46.55	2.26	5.06	0.04	5.06	0.56	0.92
48.03	2.20	4.51	1.02	4.51	-0.07	0.66
49.60	2.49	4.27	0.39	4.27	0.49	0.04
51.17	2.34	4.15	-0.33	4.15	0.00	1.68
52.73	2.01	3.36	-0.97	3.36	-0.34	0.37
54.22	1.35	2.58	2.05	2.58	-0.06	0.94
55.71	2.06	2.82	0.79	2.82	-0.08	-0.91
57.10	2.21	3.07	0.29	3.07	0.13	0.97
58.71	2.16	2.78	-0.09	2.78	0.23	1.81
60.24	1.52	3.03	-0.36	3.03	0.27	0.66
61.85	2.01	2.87	-0.27	2.87	-0.89	0.41
63.38	2.03	3.27	-0.52	3.27	0.36	0.02
64.94	2.19	3.13	-0.42	3.13	-0.08	-0.80
66.38	1.92	3.39	0.32	3.39	-1.46	-0.65
67.81	2.18	2.71	-0.29	2.71	-0.19	-0.75

69.33	2.14	2.70	0.04	2.70	-1.44	-0.48
70.88	1.89	2.94	0.03	2.94	-0.54	-0.52
72.36	2.06	3.01	-0.10	3.01	-0.19	-0.04
73.92	1.80	2.42	0.12	2.42	-0.24	-0.04
75.35	1.59	2.18	-0.30	2.18	0.19	0.78
76.85	2.01	2.23	-0.38	2.23	0.38	0.71
78.28	1.94	2.41	0.23	2.41	0.34	0.80
79.72	1.93	2.30	-0.07	2.30	0.39	0.57
81.15	1.99	2.44	0.31	2.44	0.34	0.82
82.54	1.87	2.68	0.64	2.68	0.02	-0.42
84.15	2.03	2.41	0.78	2.41	-0.23	-0.06
85.64	1.91	2.58	0.75	2.58	-0.30	0.02
87.08	1.99	2.84	0.28	2.84	-0.28	0.06
88.52	2.15	2.47	-0.27	2.47	-0.19	0.22
90.08	2.09	3.00	0.21	3.00	-0.04	1.37

- Current velocity

Velocity 1 (cm/sec)	Direction 1 (deg)	Velocity 2 (cm/sec)	Direction 2 (deg)	Velocity 3 (cm/sec)	Direction 3 (deg)
0.74	-0.04	0.85	0.01	1.33	27.51
0.87	-0.04	0.71	0.01	0.78	26.18
0.76	-0.04	1.11	0.01	1.29	14.27
0.59	-0.04	0.87	0.01	0.99	34.87
0.72	-0.04	0.49	0.01	1.04	40.88
0.58	-0.04	0.51	0.01	1.20	27.13
0.55	-0.05	0.49	0.01	1.21	40.30
0.65	-0.04	0.58	0.01	1.01	43.03
0.59	-0.04	0.76	0.01	1.22	36.67
0.52	-0.04	0.62	0.01	1.10	28.95
0.68	-0.04	0.90	0.01	1.14	27.23
0.78	-0.04	0.58	0.01	1.16	12.13
0.73	-0.04	0.85	0.01	0.96	35.81
0.21	-0.05	1.12	0.01	1.14	14.85
2.82	40.48	1.56	-85.27	1.15	138.12
2.27	-102.88	3.63	11.77	4.87	-14.73
1.46	61.96	1.86	-21.01	2.37	20.18
0.68	0.08	3.00	5.30	1.98	-7.37
0.77	0.09	2.30	17.18	1.37	10.65
0.98	0.08	1.82	1.04	1.54	9.06
0.29	0.08	1.11	8.01	1.15	27.62
1.16	0.08	1.72	9.49	1.71	14.36
0.85	0.08	1.80	3.03	2.39	-4.44
1.08	0.08	1.57	15.47	1.86	12.02
0.62	0.08	1.89	27.89	2.75	-3.88
0.73	0.08	1.10	18.09	1.91	-6.67
0.88	0.08	1.39	14.48	111.99	-79.87
0.34	0.08	1.26	-17.64	1.02	39.30
0.99	0.09	1.60	16.39	2.13	8.78
0.96	-0.04	1.53	-8.87	1.52	40.18
0.17	0.08	1.94	-36.11	2.78	-6.87
0.29	0.08	1.34	-26.30	1.44	3.80
0.93	0.08	0.99	20.04	1.31	5.63
0.70	0.08	1.19	-22.52	2.34	6.20

0.11	0.07	0.90	12.73	1.91	18.21
0.79	0.08	1.44	4.42	1.85	19.30
0.23	0.08	1.77	16.73	0.94	25.46
0.56	0.07	1.40	-3.53	1.93	3.01
0.45	0.08	1.32	-9.48	1.51	37.17
0.91	0.08	0.96	-25.24	1.82	26.95
0.73	0.08	1.47	-0.81	1.99	11.18
0.86	0.08	0.87	0.01	1.43	15.94
0.67	0.08	0.10	0.01	0.72	8.68
0.80	0.07	1.08	-15.60	1.73	22.81
0.63	0.08	0.92	0.01	1.61	33.70
0.39	0.07	0.88	0.01	1.16	20.45
0.33	0.07	1.04	0.01	1.66	19.93
0.40	0.08	0.68	0.01	1.30	43.64
0.46	0.08	0.93	0.01	1.12	23.33
0.38	0.08	1.22	0.01	1.21	27.47
0.82	0.08	1.30	-11.38	1.60	26.13
0.57	0.08	1.29	-15.02	1.63	38.75
0.62	0.08	1.16	-5.01	2.16	28.75
0.42	0.08	1.22	-18.93	1.81	2.98
0.44	0.08	1.42	-26.59	1.29	20.03
0.70	0.08	1.47	-20.34	1.84	19.66
0.76	-0.04	1.11	-23.85	1.30	16.61
0.40	-0.05	1.23	-16.02	1.47	43.54
0.65	-0.04	1.22	-5.11	0.89	26.98

Velocity 4 (cm/sec)	Direction 4 (deg)	Velocity 5 (cm/sec)	Direction 5 (deg)
1.74	-14.80	3.40	-114.34
1.65	-17.11	3.62	-121.38
1.45	-8.25	3.56	-123.69
1.45	-7.59	3.49	-129.01
1.27	-2.90	3.46	-129.25
1.15	-0.23	3.54	-125.99
1.27	-1.43	4.17	-129.16
1.28	4.70	3.73	-125.08
1.36	1.96	3.64	-126.38
1.40	3.47	3.59	-128.68
1.38	11.21	3.53	-127.21
1.47	10.83	3.36	-126.81
1.58	13.22	3.37	-127.38
2.85	-13.57	8.17	-76.26
22.30	-55.64	10.51	-0.16
7.89	4.91	5.65	-14.50
6.01	-49.06	4.19	-107.67
5.07	-65.80	5.46	-92.50
1.97	-42.43	1.50	-106.44
3.23	-6.53	5.85	-143.05
1.64	12.46	9.51	-160.16
2.57	-56.32	9.00	-169.85
3.56	-31.78	8.18	-157.63
2.72	-25.73	7.41	176.55
3.22	-44.67	6.98	-160.00
3.39	-28.99	5.43	-176.59
1.10	-0.19	4.52	-155.96

2.74	-58.60	5.64	-172.04
1.01	-20.38	3.43	161.49
2.71	20.58	3.44	-153.57
1.84	-37.82	2.64	157.59
1.16	68.82	3.94	-174.98
1.88	52.21	5.19	-178.04
1.45	46.92	3.13	-175.76
1.89	48.64	3.48	180.42
2.89	-37.81	2.21	172.52
1.13	-14.23	3.35	-148.87
1.94	-44.65	3.70	-154.91
2.53	20.48	2.74	-158.76
1.54	16.92	2.78	-129.79
1.77	59.66	2.47	-158.81
2.91	-23.50	2.55	-127.25
1.59	-10.53	3.21	-142.78
2.66	-7.15	2.15	-153.06
2.22	3.24	2.93	-170.44
1.82	1.21	2.33	-178.87
2.56	-9.39	2.11	-169.38
1.96	-11.02	2.22	-150.82
2.44	6.52	3.55	-152.99
2.64	-8.16	2.89	-117.16
3.32	-6.80	2.16	-141.43
2.29	5.38	2.59	-114.15
2.80	-8.69	1.97	-123.11
1.75	-4.43	2.20	-127.40
2.64	-8.66	1.44	-111.55
1.68	-11.21	1.52	-118.53
2.44	-11.34	1.80	-116.45
2.47	-6.07	2.32	-122.47
2.87	22.89	1.86	-103.63

- Wave height

Submarine Explosion without Chamber
Intensity : 4 tubes

Time (second)	Height 206 (cm)	Height 207 (cm)	Height 208 (cm)	Height 209 (cm)	Height 210 (cm)	Height 211 (cm)
0.00	0.00	0.00	0.00	0.00	0.00	0.00
1.57	0.05	0.07	-0.52	-0.02	0.03	-0.01
3.11	0.05	0.14	-0.08	0.17	0.18	-0.25
4.56	0.02	0.07	0.01	0.31	-0.06	0.03
5.98	0.03	-0.23	0.03	0.16	-0.13	-0.10
7.43	0.01	-0.26	0.05	0.13	-0.25	-0.06
8.98	-0.01	-0.28	-0.11	0.34	-0.25	-0.09
10.48	0.01	0.15	-0.62	0.36	-0.11	0.01
11.95	-0.23	0.07	-0.31	0.00	-0.06	-0.04
13.50	0.06	-0.23	0.02	0.39	-0.03	0.08
14.92	-0.01	-0.25	-0.60	0.03	0.15	-0.23
16.41	0.01	0.14	-0.01	0.41	-0.05	0.04
17.79	0.07	0.18	-0.02	0.43	-0.02	-0.06
19.23	-0.16	-0.16	0.11	0.23	-0.06	-0.01
20.74	0.07	-0.01	-0.01	-0.01	-0.04	0.09
22.18	0.01	0.07	-0.01	-0.04	0.09	0.00
23.58	0.07	0.19	-0.01	0.06	-0.05	0.00
25.02	0.05	-0.18	-0.03	0.35	-0.06	-0.05
26.45	0.05	-0.14	-0.07	0.06	-0.34	-0.02
28.06	0.17	-4.24	-0.14	1.37	-0.16	-0.07
29.46	-9.57	7.69	-0.58	-11.37	0.08	-0.02
30.84	-4.28	-11.17	0.02	-9.10	-0.01	0.03
32.28	-8.36	3.10	-2.67	1.32	-0.34	0.00
33.95	-0.25	3.33	-5.67	3.74	-0.15	-0.07
35.51	0.16	0.19	-6.15	1.46	-0.05	-0.03
37.05	0.18	-0.50	-0.60	-0.60	-2.45	1.26
38.48	-0.55	0.63	-1.27	3.05	-2.29	-0.72
39.92	-1.63	0.31	-0.75	-0.68	2.87	0.68
41.49	-1.61	-0.23	-2.94	0.23	0.73	-0.05
43.00	-0.65	-0.21	-2.80	-1.88	-2.44	0.28
44.58	-0.67	-2.88	-2.44	-2.23	-1.27	1.25
46.20	-1.97	-0.35	-2.02	-1.57	1.53	-0.55
47.77	-1.09	-0.27	-0.89	0.75	0.96	1.02
49.35	-0.32	-1.76	-1.15	-1.51	-0.82	0.91
50.87	-4.54	-0.78	-2.44	-2.20	0.30	1.10
52.31	0.24	-0.38	-4.01	-0.18	-1.80	0.15
53.70	-0.84	-2.40	-1.90	-0.85	0.97	0.11
55.17	-0.83	0.40	-2.38	-1.07	0.78	0.67
56.79	-0.74	0.43	-3.44	0.49	0.25	1.20
58.41	-1.87	0.13	-3.70	-0.54	0.84	1.24
59.98	-0.56	-0.19	-4.63	-1.63	0.67	0.36
61.46	-3.66	-0.18	-4.98	-2.00	0.07	0.73
62.85	-0.73	-1.02	-0.44	-1.32	0.33	-0.13
64.47	-2.52	0.17	-0.64	0.37	-1.76	0.61
65.91	-0.83	-0.40	-2.21	0.15	0.76	0.80
67.39	-0.55	-0.01	-4.40	-0.79	0.86	0.07
68.80	-2.01	-0.72	-2.31	-0.77	0.51	1.20
70.39	-1.41	-0.16	-3.06	-0.19	0.26	1.23

72.01	-1.84	0.17	-0.82	-0.54	0.61	0.46
73.57	-0.64	-1.86	-0.78	-1.35	0.06	0.47
75.18	-0.66	-1.20	-1.49	-0.65	0.07	0.93
76.70	-2.57	-1.57	-4.62	-1.32	-0.72	0.65

- Current velocity

Velocity 1 (cm/sec)	Direction 1 (deg)	Velocity 2 (cm/sec)	Direction 2 (deg)	Velocity 3 (cm/sec)	Direction 3 (deg)
0.53	-0.04	0.69	-72.63	1.96	55.43
0.21	-0.04	0.78	0.01	0.81	25.65
0.23	-0.04	0.71	0.01	1.11	-4.05
0.51	-0.04	0.50	0.01	1.15	-7.98
0.32	-0.04	0.90	0.01	0.97	-5.02
0.54	-0.04	0.77	0.01	0.90	-8.30
0.43	-0.05	0.82	0.01	1.44	-2.72
0.63	-0.05	0.54	0.01	0.80	-23.31
0.38	-0.04	0.65	0.01	0.75	-7.55
0.18	-0.05	0.51	0.01	0.56	-12.44
0.54	-0.04	0.46	0.01	0.88	-7.21
0.40	-0.04	0.42	0.01	0.93	-9.57
0.22	-0.04	0.40	0.01	0.96	-3.34
0.22	-0.04	0.54	0.01	0.91	-1.31
0.27	-0.04	0.47	0.01	0.75	-15.67
0.15	-0.04	0.44	0.01	1.08	-3.12
0.37	-0.04	0.17	0.01	1.15	-12.95
0.27	-0.04	0.55	0.01	0.77	-24.28
0.49	-0.05	0.58	0.01	1.38	4.15
0.73	-0.04	4.12	-5.57	3.17	-19.43
5.49	-0.95	4.04	-26.95	6.94	-27.47
1.00	67.66	1.36	-115.49	1.55	143.60
2.21	-7.54	2.82	8.16	7.37	-24.36
0.76	-0.04	0.37	0.01	0.63	135.40
0.57	-0.04	0.80	0.01	1.61	-11.13
0.37	-0.04	-0.01	0.02	2.57	-10.58
0.73	-0.04	0.35	0.01	2.36	-2.72
0.91	-0.04	0.84	-36.49	1.41	-20.98
0.42	-0.05	1.06	12.80	1.71	-7.91
1.11	-0.04	-0.02	0.01	1.06	-64.27
1.09	-58.96	0.88	-0.03	0.85	84.62
0.08	-0.04	1.19	-18.63	1.49	23.68
0.32	-0.04	0.74	0.01	2.57	-37.56
0.26	-0.05	0.34	0.01	1.29	0.18
0.29	-0.04	0.46	-0.04	1.83	-4.63
0.91	-0.04	1.33	29.02	1.50	-26.17
0.87	-0.04	0.96	-46.25	1.64	29.87
0.83	-0.05	1.06	0.01	1.51	-11.28
0.82	-0.04	0.82	0.01	1.72	-41.66
0.62	-0.04	0.77	0.01	2.26	-13.12
0.54	-0.04	-0.01	0.01	0.75	39.93
0.36	-0.04	0.44	-0.04	1.27	16.19
0.60	-0.04	1.60	-58.31	1.97	-26.68
0.28	-0.04	0.82	0.01	1.44	-37.44
0.44	-0.04	0.44	0.01	1.34	-26.43

0.56	-0.04	0.00	0.01	1.16	65.67
0.27	-0.04	0.46	-0.04	2.04	7.75
0.11	-0.04	1.11	0.01	1.22	-26.04
0.57	-0.05	0.07	0.01	0.49	-7.51
0.23	-0.04	0.58	0.01	0.94	27.88
0.38	-1.91	-0.01	0.01	1.20	-0.01
0.10	-0.04	-0.01	0.01	1.21	7.43

Velocity 4 (cm/sec)	Direction 4 (deg)	Velocity 5 (cm/sec)	Direction 5 (deg)
2.18	-46.39	3.49	-109.34
1.96	-58.22	3.91	-109.67
1.59	-60.03	3.97	-109.37
1.47	-39.00	3.43	-111.46
1.53	-48.45	3.65	-119.10
1.91	-31.05	3.97	-110.54
1.39	-52.05	3.58	-106.95
1.65	-51.68	3.77	-119.88
1.94	-27.23	3.16	-114.72
1.17	-17.15	3.52	-118.88
1.50	-38.35	3.36	-113.78
1.49	-12.41	3.52	-118.63
1.51	-29.17	3.29	-117.61
1.71	-45.96	3.62	-117.26
1.64	-40.20	3.54	-114.15
1.83	-37.64	3.78	-114.32
1.47	-53.39	3.37	-109.55
1.53	-57.56	2.97	-116.46
4.18	-8.77	5.42	-120.63
25.52	132.93	18.32	-118.24
6.47	-32.49	9.20	-28.95
15.01	-47.15	12.49	-134.87
2.12	-75.36	4.31	-137.66
1.99	53.54	2.06	33.98
0.69	-0.19	2.33	-115.91
2.07	-85.09	2.62	-114.95
1.31	0.12	2.29	-135.29
1.54	-5.94	2.71	-112.90
1.21	-91.88	3.26	-105.93
1.75	-88.26	0.87	-124.23
2.04	-56.13	1.83	-97.84
1.91	78.24	4.23	-114.63
1.42	-78.04	3.09	-123.11
0.86	125.93	2.08	-113.18
2.68	-36.21	2.96	-135.47
1.39	8.81	4.47	-100.13
2.28	-10.34	2.44	-126.16
5.34	-59.29	2.58	-117.64
1.53	-55.54	3.07	-142.46
1.55	-23.40	2.37	-138.02
1.15	-60.06	2.50	-119.45
1.10	-20.70	3.10	-126.13
2.27	-27.73	3.10	-115.55
1.46	-23.81	3.79	-112.66
2.37	3.90	2.46	-136.86

0.91	-27.24	1.79	-124.10
1.42	61.86	2.76	-113.41
2.02	-33.90	2.86	-99.24
1.12	4.29	3.17	-121.61
2.57	-35.63	2.96	-134.50
1.51	-25.10	2.59	-114.86

- Wave height

Submarine Explosion without Chamber
Intensity : 6 tubes

Time (Second)	Height 206 (cm)	Height 207 (cm)	Height 208 (cm)	Height 209 (cm)	Height 210 (cm)	Height 211 (cm)
0.00	0.00	0.00	0.00	0.00	0.00	0.00
1.47	0.03	0.10	-0.41	0.00	-0.03	-0.08
2.96	0.03	0.69	0.43	1.30	0.03	-0.05
4.54	0.04	0.81	0.51	3.00	0.01	-0.12
5.97	0.06	1.04	0.58	2.87	-0.01	-0.25
7.48	0.05	0.96	0.30	2.97	-0.04	-0.28
9.02	0.05	0.76	0.48	2.23	0.09	-0.62
10.45	0.04	1.01	0.24	3.12	-0.02	-0.27
11.94	0.03	1.17	0.41	2.89	-0.15	-0.09
13.47	0.04	0.87	0.48	1.97	-0.02	-0.28
14.90	0.04	-0.03	0.62	2.18	-0.36	-0.14
16.46	0.01	-0.81	0.48	1.78	-0.03	-0.33
18.03	0.02	-0.95	0.35	2.52	-0.01	-0.33
19.58	0.04	-8.35	0.37	-13.83	-0.02	-0.27
21.19	-3.30	10.71	0.23	-18.39	-0.35	0.59
22.80	-1.80	-11.82	0.97	-8.26	-0.10	-0.09
24.25	-6.86	4.07	-3.55	9.07	0.18	-0.30
25.68	2.53	4.80	-4.73	7.56	-0.02	-0.20
27.29	2.54	2.85	-7.21	0.06	-0.02	-0.23
28.79	-0.61	3.88	-5.71	4.23	-1.83	3.65
30.39	1.85	2.06	-1.90	-0.82	-1.62	-2.60
31.92	0.83	1.11	-3.41	0.32	-2.92	-4.75
33.40	-1.52	-1.97	-4.61	-0.92	3.26	1.48
34.87	1.39	-0.43	-3.60	-2.33	-1.07	-0.69
36.39	1.96	-0.62	-2.84	-0.42	2.87	0.96
37.83	0.99	-0.44	-3.07	-2.33	1.07	0.86
39.36	0.76	1.47	-3.75	0.04	1.98	-1.69
40.76	-1.44	-1.68	-4.71	1.26	0.29	0.45
42.38	2.16	0.50	-2.86	-2.32	-1.02	1.66
43.97	1.69	-4.26	-1.36	-1.39	-1.33	-3.09
45.33	0.23	1.88	-4.82	2.12	0.30	-1.65
46.86	0.62	1.59	-2.49	1.37	1.00	-1.14
48.35	1.34	-0.23	-2.94	-0.32	1.08	0.96
49.80	2.28	-1.64	-5.53	0.44	1.07	2.40
51.30	1.31	1.52	-5.32	0.82	1.43	0.23
52.83	0.73	0.67	-6.80	0.68	-1.89	0.14
54.37	-1.56	-1.17	-1.25	-1.18	0.06	0.79
55.78	0.25	-0.40	-2.15	-0.18	-0.15	1.28
57.22	1.66	0.01	-2.99	0.88	-0.27	0.07
58.71	0.51	0.57	-5.00	1.04	0.69	-1.11
60.21	0.26	-0.20	-4.25	-1.03	0.65	1.57
61.77	1.21	0.18	-4.17	1.05	1.25	2.41
63.20	1.03	0.78	-2.96	-0.60	1.38	1.28
64.58	-0.67	0.34	-4.39	-0.95	1.53	0.14
66.02	-0.80	1.16	-4.13	-1.15	0.62	-0.92
67.46	-0.06	0.95	-4.28	0.39	-0.74	1.46
68.89	0.25	1.12	-4.41	0.92	-0.71	1.08
70.33	1.74	0.58	-5.45	0.38	-1.38	0.66
71.85	1.69	1.40	-3.97	-0.27	0.43	-1.48

73.26	1.54	0.95	-4.11	0.12	1.37	-0.26
74.71	1.37	0.39	-3.01	0.29	-0.37	0.56
76.13	1.34	1.05	-4.07	-0.70	-0.64	0.61
77.61	0.12	1.20	-5.47	0.52	-0.07	0.49
79.12	1.36	-0.56	-3.65	-0.16	0.84	-0.15
80.62	1.26	1.07	-3.42	0.63	0.34	0.48
82.14	0.01	-0.28	-3.42	-0.39	0.43	0.74
83.67	0.68	0.97	-4.72	-0.78	0.18	0.78
85.13	1.60	-0.80	-4.28	-0.20	-0.73	-1.78
86.72	0.75	-0.19	-3.96	-0.66	-1.31	-0.50
88.22	0.93	1.00	-4.68	-0.95	-0.98	-0.06
89.72	0.89	1.09	-4.15	-0.83	0.09	1.51

- Current velocity

Velocity 1 (cm/sec)	Direction 1 (deg)	Velocity 2 (cm/sec)	Direction 2 (deg)	Velocity 3 (cm/sec)	Direction 3 (deg)
0.22	-0.05	-0.01	0.01	0.88	37.91
0.52	-0.05	-0.02	0.01	0.51	3.27
0.37	0.08	-0.02	-0.03	1.24	40.89
0.17	0.08	-0.02	-0.04	0.94	23.26
0.18	0.08	-0.02	-0.03	1.20	14.67
0.12	0.08	-0.02	-0.04	0.77	28.84
0.25	0.09	-0.02	-0.03	0.83	44.75
0.33	-0.05	-0.02	-0.03	1.00	27.02
0.39	-0.05	-0.01	0.02	1.09	3.83
0.28	-0.05	-0.01	0.01	0.85	18.13
0.21	-0.05	0.15	0.01	0.94	36.54
0.24	-0.05	0.24	0.01	0.84	40.40
0.36	-0.05	0.13	0.01	1.01	27.51
0.56	-0.05	1.41	1.34	1.46	6.84
5.99	-23.12	9.72	-13.56	10.02	-14.20
3.72	73.13	1.11	-170.21	6.72	136.62
0.93	-104.02	3.64	22.49	2.95	-23.92
3.30	63.37	1.58	-19.24	1.91	124.70
0.30	0.09	1.27	47.15	0.88	-5.55
0.12	0.08	1.24	25.02	0.60	84.66
0.17	0.09	0.98	-0.04	1.26	39.81
0.75	-0.05	1.38	8.77	2.15	-20.39
0.47	-0.05	2.50	39.93	2.19	24.57
1.04	-42.26	1.66	53.50	2.27	-39.91
1.65	-27.54	1.60	48.72	1.20	39.84
0.31	0.09	0.97	9.75	1.84	49.07
0.79	0.08	1.75	-12.07	1.64	11.02
1.80	89.07	1.04	-32.78	2.05	54.32
1.12	44.38	1.30	28.29	3.30	-21.30
1.05	8.33	2.00	-22.74	1.80	46.14
0.28	0.08	1.49	34.03	3.96	-21.69
0.19	0.09	1.08	26.07	1.73	24.36
0.51	0.08	1.38	4.73	1.82	39.73
0.66	-0.05	1.17	6.98	2.37	-2.11
0.53	0.09	1.22	12.28	2.03	41.54
0.87	62.17	1.67	42.69	2.13	76.37

0.62	74.70	1.37	29.88	1.56	-19.54
1.12	-30.79	1.82	-1.30	2.30	28.58
0.95	0.10	1.29	44.26	2.47	19.78
0.39	0.08	1.03	17.54	2.76	81.67
0.79	0.09	1.59	33.62	1.27	-12.39
0.63	0.08	1.58	14.19	1.07	12.37
0.76	0.08	1.64	14.64	1.12	-27.32
0.81	0.08	0.94	9.62	1.18	27.48
0.58	0.08	1.30	29.62	1.72	-4.92
0.78	0.09	0.87	21.97	1.30	23.00
0.32	0.08	1.40	28.04	1.16	-17.35
0.64	0.08	0.56	3.54	0.98	80.44
0.98	0.08	0.99	-10.21	1.55	4.76
1.08	0.08	0.99	-3.00	1.13	22.27
0.71	-3.50	1.16	-21.85	1.43	66.12
0.83	7.41	1.01	-13.89	1.54	4.90
0.89	10.73	0.94	-36.11	1.56	39.56
0.53	0.09	1.32	-13.39	2.03	42.01
0.59	0.08	1.18	12.88	0.87	42.12
0.82	-0.05	1.42	-0.25	1.67	39.43
0.58	-0.05	0.76	2.21	1.65	44.44
0.67	-0.05	1.55	20.83	1.39	47.61
0.38	0.08	1.07	36.02	1.62	61.62
0.57	0.08	0.74	19.86	1.53	0.84
0.19	0.09	1.11	-0.04	2.18	3.52

Velocity 4 (cm/sec)	Direction 4 (deg)	Velocity 5 (cm/sec)	Direction 5 (deg)
1.45	-24.71	3.26	-129.28
1.68	-51.88	3.01	-118.42
2.11	-45.16	3.80	-127.73
1.87	-34.05	3.57	-121.86
1.62	-43.84	3.84	-118.74
1.79	-52.38	3.70	-118.40
1.46	-29.73	3.92	-121.76
1.83	-30.92	3.38	-114.89
1.72	-26.06	3.22	-116.15
2.05	-23.97	3.04	-115.23
2.01	-43.38	3.57	-120.59
1.70	-42.04	3.61	-125.81
1.69	-47.35	3.93	-118.45
10.06	-42.71	6.58	-110.20
22.84	84.16	6.33	-27.44
2.73	-3.87	14.40	-149.70
4.72	47.98	7.63	64.95
4.20	27.62	4.47	-85.67
5.69	105.37	4.57	-96.96
2.89	80.79	2.04	143.82
5.16	77.36	2.08	-134.82
4.42	66.22	4.18	-110.83
1.71	50.44	3.85	-98.22
2.22	-24.24	1.64	164.91
2.17	7.27	2.19	-125.67
3.89	60.02	1.30	-141.82

2.96	109.27	4.92	-105.27
3.34	80.23	2.12	-174.01
2.40	4.52	0.84	-68.34
1.30	64.59	1.97	-108.63
5.48	-23.32	2.00	-97.06
4.54	92.55	4.46	-131.09
3.57	-11.42	4.49	-120.80
1.49	13.56	2.65	-102.84
2.25	57.31	2.56	-126.24
2.70	43.94	1.99	-176.73
4.51	4.96	3.95	-122.15
3.19	24.71	3.81	-95.03
1.00	-26.67	1.63	-108.95
2.86	9.40	5.21	-130.88
3.76	-6.86	2.57	-148.71
3.86	18.08	2.49	-132.07
3.25	-22.02	2.57	-114.60
3.91	-17.50	2.92	-123.30
0.92	27.39	3.16	-133.12
2.60	6.40	3.71	-125.17
2.34	17.98	2.97	-124.45
3.57	-24.37	2.96	-140.15
1.68	11.30	2.70	-158.59
2.44	29.50	3.40	-118.96
3.47	-10.55	2.46	-131.36
2.65	51.34	2.33	-118.98
2.38	6.60	3.14	-113.07
2.66	-5.95	3.10	-120.17
3.51	35.92	2.46	-131.42
1.71	24.35	4.21	-136.03
3.02	-20.78	3.91	-143.79
2.60	6.33	3.28	-126.37
2.93	23.15	3.26	-140.64
3.08	-3.26	4.22	-135.37

- Wave height

Submarine Explosion with Chamber
Intensity : 6 tubes

Time (second)	Height 205 (cm)	Height 206 (cm)	Height 207 (cm)	Height 208 (cm)	Height 209 (cm)	Height 210 (cm)	Height 211 (cm)
0.00	0.00	0.00	0.00	0.00	0.00	0.00	0.00
1.53	0.22	0.04	-0.01	-0.05	0.13	-0.14	-0.04
2.96	0.25	0.24	0.01	-0.04	0.17	0.61	-0.07
4.45	0.25	0.29	0.17	-0.07	0.45	-0.56	0.05
5.89	0.23	0.31	0.34	-0.04	0.14	-0.26	0.05
7.27	0.25	0.29	0.08	-0.13	0.37	-0.23	0.00
8.76	0.26	0.25	0.25	-0.26	0.40	-0.26	-0.03
10.26	0.22	0.19	0.21	-0.15	0.35	-0.29	0.06
11.75	0.23	0.06	-0.03	-0.17	-0.19	-0.35	-0.07
13.19	0.21	0.06	0.09	-0.30	-0.17	-0.39	-0.06
14.73	0.18	-0.03	-0.30	-0.50	-0.18	-0.40	-0.07
16.24	0.16	-0.11	-0.05	-0.71	-0.25	-0.44	-0.02
17.74	0.14	-0.08	-0.25	-0.82	-0.33	-0.31	-0.03
19.12	0.08	-0.11	-0.21	-0.47	-0.36	-0.32	-0.06
20.61	0.01	-0.12	0.02	-0.35	-0.39	-0.23	-0.01
22.05	0.05	-0.09	-0.26	-0.26	-0.08	-0.60	-0.07
23.48	0.03	-0.10	0.04	-0.99	-0.22	-0.39	-0.62
25.04	-0.08	-0.13	-0.36	-0.93	-0.23	-0.57	-0.55
26.48	-0.05	-0.09	0.02	-1.10	-0.33	-0.67	-0.58
27.97	-0.17	-0.19	-0.40	-0.98	-0.36	-0.87	-0.87
29.41	-0.40	-0.49	-0.36	-1.26	-0.35	-0.72	-0.37
30.79	-0.51	-0.68	-0.62	-1.09	-0.39	-0.71	-0.58
32.22	-0.46	-0.77	-0.97	-0.93	-0.73	-0.69	-0.41
33.71	-0.60	-0.50	-0.52	-0.92	-0.79	-0.65	-0.38
35.09	-0.51	-0.64	-0.88	-0.98	-0.54	-0.58	-0.30
36.53	-0.52	-0.55	-0.39	-0.35	-0.43	-0.55	-0.21
37.97	-0.51	-0.26	-0.33	-0.54	-0.26	-0.69	-0.39
39.40	-0.51	-0.08	0.10	-0.54	-0.36	-0.40	-0.47
40.84	-0.11	0.06	-0.36	-0.51	-0.14	-0.59	-0.43
42.33	-0.11	0.07	-0.04	-0.37	-0.17	-0.70	-0.48
43.71	0.01	0.05	-0.22	-0.36	-0.05	-0.73	-0.51
45.14	0.01	0.05	0.03	-0.37	-0.37	-0.67	-0.55
46.58	0.18	0.06	-0.18	-0.37	0.11	0.18	-0.71
48.02	0.19	0.08	0.08	-0.42	-0.23	-0.88	-0.34
49.45	0.18	0.10	-0.12	-0.33	0.12	-0.23	-0.10
50.89	0.17	-0.01	0.08	-0.27	-0.22	-0.15	-0.06
52.32	0.14	-0.05	-0.19	-0.27	0.07	-0.14	0.15
53.76	0.11	-0.05	-0.02	-0.15	-0.26	-0.07	0.21
55.25	0.08	-0.15	-0.19	-0.08	-0.15	-0.18	0.35
56.69	0.06	-0.09	-0.02	-0.20	-0.12	-0.08	0.04
58.12	-0.05	-0.08	-0.25	-0.26	-0.04	0.06	0.16
59.61	-0.24	-0.09	-0.19	-0.33	-0.20	-0.13	0.05
61.00	-0.29	-0.13	-0.36	-0.34	-0.05	-0.30	-0.08
62.43	-0.42	-0.06	0.06	-0.51	-0.33	-0.51	-0.32
63.87	-0.42	-0.07	-0.35	-0.50	0.02	-0.90	-0.61
65.42	-0.48	-0.02	-0.15	-0.50	-0.01	-1.02	-0.68
66.92	-0.40	-0.02	-0.03	-0.51	-0.17	-1.01	-0.84

68.40	-0.41	-0.02	-0.23	-0.58	-0.07	-1.43	-0.72
69.92	-0.43	-0.01	-0.08	-0.66	-0.10	-1.09	-0.88
71.45	-0.42	-0.07	-0.08	-0.82	-0.42	-1.05	-0.88
72.97	-0.39	-0.11	-0.70	-1.11	-0.62	-0.92	-0.77
74.40	-0.42	-0.19	-0.50	-1.44	-0.74	-0.89	-0.74
75.89	-0.41	-0.29	-0.82	-1.26	-0.69	-0.85	-0.71
77.29	-0.38	-0.27	-0.64	-1.26	-0.71	-0.83	-0.72
78.71	-0.40	-0.39	-0.49	-1.11	-0.94	-0.80	-0.64
80.15	-0.43	-0.13	-0.78	-1.01	-0.63	-0.95	-0.76
81.58	-0.28	-0.13	-0.23	-0.98	-0.52	-0.60	-0.83
83.02	-0.28	-0.07	-0.36	-0.60	-0.36	-0.60	-0.68
84.47	-0.24	-0.07	-0.13	-0.55	-0.05	-0.65	-0.70
85.94	-0.12	-0.04	-0.16	-0.51	-0.13	-0.60	-0.62
87.38	-0.15	0.03	-0.27	-0.57	-0.20	-0.60	-0.64
88.82	-0.17	-0.01	0.01	-0.51	-0.45	-0.64	-0.78
90.28	-0.18	-0.04	-0.33	-0.34	-0.07	-0.62	-0.39
91.81	-0.22	-0.05	-0.34	-0.34	-0.29	-0.55	-0.07
93.36	-0.26	-0.07	-0.35	-0.31	-0.06	-0.35	-0.40
94.83	-0.40	-0.04	-0.01	-0.36	-0.27	-0.53	-0.18
96.30	-0.43	-0.02	-0.28	-0.27	-0.37	-0.52	-0.21
97.79	-0.42	-0.05	-0.24	-0.36	-0.29	-0.56	-0.51
99.35	-0.36	-0.02	-0.01	-0.22	-0.03	-0.54	-0.14
100.90	-0.38	5.73	44.63	9.64	22.76	-0.27	-0.12
102.50	-0.24	-8.14	-11.74	9.62	-21.46	-0.31	0.18
103.90	-0.14	11.20	-2.17	19.28	-2.60	-0.75	-0.38
105.60	-0.06	5.43	13.90	5.77	-5.20	-0.18	0.13
107.20	-0.05	3.74	8.59	-5.90	5.14	0.01	0.45
108.70	8.52	2.87	5.30	9.46	6.69	0.60	3.46
110.30	-3.78	4.65	6.84	18.90	5.14	-0.10	-1.19
111.90	-3.94	0.10	7.83	14.18	5.66	-2.83	-5.03
113.40	-1.84	1.56	2.32	10.73	2.33	-3.69	5.74
115.00	0.17	2.19	9.59	5.24	5.77	-7.56	-2.97
116.60	1.17	-1.76	9.12	7.50	6.64	2.89	5.86
118.10	-3.89	1.10	6.25	10.73	3.14	4.54	1.64
119.70	0.84	-0.43	3.07	5.07	4.94	2.01	1.63
121.20	1.17	2.26	6.74	4.37	3.08	-2.66	3.41
122.70	1.86	1.09	4.55	4.05	1.01	-5.25	-0.62
124.20	1.14	2.42	6.20	18.48	3.60	-3.17	-5.75
125.80	-0.16	1.79	6.76	8.21	7.69	-4.82	-4.62
127.30	-1.84	1.13	8.35	8.53	6.89	-0.18	0.26
129.00	-2.39	2.75	7.84	14.38	4.82	-0.12	1.80
130.60	1.85	2.01	1.77	7.43	5.29	1.99	3.06
132.20	0.78	1.59	5.61	-0.01	4.85	-0.60	2.43
133.90	-2.39	0.87	4.83	9.63	3.20	0.66	0.76
135.40	0.14	-0.05	4.94	8.95	3.32	0.63	0.97
137.00	0.60	2.28	5.14	13.70	6.44	-2.23	0.67
138.70	1.03	1.00	8.09	9.83	6.79	-2.21	-2.91
140.40	-1.56	3.15	5.58	7.06	2.64	0.05	0.72
142.00	1.42	2.39	6.87	9.42	5.68	-0.36	2.72
143.40	-0.37	2.24	5.72	11.35	5.64	1.01	1.85
144.90	1.35	0.80	5.36	13.43	4.81	0.69	-0.07
146.40	-0.21	2.21	4.54	9.88	4.73	0.25	-0.31
147.90	0.30	2.08	5.00	10.32	5.83	-1.82	2.55
149.40	-0.54	1.68	5.23	9.24	6.65	-0.17	0.51
151.10	0.68	2.12	5.12	11.68	6.23	0.11	-0.01
152.70	-0.15	2.65	5.41	9.63	4.68	0.29	-1.92

154.20	-1.99	1.04	5.51	8.97	4.33	-0.66	0.23
155.60	-2.24	1.25	2.61	7.68	3.96	-0.95	0.36
157.10	-3.86	0.63	4.97	6.77	3.97	-0.57	1.06
158.50	-0.66	1.83	3.86	8.52	4.12	-0.76	-1.69
160.00	0.06	3.06	4.69	12.08	5.42	0.49	-0.72
161.80	-1.12	1.52	5.67	10.93	6.65	1.38	0.01
163.40	-0.20	1.58	5.17	10.68	5.35	0.14	-0.15
165.20	-0.11	1.36	3.23	13.81	5.61	-0.51	-3.68
166.70	-1.70	1.03	4.43	12.13	2.83	-2.94	0.64
168.30	-0.88	1.16	4.03	4.68	3.38	-0.11	0.54
169.80	-0.45	1.42	2.48	7.14	5.12	0.48	1.15
171.30	0.22	0.61	5.24	8.30	6.52	1.81	-1.16
172.90	-0.23	2.11	4.51	12.86	6.07	0.32	0.43
174.60	0.17	1.96	3.15	11.68	4.21	-0.87	0.93
176.00	-0.92	1.44	3.86	13.67	4.82	-2.77	-0.42
177.50	-0.57	1.68	4.00	11.05	6.39	0.45	0.21
179.00	-0.06	1.30	5.28	6.28	6.92	1.07	0.64
180.70	-0.23	1.97	5.04	8.99	4.97	0.69	-0.24
182.30	-0.12	1.74	3.41	12.05	3.64	0.60	0.31
183.80	-0.08	1.14	3.34	10.84	4.00	0.39	0.01
185.30	-0.69	1.18	3.48	10.62	4.13	6.11	8.03

- Current velocity

Velocity 1 (cm/sec)	Direction 1 (deg)	Velocity 2 (cm/sec)	Direction 2 (deg)	Velocity 3 (cm/sec)	Direction 3 (deg)
1.92	1.68	0.98	19.29	1.67	25.21
1.02	3.87	1.05	7.85	1.06	26.25
1.49	-26.61	1.56	-21.85	1.27	18.50
1.30	-5.13	1.07	-25.86	1.68	19.24
1.22	-3.20	1.27	-20.46	1.38	21.45
0.89	4.34	1.11	-22.02	1.78	40.78
0.63	-1.20	0.91	1.56	1.75	43.86
1.05	-8.62	1.10	-22.29	1.98	39.74
1.01	-5.57	1.05	-14.40	1.89	25.33
1.25	1.59	1.12	-4.81	1.42	40.36
0.88	-4.12	1.59	-5.18	1.59	31.02
0.96	5.23	1.52	-5.23	2.03	41.49
1.18	-8.60	1.41	-10.92	1.42	28.30
1.29	-6.87	1.36	-17.77	1.78	29.78
1.06	-10.87	1.02	6.65	1.76	43.23
1.02	-10.57	1.32	5.65	2.14	27.92
1.12	-24.16	0.81	-1.28	2.01	29.69
1.18	-20.67	0.89	6.57	1.51	25.10
1.18	-11.32	1.26	-18.54	1.69	31.46
1.14	-15.03	1.77	-24.92	1.44	16.68
1.23	-27.78	1.32	-12.82	1.72	26.40
1.23	-25.66	1.15	-7.85	1.79	12.00
1.03	-30.03	1.43	-14.78	2.10	27.69
1.09	-26.08	1.27	-13.26	1.78	20.79
1.09	-19.54	1.36	-18.67	1.89	24.96
0.85	-22.38	1.48	-15.05	1.78	22.68
1.03	-19.67	1.23	-17.35	1.76	25.32
0.77	-15.39	1.06	-12.14	1.16	27.39

1.01	3.68	1.32	-12.49	1.81	25.82
0.83	5.65	1.51	-6.18	1.45	24.89
0.94	4.55	1.02	0.68	1.33	22.64
0.99	-3.02	1.46	-5.48	1.73	29.43
0.77	7.74	1.54	-1.87	1.21	11.87
0.73	7.34	1.30	-9.62	1.49	26.41
0.95	-7.42	1.37	0.60	1.76	27.57
1.07	-13.73	1.75	-0.72	1.44	28.32
1.13	-24.81	1.33	-13.57	1.43	21.30
1.15	-36.46	1.23	-20.34	1.50	8.57
1.32	-34.82	1.33	-18.90	1.46	8.72
1.11	-41.26	1.33	-27.41	1.76	17.53
1.18	-43.35	1.26	-25.91	1.19	8.21
0.98	-30.08	1.20	-25.75	1.09	18.09
0.81	-28.35	1.07	-21.15	1.38	9.67
0.79	-29.60	1.02	-26.77	0.62	22.13
0.66	-32.24	1.05	-31.56	1.18	2.94
0.78	-29.61	1.08	-16.95	1.52	21.37
0.75	-9.38	0.82	-28.88	1.11	38.80
0.89	-23.70	0.92	-19.84	0.88	36.24
0.58	-27.88	0.98	-16.25	1.26	39.40
0.59	-15.26	0.95	-30.85	1.42	20.76
0.85	-11.13	1.07	-14.04	1.22	29.25
0.88	-9.94	0.99	-10.32	1.33	35.68
0.85	-10.73	0.91	-11.83	1.34	18.19
1.08	-7.99	1.17	-7.21	0.70	26.64
1.08	-8.69	1.13	-10.32	1.59	25.31
0.72	-3.28	1.18	-7.81	1.83	23.93
0.79	4.96	1.16	-9.10	1.38	14.46
0.68	7.57	1.28	-7.34	1.87	10.07
0.52	-0.04	1.21	-11.74	2.05	22.18
0.52	-0.04	1.13	-3.24	1.24	28.04
0.44	-0.04	1.17	-7.75	1.79	26.33
0.65	-0.04	1.21	-3.38	1.13	21.54
0.68	-15.13	1.21	-23.65	1.62	23.15
0.59	-8.28	0.88	-24.41	1.25	33.74
0.58	-22.38	0.88	-24.86	1.17	37.25
0.58	-0.04	1.10	-13.78	1.34	23.17
0.81	-0.04	1.05	-24.41	1.13	30.12
0.55	-0.04	0.91	-23.29	1.62	16.16
0.58	-0.04	0.73	-22.90	1.18	38.32
5.70	-160.46	5.22	-173.71	9.96	155.50
4.45	-174.24	12.90	-170.99	7.02	-113.64
2.92	39.43	4.05	9.13	7.01	-8.13
3.37	118.45	1.70	9.89	2.94	-1.03
1.54	69.38	6.98	45.44	3.66	8.79
1.09	55.66	0.96	13.04	2.08	1.29
1.39	139.12	3.49	55.91	6.12	15.78
0.80	20.98	3.00	12.03	3.18	13.03
2.03	99.00	3.58	27.47	5.29	-4.79
3.50	78.78	2.71	-23.15	2.37	-23.41
2.33	48.25	3.31	24.71	5.81	-21.00
0.54	70.06	3.04	5.14	5.98	-4.98
1.46	37.67	2.34	4.15	4.36	0.54
0.85	37.01	3.08	42.65	2.98	16.55
1.19	107.64	3.37	23.08	3.13	49.29

1.51	54.51	2.89	11.23	3.50	5.77
2.23	68.55	3.28	-19.40	2.99	-22.89
0.39	-0.04	2.34	-19.90	3.64	-7.91
1.18	-4.90	1.80	-22.10	1.93	9.62
0.54	6.58	2.20	-3.49	3.50	17.61
1.26	81.42	2.79	38.71	3.75	27.48
1.91	55.12	3.25	0.99	3.53	9.76
0.83	53.28	2.92	6.53	3.08	-8.51
0.31	0.08	1.99	-8.58	3.47	-25.23
0.58	38.11	1.25	23.35	1.18	80.21
1.26	82.20	2.25	-8.88	3.19	-18.00
1.26	72.41	2.17	-29.01	1.46	-15.75
1.33	93.01	2.17	-3.87	2.47	-21.01
0.49	0.09	1.44	-11.52	1.41	9.54
1.03	0.09	1.68	-11.95	3.11	-23.61
1.58	-42.48	2.56	0.93	2.41	13.56
1.57	-42.58	2.07	-9.78	3.28	-29.33
0.62	-154.86	1.40	-21.65	1.64	-6.98
1.67	171.78	1.75	-4.58	2.66	1.98
1.77	-164.70	1.30	-9.56	2.38	29.28
1.44	102.07	1.91	-22.96	2.39	13.05
1.66	158.92	0.95	-7.33	1.79	-18.26
0.90	138.79	2.30	-23.56	2.63	-2.91
1.26	120.19	1.88	11.77	2.56	27.56
0.54	0.08	1.51	21.94	2.81	28.01
0.68	0.08	1.41	-50.37	1.06	-44.26
1.14	176.36	1.42	-13.93	1.97	19.64
0.81	0.08	0.94	-40.20	1.07	23.91
0.80	142.77	1.54	-12.74	2.36	5.00
1.07	96.95	1.88	21.44	2.40	4.61
0.69	0.08	1.83	-22.40	1.57	-5.93
0.43	0.08	0.88	-28.69	1.46	10.78
0.07	0.08	1.71	-5.71	1.58	12.08
0.22	0.07	1.35	5.11	2.94	16.63
1.08	3.14	1.87	-2.91	1.69	-6.78
0.87	-0.04	1.19	-39.95	1.06	-3.14
0.98	-150.00	0.52	0.01	1.18	-13.78
0.69	-0.04	1.71	-49.42	2.13	8.32
0.78	-0.04	1.82	-9.81	2.80	6.72

Velocity 4 (cm/sec)	Direction 4 (deg)	Velocity 5 (cm/sec)	Direction 5 (deg)
2.87	6.32	3.47	-108.60
2.37	-10.15	3.48	-110.84
2.33	-5.53	3.44	-104.54
1.75	10.68	3.55	-114.78
1.52	8.16	3.20	-111.90
2.20	6.68	2.98	-115.02
2.07	6.69	3.05	-105.64
1.76	14.40	3.24	-109.17
1.96	18.78	3.54	-110.84
2.22	-3.98	3.26	-113.22
2.25	11.79	3.69	-116.98
2.21	8.29	3.00	-113.19

1.95	17.38	3.64	-120.35
2.14	10.27	3.47	-112.41
2.01	3.34	3.19	-121.07
2.35	10.14	3.40	-110.72
2.34	9.99	3.16	-110.84
2.30	7.57	3.34	-109.38
2.19	8.67	2.95	-107.25
2.23	9.89	3.28	-102.03
2.25	5.77	3.17	-104.82
2.31	26.30	3.39	-109.30
2.28	6.85	3.33	-101.06
2.44	14.33	3.96	-101.24
2.60	-8.03	3.70	-100.11
2.32	5.03	3.52	-105.76
2.23	3.60	3.60	-108.65
2.19	4.26	3.62	-109.58
2.15	23.05	3.59	-110.85
2.39	20.00	3.27	-111.45
1.98	16.89	3.39	-111.86
2.12	5.92	4.01	-108.34
2.14	6.97	3.41	-109.76
1.93	22.75	3.90	-108.58
1.67	20.06	3.38	-118.67
1.72	9.41	3.33	-114.11
1.79	16.40	3.52	-119.45
2.29	14.73	3.63	-116.96
2.08	9.56	3.84	-120.89
2.26	-10.19	3.77	-118.65
2.07	-5.65	3.65	-118.33
1.96	-10.78	3.77	-116.69
1.69	-9.25	3.85	-124.15
2.06	-4.99	3.70	-116.38
1.82	-8.06	3.88	-113.05
2.05	-4.75	3.33	-118.50
1.78	-0.79	3.46	-123.64
1.56	1.24	3.33	-128.75
1.88	20.10	3.13	-125.67
1.47	1.42	2.53	-117.88
1.76	9.18	2.97	-114.60
1.79	18.33	2.61	-112.28
2.10	7.60	3.10	-117.32
1.93	5.73	3.23	-116.82
2.12	2.88	2.35	-119.12
2.13	14.42	2.65	-120.02
2.26	9.98	3.70	-114.48
1.91	1.35	2.78	-117.24
2.22	-14.72	3.05	-116.23
2.11	6.93	2.66	-112.88
2.26	-17.23	3.32	-114.71
2.07	-8.02	3.05	-116.01
2.29	-10.92	2.88	-116.45
2.11	-1.22	3.25	-124.89
1.61	-11.33	3.24	-126.40
1.58	-11.60	3.17	-119.49
1.84	-7.31	3.50	-120.71
1.74	-8.88	3.32	-114.36

7.43	91.21	5.80	-68.80
10.04	-55.56	17.08	-153.56
24.84	-73.68	8.09	-100.90
10.05	46.24	7.80	-100.31
6.03	15.29	8.34	-64.81
4.08	-4.59	6.02	-80.22
5.50	-20.66	3.26	158.83
4.04	62.65	4.90	128.45
6.54	46.86	4.38	175.71
7.31	-54.02	6.69	-143.42
7.46	-26.79	2.71	-178.12
4.25	-13.01	3.56	-161.48
7.23	-27.78	3.95	124.97
5.56	-28.18	4.32	177.46
1.35	27.50	2.86	145.28
5.87	-10.52	3.32	176.45
4.96	-6.93	2.48	-171.38
5.61	-14.69	5.46	172.93
5.37	-38.67	1.56	-145.42
2.46	-61.09	2.09	-144.43
5.52	-25.04	0.99	-31.68
2.83	-8.23	2.57	153.24
5.55	-9.99	3.03	159.86
5.99	-47.85	2.07	-101.28
6.68	-56.85	3.64	-143.54
5.16	-15.32	3.92	174.32
5.00	-45.66	1.97	-134.15
4.39	-10.88	2.57	-145.56
3.97	-29.97	1.36	-39.13
4.84	-10.07	3.79	-136.53
2.44	-11.12	2.99	-142.56
3.75	-15.88	2.31	-126.33
5.53	-28.91	3.08	-120.38
4.75	-28.18	4.17	-123.87
2.26	-5.61	3.42	-152.85
2.18	-39.92	5.22	-122.55
5.84	-39.46	4.28	-117.35
2.37	-11.58	2.10	-99.13
5.06	-27.41	3.23	-144.21
3.98	1.05	1.32	-106.36
4.89	-28.04	1.92	-121.29
1.57	-15.90	2.74	-116.90
0.95	49.81	3.33	-120.58
4.38	-22.48	2.20	-99.94
2.42	13.61	3.46	-101.85
4.02	-23.58	2.04	-134.81
4.44	-7.94	1.78	-128.14
1.84	17.90	3.45	-104.53
4.01	-15.32	3.29	-104.22
3.91	-8.17	3.74	-131.90
2.14	-29.25	2.87	-114.88
2.63	-30.06	2.14	-124.28
2.97	-15.86	3.95	-109.16
5.10	-12.03	3.06	-113.22
2.42	3.54	2.26	-128.47

- Wave height

Submarine Explosion with Chamber
Intensity : 7 tubes

Time (second)	Height 203 (cm)	Height 206 (cm)	Height 207 (cm)	Height 208 (cm)	Height 209 (cm)	Height 210 (cm)	Height 211 (cm)
0.00	0.00	0.00	0.00	0.00	0.00	0.00	0.00
1.48	-0.01	0.02	-0.09	0.08	0.08	0.07	0.10
3.01	-0.01	0.05	0.06	0.05	0.11	0.07	0.00
4.62	0.00	0.05	0.15	0.03	0.04	0.03	0.02
6.24	0.00	0.03	0.03	0.08	-0.08	0.12	-0.01
7.73	-0.01	0.02	-0.09	0.08	0.01	0.04	-0.05
9.17	0.03	0.07	-0.09	0.10	-0.01	-0.29	0.20
10.73	0.02	0.13	-0.17	0.09	-0.16	-0.27	0.09
12.34	0.01	0.13	-0.15	0.07	-0.01	0.03	-0.06
13.96	0.00	0.12	-0.01	-0.02	0.06	0.05	0.06
15.45	-0.02	0.07	-0.15	0.07	0.07	0.19	0.00
16.92	-0.01	0.09	0.19	0.05	-0.15	0.06	0.02
18.45	-0.01	0.10	0.07	0.08	-0.06	0.07	0.00
20.06	-0.02	0.13	-0.16	0.07	-0.19	0.15	0.02
21.68	-0.04	0.13	-0.23	0.06	-0.19	0.03	0.01
23.17	-0.04	0.09	0.13	0.11	-0.23	0.07	0.04
24.73	-0.05	0.06	-0.02	0.07	-0.12	0.08	0.00
26.22	-0.03	0.10	0.00	0.08	-0.04	0.70	-0.12
27.66	-0.02	0.12	-0.13	0.04	0.01	0.00	-0.02
29.22	-0.02	0.10	-0.17	0.02	-0.16	0.13	-0.29
30.84	-0.01	0.10	-0.05	0.05	0.01	0.00	-0.35
32.45	-0.01	0.10	0.03	0.05	0.10	-0.12	0.17
34.07	-0.01	0.08	0.18	0.19	0.06	0.04	-0.04
35.74	-0.01	0.07	0.03	0.03	-0.21	0.06	0.07
37.30	0.01	0.09	-0.08	-0.02	-0.19	0.04	-0.03
38.91	0.01	0.08	-0.22	0.07	-0.27	0.05	0.00
40.53	0.01	0.07	-0.20	0.04	-0.15	0.07	0.02
42.14	0.00	0.09	-0.18	0.15	0.00	0.07	0.02
43.76	-0.01	0.11	-0.05	0.03	0.06	0.15	0.00
45.27	0.00	0.07	-0.13	0.05	-0.03	0.04	-0.03
46.82	-0.02	0.05	-0.36	0.03	-0.19	0.07	0.00
48.43	-0.02	0.06	-0.17	0.04	-0.05	0.07	-0.01
50.04	0.00	0.07	-0.13	0.12	0.06	0.03	-0.02
51.66	0.00	0.08	0.05	0.07	0.03	0.14	-0.01
53.16	0.03	0.11	-0.27	0.05	0.06	0.02	-0.08
54.71	0.01	0.09	-0.24	0.06	-0.07	0.04	-0.01
56.33	0.01	0.07	-0.15	0.19	0.04	0.05	0.00
57.94	0.01	0.06	0.05	0.05	0.02	0.02	0.00
59.46	0.01	0.05	-0.14	0.05	0.02	0.06	0.17
61.05	0.02	0.04	-0.35	0.05	0.02	0.05	0.01
62.62	0.04	0.04	-0.22	0.10	-0.03	0.07	0.03
64.12	0.02	0.06	-0.34	0.09	-0.18	-0.08	-0.12
65.66	0.02	0.06	-0.40	0.06	-0.30	0.05	-0.01
67.28	0.02	0.07	-0.29	0.09	-0.26	0.05	0.02
68.90	0.01	0.05	-0.33	0.09	-0.12	0.05	0.04
70.51	0.02	0.05	-0.19	0.02	-0.02	0.05	-0.01
72.13	0.03	0.07	-0.06	0.11	0.04	0.06	-0.02
73.74	0.03	0.06	0.04	0.07	0.00	-0.02	-0.01

75.27	0.05	0.09	-0.27	0.02	0.03	0.03	0.12
76.79	0.04	0.11	-0.24	0.09	-0.12	0.03	0.04
78.33	0.03	0.04	-0.03	0.09	-0.18	-0.29	0.22
79.85	0.02	0.04	-0.24	0.11	-0.22	0.05	0.09
81.34	0.01	0.03	-0.13	0.15	-0.12	0.15	0.02
82.90	0.05	0.07	-0.06	0.22	0.04	-0.26	0.30
84.42	0.04	0.04	-0.25	0.10	-0.03	0.06	0.04
86.03	0.04	0.05	-0.13	0.11	0.04	0.07	0.04
87.57	0.02	0.04	-0.27	0.04	-0.11	0.00	0.01
89.18	0.04	0.06	-0.14	0.09	0.00	0.19	0.01
90.68	0.05	0.08	-0.14	0.10	-0.15	0.06	-0.02
92.14	0.06	0.12	-0.10	0.07	0.00	-0.25	0.26
93.67	0.06	0.09	0.01	0.14	0.09	0.05	0.09
95.19	0.05	0.06	-0.25	0.05	-0.03	0.09	0.01
96.73	0.07	0.07	-0.25	0.10	-0.24	-0.25	-0.06
98.34	0.06	0.05	-0.32	0.08	-0.14	-0.12	-0.01
99.84	0.07	0.08	0.00	0.08	-0.23	0.06	0.05
101.40	0.07	0.06	-0.07	0.05	-0.09	0.02	0.02
103.00	0.07	0.06	-0.20	0.12	-0.18	0.21	0.03
104.50	0.06	0.04	-0.08	0.09	-0.06	0.08	0.01
105.90	0.09	0.07	-0.15	0.08	-0.16	0.01	-0.30
107.50	0.09	0.09	-0.24	0.16	-0.28	0.07	0.10
109.10	0.08	0.02	-0.32	0.18	-0.29	0.06	0.03
110.60	0.09	0.06	0.06	0.11	-0.18	-0.12	0.24
112.20	0.08	0.07	0.04	0.08	0.01	-0.11	0.00
113.80	0.10	0.07	0.05	0.11	-0.03	0.13	0.25
115.50	0.10	0.07	0.03	0.10	-0.29	0.01	0.19
117.00	0.11	0.07	-0.04	0.09	-0.19	0.06	0.04
118.60	0.12	0.08	-0.19	0.17	-0.20	0.09	0.06
120.10	0.09	0.06	-0.04	0.06	-0.05	0.24	0.05
121.70	0.08	0.06	-0.01	0.12	0.06	0.16	0.30
123.30	0.06	0.08	53.14	0.12	55.16	0.27	-0.15
124.80	0.01	2.05	-31.06	3.76	-36.86	0.50	0.13
126.40	-2.42	-3.80	-11.92	2.84	-3.08	0.79	-0.02
128.10	0.62	6.57	40.39	-3.97	-13.90	0.62	0.39
129.70	0.39	2.95	8.71	-13.76	4.98	19.56	3.49
131.30	5.53	10.10	19.35	-4.73	8.45	-3.71	2.22
132.90	-5.42	14.28	18.28	8.36	8.44	1.77	-3.29
134.50	-7.97	2.53	14.65	3.57	13.23	-7.98	-8.29
136.10	-5.16	4.66	7.34	0.70	4.12	-17.26	-7.71
137.80	2.02	2.68	7.95	6.47	5.40	-1.99	-3.00
139.50	2.24	7.12	11.60	3.05	6.72	3.24	3.22
141.00	-2.96	7.12	6.83	-2.67	4.02	10.59	0.48
142.60	0.07	6.74	12.57	-1.73	12.16	6.81	3.36
144.10	2.58	4.45	6.65	-4.07	6.18	-5.34	1.45
145.70	3.02	4.33	10.79	-3.56	5.17	-7.95	-4.87
147.40	-0.62	1.95	14.38	6.05	10.49	-0.94	-10.14
148.90	-1.50	6.78	14.27	0.72	14.62	-2.69	1.12
150.50	-4.44	5.44	19.83	-4.79	12.57	2.12	10.26
152.10	1.58	4.98	12.44	6.13	5.57	-2.74	3.10
153.60	5.05	7.53	6.44	-3.69	6.28	1.03	2.85
155.20	4.57	6.23	8.22	-10.01	4.28	5.83	4.91
156.90	0.56	0.82	10.87	2.03	8.78	0.74	0.94
158.40	2.27	5.18	10.63	4.94	8.82	-2.50	-6.05
159.90	-2.51	4.10	9.51	2.98	8.12	-5.39	-3.12
161.60	-4.47	5.82	8.88	5.75	9.48	-7.24	-0.85

163.10	-5.41	9.76	7.98	-0.48	4.48	0.26	3.64
164.70	1.13	5.21	11.29	-3.27	10.85	5.18	5.35
166.20	-2.92	9.30	10.01	4.51	10.59	4.01	4.15
167.70	-1.94	6.71	9.36	4.20	3.93	4.41	-2.23
169.30	-2.85	6.55	4.00	1.84	6.52	2.57	0.61
171.00	1.73	3.67	3.88	0.14	7.49	-2.79	2.19
172.50	1.75	7.97	8.60	1.80	9.45	1.07	-1.85
174.20	2.24	4.21	10.19	3.06	14.73	-0.51	-5.42
175.80	0.04	9.88	7.22	-1.13	10.02	1.16	-5.01
177.40	-0.44	4.59	9.09	-1.20	7.86	-2.70	1.88
179.00	0.56	5.28	4.00	-2.62	4.85	-5.38	3.31
180.60	0.71	6.17	6.02	-1.83	9.11	-2.63	-0.53
182.20	0.87	10.11	8.14	-1.16	10.57	2.86	-0.76
183.90	-1.95	5.55	11.89	1.32	12.78	0.75	1.13
185.60	-1.52	7.31	9.07	5.82	11.49	1.12	1.39
187.30	0.93	6.46	4.47	6.77	7.95	-2.63	0.81
188.80	-5.13	0.95	5.72	2.62	4.83	-2.35	-2.40
190.40	-2.29	6.42	1.17	-6.48	3.28	2.03	0.90
191.90	-1.28	5.72	2.85	-3.41	8.78	3.98	2.92
193.50	0.82	6.46	9.85	-2.25	10.82	5.38	0.15
195.20	1.01	7.66	8.80	1.23	14.18	1.28	-0.03
196.80	0.54	6.83	5.54	6.24	8.67	-2.92	1.61
198.30	-1.19	6.54	8.16	4.01	6.60	-6.05	0.19
199.80	-1.07	7.13	8.20	2.47	11.23	0.92	0.76
201.40	-0.79	6.21	11.28	-5.55	13.53	1.71	0.74
203.10	1.09	7.73	7.80	-2.66	10.00	4.40	1.18
204.60	0.96	6.03	2.31	0.68	4.47	-0.66	0.94
206.20	-2.23	3.86	2.62	-0.93	4.13	0.54	1.12
207.80	0.51	5.87	5.85	0.39	9.57	-2.94	2.01
209.30	0.66	6.62	7.78	1.96	12.84	1.52	0.67
211.00	2.55	6.96	11.01	3.28	14.13	0.61	0.73
212.50	-1.78	6.79	11.77	2.24	13.72	1.95	-2.88
214.10	-2.27	6.48	6.00	1.64	7.55	-1.54	-2.30
215.70	1.20	6.71	3.29	-4.46	4.46	-1.52	2.10
217.20	0.84	6.05	6.22	1.01	9.41	0.89	2.13
218.90	0.60	6.26	7.55	1.11	10.38	1.91	1.66
220.50	0.46	5.53	8.73	-0.26	12.23	2.55	-1.08
222.20	-0.04	6.08	8.07	2.09	9.53	0.53	-0.07
223.80	0.80	5.33	7.07	-0.40	8.07	-4.58	0.33
225.50	0.54	5.67	4.72	-2.18	7.60	-4.18	-0.87
227.10	-1.80	6.70	6.69	1.23	10.92	0.49	0.86
228.70	-2.73	6.54	8.15	2.71	12.01	2.30	1.97
230.30	0.01	6.43	7.86	-0.57	11.32	2.70	2.33
231.90	-0.12	6.26	6.86	-3.70	9.72	1.07	0.39

- Current velocity

Velocity 1 (cm/sec)	Direction 1 (deg)	Velocity 2 (cm/sec)	Direction 2 (deg)	Velocity 3 (cm/sec)	Direction 3 (deg)
1.15	-6.41	0.73	-24.93	0.54	24.64
0.89	-39.11	0.61	0.01	0.77	0.18
0.98	-33.67	0.90	0.01	0.81	0.18
0.82	-38.44	0.65	0.01	0.79	0.18
0.98	-24.41	0.57	0.01	0.94	0.18
1.04	-25.44	0.91	0.01	0.89	0.18

0.89	-35.79	0.81	0.01	0.97	0.18
1.00	-30.77	0.75	0.01	0.89	0.18
0.79	-43.54	0.74	0.01	0.92	0.18
0.76	-28.48	0.84	0.01	0.76	0.18
0.75	-25.42	0.61	0.01	0.69	0.18
0.75	-33.99	0.46	0.01	0.78	0.18
0.68	-34.64	0.63	0.01	0.80	0.18
0.69	-29.66	0.77	0.01	0.90	0.18
0.82	-23.92	0.64	0.01	0.80	0.18
0.77	-28.80	0.72	0.01	0.92	0.18
0.81	-21.59	0.70	0.01	0.87	0.18
0.77	-21.30	0.65	0.01	0.85	0.18
0.81	-34.71	0.63	0.01	0.89	0.18
0.75	-27.23	0.70	0.01	0.90	0.18
0.72	-35.99	0.72	0.01	0.71	0.18
0.73	-39.71	0.58	0.01	0.79	0.18
0.84	-44.84	0.78	0.01	0.76	0.18
0.73	-32.61	0.59	0.01	0.74	0.18
0.74	-43.31	0.66	0.01	0.86	0.18
0.67	-39.50	0.68	0.01	0.87	0.18
0.81	-43.72	0.91	0.01	0.73	0.18
0.86	-31.79	0.88	0.01	0.79	0.18
0.78	-38.89	0.44	0.01	0.82	0.18
0.82	-42.08	0.61	0.01	0.85	0.18
0.89	-36.98	0.76	0.01	1.00	0.18
0.81	-37.10	0.59	0.01	0.85	0.18
0.82	-34.21	0.89	0.01	0.73	0.18
0.91	-44.63	0.63	0.01	0.56	0.18
0.82	-52.10	0.60	0.01	0.45	0.18
0.78	-37.80	0.52	0.01	0.81	0.18
0.71	-37.58	0.79	0.01	0.77	0.18
0.89	-36.37	0.35	0.01	0.80	0.18
0.80	-39.26	0.68	0.01	0.84	0.18
0.80	-44.75	0.48	0.01	0.63	0.18
0.86	-39.72	0.60	0.01	1.01	0.18
0.79	-35.92	0.81	0.01	0.92	0.18
1.00	-47.19	0.56	0.01	1.04	0.18
0.98	-41.21	0.85	0.01	0.93	0.18
0.74	-42.45	0.63	0.01	0.77	0.18
1.08	-44.18	0.92	0.01	0.87	0.18
0.93	-43.09	0.97	0.01	0.86	0.18
0.89	-39.75	0.60	0.01	0.82	0.18
0.85	-42.30	0.72	0.01	0.78	0.18
0.81	-35.43	0.37	0.01	1.00	0.18
0.71	-38.29	0.68	0.01	0.83	0.18
0.79	-28.72	0.62	0.01	0.88	0.18
0.86	-42.01	0.79	0.01	0.89	0.18
0.83	-28.92	0.59	0.01	0.78	0.18
0.77	-34.78	0.78	0.01	0.78	0.18
0.88	-25.06	0.82	0.01	1.01	0.18
0.84	-39.86	0.66	0.01	0.88	0.18
0.86	-27.08	0.57	0.01	0.94	0.18
0.84	-41.01	0.60	0.01	0.84	0.18
0.88	-41.98	0.41	0.01	0.74	0.18
0.87	-40.12	0.52	0.01	0.93	0.18
0.92	-42.58	0.80	0.01	0.71	0.18

0.78	-34.46	0.63	0.01	0.76	0.18
0.75	-41.96	0.71	0.01	0.53	0.18
0.83	-40.06	0.55	0.01	0.81	0.18
0.87	-27.17	1.04	0.01	0.73	0.18
0.87	-28.90	0.68	0.01	0.77	0.18
0.88	-27.41	0.56	0.01	0.80	0.18
0.95	-34.66	0.73	0.01	1.03	0.18
0.68	-34.67	0.72	0.01	1.04	0.18
0.89	-29.60	0.88	0.01	1.02	0.18
1.01	-36.14	0.71	0.01	0.89	0.18
0.99	-43.17	0.68	0.01	0.90	0.18
0.85	-28.75	0.51	0.01	0.76	0.18
0.84	-41.22	0.77	0.01	0.71	0.18
0.81	-34.31	0.63	0.01	0.75	0.18
0.87	-29.29	0.62	0.01	0.65	0.18
0.93	-43.79	0.64	0.01	0.95	0.18
0.84	-26.80	0.59	0.01	0.72	0.18
1.74	158.88	14.09	-110.71	24.92	-152.83
14.89	30.55	5.52	-4.00	17.51	-76.75
7.03	56.40	24.32	14.72	23.80	-22.24
7.16	65.21	19.07	23.84	25.14	-18.99
5.51	81.76	2.19	39.00	5.52	5.54
1.35	63.28	0.18	9.47	4.05	-11.05
2.45	80.06	6.50	41.67	4.31	8.22
1.84	-52.23	4.42	11.86	4.77	67.39
1.57	169.37	5.44	39.14	5.77	-11.15
1.84	-59.75	5.10	9.53	7.47	-42.31
4.38	-4.00	3.54	33.75	3.03	-12.07
2.04	-36.65	5.14	-19.96	3.44	76.11
1.89	83.59	3.99	11.81	2.89	3.42
4.40	129.24	1.24	61.72	1.59	40.55
3.91	94.54	3.77	27.98	7.43	10.49
0.17	0.08	3.24	-5.51	5.62	-3.47
1.52	46.19	3.73	6.33	4.45	-16.78
2.61	-4.11	2.76	-55.09	1.63	-40.62
1.27	-6.12	0.21	-0.03	3.07	-31.46
1.57	-5.56	1.83	-29.74	1.76	-10.12
2.33	79.46	2.31	44.53	5.73	66.16
2.32	72.02	3.79	19.06	3.26	10.08
1.94	102.96	2.59	-35.29	2.39	-61.07
0.66	0.09	3.80	-29.14	4.21	-23.75
1.79	118.50	3.09	7.85	2.14	115.91
3.05	142.36	1.17	64.63	3.24	-9.01
1.84	180.33	0.84	29.61	1.57	40.10
0.63	-140.00	2.62	10.71	0.89	30.21
0.57	-0.04	2.21	36.84	1.69	-1.62
1.08	8.33	2.91	-0.93	5.47	6.12
0.72	-0.05	2.10	-14.16	3.73	17.97
2.01	-81.65	2.14	-9.06	3.15	-41.77
3.22	-118.56	1.14	69.43	1.60	85.97
3.72	-156.17	1.81	1.17	0.99	89.06
2.18	-111.02	0.63	0.01	0.81	51.78
2.23	-146.62	1.55	-27.65	2.71	-22.18
2.32	-109.20	3.19	-15.74	2.99	25.03
1.55	-157.16	4.13	21.26	3.41	20.49
2.10	-106.96	1.57	6.30	2.92	57.58

2.79	-135.40	0.79	-64.72	0.97	26.53
2.07	-123.12	0.85	-5.12	1.04	49.23
1.01	-172.67	1.84	-25.20	1.79	53.14
1.84	-155.74	2.49	27.37	3.17	29.17
0.72	-0.05	3.70	5.40	3.49	-14.45
2.51	-101.67	1.62	-33.88	4.05	25.05
0.64	-123.22	2.00	-6.08	1.08	100.79
1.53	-56.07	2.35	12.57	2.48	92.14
0.34	-0.05	3.22	29.65	3.01	13.77
1.05	-0.05	2.32	-6.85	3.09	-3.59
2.60	-102.61	0.91	-19.17	0.95	-171.38
2.55	-123.10	-0.01	0.01	0.69	-8.89
2.38	-138.67	2.07	-6.89	1.53	26.66
1.08	-61.30	3.01	4.07	3.43	-15.04
1.02	0.09	3.16	10.04	3.30	24.93
2.63	163.28	1.19	38.67	1.68	29.80
0.95	-147.58	1.45	44.09	1.94	89.33
2.41	-106.88	1.23	-80.57	1.04	-0.01
1.20	-104.47	0.59	-13.89	1.46	-6.73
1.16	-104.88	2.60	-5.31	2.87	-10.95
0.78	0.09	2.81	0.16	3.10	5.93
0.42	-0.05	2.97	36.89	2.89	38.53
1.65	169.52	1.37	70.44	0.16	-0.01
0.90	169.34	2.06	89.47	0.91	18.20
0.76	102.95	0.50	-0.03	1.88	-19.57
1.22	179.24	1.05	52.33	4.18	-16.39
0.16	0.08	1.57	33.53	2.22	4.92
1.20	-0.05	1.50	79.60	1.72	81.35
0.11	-0.04	0.79	-0.03	1.01	46.48
0.54	-0.05	2.11	86.66	0.00	0.00

- Wave height

Submarine Explosion with Chamber
Intensity : 9 tubes

Time (second)	Height 203 (cm)	Height 206 (cm)	Height 207 (cm)	Height 208 (cm)	Height 209 (cm)	Height 210 (cm)	Height 211 (cm)
0.00	0.00	0.00	0.00	0.00	0.00	0.00	0.00
1.56	-0.03	-0.10	0.05	-0.07	0.04	0.15	-0.09
3.13	0.33	-0.05	0.04	-0.10	0.00	-0.11	0.22
4.61	0.28	0.03	0.32	-0.25	0.19	-0.11	-0.04
6.18	0.21	0.10	0.30	-0.20	0.24	-0.64	0.03
7.79	0.13	0.13	0.42	-0.12	-0.04	-0.42	-0.48
9.49	0.11	0.19	0.38	-0.32	0.29	-0.78	-0.22
11.04	0.08	0.26	0.17	0.00	0.30	-0.59	-0.38
12.64	0.13	0.25	0.42	-0.05	0.31	-0.52	-0.36
14.25	0.16	0.29	0.39	-0.06	0.00	-0.07	-0.29
15.91	0.15	0.26	0.34	-0.01	0.10	-0.22	-0.16
17.48	0.08	0.19	0.38	0.06	0.14	-0.12	-0.05
18.94	0.04	0.11	0.17	-0.03	0.23	0.34	-0.34
20.53	-0.07	0.02	0.41	0.01	-0.01	0.11	-0.05
21.99	-0.12	-0.06	0.32	0.01	-0.21	0.10	0.08
23.53	-0.26	-0.20	0.10	-0.10	-0.25	0.16	0.41
25.02	-0.27	-0.22	0.08	-0.31	-0.46	0.30	0.35
26.48	-0.32	-0.31	-0.06	-0.13	-0.30	0.20	0.17
27.91	-0.40	-0.29	-0.08	-0.10	-0.17	1.00	0.07
29.45	-0.42	-0.40	0.12	-0.15	-0.36	0.07	0.22
31.12	-0.44	-0.10	0.02	-0.07	-0.29	-0.34	-0.12
32.56	-0.47	-0.04	0.19	-0.09	-0.27	-0.50	-0.31
34.05	-0.49	0.09	0.23	-0.07	-0.10	-0.69	-0.95
35.63	-0.48	0.15	0.49	-0.17	-0.03	-1.05	-0.36
37.07	-0.48	0.29	0.49	-0.31	0.07	-0.76	-0.70
38.66	-0.49	0.33	0.37	-0.43	0.00	-1.27	-0.79
40.13	-0.42	0.17	0.33	-0.40	-0.16	-0.86	-0.71
41.56	-0.41	0.09	0.17	-0.55	-0.12	-0.63	-0.52
43.04	-0.41	0.06	0.23	-0.43	-0.23	-0.07	-0.53
44.63	-0.43	-0.06	0.13	-0.37	-0.34	-0.08	-0.12
46.10	-0.45	-0.08	0.28	-0.33	-0.22	0.16	0.15
47.65	-0.47	0.05	0.15	-0.07	-0.07	0.23	0.41
49.37	-0.49	0.11	0.28	0.17	0.16	0.15	0.13
51.00	-0.54	0.15	0.47	0.15	0.24	0.14	0.39
52.48	-0.58	0.14	0.34	0.10	0.24	0.26	0.14
53.91	-0.63	0.20	0.32	-0.03	0.08	0.15	0.13
55.35	-0.67	0.22	0.49	0.03	0.06	0.01	0.14
56.79	-0.72	0.13	0.49	-0.03	0.24	-0.47	0.10
58.22	-0.77	0.00	0.20	-0.02	0.21	0.00	0.15
59.66	-0.85	-0.01	-5.60	0.11	-8.94	0.00	0.10
61.13	-0.92	6.66	-6.29	0.20	0.81	0.07	0.24
62.73	-0.95	10.01	-1.97	0.39	10.71	-0.40	0.40
64.33	-0.97	-6.04	-0.66	-1.84	9.98	0.06	0.21
65.76	-0.99	-0.38	2.23	0.06	13.42	-0.35	0.43
67.32	-1.02	8.25	4.57	-0.69	10.98	-0.26	0.12
68.99	-1.04	6.79	1.75	2.18	11.50	-0.31	-0.57
70.55	-0.99	3.05	3.23	-0.36	0.77	-0.72	-2.21
72.27	-0.80	2.11	1.83	0.94	0.48	0.54	0.50

73.90	-0.73	1.87	2.12	-0.02	0.77	1.45	-0.35
75.40	-0.66	0.73	1.20	-0.20	-0.42	-0.06	-0.99
77.14	-0.83	3.95	2.30	-1.06	0.00	0.99	0.35
78.72	-0.62	1.93	2.19	0.62	1.23	0.59	2.04
80.48	-0.34	1.46	1.11	0.54	0.25	-0.88	-0.41
81.99	-0.90	1.05	0.69	-0.18	-0.20	0.11	0.29
83.53	-1.03	1.94	0.81	0.77	0.14	0.75	-0.97
84.99	-1.05	2.22	0.94	-0.26	0.48	2.12	1.31
86.67	-0.99	1.90	0.80	-1.43	-1.55	0.60	1.18
88.32	-2.22	1.51	0.54	-0.31	-0.20	0.36	-0.11
89.81	-0.93	1.31	0.95	0.09	0.39	0.22	-1.86
91.33	-1.11	1.63	0.92	1.37	-0.04	-1.38	0.44
92.88	-1.41	1.97	1.13	1.80	0.29	-0.82	-0.10
94.49	-1.48	2.12	1.24	0.79	1.19	-1.77	-0.82
96.10	-0.99	2.43	1.41	-0.57	0.96	-0.41	0.30
97.56	-1.33	3.29	1.01	1.24	-0.55	-0.14	-0.08
99.09	-1.31	2.46	1.47	0.66	0.92	-0.73	0.35
100.80	-1.02	1.98	1.54	1.21	0.48	-0.26	-0.28
102.40	-1.16	2.22	1.27	0.33	0.70	-0.01	0.07
104.20	-1.27	2.97	0.83	0.03	0.70	0.23	-0.15
105.80	-1.02	2.30	0.86	0.48	0.73	-0.40	0.70
107.40	-1.32	2.58	0.96	-0.24	-0.08	0.78	-0.11
109.00	-1.17	1.74	0.67	0.15	0.47	0.24	-0.07
110.60	-1.20	1.64	0.72	0.49	1.02	0.25	0.08
112.20	-1.19	2.17	1.17	-0.16	1.04	-0.14	0.47
113.90	-1.31	2.52	0.90	-0.54	0.22	-0.02	0.58
115.40	-1.47	1.58	0.92	-0.39	0.65	0.28	0.32
116.90	-1.35	2.97	1.06	0.29	0.57	-0.10	-0.30
118.50	-1.52	2.20	1.06	0.53	0.76	-0.41	0.00
120.00	-1.72	2.28	0.89	0.44	0.78	-0.28	-0.20
121.50	-1.91	2.10	1.04	-0.29	0.99	-1.15	-1.06
123.00	-1.95	1.50	0.24	0.22	-0.29	-0.25	-0.31
124.40	-2.15	1.35	0.68	-0.30	-0.01	-0.43	-0.25
125.90	-2.05	1.97	0.34	-0.44	-0.25	-0.06	0.82
127.40	-1.97	1.66	0.42	-0.47	0.74	0.28	0.25
128.90	-1.66	1.99	1.08	-0.15	0.58	-0.33	0.80
130.50	-1.79	1.98	1.33	0.30	1.26	-0.69	0.03
132.20	-1.68	1.91	1.16	0.48	0.48	-1.18	-0.21
133.80	-1.75	2.02	1.18	0.65	0.91	-0.48	-0.22
135.20	-1.54	2.10	0.68	-0.05	1.26	-0.73	-0.44
136.80	-1.20	1.72	1.00	-0.54	1.12	-0.21	-0.22
138.30	-1.35	2.68	0.96	-0.44	0.85	-0.08	-0.06
139.90	-1.34	1.85	0.97	0.09	0.50	-0.21	0.51
141.30	-1.57	1.60	0.46	0.38	0.44	-0.18	0.21
142.90	-1.49	1.60	0.56	0.37	1.39	0.13	-0.18
144.50	-1.60	1.79	0.92	0.04	1.42	0.28	0.42
146.00	-1.82	2.05	1.07	0.40	1.08	0.45	0.54
147.50	-1.89	1.88	0.94	0.40	0.42	0.28	0.15
149.00	-2.04	1.69	0.44	0.26	0.56	-0.16	0.19
150.50	-2.12	1.95	0.23	-0.24	0.48	-0.17	-0.09
151.90	-2.08	1.80	0.04	0.11	0.09	-0.18	-0.14
153.50	-2.04	2.03	0.54	-0.05	0.19	-0.38	-0.09
155.10	-2.17	1.88	0.85	0.06	0.85	-0.46	-1.28

- Current velocity

Velocity 1 (cm/sec)	Direction 1 (deg)	Velocity 2 (cm/sec)	Direction 2 (deg)	Velocity 3 (cm/sec)	Direction 3 (deg)
1.50	-10.67	1.62	-8.39	1.35	43.33
1.26	-0.04	1.18	-3.76	1.90	39.68
1.73	0.80	1.30	5.98	1.76	39.54
1.47	-36.88	1.74	2.36	1.81	45.99
0.90	-4.65	1.68	3.18	2.39	42.74
0.91	-0.04	1.56	6.41	1.37	37.00
1.09	1.61	1.39	0.05	1.73	61.39
1.23	-7.01	1.84	2.47	1.73	48.73
0.74	2.74	1.74	12.63	2.19	53.96
1.20	3.74	1.55	4.69	1.96	42.72
1.05	4.29	1.57	6.18	2.01	53.58
0.97	-2.72	1.82	11.90	1.87	47.66
1.22	-6.41	1.47	2.93	1.81	40.42
1.26	-3.52	1.60	4.28	1.84	47.85
1.26	-4.08	1.77	9.43	1.58	41.21
1.07	-13.09	1.91	4.51	1.82	28.58
1.12	-23.83	1.77	6.33	1.58	36.90
1.30	-21.45	1.57	13.35	1.50	43.76
1.15	-24.90	1.85	-8.44	1.52	28.96
1.05	-37.37	1.45	0.35	1.69	45.86
1.05	-24.74	1.37	-5.49	1.59	30.24
1.02	-28.46	1.19	-2.78	1.30	44.49
0.82	-27.22	1.25	-2.61	1.68	35.77
0.65	-21.41	1.27	-7.99	1.27	43.21
0.67	-13.79	1.35	-9.49	1.99	54.78
0.58	-14.63	1.25	-22.42	1.66	69.03
0.72	3.57	1.16	7.71	1.69	54.85
0.82	5.95	1.52	24.21	1.59	49.36
1.06	-6.53	1.75	11.86	1.64	51.14
0.95	-3.91	1.45	12.93	1.80	49.62
1.20	-0.04	1.44	-0.78	1.62	43.60
0.98	-0.04	1.61	0.97	1.67	40.66
1.26	-0.04	1.47	5.59	1.70	30.15
0.93	-0.04	1.58	15.23	1.48	29.89
1.13	-0.04	1.68	-20.97	1.52	19.33
0.94	-0.04	1.96	-14.28	1.47	23.78
1.03	-0.04	1.68	-7.78	1.41	23.13
0.81	-0.04	1.49	-10.09	1.51	30.29
0.94	-0.04	1.59	-10.46	1.64	22.11
1.09	-12.25	1.72	-4.53	1.64	17.98
1.14	0.03	5.60	8.88	7.46	-10.09
0.36	0.07	1.68	16.40	1.57	38.53
0.76	-0.71	2.50	30.06	3.50	-15.62
0.81	0.07	1.69	-14.50	1.94	8.77
0.76	0.07	2.33	5.42	1.74	52.18
0.68	0.07	1.52	8.49	1.58	25.48
0.97	0.07	2.24	1.99	1.55	15.67
0.69	0.07	2.45	-0.27	1.64	25.67
0.57	0.07	1.67	25.53	1.49	4.65
0.96	0.07	1.91	1.87	2.36	38.60
1.10	28.48	1.69	3.18	2.48	54.32

0.82	5.54	2.09	9.24	1.49	48.58
1.18	16.84	1.83	7.40	2.43	38.89
1.00	-2.43	2.10	-10.63	2.61	14.19
1.35	15.00	1.40	-7.88	2.30	1.00
1.41	-22.66	1.80	-7.63	2.14	37.19
1.65	-4.38	1.63	-2.62	1.98	37.69
1.60	-4.30	1.60	-4.32	2.39	18.69
1.28	-16.29	1.81	-6.87	2.18	23.25
0.88	-8.74	1.36	-14.49	2.28	36.76
1.34	-5.40	1.53	-16.93	1.56	23.89
1.17	-8.47	1.85	-28.29	1.55	10.27
0.91	-20.30	1.35	-3.56	1.82	52.27
1.02	6.53	1.90	-20.86	1.93	14.38
0.83	0.61	1.15	-7.24	2.01	54.21
0.33	14.23	1.43	-5.90	1.76	40.29
0.67	-0.04	1.43	-2.46	1.79	48.01
0.73	-0.04	1.43	0.61	2.05	43.39
0.59	-0.04	1.55	-8.68	2.16	50.16
0.85	-0.04	1.86	-2.93	1.55	7.37
0.80	-0.04	1.42	-5.33	1.77	16.66
0.92	-0.04	1.77	-2.86	2.15	7.56
1.34	-0.04	1.31	9.77	2.20	4.58
1.29	-0.04	1.89	11.65	1.78	14.67
1.17	-4.83	1.74	-17.13	2.01	10.45
1.50	5.30	1.58	-14.54	1.60	15.44
1.17	-5.70	1.14	-10.44	1.33	7.01
1.52	-13.94	1.17	-11.56	1.56	10.14
1.07	-16.88	1.45	-14.15	1.91	10.19
0.87	-16.44	1.44	-15.15	1.62	10.35
1.14	-5.95	1.47	-2.72	1.44	19.03
0.97	-8.87	1.56	-14.94	1.47	4.15
0.76	7.42	1.46	-13.15	1.53	38.08
0.76	2.69	1.36	-5.67	1.17	26.97
0.75	-1.11	1.32	-8.04	1.41	40.14
0.92	5.25	1.10	-0.99	1.28	44.83
0.73	4.74	1.01	-3.37	1.27	19.56
0.98	4.10	1.25	-5.75	1.25	44.83
1.11	-6.85	1.19	-9.07	1.62	37.83
1.19	4.10	1.20	-8.19	1.41	38.29
1.33	-5.03	1.59	-2.79	1.82	43.84
1.26	-7.97	1.50	-4.69	1.32	28.53
1.37	-4.36	1.32	-22.79	1.52	27.20
1.39	-6.78	1.31	-5.39	1.26	4.84
1.34	0.10	1.11	-16.50	1.61	27.91
1.59	-4.93	1.18	-28.42	1.41	5.34
1.25	-7.39	1.13	-10.81	2.45	5.05
1.24	-3.70	1.29	-17.11	1.91	-0.41
1.28	7.42	1.37	-1.16	1.83	11.49
0.97	2.10	0.96	16.24	1.39	24.10
0.70	-0.04	0.86	9.00	0.00	0.00

Velocity 4 (cm/sec)	Direction 4 (deg)	Velocity 5 (cm/sec)	Direction 5 (deg)
1.80	4.71	3.48	-120.05
1.49	3.06	2.89	-112.97

1.78	4.88	2.29	-124.75
1.71	18.22	2.77	-121.31
1.72	23.63	3.32	-127.68
1.82	31.94	3.47	-132.35
1.54	25.42	3.21	-126.93
1.77	22.29	1.77	-121.87
2.26	30.88	2.55	-124.72
1.72	43.14	2.75	-137.84
1.91	27.93	2.34	-133.69
1.96	21.72	2.53	-122.70
1.86	34.98	2.35	-128.64
1.72	27.90	2.86	-120.79
1.99	11.85	2.88	-118.26
1.57	7.61	2.02	-126.21
2.05	6.23	2.95	-126.73
1.65	3.64	3.00	-120.24
1.76	1.63	3.00	-117.60
1.54	-3.78	3.23	-123.66
1.97	-15.38	3.20	-127.82
1.40	6.10	3.41	-127.47
1.74	11.87	3.01	-130.29
1.41	21.48	3.13	-128.42
1.29	25.99	2.65	-126.00
1.36	27.58	3.15	-125.95
1.61	20.72	2.69	-108.32
1.73	41.89	2.93	-128.83
1.87	42.19	2.79	-131.03
1.72	39.31	3.58	-131.00
1.85	18.08	2.91	-131.93
1.46	30.67	2.88	-121.75
1.83	2.09	2.79	-121.65
2.39	4.12	3.11	-118.17
1.99	6.64	3.15	-119.92
2.20	-8.52	2.89	-120.90
2.18	-6.68	3.04	-117.30
1.98	10.69	3.08	-122.95
1.60	22.98	0.93	-138.09
7.70	-32.00	9.50	-109.82
5.11	121.17	15.71	-101.42
6.25	106.73	15.23	-101.77
5.63	-32.07	15.54	147.56
4.80	-35.55	12.10	-44.29
3.43	19.43	9.86	-80.05
3.44	38.03	3.88	-4.10
0.96	64.39	3.92	-72.67
1.59	15.86	3.95	-41.69
1.16	12.50	2.32	-36.20
1.65	76.64	2.37	-92.37
1.85	47.81	2.90	-94.28
2.10	28.15	3.38	-100.57
2.85	45.36	1.89	-100.67
3.12	-8.31	3.69	-64.78
1.52	-6.32	3.13	-98.47
1.73	27.29	2.93	-122.36
3.49	10.13	3.01	-94.34
3.74	-20.85	2.76	-100.06

2.73	8.29	2.34	-114.42
2.76	-18.50	4.32	-106.57
2.26	-18.88	4.61	-98.55
1.72	-39.40	4.06	-94.85
2.01	-22.25	3.81	-117.10
2.38	-2.73	3.85	-111.57
1.61	-8.83	3.70	-112.28
1.10	-23.28	2.60	-112.51
1.62	-3.70	2.92	-118.33
2.17	-17.19	3.41	-122.00
3.05	0.63	2.87	-119.20
2.42	18.84	3.36	-117.41
3.02	-8.07	3.21	-127.27
2.67	15.57	3.80	-126.30
2.29	8.00	3.43	-114.33
2.73	-25.93	3.11	-111.62
2.47	-4.07	3.14	-123.01
2.15	-14.12	3.77	-123.65
2.31	12.14	3.39	-128.53
1.47	-16.70	3.92	-108.23
2.17	-17.42	2.90	-124.46
2.33	-9.21	3.51	-105.87
2.48	-2.74	3.85	-132.96
1.82	20.27	3.68	-113.92
2.40	-4.56	3.66	-128.32
2.32	-6.01	3.34	-122.02
1.67	12.25	3.00	-119.52
2.02	-13.49	3.89	-121.66
1.86	13.75	3.54	-118.71
1.57	-16.83	3.60	-108.15
2.46	15.30	3.14	-125.02
2.18	5.20	3.04	-129.29
1.82	14.25	3.27	-116.30
1.66	6.88	3.20	-121.71
2.14	8.06	3.61	-104.60
2.24	-22.49	3.93	-123.65
2.54	-24.77	3.40	-107.33
1.94	-3.89	3.64	-108.52
2.57	-18.60	3.46	-118.25
2.68	13.04	4.13	-118.02
2.17	3.58	4.08	-110.83
1.53	-1.59	3.54	-112.29

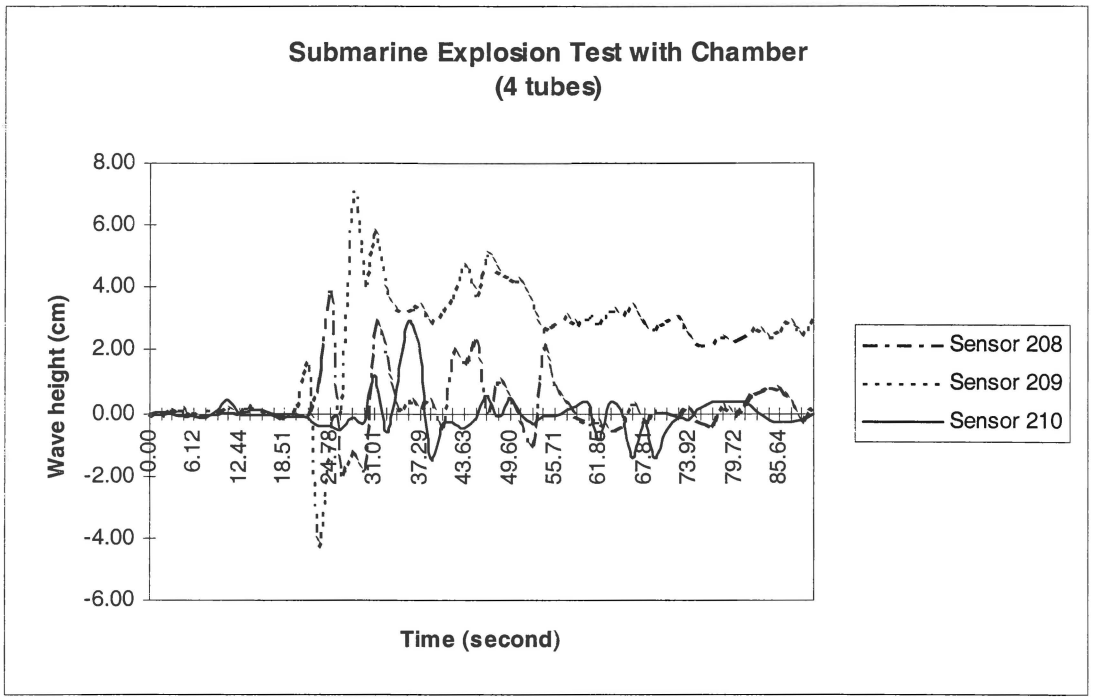
Submarine Explosion Test with Chamber
(4 tubes)
Wave height (cm)
8.00
6.00
4.00
2.00
0.00
-2.00
-4.00
-6.00
0.00
6.12
12.44
18.51
24.78
31.01
37.29
43.63
49.60
55.71
61.85
67.81
73.92
79.72
85.64
Time (second)
Sensor 208
Sensor 209
Sensor 210

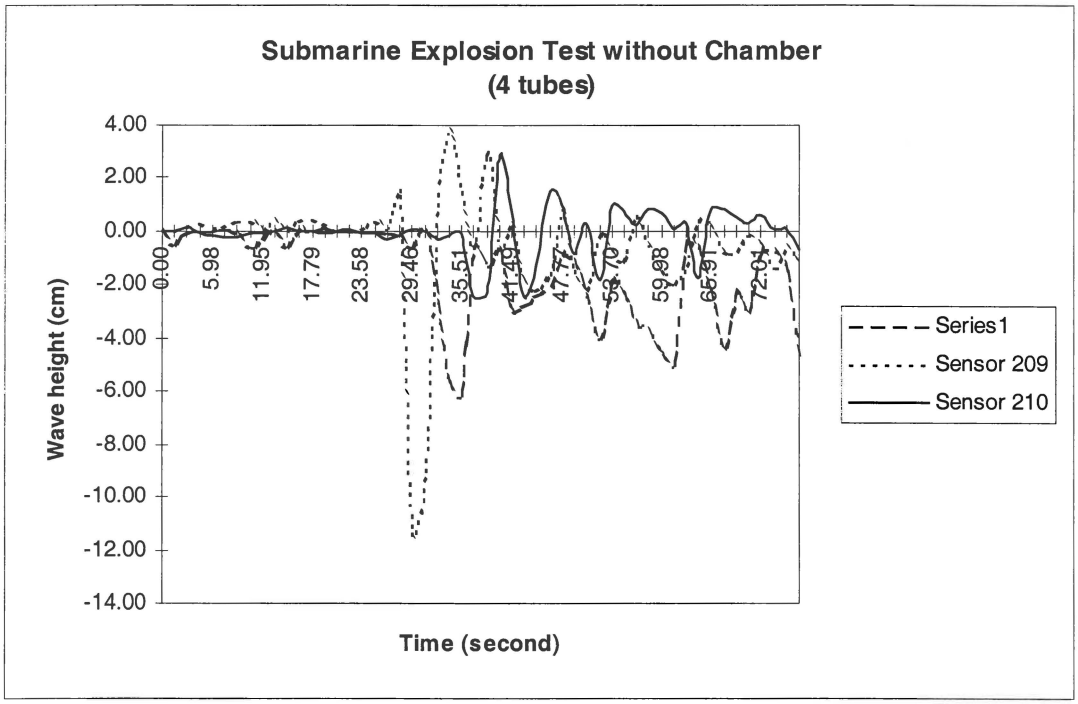
Submarine Explosion Test without Chamber
(4 tubes)
Wave height (cm)
4.00
2.00
0.00
-2.00
-4.00
-6.00
-8.00
-10.00
-12.00
-14.00
0.00
5.98
11.95
17.79
23.58
29.46
35.51
41.49
47.77
53.70
59.08
65.91
72.01
Time (second)
Series1
Sensor 209
Sensor 210

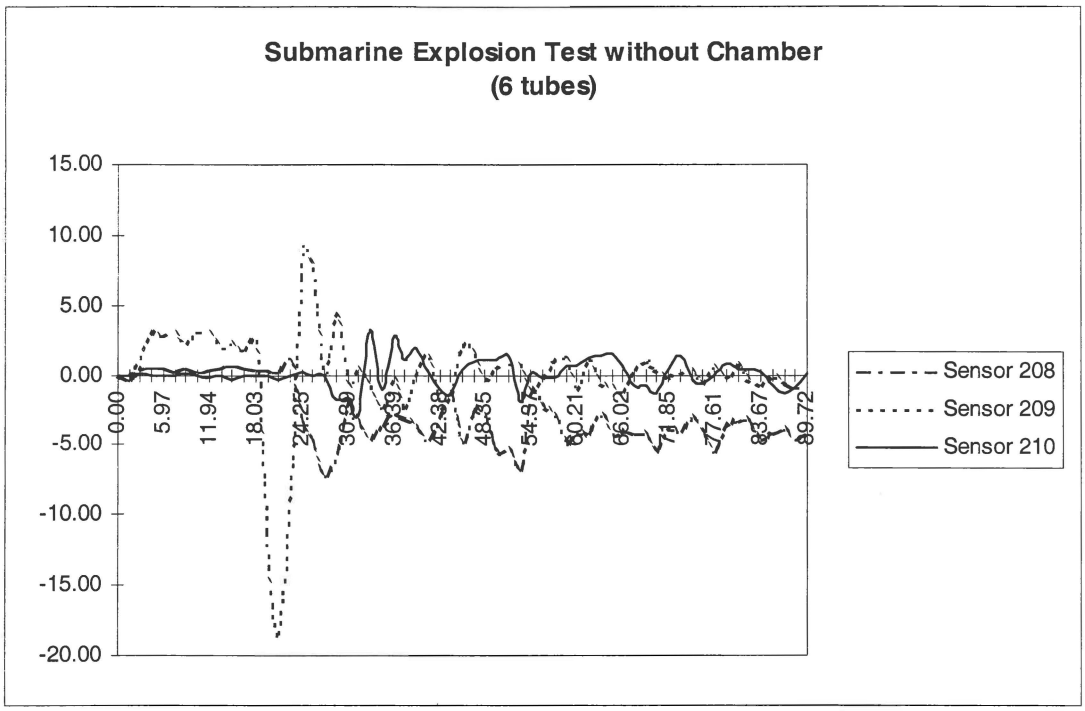
Submarine Explosion Test without Chamber
(6 tubes)
15.00
10.00
5.00
0.00
-5.00
-10.00
-15.00
-20.00
0.00
5.97
11.94
18.03
24.25
30.90
36.39
42.38
48.35
54.97
60.21
66.02
71.85
77.61
83.67
89.72
Sensor 208
Sensor 209
Sensor 210

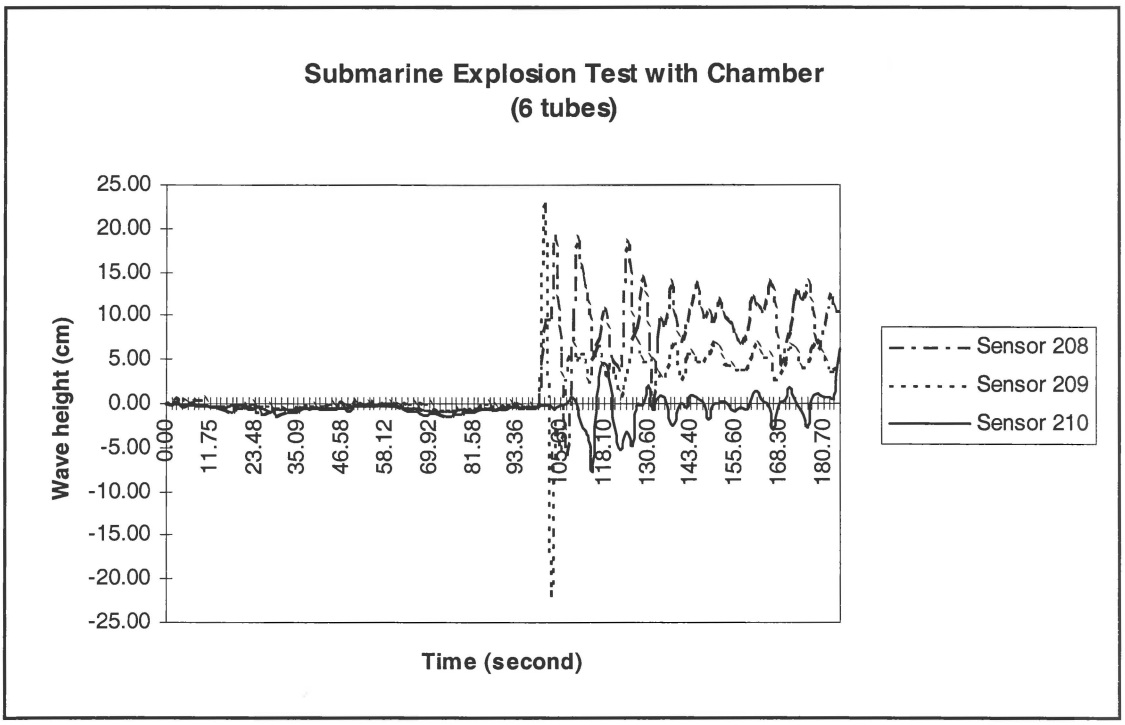
Submarine Explosion Test with Chamber
(6 tubes)
Wave height (cm)
25.00
20.00
15.00
10.00
5.00
0.00
-5.00
-10.00
-15.00
-20.00
-25.00
0.00
11.75
23.48
35.09
46.58
58.12
69.92
81.58
93.36
118.10
130.60
143.40
155.60
168.35
180.70
Time (second)
Sensor 208
Sensor 209
Sensor 210

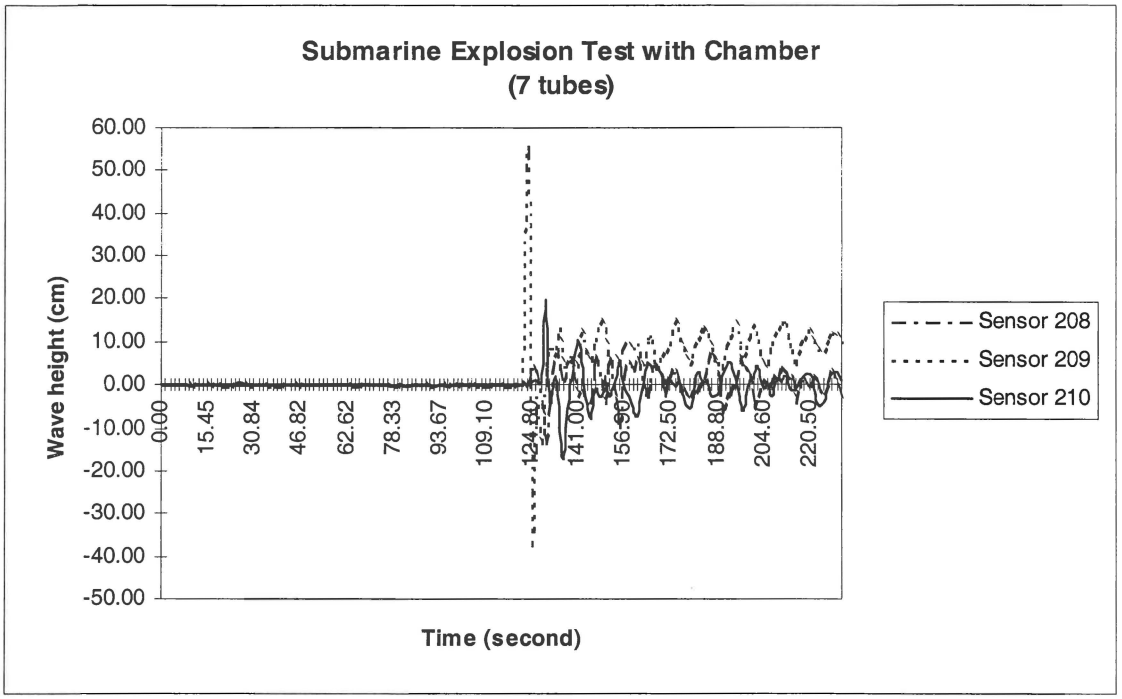
Submarine Explosion Test with Chamber
(7 tubes)
Wave height (cm)
60.00
50.00
40.00
30.00
20.00
10.00
0.00
-10.00
-20.00
-30.00
-40.00
-50.00
0.00
15.45
30.84
46.82
62.62
78.33
93.67
109.10
124.80
141.00
156.90
172.50
188.80
204.60
220.50
Time (second)
Sensor 208
Sensor 209
Sensor 210

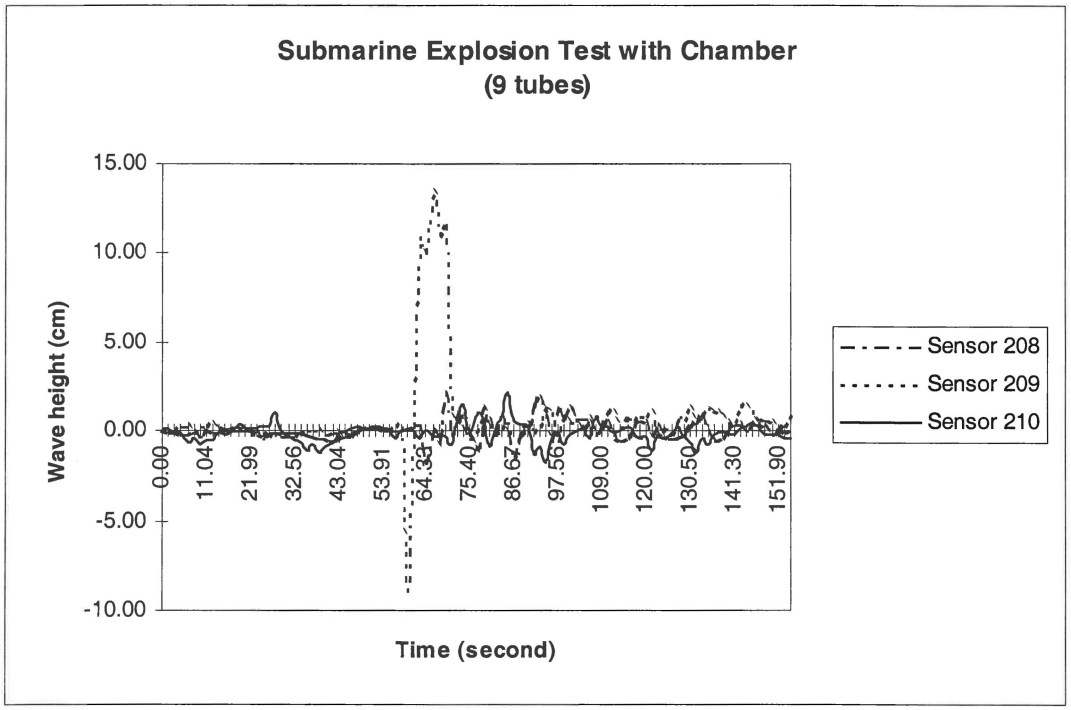
Submarine Explosion Test with Chamber
(9 tubes)
Wave height (cm)
15.00
10.00
5.00
0.00
-5.00
-10.00
0.00
11.04
21.99
32.56
43.04
53.91
64.33
75.40
86.67
97.56
109.00
120.00
130.50
141.30
151.90
Time (second)
Sensor 208
Sensor 209
Sensor 210

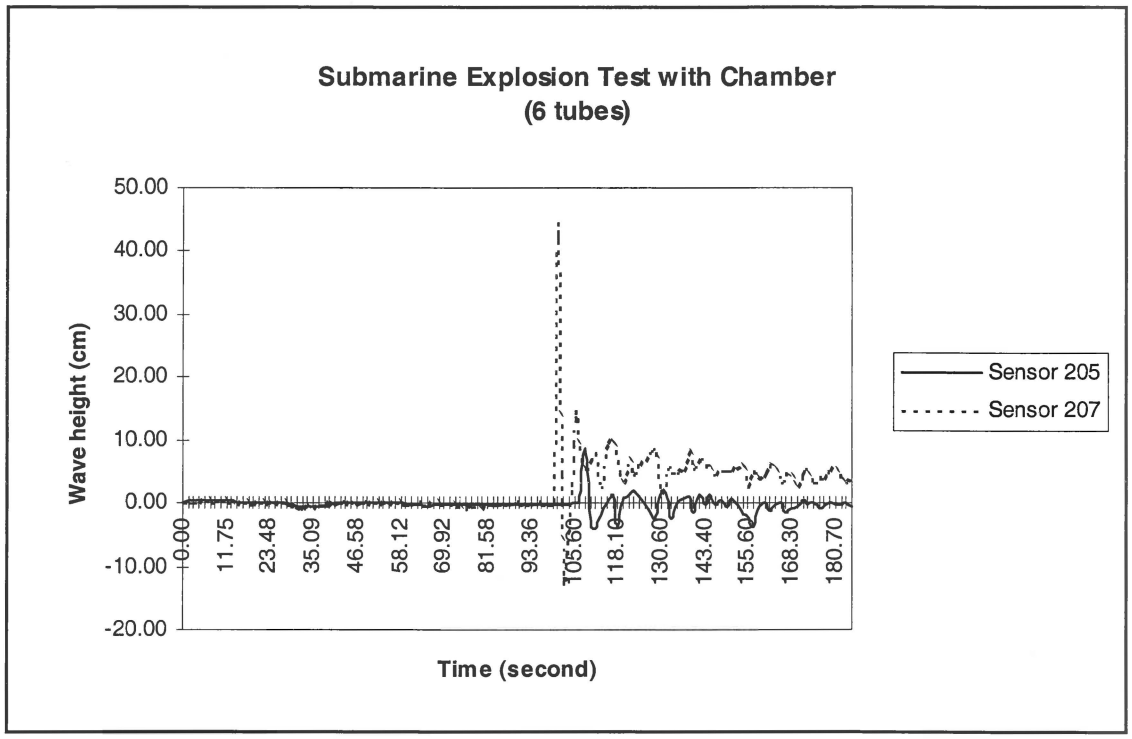
Submarine Explosion Test with Chamber
(6 tubes)
Wave height (cm)
50.00
40.00
30.00
20.00
10.00
0.00
-10.00
-20.00
0.00
11.75
23.48
35.09
46.58
58.12
69.92
81.58
93.36
105.60
118.10
130.60
143.40
155.60
168.30
180.70
Time (second)
Sensor 205
Sensor 207

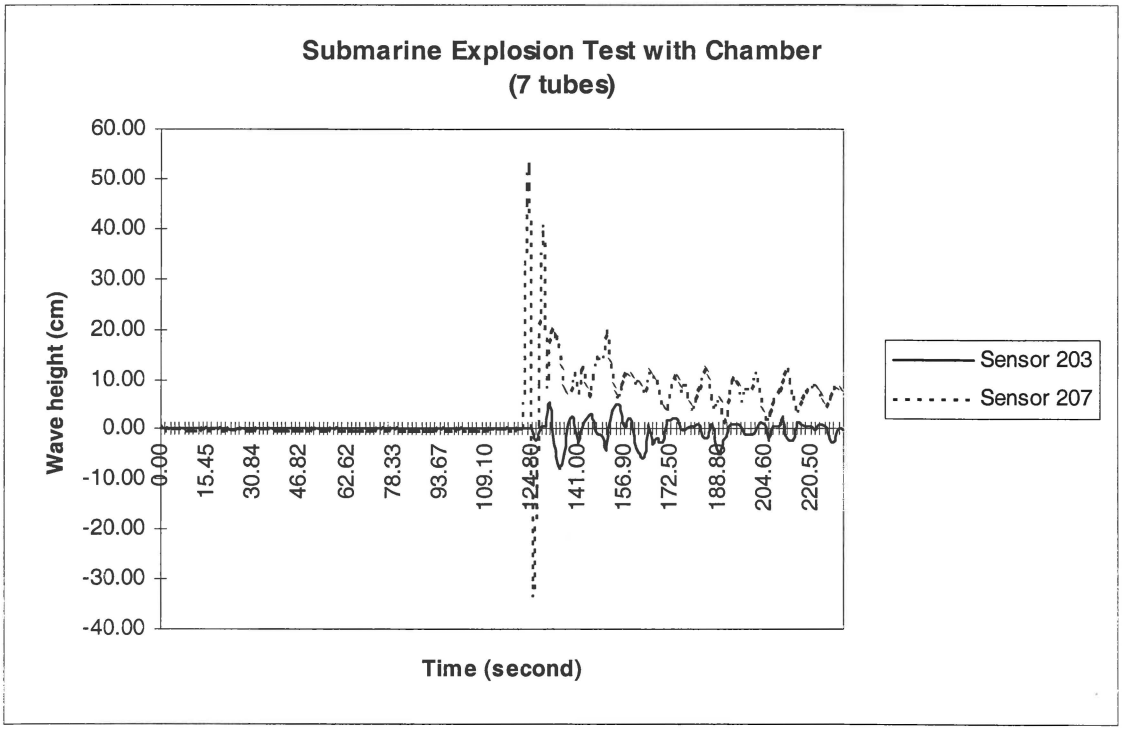
Submarine Explosion Test with Chamber
(7 tubes)
Wave height (cm)
60.00
50.00
40.00
30.00
20.00
10.00
0.00
-10.00
-20.00
-30.00
-40.00
0.00
15.45
30.84
46.82
62.62
78.33
93.67
109.10
124.80
141.00
156.90
172.50
188.80
204.60
220.50
Time (second)
Sensor 203
Sensor 207

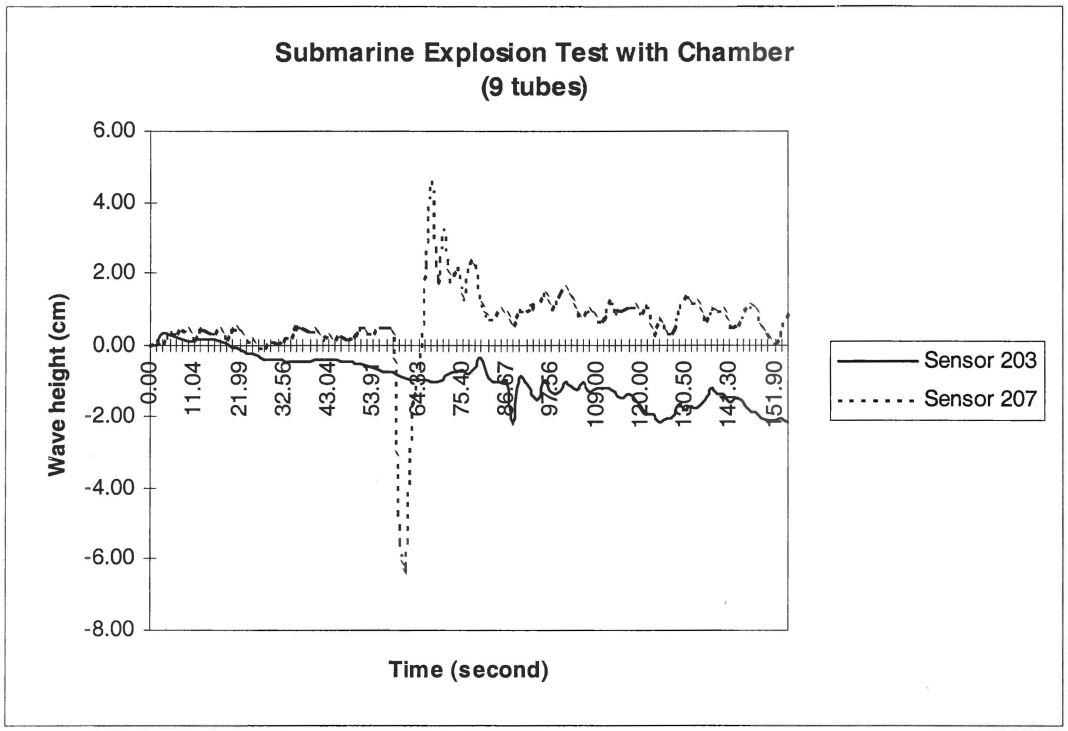
Submarine Explosion Test with Chamber
(9 tubes)
6.00
4.00
2.00
0.00
-2.00
-4.00
-6.00
-8.00
Wave height (cm)
0.00
11.04
21.99
32.56
43.04
53.91
64.93
75.40
86.67
97.56
109.00
120.00
130.50
141.30
151.90
Time (second)
Sensor 203
Sensor 207

FREE FALL OF CIRCULAR PLATE TEST

- Wave height

Free Fall of Circular Plate Test 1							
Time (second)	Height 1 (cm)	Height 2 (cm)	Height 3 (cm)	Height 4 (cm)	Height 5 (cm)	Height 6 (cm)	Height 7 (cm)
0	-0.05	0.23	0.12	0.31	0.22	0.08	-0.25
2.57	0.13	0.21	0.10	0.33	0.27	0.08	-0.26
5.02	0.14	0.22	0.10	0.31	0.28	0.07	-0.28
7.63	0.13	0.22	0.13	0.30	0.23	0.03	-0.29
10.15	0.14	0.20	0.10	0.43	0.38	-0.05	-0.30
12.8	0.19	0.25	0.13	0.32	0.23	0.09	-0.77
15.4	0.14	0.20	0.14	0.35	0.24	0.10	5.44
17.92	8.28	0.23	0.09	0.30	0.69	-0.03	2.36
20.56	-7.16	0.77	3.29	-1.83	1.49	0.74	1.50
23.07	0.05	-6.63	-6.69	4.54	-2.90	-1.84	4.62
25.52	-1.86	-1.44	1.35	9.59	0.66	0.24	-0.58
28.2	2.70	-1.48	4.69	3.65	3.57	2.03	1.90
30.79	-1.80	2.95	1.80	1.20	1.40	2.36	-1.03
33.26	-1.64	1.24	3.10	4.13	1.73	-0.15	1.71
35.89	2.65	-1.42	1.11	-2.23	1.54	2.90	-3.39
38.45	3.50	-0.51	0.94	-1.50	2.10	-1.06	3.72
41.2	2.23	1.27	1.20	6.57	1.09	0.81	1.25
43.89	2.36	1.18	-0.99	0.26	1.12	-0.66	1.07
46.76	4.45	-2.44	2.32	-2.02	2.18	-0.20	1.74
49.51	-0.62	0.00	0.70	2.62	-1.05	1.78	1.54
52.06	0.10	-0.11	0.03	1.05	3.06	1.56	2.34
54.7	1.74	-2.09	-1.95	0.46	1.97	-0.95	1.42
57.35	1.32	0.54	0.12	0.01	0.38	0.94	2.33
60.13	1.05	1.76	0.44	0.15	-0.73	1.14	1.75
62.8	0.42	1.51	0.96	1.32	2.01	1.47	1.54
65.48	1.77	1.31	-0.01	0.51	1.46	1.47	1.73
68.11	1.21	1.31	2.72	0.67	2.00	0.38	-0.54
70.92	0.73	2.85	0.71	0.81	1.00	-1.77	3.38
73.37	1.04	2.29	0.21	2.28	0.32	0.92	0.96
75.97	1.38	1.57	0.79	0.16	0.51	1.65	1.53
78.58	-0.82	0.28	1.40	-0.82	2.24	1.49	1.13
81.29	0.16	-1.73	0.49	2.34	2.35	1.14	1.19
83.94	0.99	0.47	-2.09	1.41	0.24	1.20	0.82
86.48	1.02	0.47	2.21	0.10	-0.25	0.61	1.17
89.16	0.79	1.74	0.34	0.99	-1.07	1.71	1.66
91.67	0.57	1.06	0.23	1.11	1.13	-0.58	1.00
94.38	0.63	0.62	0.17	1.52	1.82	1.31	-0.09
97.18	0.78	1.53	1.48	-0.08	0.61	1.37	1.20
99.93	0.61	1.96	1.12	1.79	0.94	-0.92	0.97
102.6	1.01	0.12	0.57	-0.38	0.74	-0.21	1.01
105.2	0.88	1.74	0.31	1.13	0.76	1.31	0.92
108.1	0.84	0.98	0.81	0.81	1.35	1.27	1.02
110.5	0.14	1.27	-0.42	0.71	1.32	0.94	1.03
113.1	0.55	0.76	-0.65	0.77	-0.71	0.83	0.93
116	0.09	-0.05	0.42	-0.01	0.68	0.53	1.35

118.5	1.07	0.33	0.27	0.66	0.39	0.78	1.10
121.3	0.85	0.50	-0.12	0.85	1.04	0.39	-0.43
124	0.72	0.57	0.26	0.66	0.41	0.74	0.97
126.5	0.73	0.86	0.31	1.02	0.94	1.24	0.83
129.4	0.93	1.20	0.77	0.76	0.66	0.37	1.67
132.1	0.70	1.12	0.75	0.89	0.70	0.12	0.37
134.8	1.12	1.05	0.32	0.99	0.78	0.33	1.08
137.4	0.94	1.49	0.85	0.92	0.72	0.33	1.39
140.1	0.55	0.69	0.75	0.70	0.56	0.66	0.72
142.8	0.33	0.61	-0.11	0.69	0.59	0.73	-0.12
145.6	0.63	-0.46	0.05	0.44	1.22	0.21	0.41
148.1	0.50	0.82	-0.09	0.68	-0.27	0.40	1.14
150.8	0.38	0.22	-0.02	-0.40	0.08	0.36	0.73
153.5	0.17	0.78	-0.18	1.01	0.92	0.35	-0.23
156.3	0.47	-0.27	-0.01	0.76	1.00	0.51	0.41
159	0.51	0.92	0.10	0.88	1.03	0.30	0.65
161.6	0.46	0.80	0.77	0.73	-0.67	-0.02	0.67
164.3	0.73	0.94	0.55	0.66	0.46	0.06	0.13
166.9	0.82	0.88	0.82	0.55	0.66	0.40	0.78
169.7	0.27	1.01	0.74	0.80	0.87	0.52	0.77
172.5	0.61	0.46	0.24	0.67	0.62	0.48	0.57
174.9	0.52	0.54	0.58	0.34	0.67	0.20	0.64
177.4	-0.18	0.17	0.29	0.45	0.34	0.44	0.96
179.9	0.25	0.16	-0.16	0.28	-0.20	0.18	0.93
182.4	0.68	0.21	-0.46	0.64	0.21	-0.09	0.73
185.2	0.44	-0.06	0.19	0.35	0.49	0.62	0.58

Height 8 (cm)	Height 9 (cm)	Height 10 (cm)	Height 11 (cm)	Height 12 (cm)	Height 13 (cm)	Height 14 (cm)	Height 15 (cm)
0.38	0.17	-0.05	0.29	0.16	0.10	0.34	0.23
0.09	0.16	0.11	0.30	0.14	0.08	0.29	0.23
0.57	0.19	-0.12	0.31	0.28	0.11	0.35	0.26
0.22	0.15	-0.02	0.29	0.19	0.11	0.32	0.26
0.43	0.21	0.04	0.29	0.16	0.09	0.32	0.19
-27.25	13.93	-38.22	0.27	-0.02	0.13	0.34	0.29
2.42	-0.06	2.91	-0.13	0.63	-4.53	0.40	0.26
7.05	-0.76	3.27	13.19	4.05	-1.63	-2.64	7.44
4.41	1.46	1.60	3.70	-0.86	-0.96	1.60	0.99
3.41	3.85	0.77	-6.71	-4.36	-0.65	2.39	2.62
3.15	2.38	1.00	-5.56	0.47	1.15	2.23	2.55
3.25	2.86	1.01	6.38	0.14	-2.50	-0.81	-2.84
1.57	-1.99	2.11	6.69	4.60	-3.09	0.03	0.71
1.71	-1.24	-1.74	-2.32	0.98	1.48	1.13	3.26
3.50	3.71	2.42	0.47	-2.62	1.05	2.95	-3.21
6.24	1.94	6.77	3.21	4.05	-0.11	1.03	1.21
0.86	0.99	2.76	2.05	2.34	0.70	2.20	1.68
1.08	-3.69	-0.61	1.62	1.04	0.88	1.74	-1.05
1.97	7.44	1.99	-2.27	2.85	0.61	0.78	2.21
3.24	1.45	3.56	-0.85	-1.45	-0.50	1.10	-0.23
1.66	-1.13	2.73	0.66	1.67	-1.02	2.90	1.14
2.15	0.77	1.80	1.90	1.08	2.31	-0.82	1.27
2.22	1.55	1.88	1.76	2.95	2.58	0.79	0.78
2.45	-0.33	2.11	0.66	2.83	1.93	0.81	0.30
3.40	3.22	3.47	2.53	-0.72	1.70	1.21	1.21

2.33	1.99	2.37	0.82	2.78	1.44	2.02	0.84
1.59	-1.02	1.00	1.41	2.49	1.96	2.01	-0.94
3.55	1.34	3.56	2.02	2.39	2.10	0.64	-0.61
3.21	3.34	2.78	1.23	2.64	1.14	1.48	1.27
1.98	3.03	2.22	0.11	-0.97	0.60	-0.08	0.34
0.83	-1.14	-0.70	1.31	1.83	0.09	1.33	1.30
2.75	-0.78	2.34	1.41	2.61	-0.03	-0.25	0.23
2.93	3.05	2.19	0.81	3.30	0.86	0.26	0.54
2.29	5.22	2.49	-2.58	1.42	1.42	0.64	0.68
2.82	-3.65	4.05	1.34	0.13	1.84	0.67	0.33
2.92	-0.81	2.42	1.64	1.20	0.47	0.88	1.12
0.06	-0.30	-0.91	1.10	1.47	1.59	0.45	0.40
2.07	0.43	3.35	1.46	-1.05	0.54	0.19	0.75
4.13	1.71	4.27	1.46	1.49	1.58	0.77	0.81
2.21	1.86	1.15	0.41	0.99	1.86	1.16	-0.53
2.05	0.91	0.54	0.67	2.45	0.74	0.04	0.85
2.42	1.73	2.83	1.53	1.38	0.49	-0.38	0.83
2.46	0.85	2.59	1.26	-0.27	0.22	1.00	0.55
1.78	-0.74	0.18	-1.25	2.05	0.28	1.07	0.72
2.45	1.87	3.51	0.73	0.57	1.16	0.52	0.51
2.52	-0.32	3.04	1.72	0.22	-0.10	0.20	0.74
2.29	0.11	0.79	-1.75	1.00	0.59	1.00	0.65
0.92	0.93	-0.26	0.69	0.57	0.12	0.62	0.50
2.77	0.68	3.32	1.47	1.86	1.51	0.38	0.55
3.00	0.28	3.16	0.44	0.20	0.32	0.61	0.47
1.24	-1.16	0.58	-0.73	1.03	1.40	1.45	-0.30
1.95	2.44	2.89	1.25	0.42	0.91	0.79	0.06
3.01	-1.23	3.63	1.50	0.90	0.33	0.83	0.64
0.48	1.71	0.13	-0.57	1.41	0.43	0.77	0.62
1.37	1.71	0.24	-0.35	0.88	0.24	0.95	0.60
2.67	1.50	2.69	1.23	2.17	0.47	0.12	0.64
2.62	0.71	3.03	1.18	1.44	0.83	0.71	0.31
1.48	0.00	1.47	-0.88	-0.44	0.46	0.64	0.42
2.34	1.89	2.03	1.19	-0.45	-0.01	0.51	0.45
2.08	0.20	2.07	1.36	1.43	0.62	0.22	0.20
1.95	-1.03	1.74	0.73	1.59	0.82	0.54	0.41
1.90	0.99	2.50	-0.07	0.35	0.65	0.68	0.27
2.19	0.69	2.53	0.92	0.68	0.77	0.86	-0.29
2.13	1.33	2.42	0.72	1.61	0.44	0.76	0.28
1.41	0.29	1.88	0.94	0.51	0.70	0.80	0.37
1.67	0.72	1.26	0.78	0.83	0.26	0.35	0.48
1.89	1.65	1.99	0.04	0.55	0.57	0.76	0.29
2.17	0.35	1.99	0.52	1.45	0.61	0.59	0.15
2.03	1.18	1.58	0.80	1.11	0.27	0.63	0.36
1.93	0.71	2.27	0.80	0.63	0.28	0.58	0.33
0.59	-0.03	-0.17	0.43	1.06	0.24	0.46	0.25

- Current velocity

Velocity 1 (cm/sec)	Direction 1 (deg)	Velocity 2 (cm/sec)	Direction 2 (deg)	Velocity 3 (cm/sec)	Direction 3 (deg)	Velocity 4 (cm/sec)	Direction 4 (deg)
0.11	43.31	0.20	-0.21	0.42	-128.06	0.44	-32.07
0.14	70.23	0.25	-0.21	0.37	-131.31	0.45	-27.05
0.09	45.38	0.17	-0.22	0.41	-128.73	0.46	-28.73

0.14	75.10	0.10	-0.21	0.37	-127.49	0.57	-28.17
0.14	86.37	0.15	-0.21	0.32	-130.59	0.46	-48.85
6.94	-161.06	2.25	27.46	1.00	29.64	5.22	19.03
4.78	148.84	4.11	101.99	2.51	43.11	7.96	6.00
1.42	124.13	0.85	102.12	1.29	82.39	3.75	18.07
0.38	142.90	0.53	178.08	1.89	120.39	2.50	16.32
1.90	69.07	0.75	141.78	2.42	109.87	3.46	9.18
1.49	59.51	1.49	173.71	2.14	-125.60	2.50	15.39
1.55	135.90	0.86	-24.20	0.58	-122.06	2.40	5.22
0.25	94.61	1.02	148.65	1.36	99.36	2.50	42.88
1.06	106.20	1.57	136.99	1.49	97.61	2.50	32.65
1.35	164.10	1.40	106.76	0.77	41.03	3.41	13.84
1.90	5.67	1.33	-36.93	0.62	-11.05	1.55	-18.22
1.15	2.77	0.99	57.00	0.62	96.67	2.01	21.88
1.27	30.13	1.07	98.45	1.18	95.23	2.14	24.20
1.81	77.14	1.23	121.93	0.45	25.42	1.24	-27.56
1.46	89.62	0.99	157.75	0.14	-0.04	1.06	1.37
0.84	-155.44	1.39	179.53	0.69	-155.03	0.87	-18.42
0.90	35.01	0.65	-23.44	0.21	-183.49	1.25	11.20
0.22	64.77	0.68	78.89	1.28	90.78	2.10	15.93
0.67	90.44	1.28	153.78	0.05	0.09	1.14	-17.75
0.66	9.66	0.42	136.15	0.22	-138.49	0.57	-3.19
0.49	87.34	0.36	149.14	0.80	95.81	1.16	17.22
0.45	181.39	1.57	113.63	0.87	-4.26	2.07	-11.82
1.28	24.68	0.61	65.28	0.75	57.64	1.66	20.67
0.38	16.08	0.27	-44.64	0.07	-0.05	0.82	-14.66
1.20	-38.39	0.20	24.98	0.38	-8.24	0.99	-28.72
0.25	-42.56	1.22	91.07	1.27	94.41	1.46	-0.07
0.88	-110.03	1.00	91.10	0.65	61.79	1.59	-34.95
1.13	-58.96	0.40	80.11	0.07	-0.04	0.23	-4.28
0.21	15.65	0.78	100.90	0.45	72.86	1.38	-20.06
0.27	-19.14	0.29	-161.66	0.33	-126.92	0.32	-5.51
1.26	-4.47	0.66	-137.95	0.32	-148.49	0.50	-43.06
0.58	-152.53	0.36	151.23	0.65	51.68	2.01	10.18
0.23	31.13	1.38	136.63	1.20	112.28	0.71	27.39
1.30	-37.11	0.53	-136.07	0.52	-63.01	1.15	-74.32
0.55	-57.56	0.34	-76.07	0.13	-41.89	0.71	19.25
0.65	180.93	0.61	89.90	0.58	45.54	1.46	15.49
1.30	18.26	0.20	102.13	0.35	69.72	0.17	23.47
1.34	-22.36	0.65	-120.23	0.34	147.27	0.47	-60.72
0.66	40.40	0.10	102.08	0.26	148.21	0.85	10.50
0.73	15.93	0.61	-92.43	0.38	183.47	0.92	11.68
1.69	-14.13	0.20	-178.49	0.52	165.40	0.37	-66.54
1.14	-23.34	0.14	-44.45	0.06	-0.04	0.60	-58.63
0.70	18.00	0.69	134.85	0.55	127.41	1.34	-13.58
0.76	109.91	0.35	151.15	0.39	174.28	0.36	22.80
1.41	-1.78	0.62	-139.75	0.91	-154.40	0.23	-163.87
0.76	39.82	0.45	47.09	0.04	0.08	1.30	-17.20
1.09	71.69	0.41	84.42	0.36	69.51	1.15	4.69
2.06	-7.37	1.01	-73.76	0.47	-152.35	0.18	0.01
1.91	-28.30	0.08	-0.21	0.09	-0.05	0.77	-1.35
0.64	-14.57	0.68	123.85	0.25	0.08	1.66	-7.44
1.09	-16.98	0.14	154.88	0.07	0.08	0.53	-43.06
2.00	-20.21	0.28	-0.21	0.23	-0.05	0.43	-51.12
1.58	-30.20	0.49	102.17	0.46	124.58	0.71	0.81
0.57	-58.13	0.38	-89.84	0.51	-74.20	0.85	-36.39

0.94	-27.31	0.71	157.81	0.42	161.75	0.28	14.37
0.27	-52.38	0.63	174.85	0.26	118.27	1.00	14.04
0.92	24.00	0.61	140.57	0.55	110.63	0.91	0.04
1.80	-23.74	0.20	-39.10	0.36	-62.53	0.94	-38.65
2.01	-8.37	0.10	181.13	0.25	-0.04	0.60	-1.14
1.80	-23.57	0.34	96.94	0.28	95.13	1.05	2.26
0.68	-14.65	0.39	158.41	0.10	0.09	0.87	4.79
0.86	8.80	0.22	120.21	0.06	0.08	0.74	-35.56
1.28	9.57	0.21	-0.21	0.07	-0.04	0.75	-0.95
1.20	-9.36	0.35	118.85	0.10	0.09	0.70	-26.42
1.60	-23.97	0.42	-108.25	0.26	-0.05	0.21	-40.40
0.88	11.45	0.54	141.73	0.13	-0.04	0.89	-13.31

Velocity 5 (cm/sec)	Direction 5 (deg)	Velocity 6 (cm/sec)	Direction 6 (deg)	Velocity 7 (cm/sec)	Direction 7 (deg)
0.81	13.38	0.29	6.13	2.04	-43.96
0.58	2.75	0.30	16.76	1.94	-45.09
0.70	8.65	0.33	13.19	1.89	-42.66
0.81	11.36	0.33	10.82	1.99	-42.87
0.62	5.65	19.13	136.17	4.78	-111.96
5.77	-48.39	12.14	-44.51	28.37	-56.31
9.10	-9.88	8.79	133.17	13.78	67.32
2.51	-14.58	5.08	175.69	8.54	47.88
2.28	-11.89	4.67	145.47	8.05	68.52
6.43	-34.09	2.02	42.23	1.78	-9.96
4.59	-30.16	0.85	140.87	5.88	43.48
3.37	-4.23	5.59	90.10	7.87	36.40
3.12	6.77	9.68	113.13	1.91	20.46
4.43	-4.94	8.64	72.59	2.70	47.42
4.79	-33.86	7.10	72.67	1.65	-6.75
1.79	-42.70	5.00	85.00	2.50	-41.28
2.03	15.02	8.75	88.24	2.70	37.48
2.39	4.65	8.43	71.38	2.60	42.41
2.38	-7.88	2.50	18.50	2.01	-19.36
1.17	18.80	5.87	77.69	1.34	-42.10
1.56	-24.68	5.59	71.56	2.03	-19.10
1.38	-10.58	2.51	18.50	0.89	18.78
2.30	0.72	4.59	55.73	0.94	-63.37
1.69	0.53	4.32	35.25	2.41	-38.95
1.06	-14.76	2.51	45.95	1.57	-46.26
1.38	9.27	1.84	-6.94	2.52	-66.92
1.78	7.36	3.42	8.30	2.33	-13.55
1.35	25.80	4.28	57.89	2.60	38.82
1.47	-31.43	1.22	-20.58	2.62	-60.13
1.25	64.78	2.43	88.46	1.58	-63.69
2.51	-26.86	5.01	12.07	2.13	-20.64
1.55	-9.53	3.66	23.75	0.91	-14.34
0.77	14.50	1.15	-22.46	1.70	-45.71
1.88	-4.89	1.93	8.67	1.54	-60.11
0.72	4.54	0.48	-136.24	2.30	-37.88
1.02	-30.19	2.02	10.76	1.72	-22.39
2.44	1.74	2.51	30.23	0.84	-100.53
0.89	39.89	1.27	69.85	0.77	39.57
1.15	-51.14	1.77	-69.48	2.50	-67.17
1.43	6.46	1.04	16.85	1.40	-39.07

1.81	20.23	2.51	28.38	1.55	-14.88
0.41	135.80	1.14	38.10	2.52	-67.27
0.84	47.62	1.59	77.79	1.77	-49.96
1.73	-24.84	2.51	-15.53	2.31	-31.28
1.17	38.30	1.65	77.72	1.24	-19.19
0.95	28.00	0.35	110.68	2.19	-92.41
0.86	-15.24	0.69	-23.66	2.54	-33.16
1.96	10.55	1.67	9.65	0.73	-33.76
0.84	37.55	0.19	-0.19	1.95	-61.03
0.71	71.16	0.22	53.30	1.73	-43.21
1.74	4.44	2.46	19.38	1.75	-26.91
0.94	11.85	1.20	-5.24	2.16	-45.76
0.99	65.56	0.73	146.74	1.97	-59.61
1.37	-15.44	1.76	-2.34	1.88	-25.79
1.96	-7.96	1.76	21.19	1.72	-45.64
0.71	42.88	0.61	-3.66	2.14	-67.07
0.75	73.51	0.94	102.75	2.09	-51.60
1.35	-12.87	1.31	7.49	2.04	-38.31
1.15	-16.16	0.53	6.50	2.48	-63.52
0.63	72.34	0.82	38.23	2.21	-55.30
1.40	52.29	1.75	60.99	1.41	-42.30
0.91	7.59	0.83	-14.12	2.55	-49.97
1.29	-9.18	1.02	3.55	2.46	-46.22
0.80	11.00	0.96	-3.52	2.41	-40.19
1.51	43.38	1.55	61.21	1.24	-22.16
0.98	0.24	0.84	3.15	2.30	-42.83
1.36	-17.95	1.37	-1.62	2.59	-49.06
1.14	23.82	1.22	7.88	2.03	-42.65
0.62	32.77	0.87	3.16	2.26	-63.93
0.78	34.79	0.14	-96.35	2.57	-56.65
1.28	-14.28	1.87	-10.18	2.63	-41.35

- Wave velocity

Free Fall of Circular Plate Test 2.

Time (second)	Height 1 (cm)	Height 2 (cm)	Height 3 (cm)	Height 4 (cm)	Height 5 (cm)	Height 6 (cm)	Height 7 (cm)
0	0.20	0.07	-0.13	0.08	0.04	-0.01	0.02
2.38	0.17	0.07	-0.15	0.06	0.22	0.06	0.02
4.92	0.20	0.12	-0.13	0.14	0.11	-0.11	0.03
7.35	0.17	0.03	-0.13	0.07	0.09	-0.02	0.02
9.74	0.19	0.06	-0.14	0.07	0.05	-0.12	0.03
12.26	0.16	0.05	-0.14	0.04	0.09	-0.13	0.03
14.8	0.20	0.02	-0.14	0.06	0.05	-0.04	0.04
17.14	0.16	0.05	-0.14	0.03	0.01	-0.05	0.04
19.56	0.19	0.07	-0.12	0.05	0.06	-0.01	0.00
22.13	0.14	0.08	-0.14	0.10	0.08	0.00	0.02
24.64	0.25	0.05	-0.15	0.06	0.01	-0.01	0.00
27.1	0.17	0.04	-0.15	0.11	0.07	-0.03	0.01
29.61	0.17	0.08	-0.13	0.07	0.18	-0.07	0.01
32.04	0.17	0.06	-0.13	0.11	0.11	-0.24	0.01
34.51	0.19	0.09	-0.15	0.05	0.03	-0.07	0.05
36.97	0.21	0.05	-0.15	0.10	0.03	-0.14	0.03
39.37	0.28	0.09	-0.15	0.04	0.04	-0.01	0.03
41.82	0.19	0.07	-0.13	0.05	0.09	0.00	0.04
44.23	0.22	0.04	-0.12	0.03	0.10	-0.02	0.00
46.66	0.16	0.10	-0.13	0.07	0.06	-0.05	-12.31
49.23	0.15	0.10	-0.12	0.07	0.07	0.07	-12.40
51.83	1.29	0.09	-0.12	0.09	0.02	-0.07	3.46
54.45	7.24	7.18	12.48	2.02	1.40	8.80	8.50
56.96	4.68	-1.43	-7.29	-4.60	-0.26	0.20	-1.66
59.58	2.85	2.58	-3.46	9.65	1.25	0.72	6.84
62.14	5.18	-1.78	7.49	3.55	3.59	2.55	2.19
64.69	4.70	0.98	-0.16	2.78	1.07	2.49	1.52
67.43	1.19	2.37	0.97	0.14	4.89	0.46	1.26
69.99	2.45	-1.11	2.60	-2.10	2.16	3.13	4.44
72.72	2.59	2.87	0.92	1.73	4.24	0.79	-2.26
75.25	0.30	2.89	2.87	2.07	5.07	1.16	7.53
77.84	1.50	1.49	2.08	5.36	-1.03	1.32	2.51
80.46	3.23	3.57	0.22	0.32	2.04	1.30	2.22
83.15	-0.85	3.37	1.31	-0.95	4.68	3.15	1.43
85.7	-3.12	2.55	-0.46	-4.36	-0.16	3.80	5.12
88.36	1.98	0.26	-1.96	-0.90	3.34	-2.52	3.25
91.07	3.34	-0.93	0.76	2.50	-0.38	0.06	3.24
93.68	2.01	2.74	2.81	1.18	1.91	1.47	2.56
96.47	0.98	-1.14	2.21	3.09	2.48	2.16	3.46
99.07	2.73	-1.83	-0.96	-0.33	3.13	2.00	5.08
101.7	2.87	1.12	2.30	1.90	2.46	2.73	2.98
104.4	2.68	1.66	2.19	2.48	1.11	-2.62	5.42
106.9	1.64	3.42	0.89	0.33	1.97	1.10	4.48
109.5	2.29	2.24	-0.09	2.58	1.20	2.23	3.61
112.3	0.30	1.12	1.83	-1.62	5.41	2.64	2.68
114.9	1.04	0.31	-2.09	0.95	1.09	1.86	2.83
117.6	0.82	0.91	-0.22	1.82	2.18	1.93	3.52

120.2	1.38	1.10	0.43	0.49	1.53	0.47	2.69
122.9	0.31	1.16	1.46	-0.82	1.18	1.19	4.33
125.5	0.92	1.57	1.02	1.58	1.88	1.77	3.70
128.1	1.01	1.08	0.69	1.99	2.83	1.25	1.50
130.8	1.15	2.01	1.80	1.93	0.92	1.51	3.63
133.4	0.94	1.94	2.18	2.27	1.17	0.22	4.29
136.1	1.44	1.17	1.20	-0.47	-0.94	-2.05	3.67
138.7	1.12	1.24	0.90	-0.36	1.32	1.05	2.29
141.6	0.64	0.98	1.41	1.02	1.74	1.63	4.48
144.3	1.13	2.03	0.24	0.07	1.73	1.25	1.97
147.1	0.65	1.44	0.30	1.47	0.98	1.08	3.15
149.7	0.80	0.94	0.90	0.00	1.56	0.25	4.25
152.3	1.82	1.11	0.53	0.72	0.92	1.30	3.30
154.8	1.24	0.46	0.84	0.85	0.84	0.52	2.00
157.8	0.85	0.30	0.66	0.71	1.45	0.59	4.09
160.6	0.54	1.48	0.50	0.27	1.56	1.22	3.33
163.2	1.05	1.31	0.89	1.07	1.02	1.04	4.54
165.6	1.52	1.29	0.87	0.79	1.38	0.20	3.20
168.4	1.23	0.92	0.76	0.58	0.62	0.49	3.70
171.2	1.54	1.67	1.42	0.96	0.98	0.67	4.08
174	0.33	0.99	1.10	0.74	0.81	1.19	3.31
176.6	0.51	0.94	0.62	0.22	0.81	1.34	2.26
179.3	0.72	0.35	0.27	0.65	2.45	0.88	2.30
182	0.84	0.82	0.29	0.52	0.68	0.90	3.23
184.4	0.66	0.59	0.07	0.52	0.66	0.79	3.35
187.3	0.64	0.99	0.03	1.02	0.73	0.56	2.42
190	0.51	0.25	0.30	0.62	1.87	0.97	3.02
192.7	0.65	0.81	0.28	0.81	1.77	0.76	2.91
195.5	0.61	0.80	0.58	0.82	0.47	0.37	2.14
198.4	1.05	1.39	0.68	0.69	0.11	0.19	2.63
201.1	1.12	0.86	0.69	0.40	1.15	0.37	3.08
203.7	0.86	1.30	0.79	0.69	1.22	0.68	3.20
206.3	0.75	0.98	0.32	0.99	1.13	0.81	2.45
208.8	0.71	0.74	0.33	0.53	1.14	0.71	2.30
211.5	0.58	0.63	0.20	0.61	0.71	0.82	3.20
214	0.59	0.62	-0.10	0.61	0.55	0.63	2.78
216.4	0.80	0.48	-0.03	0.27	0.66	0.56	2.93
219	0.77	0.45	0.34	0.31	0.85	0.96	1.86
221.8	0.44	0.62	0.27	0.43	0.74	0.65	2.74
224.4	0.59	0.53	0.31	0.43	0.85	0.35	2.95
227.1	1.02	0.71	0.49	0.44	0.38	0.48	2.58
229.7	0.82	0.69	0.70	0.38	0.75	0.37	2.52
232.4	0.96	0.74	0.90	1.02	1.27	0.43	2.54
235.2	0.84	0.68	0.64	1.01	0.96	0.80	2.57
237.7	0.78	0.73	0.55	0.71	1.02	0.68	2.29

Height 8 (cm)	Height 9 (cm)	Height 10 (cm)	Height 11 (cm)	Height 12 (cm)	Height 13 (cm)	Height 14 (cm)	Height 15 (cm)
-0.02	0.03	-0.03	-0.09	0.18	0.08	-0.10	-0.04
0.20	0.06	-0.02	-0.11	-0.04	0.11	-0.14	-0.04
0.09	0.01	0.03	-0.11	0.00	-0.03	-0.14	-0.08
0.28	0.05	0.02	0.06	-0.03	0.15	-0.11	-0.05
0.11	0.08	0.22	-0.11	0.04	0.14	-0.14	-0.04
0.20	0.07	0.10	-0.13	0.40	0.09	-0.13	-0.05

0.19	0.05	-0.06	-0.11	-0.04	0.12	-0.14	-0.02
0.01	0.04	0.03	-0.08	-0.05	0.12	-0.06	-0.05
-0.15	0.12	0.18	0.24	0.43	0.12	-0.14	-0.07
0.13	0.04	-0.06	-0.10	-0.04	0.12	-0.14	-0.04
0.02	0.04	-0.18	0.06	-0.03	0.13	-0.14	-0.04
0.16	0.04	-0.40	-0.10	-0.05	0.11	-0.14	-0.05
-0.06	0.05	0.00	-0.58	0.43	0.17	-0.11	-0.04
0.07	0.12	-0.01	0.00	-0.02	0.14	-0.12	-0.06
-0.07	0.06	-0.27	-0.15	0.22	0.18	-0.08	-0.04
0.01	0.15	-0.12	-0.11	0.02	0.15	-0.15	-0.03
0.18	0.07	-0.04	-0.01	-0.01	0.21	-0.07	-0.06
0.14	0.08	-0.31	-0.13	0.08	0.10	-0.17	-0.05
0.16	0.07	0.08	-0.33	-0.22	0.15	-0.13	-0.06
-22.72	0.11	-46.99	-0.11	-0.04	0.16	-0.13	-0.04
6.83	10.75	-9.52	-0.01	0.03	3.35	-1.15	-0.06
8.92	-8.90	11.03	1.56	9.93	3.15	2.21	1.66
7.12	5.71	10.35	1.48	1.50	3.67	1.74	-1.40
5.97	7.44	5.86	-8.22	-4.55	3.29	3.16	-3.93
4.11	2.09	3.59	0.78	3.12	-1.91	4.69	1.70
3.81	1.68	1.72	5.57	-0.88	4.60	-3.19	1.59
0.24	10.17	7.98	5.86	3.43	1.44	-0.66	1.12
1.33	-4.29	-1.35	-2.81	1.13	4.81	2.29	1.71
3.42	7.52	4.29	-0.72	-6.83	2.18	3.92	-3.30
5.73	-1.20	9.38	1.91	3.47	-0.21	-3.12	0.10
-0.81	2.46	4.09	2.84	8.22	2.58	0.01	2.59
2.87	-7.50	3.50	2.70	2.98	-1.84	-2.44	1.05
1.05	3.49	4.83	1.95	-0.49	3.35	-0.71	2.89
3.89	1.01	5.95	-0.83	-2.35	3.14	1.77	-0.46
1.54	-1.66	4.91	1.74	1.01	1.58	1.65	1.07
3.42	4.89	7.56	2.42	5.41	3.37	1.96	1.49
1.50	1.52	4.11	2.73	-0.92	2.90	1.52	2.04
2.63	-3.00	5.10	0.36	5.63	-0.50	-0.50	1.53
3.85	2.44	7.49	1.98	-0.89	0.19	1.69	1.42
2.50	3.00	4.26	1.66	-2.58	0.54	0.42	1.23
0.87	-1.16	4.04	-2.80	2.02	1.96	0.91	-0.26
3.06	1.20	5.70	1.51	-1.32	2.62	1.11	-0.10
4.58	-1.67	7.49	-0.44	2.34	2.47	0.86	2.11
1.63	2.94	5.61	-0.23	0.70	1.74	0.33	0.52
-2.23	-0.33	4.58	1.22	-0.41	0.79	1.50	1.61
0.42	-1.46	4.40	1.93	3.85	1.56	1.20	1.55
3.27	1.50	8.29	2.37	0.67	2.14	0.55	1.07
0.11	4.61	3.76	-1.07	2.53	1.96	0.47	1.45
2.78	-1.14	7.66	1.50	0.84	1.41	1.43	0.19
2.16	-0.61	5.89	2.79	1.03	0.79	1.21	1.74
0.85	1.28	2.43	-0.10	2.89	2.12	1.06	1.48
1.76	1.61	5.22	0.26	0.80	0.43	0.51	-0.66
3.73	3.45	7.33	-0.02	2.00	1.35	0.59	1.33
2.68	0.50	6.15	1.23	1.62	2.10	1.51	0.23
0.63	-2.78	3.68	0.22	1.66	1.85	0.86	0.92
1.93	1.09	6.11	1.36	3.06	1.03	0.30	1.21
1.96	2.18	6.89	2.14	0.40	0.57	1.05	0.64
0.68	0.38	4.37	-1.03	2.34	1.23	1.01	0.80
1.72	0.60	5.89	1.40	2.31	1.43	0.35	0.81
2.26	2.50	6.87	2.48	1.57	1.11	0.79	1.04
0.59	-0.29	5.58	-0.68	2.36	1.37	0.81	0.84
-0.79	-0.15	2.37	0.58	1.47	0.51	0.88	0.79

1.47	2.95	6.63	1.79	1.89	1.71	0.32	0.77
2.26	1.38	6.72	2.54	-0.57	1.21	0.71	0.79
0.77	-0.47	4.84	-0.99	1.49	1.66	0.82	0.31
1.74	3.23	4.90	1.91	0.82	1.55	0.90	0.05
2.46	-0.61	7.31	2.03	0.17	1.68	0.05	0.84
0.68	0.86	3.38	0.19	1.79	1.03	0.69	0.84
1.28	0.86	2.53	0.55	0.39	1.16	0.90	0.41
1.80	0.45	5.63	1.62	1.72	0.84	-0.03	0.78
2.23	2.24	6.91	2.13	2.53	1.55	0.79	0.64
2.03	0.74	4.47	-0.27	1.15	1.60	0.85	0.75
1.43	2.40	5.48	0.15	1.33	0.84	0.84	0.73
1.22	0.40	5.90	1.99	2.30	0.78	0.03	0.57
0.96	-0.50	5.09	0.60	2.18	1.34	0.61	0.73
1.50	1.29	6.50	0.11	1.47	1.60	0.77	0.72
1.76	1.70	6.42	2.10	-0.05	1.64	0.61	0.32
1.12	0.51	4.79	1.06	1.87	1.31	0.80	0.37
1.49	0.78	4.61	2.13	0.73	1.65	0.64	0.72
0.98	0.59	4.76	0.99	1.53	0.74	0.78	0.89
0.95	1.89	5.77	0.48	1.12	0.81	0.81	0.71
0.94	0.78	5.45	1.03	2.11	1.60	0.70	0.72
1.03	2.42	5.65	1.18	2.17	1.30	0.69	0.75
1.12	0.29	5.59	1.25	1.55	0.97	0.64	0.74
-0.10	0.30	3.51	0.35	1.92	0.75	0.40	0.69
0.83	1.37	5.42	0.96	1.58	0.87	0.57	0.50
1.49	1.80	6.13	0.87	0.73	0.89	0.42	0.86
1.72	2.18	5.44	-0.77	-0.04	1.64	0.61	0.73
0.35	-0.25	4.65	0.57	1.17	1.64	0.67	0.14
1.22	0.14	5.73	1.21	1.36	1.39	0.64	0.78
1.37	1.56	5.85	1.63	0.51	1.13	0.40	0.83
0.12	1.72	4.71	0.13	0.93	0.85	0.56	0.75

- Current velocity

Velocity 1 (cm/sec)	Direction 1 (deg)	Velocity 2 (cm/sec)	Direction 2 (deg)	Velocity 3 (cm/sec)	Direction 3 (deg)	Velocity 4 (cm/sec)	Direction 4 (deg)
0.07	-0.04	0.24	-7.93	0.19	-0.05	0.35	-32.04
0.08	-0.05	0.36	-4.83	0.20	-0.05	0.42	-37.49
0.07	-0.05	0.34	-19.62	0.22	-0.05	0.47	-34.90
0.10	-0.05	0.37	-3.89	0.22	-0.05	0.46	-39.37
0.08	-0.04	0.36	0.66	0.23	-0.05	0.50	-35.18
0.06	-0.04	0.34	-47.79	0.23	-0.05	0.45	-42.04
0.10	-0.04	0.22	9.15	0.19	-0.05	0.43	-41.09
0.09	-0.04	0.32	-8.91	0.23	-0.05	0.39	-36.15
0.08	-0.04	0.26	-17.26	0.18	-0.05	0.44	-33.63
0.07	-0.04	0.27	-12.81	0.14	-0.05	0.42	-33.31
0.06	-0.04	0.25	-12.07	0.12	-0.05	0.52	-34.45
0.10	-0.04	0.48	-2.15	0.14	-0.05	0.38	-31.56
0.09	-0.04	0.31	-11.07	0.14	-0.05	0.50	-38.62
0.09	-0.04	0.30	-0.14	0.16	-0.05	0.50	-32.20
0.09	-0.04	0.43	15.92	0.20	-0.05	0.50	-36.50
0.11	-0.04	0.31	7.47	0.25	-0.05	0.40	-30.36
0.09	-0.05	0.37	15.77	0.22	-0.05	0.44	-41.47
0.10	-0.05	0.24	7.93	0.22	-0.05	0.48	-39.54
0.09	-0.05	0.19	7.48	0.23	-0.05	0.42	-29.87

8.04	144.66	7.75	82.30	4.29	15.80	11.26	2.85
10.02	130.94	7.59	67.33	6.16	52.11	11.64	9.69
4.08	125.13	3.48	88.21	2.02	104.97	4.60	28.61
4.23	111.56	2.35	112.84	2.00	107.31	3.73	32.39
4.26	105.79	4.33	108.01	1.07	39.36	3.83	-12.27
1.10	-28.96	1.40	134.42	2.31	78.15	2.29	27.33
2.25	55.27	0.19	37.02	1.63	74.59	4.38	-0.35
1.15	-41.33	1.14	119.42	2.51	115.38	2.50	42.77
1.20	75.66	1.90	101.86	2.48	95.08	2.50	20.26
1.11	-41.56	2.04	124.94	1.78	59.45	3.16	-15.94
2.12	-23.03	1.22	-74.78	1.12	-24.75	1.43	10.56
1.42	56.21	1.05	-15.93	0.63	170.45	1.78	28.12
1.47	64.65	0.55	114.13	1.60	90.79	2.50	17.64
1.23	119.56	1.44	15.16	1.50	43.56	2.48	-0.23
0.49	-96.40	0.68	-55.29	1.11	94.36	1.48	38.07
1.69	136.52	0.83	-134.28	0.87	127.03	2.09	51.14
0.33	-18.09	0.88	-91.52	0.27	41.85	1.15	2.32
1.46	52.92	0.23	-7.20	0.29	-6.13	1.84	28.41
1.39	151.68	0.53	63.72	1.14	76.84	1.73	14.28
0.86	57.71	0.61	-44.90	0.69	39.38	1.10	-13.70
0.51	-27.57	0.52	-79.23	0.19	-32.57	0.50	20.73
0.77	158.12	0.31	-102.21	0.57	100.67	1.26	-28.21
2.33	68.57	0.24	12.27	1.56	78.36	2.49	31.93
2.20	18.41	0.97	-66.53	0.73	-52.49	1.46	-15.71
1.51	-0.83	1.10	-67.06	0.74	147.95	0.81	47.79
1.83	17.85	0.32	-69.13	0.29	84.91	1.42	21.79
1.91	112.38	0.30	-177.37	0.45	164.12	1.65	2.66
1.34	5.50	0.90	-85.59	0.36	151.83	0.20	-25.26
1.87	82.85	0.50	10.29	1.07	111.45	1.86	40.11
0.64	-7.99	0.61	-38.23	1.04	155.70	0.61	9.36
1.99	-7.94	0.36	-100.90	1.62	-178.02	0.34	-49.08
0.37	48.40	0.36	28.98	0.16	-185.96	1.98	0.01
1.27	111.70	1.39	128.63	1.80	136.06	1.85	38.60
1.14	44.91	0.73	-76.00	1.29	181.21	0.49	-28.96
2.11	-1.52	0.25	-25.89	1.25	-123.51	1.00	-52.38
1.49	66.94	0.67	88.30	0.80	-171.53	1.80	1.18
1.25	88.61	0.56	63.20	1.42	161.31	1.49	29.45
0.60	44.74	0.19	0.00	2.07	-175.40	0.36	45.10
0.81	106.34	0.33	90.79	2.07	-179.47	1.28	-21.22
1.18	95.83	0.79	127.65	1.77	-168.15	1.20	3.00
0.20	0.12	0.14	149.59	1.96	174.28	0.46	-40.17
0.34	-45.13	0.45	-98.13	1.56	-161.85	0.78	-44.04
0.60	99.10	0.70	97.22	1.47	-170.05	1.76	10.28
1.37	121.67	0.21	110.74	1.31	172.73	0.93	-7.20
0.75	-28.02	0.49	-107.51	1.85	-165.34	0.51	-170.60
0.59	50.55	0.13	-0.02	0.72	173.27	1.47	4.91
1.43	112.72	0.67	68.67	1.01	162.00	1.93	2.75
0.96	27.04	0.43	-70.90	1.55	-165.90	0.09	-18.10
0.76	47.83	0.39	-64.15	1.53	-157.48	0.65	-29.66
1.19	114.33	0.11	86.93	1.20	-174.35	1.58	2.04
0.95	131.44	0.70	63.82	0.94	-161.07	0.81	-4.56
0.38	9.23	0.60	-18.84	1.25	-165.76	0.54	-25.86
0.10	57.34	0.09	40.78	1.38	-173.24	0.88	27.05
0.67	140.79	0.27	-65.52	0.97	-147.80	1.08	-34.60
0.33	-99.01	0.23	-165.50	1.49	-169.96	0.43	35.48
0.97	166.91	0.67	102.83	1.43	-174.26	1.40	23.69

0.70	157.43	0.48	94.27	0.76	159.28	0.92	0.00
0.32	11.24	0.36	-5.37	0.50	-129.14	0.96	-35.68
0.51	8.70	0.36	63.09	0.94	-171.41	0.51	-2.70
0.52	94.17	0.44	89.19	0.70	173.58	1.33	20.10
0.45	102.33	0.37	77.08	0.76	177.16	1.07	5.63
0.52	135.68	0.45	39.67	0.88	-173.82	0.84	-8.31
0.14	44.17	0.24	-0.18	0.86	-175.58	1.07	16.10
0.07	0.12	0.39	38.35	0.94	-158.42	0.80	6.03
0.42	-41.97	0.64	-53.51	1.01	-162.76	0.67	-5.11
0.34	119.77	0.78	42.45	0.73	170.46	1.13	-1.41
1.12	156.97	0.95	89.51	0.99	142.77	1.42	0.94
0.44	-101.54	0.29	147.44	1.19	163.96	0.24	23.80
0.59	-44.45	0.23	0.00	0.71	164.85	0.86	-16.05
0.28	115.91	0.92	90.22	1.22	124.71	1.24	17.13
0.32	95.21	0.75	72.10	0.83	129.47	1.17	6.85
0.84	-24.22	0.63	-38.30	0.51	145.05	0.58	11.02
0.24	-87.78	0.13	77.26	0.86	138.42	1.10	-5.04

Velocity 5 (cm/sec)	Direction 5 (deg)	Velocity 6 (cm/sec)	Direction 6 (deg)	Velocity 7 (cm/sec)	Direction 7 (deg)
0.55	6.69	0.35	21.23	2.06	-45.80
0.57	0.12	0.31	16.76	1.98	-46.38
0.57	3.00	0.36	8.73	2.01	-45.52
0.58	8.24	0.37	10.99	1.97	-48.18
0.68	2.85	0.40	4.78	2.08	-46.40
0.85	9.20	0.37	8.88	2.09	-45.14
0.76	9.02	0.35	23.37	2.04	-44.25
0.73	15.48	0.34	25.86	2.02	-43.61
0.72	4.08	0.36	29.57	2.00	-42.96
0.63	10.30	0.41	30.72	1.94	-44.62
0.54	14.74	0.38	30.26	1.90	-45.92
0.54	2.65	0.42	31.17	1.89	-48.38
0.78	11.12	0.41	25.47	2.04	-45.80
0.61	10.18	0.46	24.40	1.94	-46.00
0.66	0.21	0.37	18.87	1.98	-43.57
0.66	7.14	0.40	13.87	2.03	-46.06
0.67	1.51	0.35	3.74	1.95	-46.88
0.63	0.48	0.39	10.66	1.98	-45.43
0.71	5.74	0.32	19.59	12.68	67.98
11.48	-25.92	12.94	-88.71	28.79	19.06
16.98	-20.31	10.00	154.61	13.71	25.68
3.72	-13.18	7.99	177.22	6.39	41.59
2.00	-17.19	9.06	125.63	7.31	51.22
4.61	-20.68	10.12	115.10	3.80	31.41
7.47	-49.33	5.44	114.42	6.48	19.82
4.77	-22.20	6.46	105.65	2.19	-53.59
4.33	-13.49	11.72	113.35	0.91	-113.75
3.18	0.44	8.06	80.60	2.61	41.87
4.93	-17.36	7.76	46.14	1.87	5.22
2.51	-50.95	5.26	36.38	2.58	-56.50
1.96	18.62	3.67	64.01	2.46	-1.61
4.40	44.16	9.39	63.10	4.09	87.07
2.51	-23.75	3.95	-28.17	5.97	-54.92
0.97	66.02	4.91	66.09	0.79	174.07

1.83	49.89	2.51	36.11	1.18	-40.87
2.47	58.28	1.34	87.19	2.20	-72.39
2.43	20.90	2.13	89.85	1.53	-41.13
2.09	-3.46	3.47	19.41	1.56	-34.12
1.12	101.72	1.63	-17.06	2.90	-71.65
1.79	51.36	2.12	68.50	1.64	-105.77
2.43	-11.87	3.86	6.77	2.40	-24.52
2.51	38.02	4.84	53.38	2.03	15.88
0.79	4.53	1.94	31.85	1.73	-61.41
0.72	79.81	2.00	87.56	1.72	-53.48
1.92	19.14	3.92	75.95	1.97	6.60
1.72	15.63	4.16	27.72	1.81	38.21
0.92	18.65	1.02	32.34	1.59	-56.49
1.93	20.23	2.37	37.43	1.03	-56.44
0.88	54.60	0.85	149.66	2.61	-30.48
0.90	-35.42	1.41	45.14	1.86	-65.92
2.00	14.13	2.51	36.08	1.76	-45.97
1.49	17.50	1.39	38.19	0.58	-38.56
1.65	66.85	0.36	68.00	2.28	-44.83
0.58	56.18	0.95	51.45	1.89	-66.27
1.62	21.77	2.51	43.75	0.31	39.81
1.29	46.75	0.95	40.90	1.37	-56.19
0.96	0.23	1.37	67.29	1.12	-125.91
1.89	-27.59	2.51	-30.46	2.21	-51.26
1.98	40.91	2.42	53.15	0.72	-38.69
0.51	-37.88	1.13	-21.86	1.68	-99.57
0.54	31.57	0.61	117.78	1.38	-62.22
2.27	-2.21	2.03	9.28	0.55	7.69
0.74	12.49	0.95	174.86	2.02	-99.29
1.36	116.78	1.36	113.57	0.96	-70.77
1.83	12.65	1.52	31.33	1.82	-82.46
1.68	21.30	1.79	6.54	1.86	-55.03
1.32	69.77	1.52	98.88	1.78	-77.13
0.82	23.95	1.77	-17.15	2.25	-59.19
2.17	14.42	2.43	29.98	1.98	-73.60
0.98	-40.86	1.99	-17.55	2.57	-67.43
0.88	60.00	1.25	81.61	2.10	-92.95
1.01	20.96	1.72	25.02	2.16	-46.26
1.02	3.82	0.36	-77.71	3.06	-69.12
0.68	35.94	0.31	79.77	2.30	-53.33
1.28	48.42	1.29	66.02	2.13	-52.48
0.87	24.73	0.93	-10.93	2.60	-45.87
0.85	2.75	1.49	29.12	2.59	-57.36
0.70	32.39	1.11	-14.34	2.32	-40.35
1.50	41.83	1.72	40.80	1.37	-37.34
1.31	28.03	1.01	16.75	2.24	-54.97
1.54	-27.59	1.46	-8.07	2.64	-49.95
1.20	1.27	1.33	13.95	1.80	-41.97
0.68	10.42	1.27	-3.09	1.84	-66.88
0.70	21.52	0.34	-160.91	2.57	-60.57
1.46	-28.39	1.49	-23.77	2.61	-38.76
1.50	11.76	1.87	41.65	1.66	-38.56
0.39	87.17	0.51	114.49	2.48	-63.09
0.79	50.95	0.52	22.64	2.64	-47.33
1.32	-7.93	1.19	6.08	2.62	-42.84
1.17	37.72	1.54	42.77	2.06	-44.33

0.55	45.53	0.61	-3.03	2.39	-55.61
1.35	-16.47	0.63	9.51	2.52	-51.74

- Wave height

Free Fall of Circular Plate Test 3						
Time (second)	Height 200 (cm)	Height 201 (cm)	Height 202 (cm)	Height 203 (cm)	Height 204 (cm)	Height 205 (cm)
0	0.02	-0.13	0.09	0.30	0.15	0.02
0.42	0.21	-0.10	0.11	0.30	0.21	0.12
0.84	0.05	-0.15	0.10	0.25	0.10	0.08
1.26	0.13	-0.04	0.10	0.24	0.17	0.09
1.67	0.00	-0.09	0.09	0.29	0.09	0.11
2.1	0.03	-0.02	0.11	0.28	0.13	0.00
2.51	0.02	-0.13	0.10	0.27	0.20	0.04
2.93	0.04	-0.13	0.11	0.31	0.09	-0.04
3.36	-0.06	-0.10	0.10	0.29	0.33	0.11
3.77	0.05	-0.15	0.12	0.28	0.17	0.19
4.19	0.08	-0.12	0.11	0.26	0.18	0.10
4.61	0.02	-0.10	0.09	0.24	0.19	0.14
5.03	0.06	-0.08	0.10	0.23	0.19	0.18
5.44	0.04	-0.12	0.11	0.27	0.17	0.07
5.87	0.04	-0.14	0.12	0.27	0.20	0.03
6.28	-0.14	-0.12	0.11	0.23	0.12	0.09
6.7	0.05	-0.15	0.10	0.27	0.21	0.12
7.13	0.06	-0.12	0.11	0.31	0.13	0.13
7.54	0.00	-0.09	0.10	0.27	0.17	0.17
7.96	0.04	-0.13	0.08	0.26	0.16	0.13
8.38	0.04	-0.13	0.10	0.26	0.13	0.08
8.8	0.03	-0.14	0.10	0.23	0.20	0.11
9.21	0.03	-0.11	0.12	0.25	0.13	0.01
9.64	0.03	-0.14	0.10	0.25	0.27	0.04
10.05	0.07	-0.12	0.09	0.22	0.18	0.19
10.47	0.02	-0.19	0.08	0.28	0.18	0.06
10.9	0.02	-0.13	0.10	0.32	0.19	0.29
11.31	0.03	-0.12	0.09	0.26	0.20	0.14
11.73	0.01	-0.14	0.10	0.26	0.16	0.11
12.15	0.06	-0.09	0.11	0.29	0.21	0.07
12.57	0.03	-0.13	0.12	0.25	0.12	0.05
12.98	0.06	-0.09	0.12	0.24	0.21	0.30
13.41	0.03	-0.14	0.09	0.26	0.13	0.05
13.82	0.04	-0.11	0.12	0.25	0.17	0.10
14.24	0.02	-0.11	0.09	0.27	0.18	0.08
14.67	-0.03	-0.11	0.11	0.33	0.14	0.20
15.08	0.02	-0.06	0.11	0.26	0.37	0.08
15.5	0.02	-0.09	0.12	0.29	0.18	0.05
15.92	0.04	-0.08	0.09	0.30	0.21	0.26
16.34	0.01	-0.12	0.10	0.24	0.22	0.05
16.75	0.04	-0.09	0.10	0.23	0.20	0.06
17.18	0.03	-0.08	0.14	0.30	0.20	0.00
17.59	0.00	-0.11	0.11	0.27	0.23	0.11
18.01	0.04	-0.07	0.10	0.25	0.17	-0.03
18.44	0.00	-0.08	0.09	0.28	0.25	0.16
18.85	0.04	-0.10	0.10	0.31	0.16	0.14
19.27	0.00	-0.10	0.10	0.28	0.20	0.06

19.69	0.04	-0.10	0.12	0.29	0.15	0.14
20.11	0.04	-0.08	0.12	0.24	0.16	-0.05
20.52	0.08	-0.12	0.12	0.25	0.21	0.04
20.95	0.05	-0.05	0.13	0.28	0.13	-0.03
21.36	0.00	-0.08	0.11	0.26	0.32	0.12
21.78	0.06	-0.18	0.12	0.24	0.21	0.34
22.21	0.02	-0.08	0.12	0.29	0.21	0.15
22.62	0.02	-0.09	0.11	0.29	0.23	0.13
23.04	0.13	-0.08	0.12	0.26	0.25	0.19
23.46	0.08	-0.11	0.11	0.28	0.21	0.10
23.88	0.02	-0.05	0.09	0.28	0.25	0.03
24.29	0.00	-0.09	0.10	0.24	0.15	0.09
24.72	0.05	0.08	0.13	0.26	0.23	0.14
25.13	0.04	-0.10	0.13	0.25	0.15	0.15
25.55	0.04	-0.11	0.12	0.27	0.20	0.14
25.98	0.26	-0.09	0.10	0.29	0.19	0.43
26.39	0.05	-0.14	0.13	0.31	0.15	0.14
26.81	0.14	-0.09	0.13	0.25	0.27	0.11
27.23	0.00	-0.09	0.11	0.30	0.16	0.04
27.65	0.03	0.09	0.10	0.27	0.21	0.05
28.06	0.02	-0.12	0.12	0.23	0.21	0.11
28.49	0.05	-0.11	0.11	0.24	0.21	0.04
28.91	-0.03	-0.09	0.12	0.28	0.21	0.27
29.32	0.05	-0.14	0.13	0.24	0.22	0.21
29.75	0.14	-0.11	0.10	0.26	0.16	0.16
30.16	0.02	-0.09	0.13	0.29	0.22	0.00
30.58	0.05	-0.13	0.12	0.32	0.14	0.11
31	0.02	-0.11	0.14	0.28	0.21	-0.12
31.42	0.05	-0.12	0.12	0.28	0.15	0.02
31.83	-0.17	-0.11	0.12	0.25	0.15	0.10
32.26	0.05	-0.15	0.12	0.26	0.22	0.11
32.68	0.07	-0.11	0.14	0.25	0.11	0.30
33.09	0.03	-0.12	0.12	0.24	0.31	0.12
33.52	0.05	-0.11	0.11	0.25	0.19	0.07
33.93	0.03	-0.10	0.12	0.28	0.19	0.06
34.35	0.04	-0.12	0.11	0.27	0.22	0.12
34.77	-0.05	-0.10	0.14	0.27	0.21	0.03
35.19	0.05	-0.14	0.14	0.27	0.19	0.06
35.6	0.07	-0.15	0.13	0.27	0.23	0.11
36.03	0.03	-0.12	0.13	0.24	0.15	0.17
36.45	0.06	-0.09	0.14	0.23	0.22	0.13
36.86	0.05	-0.10	0.15	0.26	0.17	0.15
37.29	0.04	-0.10	0.14	0.28	0.20	0.15
37.7	0.06	-0.08	0.12	0.24	0.18	0.13
38.12	0.06	-0.11	0.15	0.25	0.15	0.02
38.55	0.08	-0.10	0.14	0.28	0.21	0.04
38.96	0.02	-0.10	0.13	0.29	0.17	-0.09
39.38	0.06	-0.10	0.11	0.25	0.24	0.07
39.8	0.06	-0.08	0.15	0.26	0.22	0.12
40.22	0.01	-0.09	0.12	0.24	0.21	0.22
40.63	0.06	-0.05	0.14	0.27	0.22	0.20
41.06	0.07	-0.08	0.13	0.24	0.22	0.11
41.47	0.10	-0.07	0.13	0.27	0.17	0.11
41.89	0.04	-0.08	0.13	0.28	0.23	-0.07
42.32	0.05	-0.07	0.16	0.32	0.14	0.07
42.73	0.06	-0.06	0.13	0.26	0.22	0.12

43.15	0.02	-0.09	0.13	0.30	0.14	0.12
43.57	0.02	-0.03	0.14	0.29	0.18	0.14
43.99	0.03	-0.07	0.14	0.28	0.24	0.23
44.4	0.07	-0.15	0.18	0.23	0.14	0.07
44.83	0.05	-0.05	0.15	0.31	0.37	0.27
45.24	0.05	-0.05	0.17	0.27	0.23	0.14
45.66	0.04	-0.06	0.15	0.29	0.23	0.08
46.09	0.04	-0.07	0.16	0.30	0.26	0.00
46.5	0.06	-0.01	0.17	0.35	0.25	0.11
46.92	0.00	-0.04	0.16	0.28	0.24	-0.06
47.34	0.07	-0.19	0.13	0.31	0.27	0.32
47.76	0.04	-0.04	0.17	0.26	0.18	0.18
48.17	0.05	-0.06	0.17	0.26	0.26	0.13
48.6	0.04	-0.04	0.19	0.27	0.21	0.17
49.02	0.08	-0.07	0.14	0.26	0.22	0.16
49.43	0.06	-0.01	0.10	0.26	0.21	0.03
49.86	-0.01	-0.02	0.16	0.34	0.19	0.34
50.27	0.06	-0.18	0.13	0.34	0.32	0.14
50.69	0.05	-0.04	0.15	0.28	0.18	0.16
51.12	0.07	-0.04	0.15	0.27	0.29	0.18
51.53	0.05	-0.05	0.12	0.31	0.24	0.20
51.95	0.07	-0.08	0.17	0.23	0.23	0.06
52.37	0.05	0.03	0.14	0.24	0.23	0.10
52.79	0.03	-0.03	0.14	0.27	0.25	0.16
53.2	0.07	0.14	0.15	0.25	0.21	0.08
53.63	0.06	-0.04	0.17	0.26	0.26	0.14
54.04	0.60	-0.05	0.17	0.32	0.17	0.14
54.46	10.17	-0.04	0.16	0.29	1.83	0.19
55.01	10.22	-0.04	0.16	0.33	8.57	0.18
55.53	-4.28	0.21	0.17	11.49	-0.28	0.27
56.03	-12.56	15.30	2.50	6.48	-2.53	10.54
56.5	3.60	6.10	11.12	1.70	2.97	2.72
57.09	-3.26	1.75	5.26	-1.43	-1.84	2.01
57.51	-10.73	-1.80	1.59	-3.97	2.95	3.58
57.99	4.03	-4.79	-1.20	-4.24	-5.36	1.41
58.41	-11.75	-6.77	-4.76	6.63	-5.65	3.24
58.85	4.93	10.44	-7.61	-3.10	-6.60	-1.17
59.37	7.25	-9.75	1.18	-8.47	-3.76	-2.88
59.93	-0.72	-7.40	-7.66	-10.33	2.23	-5.36
60.45	3.49	-9.96	-6.93	-6.51	3.43	-5.60
60.92	0.31	0.74	-1.01	-4.73	0.95	-1.14
61.4	5.80	-9.68	7.12	14.13	-3.33	-2.54
61.94	1.26	1.09	-1.67	6.86	-0.17	-0.71
62.42	-2.55	-1.05	1.06	8.59	-3.84	-0.83
62.88	-1.92	3.32	6.59	0.76	-4.39	2.50
63.26	11.21	-1.03	-1.23	7.82	3.38	1.77
63.86	2.56	1.31	6.05	0.92	-4.47	2.50
64.27	1.18	-1.23	10.96	4.34	4.40	4.79
64.75	4.86	-1.58	3.28	0.75	4.62	1.21
65.22	1.64	-3.58	1.84	1.10	2.73	6.15
65.65	4.62	-4.67	-1.27	-1.27	1.11	4.22
66.12	-1.17	6.99	11.07	-5.27	1.74	1.52
66.6	1.40	4.78	-2.40	-5.13	1.35	4.88
67.09	5.40	2.22	1.71	9.26	-2.49	6.39
67.55	-1.69	2.34	3.73	4.18	-0.69	0.35
67.98	3.65	6.72	0.99	0.59	4.90	-0.69

68.52	-2.06	3.85	2.87	15.96	-0.79	-0.94
68.98	-0.24	7.20	-0.69	4.14	2.46	-0.93
69.6	1.53	3.05	1.87	-0.19	5.22	-1.19
70.07	-2.31	0.53	4.54	13.12	-1.52	-1.36
70.6	-4.06	3.93	-1.00	6.33	-1.52	-1.13
71.09	0.62	0.84	3.85	5.22	-2.51	0.93
71.62	0.49	0.71	0.89	2.34	-1.99	5.16
72.06	2.22	-1.20	3.90	-1.69	-0.75	5.04
72.53	4.64	-2.47	1.27	-4.37	1.62	6.15
72.94	2.76	2.73	1.09	3.21	0.00	6.25
73.44	4.42	-2.74	1.48	-1.15	-2.61	2.87
73.84	4.26	0.75	4.35	1.08	-2.33	0.36
74.37	4.45	-2.30	1.37	-3.14	0.57	1.33
74.86	4.22	-1.15	1.72	-1.00	3.49	1.63
75.27	5.08	-3.08	2.19	-3.02	4.15	-0.94
75.76	4.67	-0.88	1.66	-4.63	4.06	-1.85
76.17	2.14	-0.73	1.52	-2.55	3.92	0.86
76.73	2.37	5.91	4.23	0.76	2.07	-0.02
77.19	4.16	1.47	1.72	-0.57	1.65	0.94
77.68	1.02	1.79	-1.55	7.68	-2.32	3.63
78.3	-2.57	2.96	2.36	0.88	1.68	4.09
78.69	-0.99	-1.99	0.07	6.79	-2.05	2.68
79.13	-3.25	1.28	2.13	5.71	2.48	0.80
79.53	-0.19	0.22	3.10	1.77	-2.16	0.18
80.04	0.45	0.96	-0.47	5.55	-1.37	0.70
80.49	1.48	0.90	-1.81	-2.02	-2.34	-0.39
80.94	4.66	4.74	-0.23	4.08	1.47	1.02
81.5	2.78	1.76	-1.81	-0.31	-0.51	2.67
81.98	2.69	4.30	-2.63	3.34	-1.92	-0.57
82.45	3.24	0.05	0.39	1.10	3.94	0.46
83.06	3.38	-0.22	-0.49	1.95	2.56	-0.27
83.6	2.13	-3.54	2.33	-1.91	-0.62	0.83
84.06	-0.32	2.14	3.25	3.24	-2.76	-0.65
84.55	3.85	2.31	2.80	0.76	-1.22	1.84
85.03	-2.94	2.11	2.24	0.94	1.41	5.09
85.49	-3.24	2.32	1.62	-1.69	4.50	3.19
85.88	0.44	2.08	1.93	-1.65	1.07	4.13
86.34	0.76	-2.43	1.63	0.69	-0.85	1.40
86.91	-0.99	-2.37	0.75	-1.84	3.43	5.47
87.42	-2.26	-1.06	0.79	-1.23	1.71	5.11
87.84	-3.38	1.01	-1.86	-3.04	-1.13	5.35
88.37	-1.59	0.99	-1.50	8.82	3.05	1.62
88.86	0.81	-2.08	-1.43	1.39	2.15	-0.96
89.38	0.74	-3.96	-0.47	0.38	0.67	-0.95
89.88	0.98	-2.58	-2.22	-0.45	2.61	1.49
90.35	1.65	-1.00	-2.31	-0.47	3.73	-0.94
90.83	2.46	-0.98	-2.81	-1.58	2.91	-2.60
91.25	3.04	-0.69	0.08	1.00	1.75	-1.71
91.74	2.15	-1.86	0.74	-1.31	1.48	0.46
92.25	1.96	-1.13	0.81	2.08	-0.77	2.24
92.68	3.48	1.04	2.31	-2.25	-1.42	1.70
93.11	3.80	-0.17	2.87	2.71	-3.72	-1.03
93.58	3.77	-1.37	4.13	2.03	-0.29	1.08
94.11	2.26	0.07	3.14	1.31	-2.15	1.29
94.55	2.42	1.22	3.29	-1.38	-2.06	0.34
95.01	3.61	3.46	3.20	5.80	-3.71	2.63

95.44	1.68	3.33	4.02	3.17	-2.24	0.77
95.86	1.85	2.83	3.86	2.49	-1.51	-0.90
96.27	1.18	1.22	2.48	2.46	0.81	-0.19
96.73	-2.65	3.28	1.59	-0.93	-1.43	2.17
97.12	1.20	3.13	0.87	2.48	1.61	4.47
97.6	1.29	3.38	1.06	2.28	1.15	3.36
98.05	-0.83	0.96	0.98	4.03	1.53	1.46
98.44	0.94	-0.59	0.80	4.88	2.51	4.62
99.03	0.73	-0.54	0.71	2.64	1.98	1.03
99.5	1.53	2.65	1.01	2.13	3.52	2.41
99.94	0.02	1.35	-0.75	-0.72	2.36	1.71
100.5	2.24	-1.08	0.37	2.97	2.40	1.14
101	2.47	-2.04	-1.15	-1.14	4.15	3.70
101.4	2.98	-2.33	-0.45	1.96	2.53	2.75
101.8	3.52	-2.82	0.83	1.74	2.34	1.01
102.3	1.33	0.34	0.99	-0.51	1.86	2.98
102.8	3.41	1.88	2.08	1.48	1.54	2.30
103.2	1.66	1.80	1.11	1.10	3.03	2.68
103.6	1.77	1.08	1.74	3.87	2.97	4.85
104.1	3.30	0.29	4.43	1.02	2.47	1.06
104.5	2.60	2.27	3.95	0.99	1.84	-1.29
105	2.30	2.42	3.41	1.25	2.11	-1.82
105.4	1.64	3.69	3.19	1.23	2.45	-0.50
105.9	2.38	3.36	3.67	4.89	1.28	1.55
106.3	3.41	3.20	2.51	3.97	0.70	-1.24
106.7	3.07	2.10	1.12	1.50	-2.55	-4.64
107.1	0.22	2.32	0.45	1.79	0.12	-3.51
107.7	-0.42	2.89	0.55	3.60	2.19	-0.89
108.2	-0.51	3.54	0.79	3.31	-1.22	-2.16
108.8	0.43	2.34	0.86	-0.97	-0.69	1.04
109.4	2.27	2.48	0.27	4.47	-1.27	1.74
109.8	1.91	2.06	-0.05	3.45	-1.19	3.26
110.3	2.14	1.87	0.49	2.09	-2.96	3.42
110.8	3.46	2.10	0.77	3.92	-4.07	3.51
111.2	2.49	2.44	-0.33	3.40	-2.41	2.82
111.7	3.19	2.26	0.43	3.82	2.49	2.71
112.2	2.53	2.18	0.89	2.03	2.02	2.47
112.6	1.25	0.15	1.91	1.13	0.87	3.16
113	0.79	-1.27	3.44	-0.31	0.50	2.55
113.5	-0.82	-1.27	3.88	-2.49	2.27	1.76
113.9	-2.56	-0.99	2.02	-1.00	3.03	3.32
114.3	-0.90	-0.78	1.35	-2.19	4.18	3.61
114.8	-0.41	-0.84	1.06	-1.67	3.19	1.11
115.2	-1.66	-1.50	0.59	-1.97	2.49	1.27

- Wave height

Free Fall of Circular Plate Test 4						
Time (second)	Height 206 (cm)	Height 207 (cm)	Height 208 (cm)	Height 209 (cm)	Height 210 (cm)	Height 211 (cm)
0	-0.64	-0.60	-0.07	-0.64	0.05	-0.18
0.49	-0.67	-0.56	0.01	-0.48	0.03	0.24
1.02	-0.65	-0.50	0.00	-0.46	-0.10	-0.15
1.53	-0.67	-0.47	-0.01	-0.58	0.06	0.10
1.92	-0.66	-0.59	-0.02	-0.61	-0.04	0.03
2.34	-0.66	-0.75	0.04	-0.46	0.07	-0.10
2.76	-0.66	-0.62	-0.04	-0.42	-0.21	0.05
3.23	-0.64	-0.68	-0.06	-0.57	0.09	-0.17
3.72	-0.63	-0.46	-0.01	-0.43	0.05	-0.18
4.2	-0.61	-0.69	-0.02	-0.43	0.12	-0.16
4.67	-0.62	-0.76	0.02	-0.39	0.16	0.01
5.18	-0.59	-0.55	-0.02	-0.48	0.08	-0.17
5.69	-0.63	-0.65	-0.03	-0.58	0.44	0.26
6.26	-0.60	-0.52	-0.05	-0.33	0.07	-0.03
6.77	-0.62	-0.48	0.02	-0.44	0.22	-0.13
7.25	-0.59	-0.42	0.02	-0.40	0.08	-0.12
7.72	-0.63	-0.57	0.00	-0.44	0.02	-0.08
8.23	-0.64	-0.55	0.00	-0.43	0.07	-0.17
8.74	-0.63	-0.37	-0.06	-0.71	-0.04	-0.19
9.16	-0.61	-0.59	0.03	-0.48	0.11	-0.17
9.6	-0.61	-0.51	0.06	-0.53	0.42	0.25
10.18	-0.65	-0.60	-0.02	-0.41	0.03	-0.16
10.74	-0.65	-0.83	0.05	-0.43	0.07	-0.12
11.25	-0.62	-0.80	0.01	-0.42	0.16	-0.38
11.79	-0.63	-0.58	-0.01	-0.68	0.14	-0.15
12.21	-0.64	-0.66	0.03	-0.42	0.11	-0.19
12.7	-0.60	-0.86	0.07	-0.49	0.17	-0.12
13.17	-0.61	-0.77	-0.03	-0.58	0.04	-0.08
13.64	-0.57	6.54	-0.03	28.65	0.04	-0.04
14.14	-0.51	75.47	-0.07	-29.32	0.05	-0.16
14.66	41.08	-33.31	0.02	-25.96	0.07	-0.17
15.2	-12.82	41.45	0.27	-18.98	0.24	-0.34
15.74	5.26	-35.79	18.16	-25.11	0.09	-0.11
16.22	-5.47	-19.61	9.01	-20.66	-0.05	-0.42
16.68	-2.11	-16.18	4.19	7.32	0.06	-0.10
17.18	-9.78	0.03	8.40	14.02	0.15	-0.10
17.73	-13.39	-9.97	1.49	5.49	0.07	-0.03
18.25	4.53	4.91	-1.04	-1.93	0.06	-0.12
18.79	2.01	-5.70	-5.06	4.53	0.48	0.34
19.34	1.87	10.60	-9.30	9.19	0.04	-0.07
19.81	9.94	6.61	-10.86	10.63	0.10	0.25
20.4	-4.06	2.76	-9.18	12.04	17.21	2.19
20.89	2.85	3.46	-9.24	13.17	6.91	7.15
21.34	0.98	19.57	-6.85	9.75	-0.36	6.10
21.89	2.44	-0.89	-1.00	7.19	2.06	2.46
22.33	0.86	4.26	-0.69	12.36	1.53	1.02
22.78	5.41	2.33	10.46	11.63	0.39	0.03

23.22	6.97	2.90	2.42	7.97	2.21	-1.83
23.76	1.49	1.03	4.27	7.37	3.38	-5.11
24.17	2.92	-1.12	9.29	2.55	-0.29	-7.52
24.72	-1.98	2.69	2.30	7.77	-3.64	-7.31
25.22	-4.89	2.96	6.50	5.40	-9.37	-5.71
25.66	0.77	2.23	6.46	3.86	-4.60	-4.25
26.05	3.79	1.35	1.29	2.85	-4.16	-3.32
26.45	1.06	0.90	-0.72	4.45	-8.53	-4.16
27.02	-2.13	-0.92	-2.42	3.40	-4.82	-1.97
27.41	0.85	5.31	-6.15	4.08	-8.70	2.00
27.95	3.15	7.03	-0.99	5.66	-3.18	-3.85
28.36	1.44	4.50	0.32	2.77	-2.66	5.46
28.9	1.16	-0.68	-1.01	4.23	-4.77	-1.21
29.33	1.11	4.86	-2.00	9.60	1.44	-0.44
29.97	0.38	4.43	1.07	7.05	5.40	1.98
30.48	0.86	1.34	4.18	3.05	7.40	-1.32
31.05	0.98	-0.11	2.12	5.44	6.61	-1.08
31.49	1.88	-1.16	-1.82	1.31	5.85	1.72
31.95	0.20	5.11	-4.64	5.26	6.74	1.35
32.43	3.00	5.21	-2.85	8.48	8.06	3.17
32.93	-0.40	-1.06	-2.37	5.27	6.64	3.92
33.38	1.06	1.71	-3.60	8.90	9.23	5.46
33.85	0.59	2.12	-5.65	8.52	0.76	3.72
34.4	0.76	4.64	-6.21	2.61	-1.08	3.24
34.82	1.07	1.12	0.49	3.77	-4.38	4.87
35.26	-1.02	2.34	-4.31	5.35	-4.33	2.50
35.66	2.01	-0.65	-1.37	2.23	-3.47	-1.19
36.14	0.93	2.00	-3.52	2.19	-2.82	-1.03
36.62	2.04	-3.28	-2.86	2.25	-5.22	0.44
37.08	-0.68	2.79	2.44	3.51	-4.47	-6.31
37.47	3.21	-0.83	-0.71	1.07	-1.87	-8.65
37.94	-3.87	4.80	1.27	5.73	-2.02	-9.42
38.42	2.36	4.32	2.19	5.07	0.87	-12.66
38.9	1.12	2.86	5.56	8.84	-1.11	-5.31
39.43	1.42	5.56	1.57	7.94	0.10	0.37
39.94	2.61	1.03	3.39	8.73	-2.39	-1.65
40.45	1.92	7.51	-1.49	10.31	-0.29	-2.11
41	1.15	3.47	-1.64	10.81	0.51	2.43
41.53	2.54	6.46	-3.73	5.99	2.24	5.02
41.94	0.67	5.87	4.15	7.21	2.63	2.24
42.43	2.29	1.17	4.73	4.99	-0.65	3.45
42.89	2.92	2.23	2.88	4.99	-2.85	1.04
43.34	1.87	1.15	2.49	2.30	0.63	6.08
43.78	2.03	2.81	1.15	5.62	1.39	3.76
44.22	1.68	0.96	1.80	3.69	2.12	-1.28
44.64	1.42	3.55	0.36	3.92	2.85	-2.62
45.12	1.54	1.14	-4.41	5.04	4.25	1.73
45.54	1.27	1.51	-6.81	4.63	1.86	4.71
45.95	3.44	-0.72	-5.79	3.98	3.88	3.89
46.38	1.68	2.96	-4.36	3.47	1.03	1.32
46.84	-0.14	1.38	-4.60	1.65	2.74	1.07
47.33	0.83	-0.58	2.22	6.79	1.87	0.95
47.9	-0.23	2.17	3.69	8.67	1.80	4.75
48.41	-0.38	0.59	4.18	3.83	3.99	1.17
48.89	0.19	0.34	3.32	3.24	2.77	-2.25
49.36	-0.35	0.61	7.99	4.85	-0.65	0.30

49.98	1.01	4.28	2.13	5.98	-2.40	0.41
50.43	0.24	2.29	0.81	5.10	-2.47	-0.88
50.86	1.65	0.91	1.18	5.08	-1.65	-1.44
51.28	2.46	1.96	1.97	6.53	-2.10	-2.72
51.78	1.11	4.74	3.91	4.32	-1.46	-4.88
52.18	0.95	4.60	0.78	9.87	-1.35	-3.09
52.66	1.10	0.87	2.15	2.93	-0.69	-1.70
53.07	2.05	0.56	3.84	3.59	-2.93	1.72
53.56	1.51	1.95	-0.67	4.57	1.15	1.12
54.03	1.86	-0.28	-3.20	5.13	1.30	1.32
54.47	2.13	0.94	-1.95	3.90	-0.83	4.34
54.87	1.23	4.31	-2.97	5.24	-0.92	3.08
55.35	1.02	4.76	-1.02	4.19	1.49	2.03
55.77	1.25	4.08	2.24	7.28	-0.62	2.95
56.31	-0.70	2.40	-1.77	4.02	2.20	4.21
56.79	2.21	0.95	5.03	5.97	3.41	1.36
57.27	0.89	2.56	4.75	6.81	1.01	-0.52
57.73	0.63	0.92	-2.40	2.95	3.27	0.85
58.12	0.82	4.42	2.97	3.12	0.85	-2.89
58.52	0.77	2.68	-1.62	4.63	3.05	-2.03
58.94	1.19	-0.18	2.34	6.71	0.38	-2.22
59.48	1.07	0.68	2.56	3.30	1.64	0.62
59.95	0.45	0.61	0.68	3.62	5.01	1.27
60.38	0.84	1.23	2.43	4.71	0.68	-0.48
60.85	1.27	0.18	-2.65	5.14	-2.25	6.00
61.29	1.16	1.74	-1.83	4.79	-0.88	5.36
61.69	0.88	0.75	-5.57	1.88	-1.80	1.53
62.18	0.79	3.06	-2.42	2.86	-1.18	1.89
62.59	0.73	4.18	-2.47	3.66	2.29	1.26
63.01	1.74	2.05	0.95	4.06	3.54	0.96
63.49	2.47	1.72	0.80	5.37	3.69	1.81
63.9	1.37	2.23	0.13	5.91	0.51	0.42
64.46	0.94	4.50	7.43	6.48	1.00	-4.28
64.93	1.08	4.03	2.44	8.24	1.46	-1.15
65.5	1.22	4.16	1.77	7.52	0.79	-0.54
65.95	0.71	2.77	2.22	6.76	1.51	-2.72
66.42	1.22	2.69	1.32	6.21	1.81	-3.24
66.89	1.02	1.39	-1.22	2.66	0.89	-4.37
67.38	2.13	1.57	-0.23	3.46	-0.71	-2.45
67.92	-0.25	3.35	-0.79	6.14	-1.88	2.42
68.39	0.90	0.14	2.05	5.74	0.94	-0.23
69	0.72	1.84	-1.33	4.54	-0.83	-0.68
69.46	0.77	0.01	-3.85	1.63	-1.67	1.87
69.95	0.44	2.04	-2.69	3.63	-1.89	0.27
70.47	0.42	3.95	-0.73	4.56	-0.90	4.12
70.93	-0.06	1.27	-1.35	5.04	-0.15	0.64
71.45	0.81	0.59	-3.91	3.11	-0.07	-1.18
71.99	1.79	0.69	-1.10	4.51	-0.20	-3.07
72.47	1.20	0.86	1.15	5.05	0.81	-0.94
72.88	2.64	2.36	2.55	6.95	4.22	-1.33
73.3	1.78	2.98	-0.54	6.95	1.32	-0.99
73.78	1.35	4.13	0.40	6.80	0.92	1.48
74.22	1.26	4.19	-1.16	7.33	0.89	0.15
74.67	0.72	4.18	3.08	8.78	2.89	0.09
75.21	1.43	3.61	-1.18	7.98	-0.49	1.41
75.78	1.07	1.53	-0.82	7.33	-0.35	1.33

76.27	1.08	1.52	2.75	6.40	1.24	-0.27
76.76	1.05	1.02	1.86	5.00	0.32	0.12
77.25	1.02	1.40	-0.59	6.16	-1.28	-1.23
77.83	0.99	-0.05	4.80	4.34	-1.37	-1.96
78.33	0.68	1.84	1.50	6.72	-1.56	-1.04
78.87	0.77	1.21	3.22	4.51	-2.30	-1.94
79.28	-0.48	1.99	1.08	3.32	-1.85	-3.14
79.77	0.21	3.09	1.48	2.27	-1.81	0.07
80.3	1.11	-0.78	-0.14	2.55	1.19	-1.67
80.84	-0.03	-1.35	-3.96	1.69	1.26	0.95
81.31	0.86	-1.16	-2.20	0.36	1.15	1.71
81.8	0.78	0.50	-4.57	2.24	0.22	4.48
82.34	0.68	-1.18	-4.11	3.57	3.07	3.61
82.75	0.99	-0.52	-0.94	3.42	1.52	0.96
83.23	0.14	0.15	-1.77	5.61	3.58	2.83
83.71	0.23	3.77	-1.44	4.35	3.53	2.75
84.18	0.82	4.20	-1.39	5.38	4.16	0.30
84.65	0.04	3.05	-1.67	6.62	3.41	-0.92
85.04	0.73	4.02	-2.75	7.21	1.48	-1.42
85.44	0.81	3.41	-1.53	8.35	1.99	-2.23
85.95	0.95	3.10	0.66	7.52	1.33	-0.32
86.45	0.53	3.57	2.31	5.87	1.65	1.64
86.88	0.69	1.94	4.16	3.11	-0.87	0.92
87.45	0.67	-0.32	2.61	4.26	-1.57	0.41
88.02	1.58	0.34	7.35	3.10	-2.23	1.40

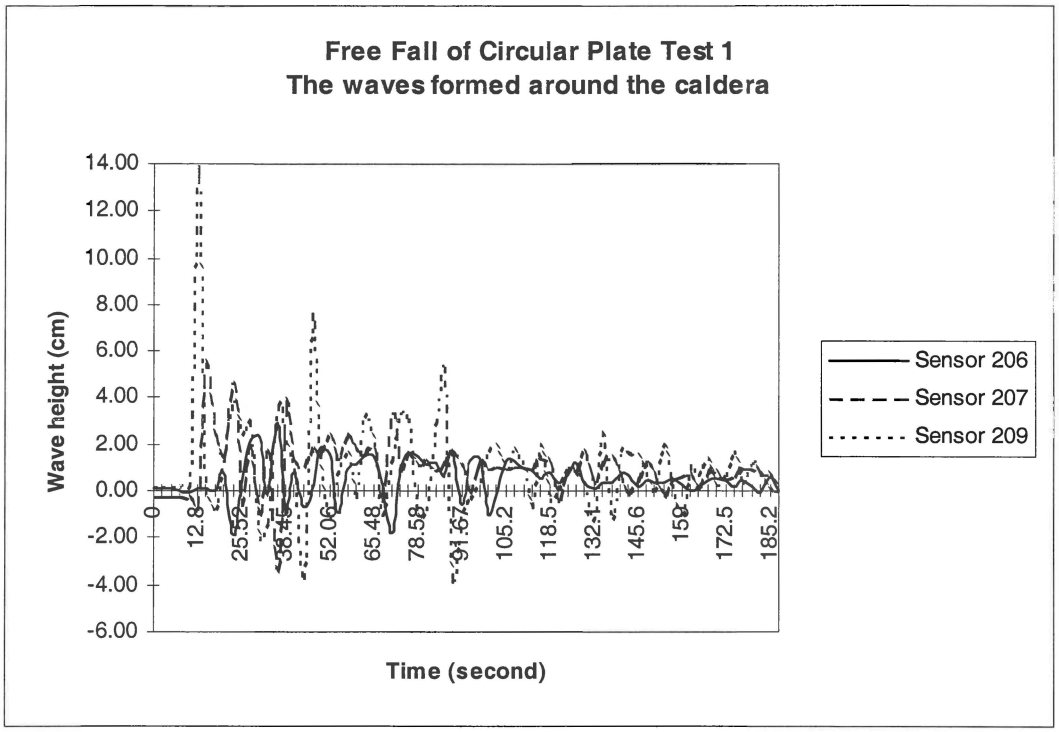
Free Fall of Circular Plate Test 1
The waves formed around the caldera
Wave height (cm)
14.00
12.00
10.00
8.00
6.00
4.00
2.00
0.00
-2.00
-4.00
-6.00
0
12.8
25.52
38.45
52.06
65.48
78.58
91.67
105.2
118.5
132.1
145.6
159
172.5
185.2
Time (second)
Sensor 206
Sensor 207
Sensor 209

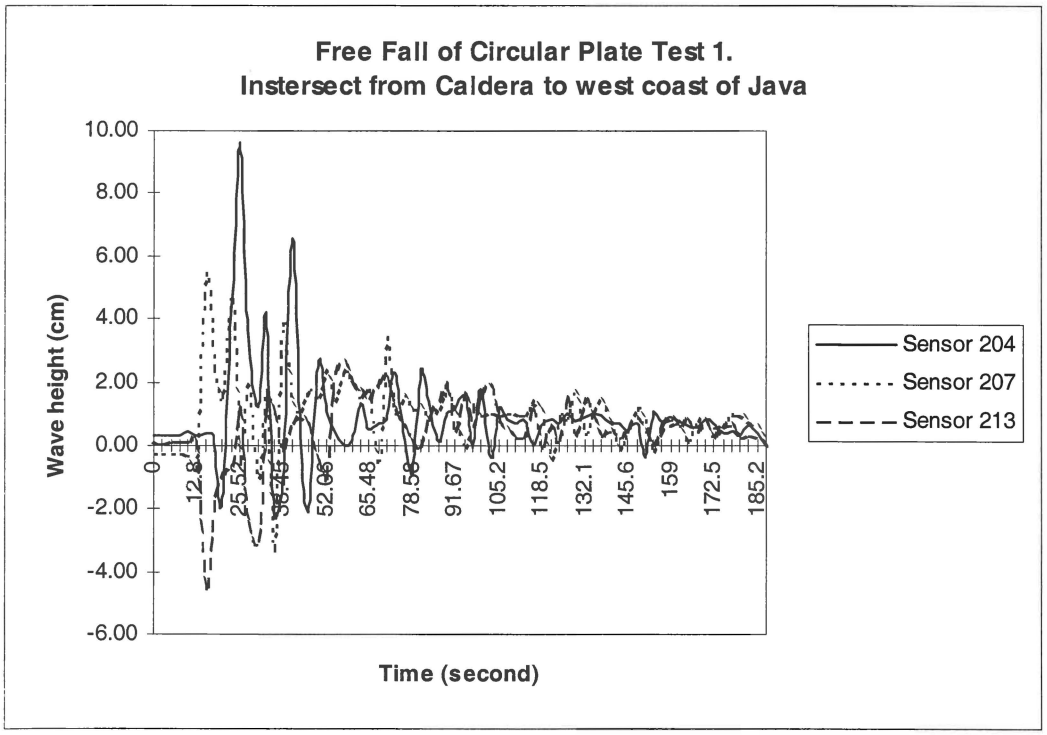
Free Fall of Circular Plate Test 1.
Instersect from Caldera to west coast of Java
Wave height (cm)
10.00
8.00
6.00
4.00
2.00
0.00
-2.00
-4.00
-6.00
0
12.8
25.52
38.45
52.06
65.48
78.58
91.67
105.2
118.5
132.1
145.6
159
172.5
185.2
Time (second)
Sensor 204
Sensor 207
Sensor 213

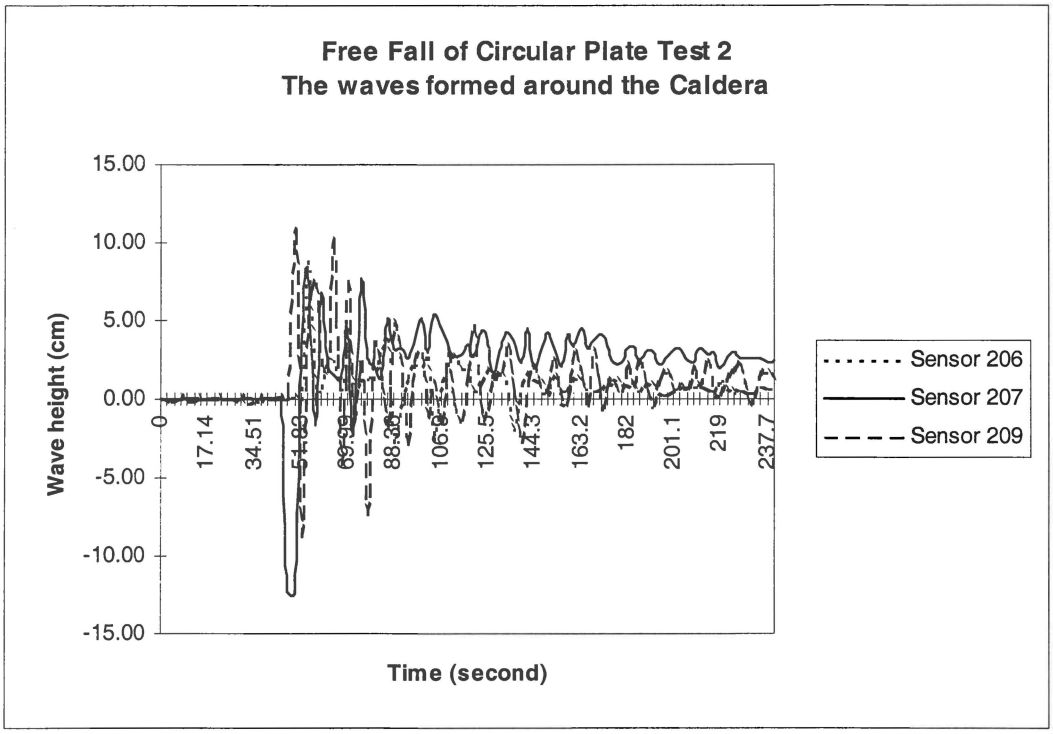
Free Fall of Circular Plate Test 2
The waves formed around the Caldera
15.00
10.00
5.00
0.00
-5.00
-10.00
-15.00
Wave height (cm)
0
17.14
34.51
54.09
69.99
88.36
106.9
125.5
144.3
163.2
182
201.1
219
237.7
Time (second)
Sensor 206
Sensor 207
Sensor 209

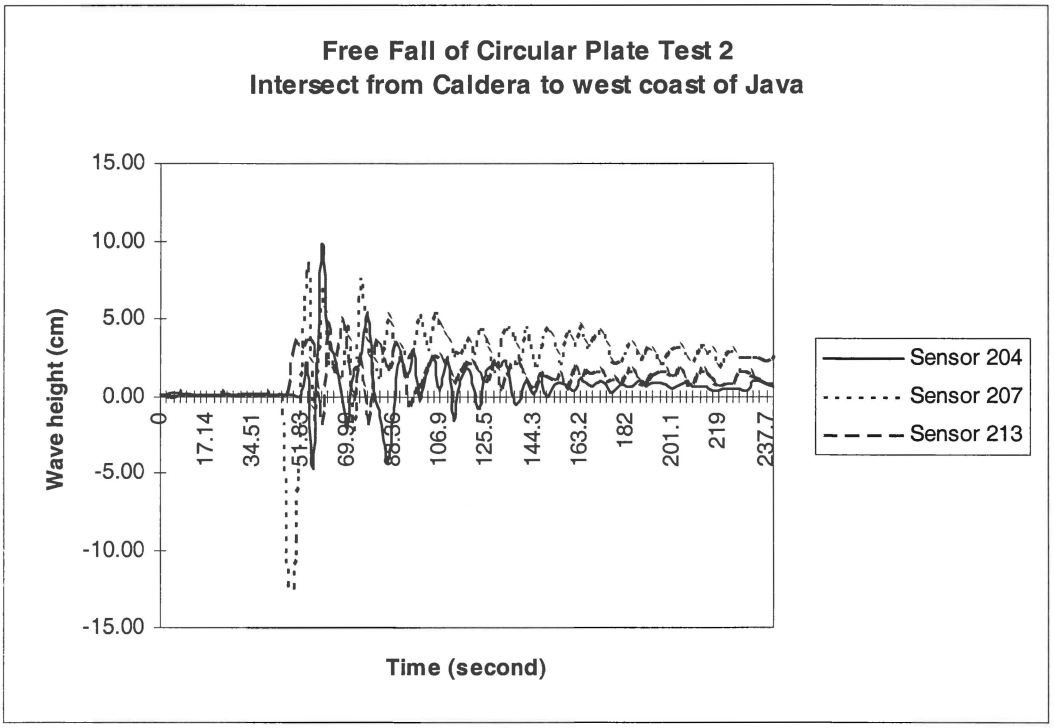
Free Fall of Circular Plate Test 2
Intersect from Caldera to west coast of Java
15.00
10.00
5.00
0.00
-5.00
-10.00
-15.00
Wave height (cm)
0
17.14
34.51
51.83
69.99
88.36
106.9
125.5
144.3
163.2
182
201.1
219
237.7
Time (second)
Sensor 204
Sensor 207
Sensor 213

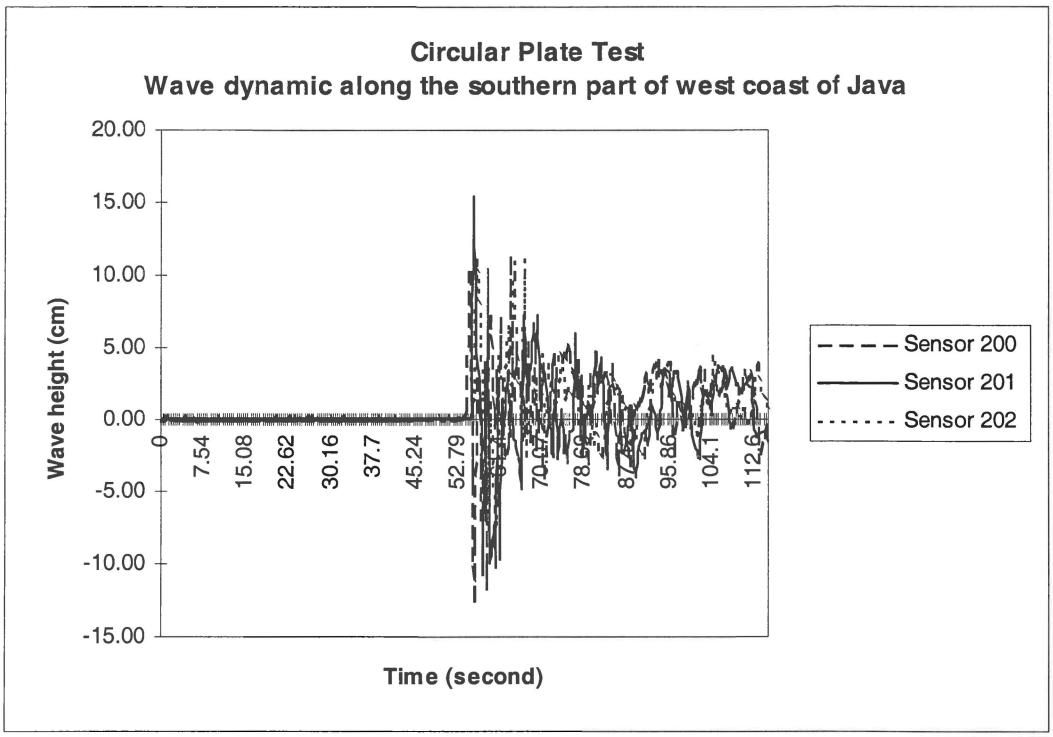
Circular Plate Test
Wave dynamic along the southern part of west coast of Java
Wave height (cm)
20.00
15.00
10.00
5.00
0.00
-5.00
-10.00
-15.00
0
7.54
15.08
22.62
30.16
37.7
45.24
52.79
70.07
78.60
87.42
95.86
104.1
112.64
Time (second)
Sensor 200
Sensor 201
Sensor 202

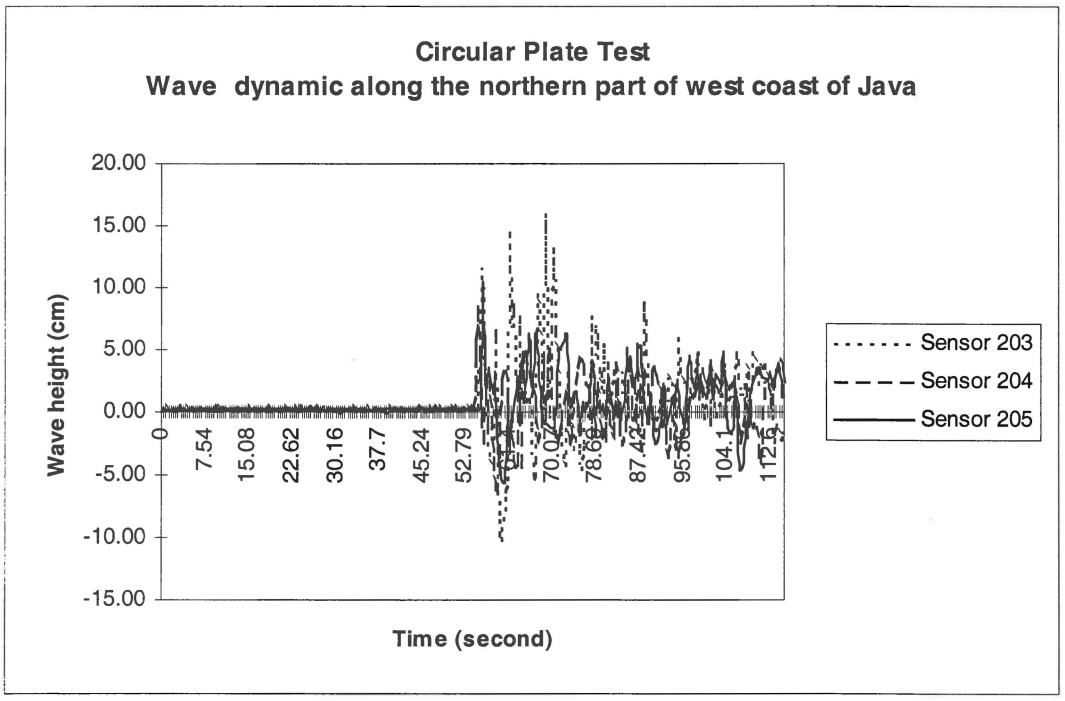
Circular Plate Test
Wave dynamic along the northern part of west coast of Java
Wave height (cm)
20.00
15.00
10.00
5.00
0.00
-5.00
-10.00
-15.00
0
7.54
15.08
22.62
30.16
37.7
45.24
52.79
70.07
78.60
87.42
95.86
104.1
112.64
Time (second)
Sensor 203
Sensor 204
Sensor 205

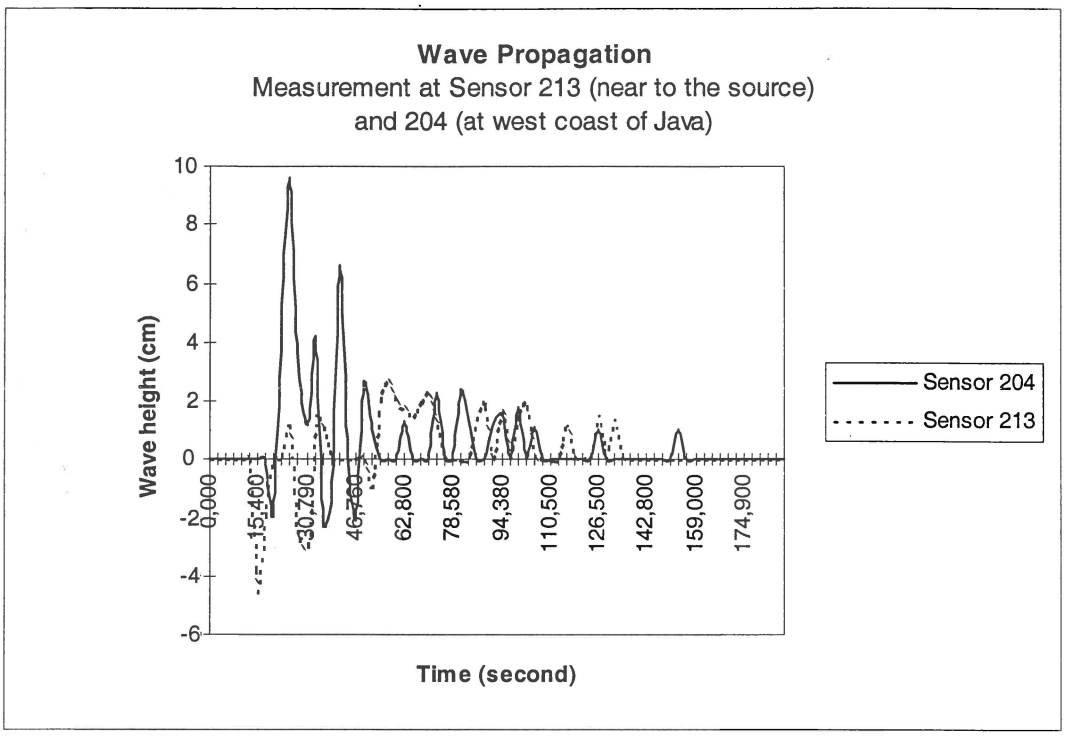
Wave Propagation
Measurement at Sensor 213 (near to the source)
and 204 (at west coast of Java)
Wave height (cm)
10
8
6
4
2
0
-2
-4
-6
0,000
15,400
30,790
46,760
62,800
78,580
94,380
110,500
126,500
142,800
159,000
174,900
Time (second)
Sensor 204
Sensor 213

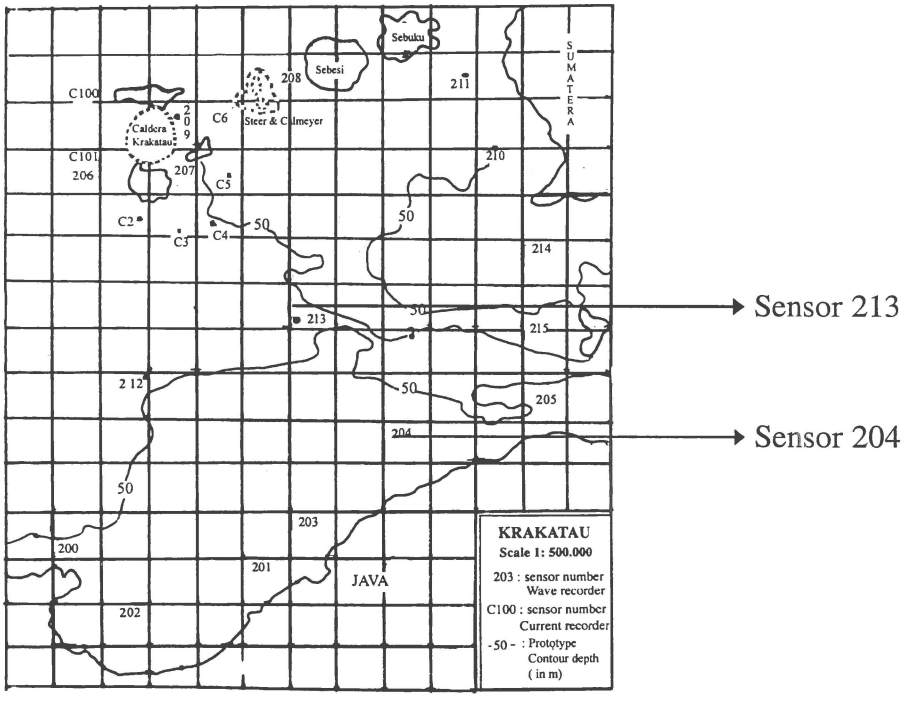
Sebuku
Sebesi
208
211
C100
C6
Steer & Culmeyer
Caldera Krakatau
209
C101
206
207
C5
210
C2
C3
C4
50
214
213
215
212
205
204
203
200
201
202
JAVA
SUMATERA
KRAKATAU
Scale 1: 500.000
203 : sensor number
Wave recorder
C100 : sensor number
Current recorder
-50- : Prototype
Contour depth
(in m)
Sensor 213
Sensor 204

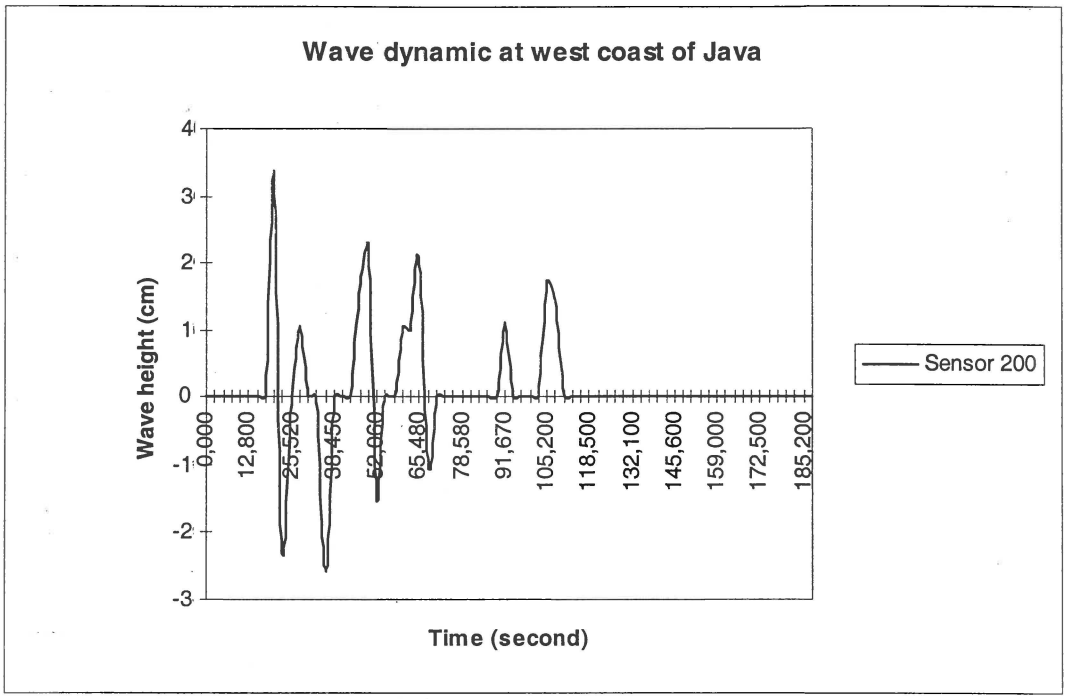
Wave dynamic at west coast of Java
Wave height (cm)
4
3
2
1
0
-1
-2
-3
0,000
12,800
25,520
38,450
52,060
65,480
78,580
91,670
105,200
118,500
132,100
145,600
159,000
172,500
185,200
Time (second)
Sensor 200

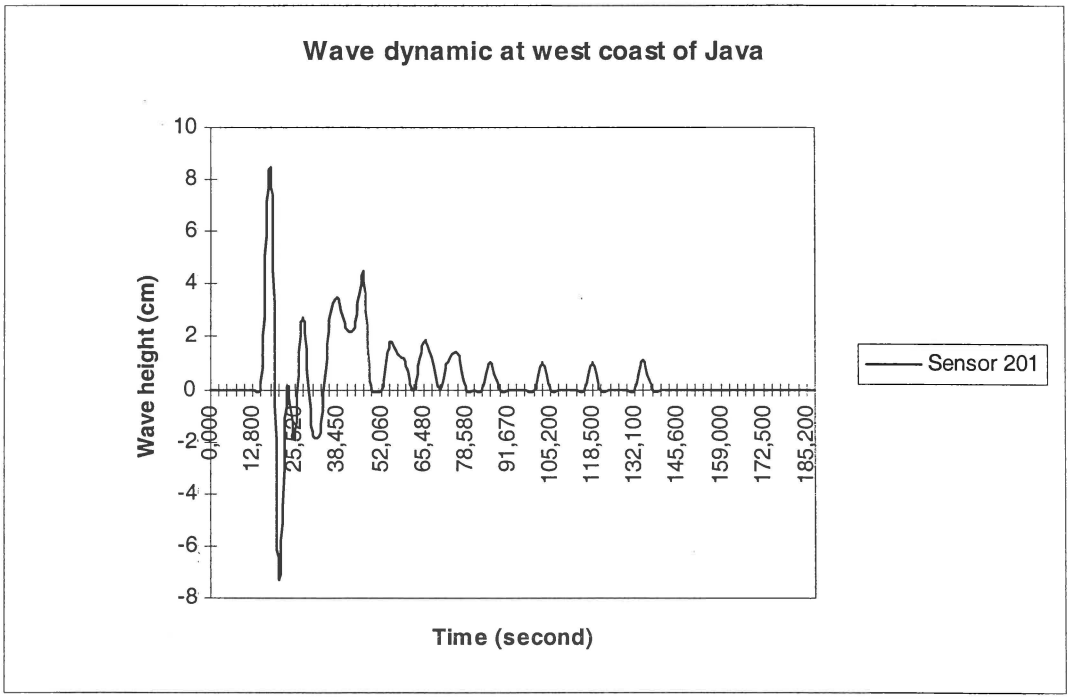
Wave dynamic at west coast of Java
Wave height (cm)
10
8
6
4
2
0
-2
-4
-6
-8
0,000
12,800
25,520
38,450
52,060
65,480
78,580
91,670
105,200
118,500
132,100
145,600
159,000
172,500
185,200
Time (second)
Sensor 201

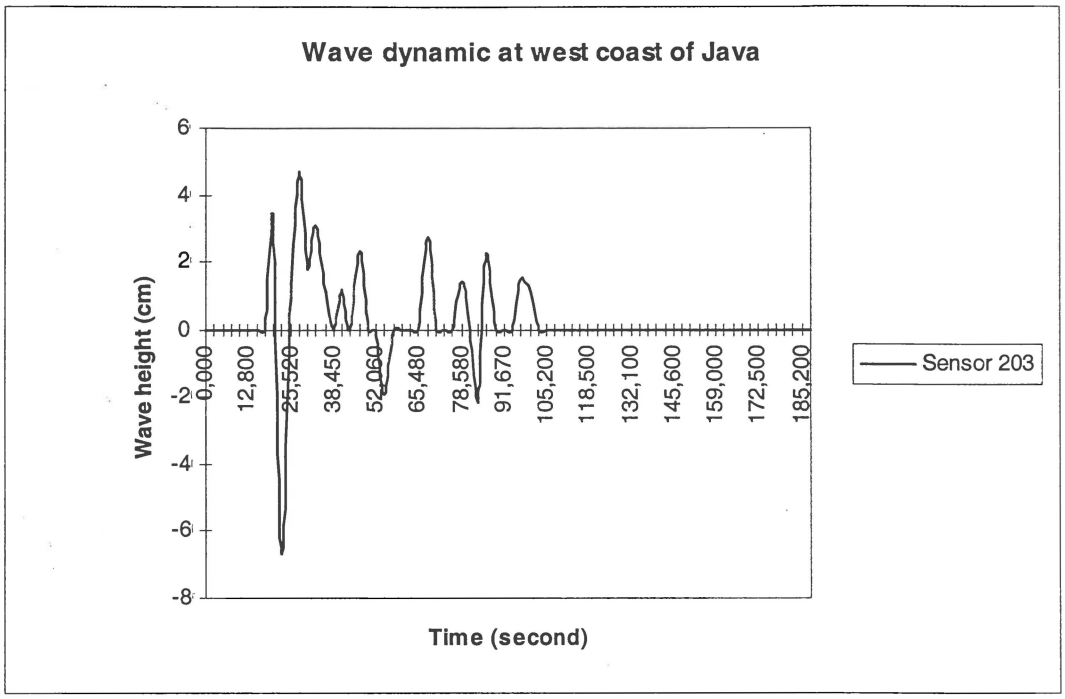
Wave dynamic at west coast of Java
Wave height (cm)
6
4
2
0
-2
-4
-6
-8
0,000
12,800
25,520
38,450
52,060
65,480
78,580
91,670
105,200
118,500
132,100
145,600
159,000
172,500
185,200
Time (second)
Sensor 203

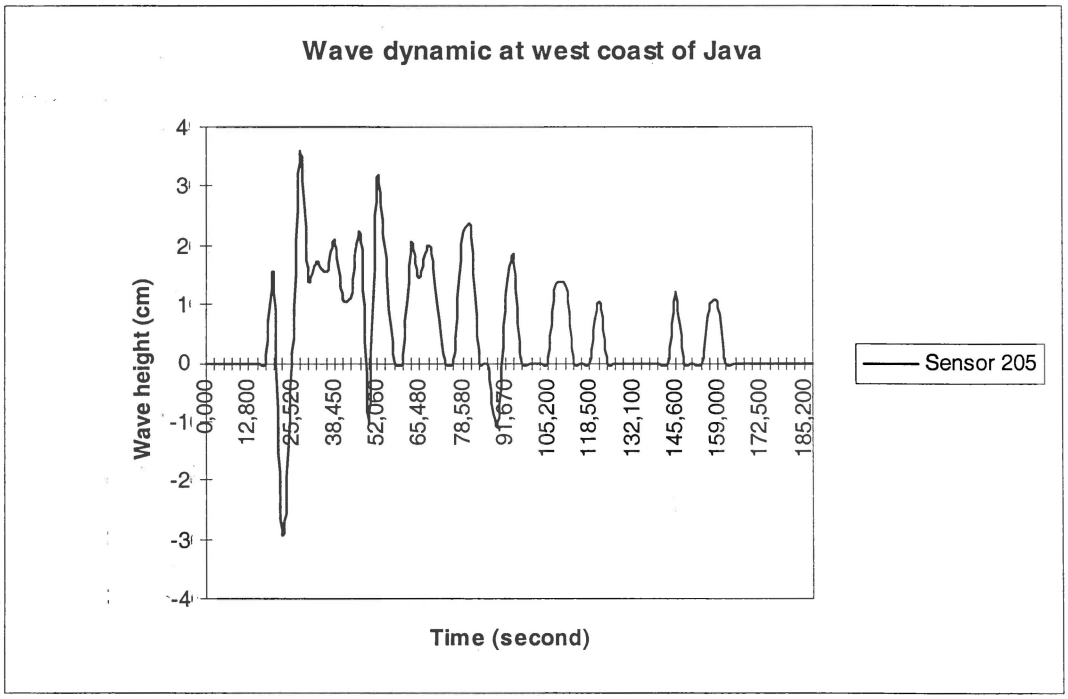
Wave dynamic at west coast of Java
Wave height (cm)
4
3
2
1
0
-1
-2
-3
-4
0,000
12,800
25,520
38,450
52,060
65,480
78,580
91,670
105,200
118,500
132,100
145,600
159,000
172,500
185,200
Time (second)
Sensor 205

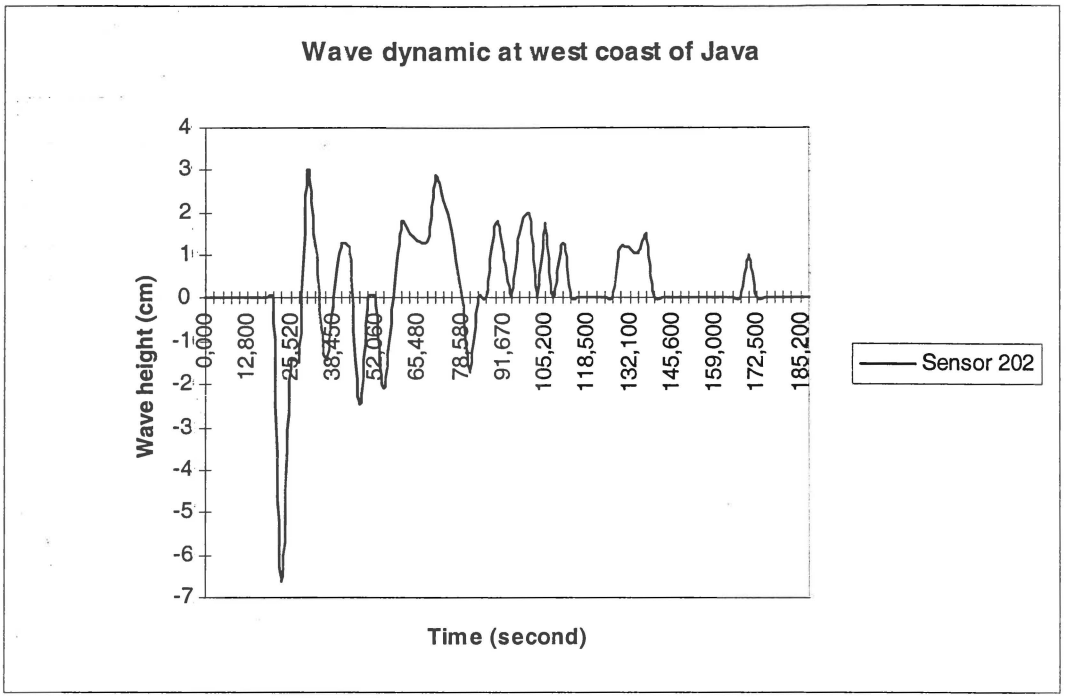
Wave dynamic at west coast of Java
Wave height (cm)
4
3
2
1
0
-1
-2
-3
-4
-5
-6
-7
0,000
12,800
25,520
38,450
52,060
65,480
78,580
91,670
105,200
118,500
132,100
145,600
159,000
172,500
185,200
Time (second)
Sensor 202

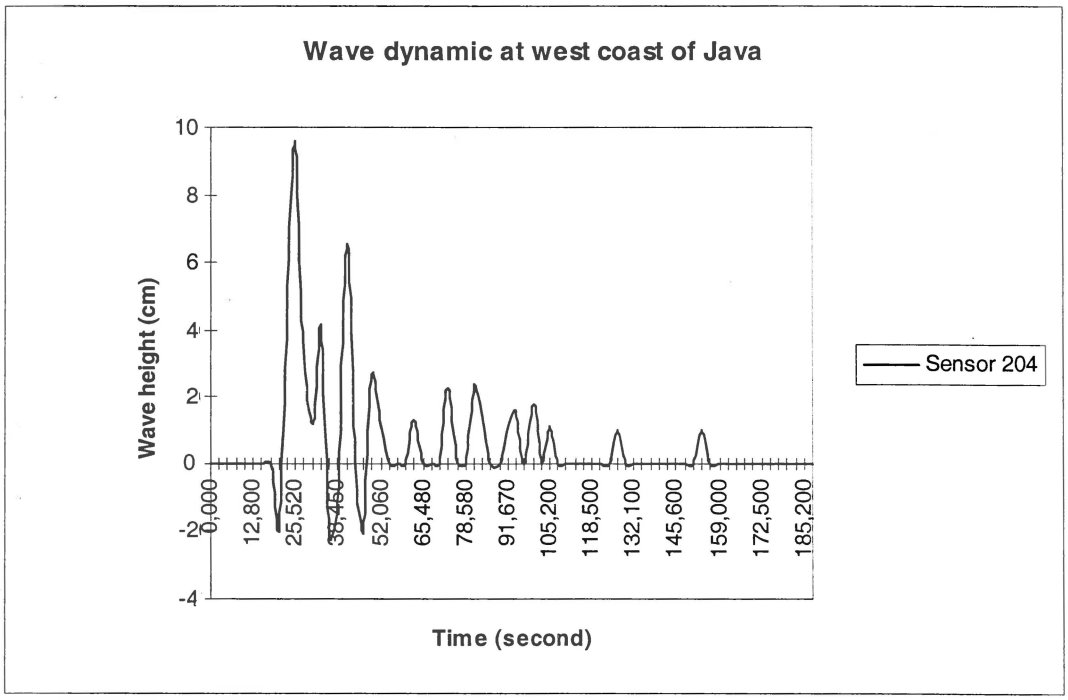
Wave dynamic at west coast of Java
Wave height (cm)
10
8
6
4
2
0
-2
-4
0,000
12,800
25,520
38,450
52,060
65,480
78,580
91,670
105,200
118,500
132,100
145,600
159,000
172,500
185,200
Time (second)
Sensor 204